Gopal B. Saha

Basics of PET Imaging

Physics, Chemistry, and Regulations

Third Edition

Springer

Basics of PET Imaging

Gopal B. Saha

Basics of PET Imaging

Physics, Chemistry, and Regulations

Third Edition

Springer

Gopal B. Saha, PhD
Emeritus Staff
Cleveland Clinic
Cleveland, OH, USA

ISBN 978-3-319-16422-9 ISBN 978-3-319-16423-6 (eBook)
DOI 10.1007/978-3-319-16423-6

Library of Congress Control Number: 2015945822

Springer Cham Heidelberg New York Dordrecht London

Printed on acid-free paper

Springer International Publishing AG Switzerland is part of Springer Science+Business Media (www.springer.com)

Dedication

With an ocean of love to my granddaughter Samira

who has been a perpetual source of my joy and inspiration

Preface

Stipulation of the third edition of the book, *Basics of PET Imaging*, has been prompted by many new developments in PET technology, equipment, and products since its second edition published in 2010. In this edition, new materials have been added, obsolete topics deleted, and pertinent contents updated. The purpose of the book remains the same as was for the previous editions—to fulfill the need for radiology and nuclear medicine professionals in their board examinations and practice.

The content of the book has been organized concisely in 14 chapters. Chapters 1 and 12 have no major change. In Chapter 2, information on detectors has been updated, and a new section on MR scanners and the principle of their operation has been added. Updated tables for specifications of PET, PET/CT, PET/MR, and animal scanners from different manufacturers have been incorporated. Chapter 3 contains a new section on PET/MR imaging. Iterative reconstruction method has been elaborated in Chapter 4. A table of PACS from different vendors has been added in Chapter 5. Chapter 6 contains a section on quality control of MR scanners. New positron emitting radionuclides with potential for human use have been included in Chapter 7, and similarly new PET radiopharmaceuticals have been added in Chapter 8. The original Chapter 9 has been split into two separate chapters to include FDA regulations in Chapter 9 and NRC regulations in Chapter 10 with updated information. Included in Chapter 11 is current updated information on reimbursement in healthcare. A new procedure for amyloid imaging in Alzheimer's patients using ^{18}F-florbetapir PET/CT imaging has been detailed in Chapter 13. A new Chapter 14 contains special topics of interest, such as absorbed doses from ^{18}F-FDG and ^{82}Rb-RbCl, SUV calculation in ^{18}F-FDG tumor imaging, and the use of infusion pump in ^{82}Rb-RbCl myocardial perfusion imaging, which were presented as appendices in past editions. In addition, four old appendices have been kept as before with minimal updating.

I would like to thank William C. Franz for his kind help in providing updated information on reimbursement in healthcare, which are included in Chapter 11. My special thanks are due to Ms Janet Foltin, Senior Editor, Clinical Medicine, of Springer Science and Business Media, Inc., who graciously encouraged and supported me in pursuing the third edition. I also sincerely thank Mr. Patrick Carr, production editor, for kind support in the production of the book. I would like to thank the SPi-Global of Chennai, India for the excellent production of the book.

Cleveland, OH, USA Gopal B. Saha, PhD

Contents

Chapter 1
Radioactive Decay and Interaction of Radiation with Matter

Atomic Structure

Matter is composed of atoms. An atom consists of a nucleus containing protons (Z) and neutrons (N), collectively called nucleons, and electrons rotating around the nucleus. The sum of neutrons and protons (total number of nucleons) is the mass number denoted by A. The properties of neutrons, protons, and electrons are listed in Table 1.1. The number of electrons in an atom is equal to the number of protons (atomic number Z) in the nucleus. The electrons rotate along different energy shells designated as K-shell, L-shell, M-shell, etc. (Fig. 1.1). Each shell further consists of subshells or orbitals, e.g., the K-shell has *s* orbital; the L-shell has *s* and *p* orbitals; the M-shell has *s*, *p*, and *d* orbitals, and the N-shell has *s*, *p*, *d*, and *f* orbitals. Each orbital can accommodate only a limited number of electrons. For example, the *s* orbital contains up to 2 electrons; the *p* orbital, 6 electrons; the *d* orbital, 10 electrons; and the *f* orbital, 14 electrons. The capacity number of electrons in each orbital adds up to give the maximum number of electrons that each energy shell can hold. Thus, the K-shell contains 2 electrons; the L-shell 8 electrons, the M-shell 18 electrons, and so forth.

A combination of a given number of protons and neutrons in a nucleus leads to an atom called the nuclide. A nuclide X is represented by ${}^{A}_{Z}X_{N}$. Some nuclides (280 or so) are stable, while others (more than 3400) are unstable. The unstable nuclides are termed the radionuclides, most of which are artificially produced in the cyclotron or reactor, with a few naturally occurring. The nuclides having the same number of protons are called the isotopes, e.g., ${}^{12}_{6}C_{6}$ and ${}^{13}_{6}C_{7}$; the nuclides having the same number of neutrons are called the isotones, e.g., ${}^{16}_{8}O_{8}$ and ${}^{15}_{7}N_{8}$; the nuclides having the same mass number are called the isobars, e.g., ${}^{131}I$ and ${}^{131}Xe$; and the nuclides with the same mass number but differing in energy are called the isomers, e.g., ${}^{99m}Tc$ and ${}^{99}Tc$.

G.B. Saha, *Basics of PET Imaging*, DOI 10.1007/978-3-319-16423-6_1

Table 1.1 Characteristics of electrons and nucleons

Particle	Charge	Mass (amu)[a]	Mass (kg)	Mass (MeV)[b]
Electron	−1	0.000549	0.9108×10^{-30}	0.511
Proton	+1	1.00728	1.6721×10^{-27}	938.78
Neutron	0	1.00867	1.6744×10^{-27}	939.07

[a]amu = 1 atomic mass unit = 1.66×10^{-27} kg = 1/12 of the mass of ^{12}C
[b]1 atomic mass unit = 931 MeV

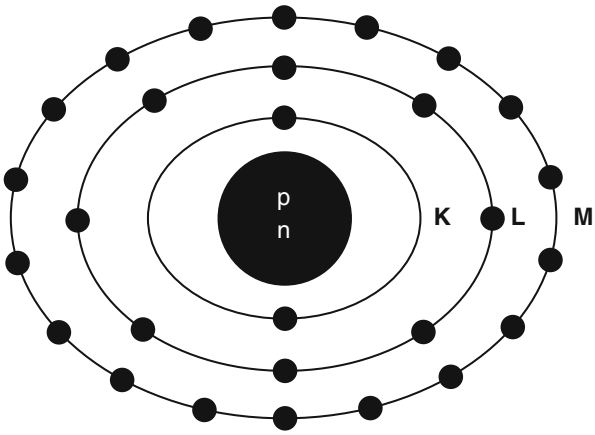

Fig. 1.1 Schematic structure of a ^{28}Ni atom. The nucleus containing protons and neutrons is at the center. The K-shell has 2 electrons, the L-shell 8 electrons, and the M-shell 18 electrons

Radioactive Decay

Radionuclides are unstable due to the unsuitable composition of neutrons and protons or excess energy and, therefore, decay by emission of radiations such as α particles, β^- particles, β^+ particles, electron capture, and isomeric transition.

α Decay

This decay occurs in heavy nuclei such as ^{235}U and ^{239}Pu. For example,

$$^{235}_{92}U_{143} \rightarrow {}^{231}_{90}Th_{141} + \alpha \tag{1.1}$$

Alpha particles are a nucleus of helium atom $^{4}_{2}He_2$ having two protons and two neutrons in the nucleus with two orbital electrons stripped off from the K-shell. The α particles are emitted with discrete energy and have a very short range in matter, e.g., about 0.03 mm in human tissues.

β^- Decay

β^- Decay occurs in radionuclides that are neutron rich. In the process, a neutron in the nucleus is converted to a proton along with the emission of a β^- particle and an antineutrino, $\overline{\nu}$.

$$n \rightarrow p + \beta^- + \overline{\nu} \tag{1.2}$$

For example,

$$^{131}_{53}\mathrm{I}_{78} \rightarrow {}^{131}_{54}\mathrm{Xe}_{77} + \beta^- + \overline{\nu}$$

The energy difference between the two nuclides (i.e., between ^{131}I and ^{131}Xe in the above example) is called the decay energy or transition energy, which is shared between the β^- particle and the antineutrino $\overline{\nu}$. Because of the random nature of decay, β^- particles are emitted with a spectrum of energy with the transition energy as the maximum energy and with an average energy equal to one-third of the maximum energy.

Positron (β^+) Decay

When a radionuclide is proton rich, it decays by the emission of a positron (β^+) along with a neutrino ν. In essence, a proton in the nucleus is converted to a neutron in the process.

$$p = n + \beta^+ + \nu \tag{1.3}$$

Since a neutron is one electron mass heavier than a proton, the right-hand side of Eq. (1.3) is two electron mass more than the left-hand side, i.e., 2×0.511 MeV $=$ 1.022 MeV more on the right side. For conservation of energy, therefore, the radionuclide must have a transition energy of at least 1.022 MeV to decay by β^+ emission. The energy beyond 1.022 MeV is shared as kinetic energy by the β^+ particle and the neutrino.

Some examples of positron-emitting nuclides are:

$$^{18}_{9}\mathrm{F}_9 \rightarrow {}^{18}_{8}\mathrm{O}_{10} + \beta^+ + \nu$$

$$^{82}_{37}\mathrm{Rb}_{45} \rightarrow {}^{82}_{36}\mathrm{Kr}_{46} + \beta^+ + \nu$$

Positron emission tomography (PET) is based on the principle of coincidence detection of the two 511-keV photons arising from positron emitters, which will be discussed in detail later.

Electron Capture

When a radionuclide is proton rich, but has energy less than 1.022 MeV, then it decays by electron capture. In the process, an electron from the nearest shell, i.e., K-shell, is captured by a proton in the nucleus to produce a neutron, and a neutrino v is emitted to conserve energy.

$$p + e^- \rightarrow n + \nu \tag{1.4}$$

Note that when the transition energy is less than 1.022 MeV, the radionuclide definitely decays by electron capture. However, when the transition energy is more than 1.022 MeV, the radionuclide can decay by positron emission and/or electron capture. The greater the transition energy above 1.022 MeV, the more likely the radionuclide will decay by positron emission. Some examples of radionuclides decaying by electron capture are:

$$^{111}_{49}\mathrm{In}_{62} + e^- \rightarrow {}^{111}_{48}\mathrm{Cd}_{63} + \nu$$

$$^{67}_{31}\mathrm{Ga}_{36} + e^- \rightarrow {}^{67}_{30}\mathrm{Zn}_{37} + \nu$$

Isomeric Transition

When a nucleus has excess energy above the ground state, it can exist in excited (energy) states, which are called the isomeric states. The lifetimes of these states normally are very short (~10^{-15} to 10^{-12} s); however, in some cases, the lifetime can be longer from minutes to years. When an isomeric state has a longer lifetime, it is called a metastable state and is represented by "*m*." Thus, having an energy state of 140 keV above ^{99}Tc and decaying with a half-life of 6 h, ^{99m}Tc is an isomer of ^{99}Tc.

$$^{99m}\mathrm{Tc} \rightarrow {}^{99}\mathrm{Tc} + \gamma$$

$$^{113m}\mathrm{In} \rightarrow {}^{113}\mathrm{In} + \gamma$$

A radionuclide may decay by α, β^-, β^+ emissions, or electron capture to different isomeric states of the product nucleus, if allowed by the rules of quantum physics.

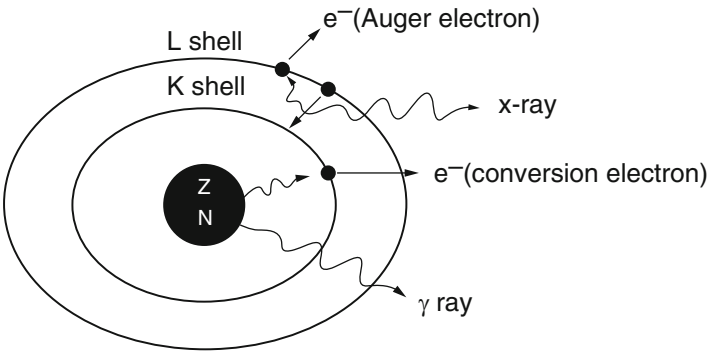

Fig. 1.2 γ-Ray emission and internal conversion process. In internal conversion process, the excitation energy of the nucleus is transferred to a K-shell electron, which is then ejected, and the K-shell vacancy is filled by an electron from the L-shell. The energy difference between the L-shell and K-shell appears as the characteristic K X-ray. The characteristic K X-ray energy may again be transferred to an L-shell electron, which is then ejected in the Auger process

Naturally, these isomeric states decay to lower isomeric states and finally to the ground states of the product nucleus, and the energy differences appear as γ-ray photons.

As an alternative to γ-ray emission, the excitation energy may be transferred to an electron, preferably in the K-shell, which is then ejected with energy $E_\gamma - E_B$, where E_γ and E_B are the γ-ray energy and binding energy of the electron, respectively (Fig. 1.2). This process is called the internal conversion, and the ejected electron is called the conversion electron. The vacancy created in the K-shell is filled by the transition of an electron from an upper shell. The energy difference between the two shells appears as a characteristic K X-ray. Similarly, characteristic L X-ray and M X-ray can be emitted if the vacancy in the L- or M-shell is filled by electron transition from upper shells. Like γ rays, the characteristic X-ray energy can be emitted as photons or be transferred to an electron in a shell which is then ejected, if energetically possible. The latter is called the Auger process, and the ejected electron is called the Auger electron.

The decay of radionuclides is represented by a decay scheme, an example of which is given for ^{68}Ga in Fig. 1.3.

Radioactive Decay Equations

General Decay Equations

The atoms of a radioactive sample decay randomly, and one cannot tell which atom will decay when. One can only talk about an average decay of the atoms in the sample. This decay rate is proportional to the number of radioactive atoms present. Mathematically,

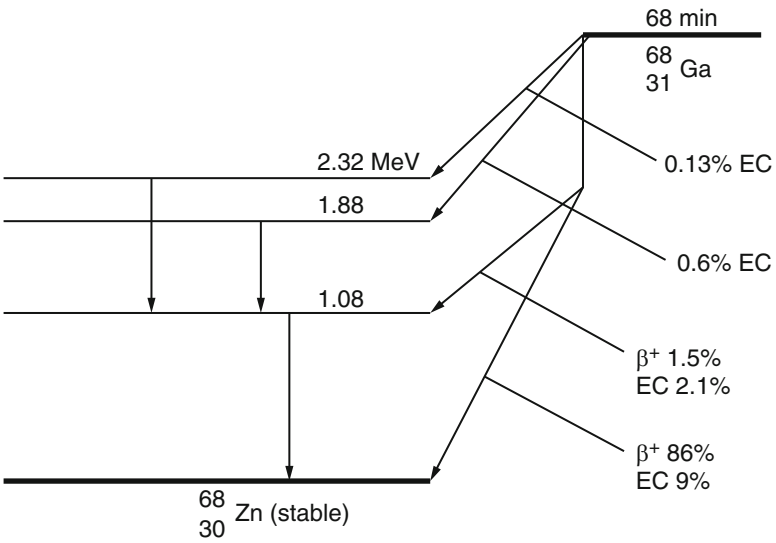

Fig. 1.3 The decay scheme of ^{68}Ga. The 87.5% of positrons are annihilated to give rise to 175% of 511-keV photons

$$-\frac{dN}{dt} = \lambda N, \tag{1.5}$$

where $-dN/dt$ is the rate of decay denoted by the term activity or radioactivity A, λ is the decay constant, and N is the number of atoms of the radionuclide present. Thus,

$$A = \lambda N, \tag{1.6}$$

Integrating Eq. (1.5) gives the activity A_t at time t as

$$A_t = A_0 e^{-\lambda t}, \tag{1.7}$$

where A_0 is the activity at time $t = 0$. The plot of A_t vs. t on a semilog scale is shown in Fig. 1.4. If one knows activity A_0 at a given time, the activity A_t at time t before or later can be calculated by Eq. (1.7).

Half-life ($t_{1/2}$): The half-life of a radionuclide is defined as the time required to reduce the initial activity to one-half. It is unique for every radionuclide and is related to the decay constant as follows:

$$\lambda = \frac{0.693}{t_{1/2}}. \tag{1.8}$$

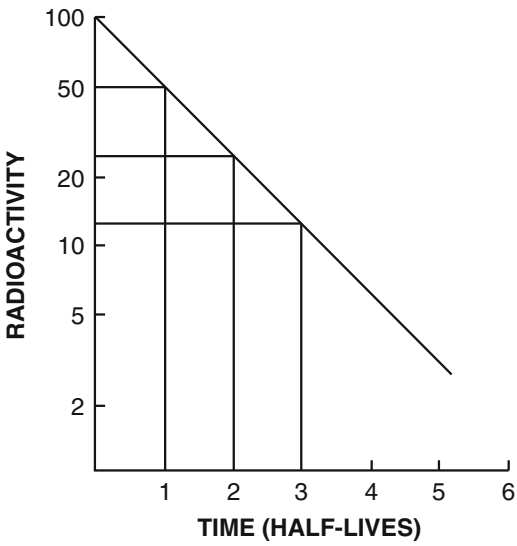

Fig. 1.4 Plot of activity A_t against time on a semilogarithmic graph indicating a *straight line*. The slope of the line is the decay constant λ of the radionuclide. The half-life $t_{1/2}$ is calculated from λ using (1.8). Alternatively, the half-life is determined by reading an initial activity and half its value and their corresponding times. The difference in time between the two readings is the half-life

The half-life of a radionuclide is determined by measuring the radioactivity at different time intervals and plotting them on semilogarithmic paper, as shown in Fig. 1.4. An initial activity and half its value are read from the straight line, and the corresponding times are noted. The difference in time between the two readings gives the half-life of the radionuclide.

The mean life τ of a radionuclide is defined by

$$\tau = \frac{1}{\lambda} = \frac{t_{1/2}}{0.693} = 1.44 t_{1/2}. \tag{1.9}$$

A radionuclide decays by 63% in one mean life.

Effective half-life: Each radionuclide decays with a definite half-life, called the physical half-life, which is denoted by T_p or $t_{1/2}$. When radiopharmaceuticals are administered to patients, analogous to physical decay, they are eliminated from the body by biological processes such as fecal excretion, urinary excretion, and perspiration. This elimination is characterized by a biological half-life (T_b) which is defined as the time taken to eliminate a half of the administered activity from the biological system. It is related to the decay constant λ_b by

$$\lambda_b = \frac{0.693}{T_b}.$$

Thus, in a biological system, the loss of a radiopharmaceutical is related to λ_p and λ_b. The net effective rate of loss (λ_e) is characterized by

$$\lambda_e = \lambda_p + \lambda_b. \tag{1.10}$$

Since $\lambda = 0.693/t_{1/2}$,

$$\frac{1}{T_e} = \frac{1}{T_p} + \frac{1}{T_b}, \tag{1.11}$$

$$T_e = \frac{T_p \times T_b}{T_p + T_b}. \tag{1.12}$$

The effective half-life is always less than the shorter of T_p or T_b. For a very long T_p and a short T_b, T_e is almost equal to T_b. Similarly, for a very long T_b and a short T_p, T_e is almost equal to T_p.

Successive Decay Equations

In a successive decay, a parent radionuclide p decays to a daughter nuclide d, and d in turn decays to another nuclide c, and we are interested in the decay rate of d over time. Thus,

$$p \rightarrow d \rightarrow c.$$

Mathematically,

$$-\frac{dN_d}{dt} = \lambda_p N_p - \lambda_d N_d. \tag{1.13}$$

On integration,

$$A_d = \frac{\lambda_d (A_p)_0}{\lambda_d - \lambda_p} \left[e^{-\lambda_p t} - e^{-\lambda_d t}\right]. \tag{1.14}$$

If the parent half-life is greater than the daughter half-life (say, by a factor of 10–100), that is, $(t_{1/2})_p > (t_{1/2})_d$ or $\lambda_d > \lambda_p$ and also if the time of decay (t) is very long, then $e^{-\lambda_d t}$ is almost zero compared to $e^{-\lambda_p t}$. Then

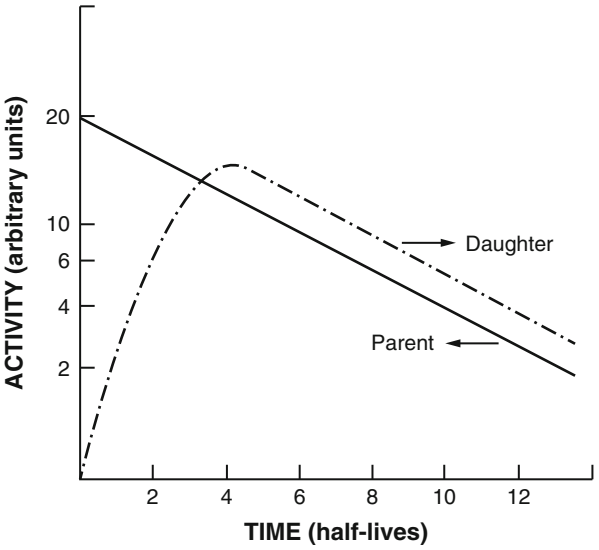

Fig. 1.5 The transient equilibrium is illustrated in the plot of activity vs. time on a semilogarithmic graph. The daughter activity increases initially with time, reaches a maximum, then transient equilibrium, and finally appears to decay following the half-life of the parent. Note that the daughter activity is higher than the parent activity in equilibrium

$$(A_{\mathrm{d}})_t = \frac{\lambda_{\mathrm{d}}}{\lambda_{\mathrm{d}} - \lambda_{\mathrm{p}}}\left(A_{\mathrm{p}}\right)_t. \tag{1.15}$$

Equation (1.15) represents a *transient equilibrium* between the parent *p* and the daughter *d* radionuclides, which is achieved after several half-lives of the daughter. The graphical representation of this equilibrium is shown in Fig. 1.5. It can be seen that after equilibrium, the daughter activity is greater than the parent activity and the daughter appears to decay following the half-life of the parent. The principle of transient equilibrium is applied to many radionuclide generators such as the ^{99}Mo–^{99m}Tc generator.

If the parent half-life is much greater than the daughter half-life (by a factor of hundreds or thousands), then λ_{p} is negligible compared to $\lambda_{\mathrm{d},}$ that is, $\lambda_{\mathrm{d}} \gg \lambda_{\mathrm{p}}$. Then Eq. (1.15) becomes

$$(A_{\mathrm{d}})_t = \left(A_{\mathrm{p}}\right)_t. \tag{1.16}$$

This equation represents a *secular equilibrium* in which the daughter activity becomes equal to the parent activity, and the daughter decays with the half-life of the parent. The ^{82}Sr–^{82}Rb generator is an example of secular equilibrium.

Units of Radioactivity

1 Ci $= 3.7 \times 10^{10}$ disintegration per second (dps)
1 mCi $= 3.7 \times 10^{7}$ dps
1 μCi $= 3.7 \times 10^{4}$ dps

Units of Radioactivity in System Internationale

1 Becquerel (Bq) = 1 dps
1 kBq $= 10^{3}$ dps $= 2.7 \times 10^{-8}$ Ci
1 Mbq $= 10^{6}$ dps $= 2.7 \times 10^{-5}$ Ci
1 GBq $= 10^{9}$ dps $= 2.7 \times 10^{-2}$ Ci

Calculations

Problem 1.1 A dosage of ^{18}F-FDG has 20 mCi at 10 a.m. Wednesday. Calculate the activity of the dosage at 7 a.m. and 2 p.m. that day. The half-life of ^{18}F is 110 min.

Answer:

$$\lambda \ \text{for}^{18}\text{F} = \frac{0.693}{110}\text{min}^{-1}$$

Time from 7 a.m. to 10 a.m. $= 43\,\text{h} = 180\,\text{min}$

Time from 10 a.m. to 2 a.m. $= 4\,\text{h} = 240\,\text{min}$

Activity of ^{18}F-FDG at 7 a.m. $= 20 \times e^{+\frac{0.693}{110}} \times 180$

$= 20 \times e^{+1.134}$

$= 62$ mCi (2.29 GBq)

Activity of ^{18}F-FDG at 2 p.m. $= 20 \times e^{-\frac{0.693 \times 240}{110}}$

$= 20 \times e^{-1.512}$

$= 20 \times 0.22 = 4.4$ mCi (163.1 MBq)

Problem 1.2 A radioactive sample decays 40% per hour. What is the half-life of the radionuclide?

Answer:

$$\lambda = 0.4\,\mathrm{h}^{-1} = \frac{0.693}{t_{1/2}}$$

$$t_{1/2} = \frac{0.693}{0.4} = 1.73\,\mathrm{h}.$$

Interaction of Radiation with Matter

Radiations are either particulate type, such as α particle and β particle, or nonparticulate type, such as high-frequency electromagnetic radiation (e.g., γ rays, X-rays), and both kinds are ionizing radiations. The mode of interaction of these two types of radiations with matter is different.

Interaction of Charged Particles with Matter

The energetic charged particles such as α particles and β particles, while passing through matter, lose their energy by interacting with the orbital electrons of the atoms in the matter. In these processes, the atoms are ionized in which the electron in the encounter is ejected or the atoms are excited in which the electron is raised to a higher energy state. In both excitation and ionization processes, chemical bonds in the molecules of the matter may be ruptured, forming a variety of chemical entities.

The lighter charged particles (e.g., β particles) move in a zigzag path in the matter, whereas the heavier particles (e.g., α particles) move in a straight path, because of the heavy mass and charge. The straight line path traversed by the charged particles is called the range R. The range of a charged particle depends on the energy, charge, and mass of the particle as well as the density of the matter it passes through. It increases with increasing charge and energy, while it decreases with increasing mass of the particle and increasing density of the matter. The range of positrons and other properties of common positron-emitters are given in Table 1.2.

A unique situation of the passage of positrons through an absorber is that as a positron loses its energy by interaction with electrons of the absorber atoms and comes to almost rest, it combines with an electron of an absorber atom. At this instant, both particles (β^+ and e^-) are annihilated as a result of matter–antimatter encounter to produce two photons of 511 keV, which are emitted in opposite directions (~180°) (Fig. 1.6). This process is called the *annihilation* process. Because the positrons have a residual momentum at the time of annihilation, the

Table 1.2 Properties of common positron emitters

Radionuclide range	Half-life	$E_{\beta+,\max}$ (MeV)	Max. β^+ range (mm) in water	Average β^+ range (mm) in water
^{11}C	20.4 min	0.97	3.8	0.85
^{13}N	10 min	1.20	5.0	1.15
^{15}O	2 min	1.74	8.0	1.80
^{18}F	110 min	0.64	2.2	0.46
^{68}Ga	68 min	1.90	9.0	2.15
^{82}Rb	75 s	3.35	15.5	4.10

Adapted by the permission of the Society of Nuclear Medicine from Brown TF, Yasillo NJ (1997) Radiation safety considerations for PET centers. J Nucl Med Technol 25:98

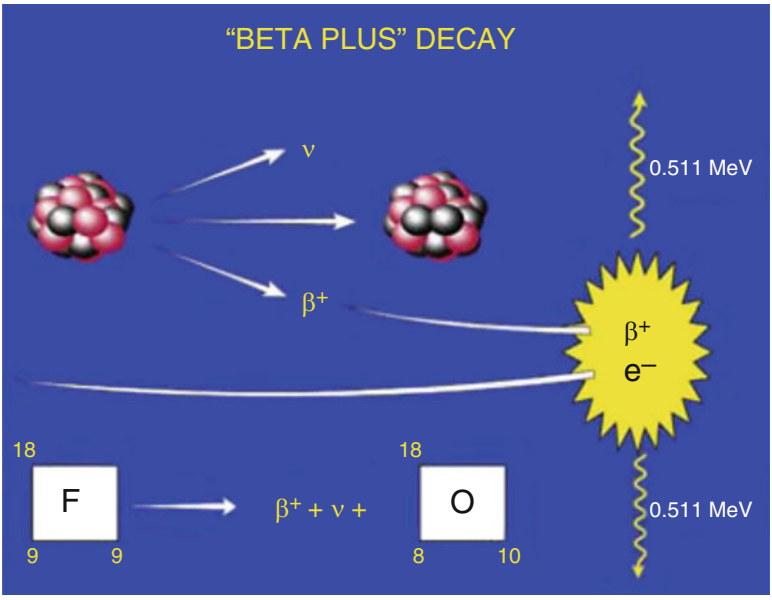

Fig. 1.6 A schematic illustration of the annihilation of a positron and an electron in the medium. Two 511-keV photons are produced and emitted in opposite directions (180°) (Reprinted with the permission of The Cleveland Clinic Center for Medical Art & Photography © 2009. All Rights Reserved)

two annihilation photons are not emitted exactly at 180°. Detection of the two 511-keV photons in coincidence by two opposite detectors is the basis of PET.

An important parameter related to the interaction of radiations with matter is linear energy transfer (LET). It is the energy deposited by a radiation per unit length of the path in the absorber and is normally given in units of kiloelectron volt per micrometer (keV/μm). The LET varies with the energy, charge, and mass of the particle. The γ radiations and β^- particles interact with matter depositing relatively

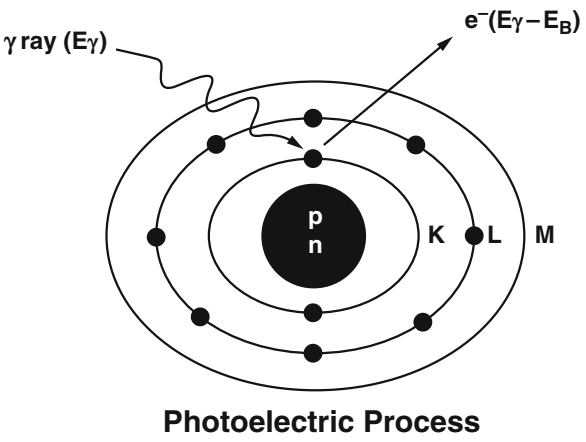

Fig. 1.7 An illustration of photoelectric effect, where a γ ray transfers all its energy E_γ to a K-shell electron and the electron is ejected with E_γ–E_B, where E_B is the binding energy of the electron in the K-shell. The characteristic K X-ray emission or the Auger process can follow, as described in Fig. 1.2

less amount of energy per unit length and so have low LET. On the other hand, α particles and protons deposit more energy per unit length because of their greater mass and charge and so have higher LET.

Interaction of γ Radiation with Matter

In the spectrum of electromagnetic radiations, γ radiations are high-frequency radiations and interact with matter by three mechanisms: photoelectric, Compton, and pair production.

Photoelectric Process: In this process, a γ radiation, while passing through an absorber, transfers its entire energy primarily to an inner shell electron (e.g., the K-shell) of an absorber atom and ejects the electron (Fig. 1.7). The ejected electron will have the kinetic energy equal to E_γ–E_B, where E_γ is the γ-ray energy and E_B is the binding energy of the electron in the shell. The probability of this process decreases with increasing energy of the γ ray, but increases with increasing atomic number of the absorber. It is roughly given by $Z^5/E_\gamma{}^3$. The vacancy in the shell is filled in by the transition of an electron from the upper shell, which is followed by emission of the energy difference between the two shells as characteristic X-rays or by the Auger process described in the internal conversion process.

Compton Scattering Process: In a Compton scattering process, a γ radiation with somewhat higher energy interacts with an outer shell electron of the absorber atom transferring only part of its energy to the electron and ejecting it (Fig. 1.8). The ejected electron is called the Compton electron and carries a part of the γ-ray energy minus its binding energy E_B in the shell, i.e., $E_\gamma^{'} - E_B$, where $E_\gamma^{'}$ is a part of the original γ ray energy E_γ that is transferred to the electron. The scattered photon carries energy equal to $E_\gamma - E_\gamma^{'} - E_B$. Thus, in Compton scattering, a scattered photon and a Compton electron are produced. The scattered photon may again,

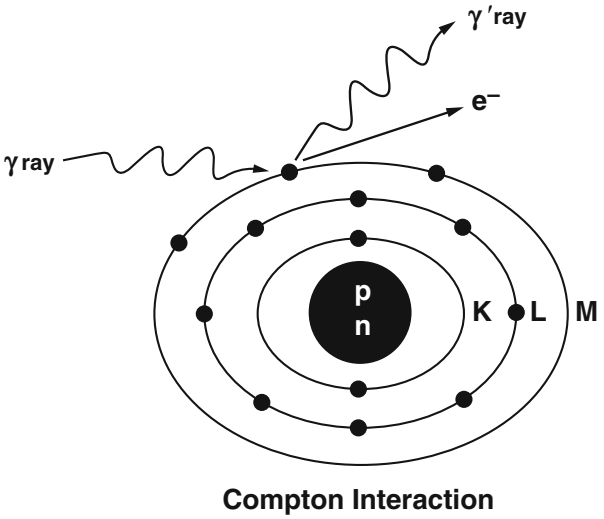

Fig. 1.8 The Compton scattering process in which a γ ray transfers only a part of its energy to an electron in a shell and is itself scattered with reduced energy. The electron is ejected from the shell with energy, $E_{\gamma}^{'}$–E_B, where $E_{\gamma}^{'}$ is the partial energy transferred by the γ ray and E_B is the binding energy of the electron in the shell. The remaining γ-ray energy appears as a scattered photon

depending on the energy and location of interaction, encounter a photoelectric process or another Compton scattering process, or leave the absorber without interaction. As the energy of the γ radiation increases, the photoelectric process decreases and the Compton scattering process increases, but the latter also decreases with photon energy above 1.0 MeV or so. The probability of Compton scattering is independent of the atomic number Z of the absorber.

Pair Production: When the γ-ray energy is higher than 1.022 MeV, the photon interacts with the nucleus of an absorber atom during its passage through it and produces a positron and an electron. This is called pair production. The excess energy beyond 1.022 MeV is shared as kinetic energy between the two particles. The probability of pair production increases with increasing photon energy above 1.022 MeV. The positron produced will undergo annihilation in the absorber as described earlier.

Attenuation of γ Radiations: When γ radiations pass through the absorber medium, they undergo one or a combination of the above three processes (photoelectric, Compton, and pair production) depending on their energy, or they are transmitted out of the absorber without any interaction. The combined effect of the three processes is called the *attenuation* of the γ radiations (Fig. 1.9). For a γ radiation passing through an absorber, the linear attenuation coefficient (μ_ℓ) of the γ radiation is given by

$$\mu_\ell = \tau + \sigma + \kappa, \tag{1.17}$$

where τ is the photoelectric coefficient, σ is the Compton coefficient, and κ is the pair production coefficient (Fig. 1.10). The linear attenuation coefficient of a

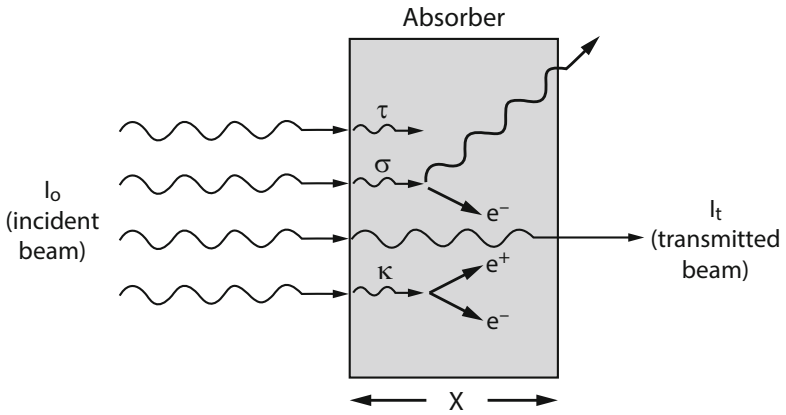

Fig. 1.9 Illustration of attenuation of a photon beam (I_0) in an absorber of thickness x. Attenuation comprises photoelectric effect (τ), Compton scattering (σ), and pair production (κ). Photons passing through the absorber without interaction constitute the transmitted beam (I_t)

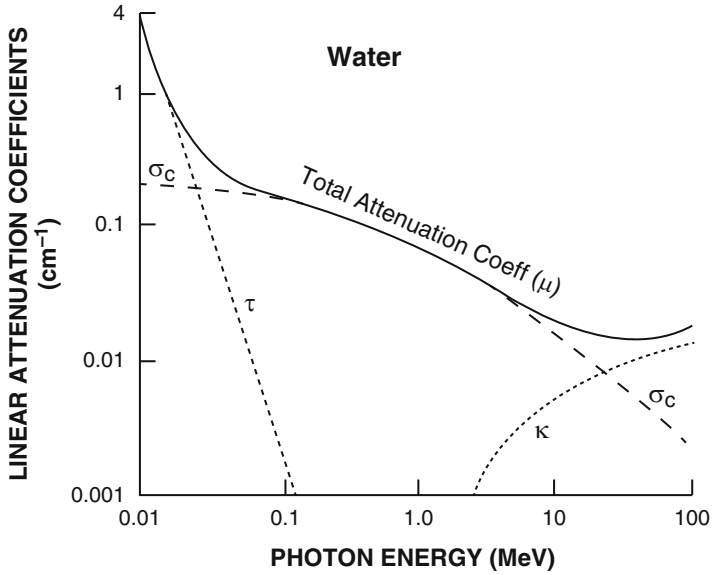

Fig. 1.10 Linear attenuation coefficient of γ rays of different energies in water (equivalent to body tissue). The relative contributions of photoelectric, Compton scattering, and pair production processes are illustrated

radiation in an absorber has the unit of cm^{-1} and normally decreases with the energy and increases with the atomic number and density of the absorber. If a photon beam I_0 passes through an absorber of thickness x, then the transmitted beam (I_t) is given by

Table 1.3 Half-value layers of 511-keV photons in different absorber materials

Absorber material	HVL (mm) (narrow beam)	HVL (mm)[a] (broad beam)
Lead	4.1	5.0
Tungsten	2.9	3.2
Iron	11.0	16.0
Concrete	33.2	64.0
Tissue	77	–

[a]Adapted from Townson JEC (2003) Radiation dosimetry and protection in PET. In: Valk PE, Bailey DL, Townsend DW, Maisey MN (eds) Positron emission tomography. Springer, New York

$$I_t = I_0 e^{-\mu_\ell x}. \tag{1.18}$$

The attenuation of a photon beam in human tissues during imaging is a critical factor to consider in both single photon emission computed tomography (SPECT) or PET, which will be discussed later.

An important quantity in the discussion of photon interaction with matter is the half-value layer (HVL), which is defined as the thickness of the absorber that attenuates initial photon beam intensity to one-half. The HVL increases with higher energy of the photon and decreases with increasing atomic number of the absorber. Lead is a high atomic number inexpensive metal that has very high absorbing power for γ radiations providing low HVL values and that is why it is commonly used for radiation protection. The HVL is related to the linear attenuation coefficient μ_ℓ as follows:

$$\mu_\ell = \frac{0.693}{\text{HVL}}. \tag{1.19}$$

The HVL for 511-keV photons in some absorbers is given in Table 1.3.

Along the same line, the tenth-value layer (TVL) is defined by the thickness of the absorber that reduces the initial intensity of the photons by a factor of 10. It is given by

$$\text{TVL} = \frac{-\ln(0.1)}{\mu_\ell} = \frac{2.30}{\mu_\ell} = 3.32\,\text{HVL}. \tag{1.20}$$

Another quantity called the mass attenuation coefficient (μ_g) is given by the linear attenuation coefficient (μ_ℓ) divided by the density (ρ) of the absorber and is given in units of cm^2/g or cm^2/mg.

Thus,

$$\mu_g = \frac{\mu_\ell}{\rho}. \tag{1.21}$$

Questions

1. The total number of nucleons in an atom is designated by (A) N; (B) Z; (C) M; (D) A.
2. Isotopes contain the same number of ____.
3. Isobars contain the same number of ____.
4. ^{99m}Tc and ^{99}Tc are two ____.
5. Isomeric transition is an alternative to gamma ray emission. True ____; False ____.
6. Gamma ray emission is an alternative to internal conversion. True ____; False ____.
7. Describe the Auger process in radioactive decay.
8. Name two nuclear decay processes in which characteristic X-rays are possibly emitted.
9. What types of radionuclides are designated as metastable isomers with symbol "m" in the mass number?
10. Why is a neutrino needed in the positron decay? In what decay is an antineutrino emitted?
11. In a β^- decay, the transition energy is 400 keV. The β^- particle is emitted with 315 keV. What is the energy of the antineutrino?
12. Describe the annihilation process.
13. Explain why two photons of 511 keV are emitted in positron annihilation.
14. If a K-shell electron whose binding energy is 25 keV is emitted as a result of internal conversion of a 135-keV photon, what is the energy of the ejected electron?
15. What types of radionuclides would decay by β^- and β^+ emission and electron capture?
16. How long will it take for the decay of three-quarters of a ^{18}F-FDG ($t_{1/2} =$ 110 min) sample?
17. What are the conditions for transient equilibrium and secular equilibrium in radioactive decay?
18. If the activity of ^{18}F-FDG is 25 mCi at 10 a.m. Wednesday, what is the activity at 2:30 p.m. the same day ($t_{1/2}$ of $^{18}\text{F} = 110$ min)?
19. ^{18}F-FDG dosages are shipped from a vendor 3 h away from the customer. What initial amount should be sent in order to have a 10 mCi dosage for the customer?

20. A radioactive sample initially gives 9500 cpm and 3 h later 2500 cpm. Calculate the half-life of the radionuclides.
21. ^{18}F-FDG has a biological half-life of 10 h in humans and a physical half-life of 110 min. What is the effective $t_{1/2}$ of the radiopharmaceutical?
22. Define linear energy transfer (LET) and range (R) of charged particles.
23. The range of a charged particulate radiation in matter increases:
    (a) as the mass increases True ____; False ____
    (b) as the charge increases True ____; False ____
    (c) as the energy decreases True ____; False ____
24. Describe photoelectric and Compton scattering processes.
25. The photoelectric interaction of a γ ray increases with:
(a) energy True ____; False ____
(b) atomic number of the absorber True ____; False ____
26. A 350-keV γ ray interacts with a K-shell electron by the photoelectric interaction. If the binding energy of the K-shell electron is 25 keV, what is the kinetic energy of the photoelectron?
27. Does Compton scattering depend on the atomic number of the absorber?
28. Describe attenuation of a photon beam through an absorber.
    (a) Does it depend on density and atomic number of the absorber?
    (b) Define linear attenuation coefficient and HVL of a γ ray in an absorber.
29. If 1 mCi of a radionuclide is adequately shielded by 6 HVLs of lead, how many HVLs would be needed to have equal shielding for (a) 5 mCi and (b) 8 mCi of the radionuclide?
30. How many HVLs are approximately equivalent to three-tenth-value layers?
31. If 15 % of the 511-keV photons of ^{18}F are transmitted after passing through a lead brick of 7 cm thickness, calculate the HVL of the 511-keV photon in lead.
32. Two annihilation photons are emitted exactly at 180? True ____; False ____.
33. A positron and an electron annihilate because (a) they have the same energy; (b) they have opposite momentum; or (c) it is matter–antimatter encounter?

References and Suggested Reading

Bushberg JT, Seibert JA, Leidholdt Sr EM, Boone JM. The essential physics of medical imaging. 3rd ed. Philadelphia: Lippincott, Williams & Wilkins; 2011.

Cherry SR, Sorenson JA, Phelps ME. Physics in nuclear medicine. 3rd ed. Philadelphia: W.B. Saunders; 2012.

Friedlander G, Kennedy JW, Macias ES, Miller JM. Nuclear and radiochemistry. 3rd ed. New York: Wiley; 1981.

Saha GB. Physics and radiobiology of nuclear medicine. 4th ed. New York: Springer; 2013.

Chapter 2
PET Scanning Systems

Background

The detection and measurement of radiation is based on the interaction of radiations with matter discussed in Chap. 1. In gases, ionizing radiations, particulate or electromagnetic, interact with gas molecules to produce positive and negative ions, which are then collected as current or count by the application of a voltage. The amount of ionization is proportional to the amount of energy deposited by the radiation. At low voltages, the ionization is measured as current that is proportional to the amount of radiation. Dose calibrators, pocket dosimeters, and ionization chambers operate on this principle at low voltages (~150 V). At high voltages (~900 V), ions are multiplied in an avalanche of interactions producing a pulse that is independent of the energy and type of radiation. Each event of interaction is detected as a count, and this principle is applied in Geiger–Müller (GM) counters, which are used as radiation survey meters.

Liquid scintillation detectors operate on the principle of interaction of radiations with a special type of scintillating liquid that emits light upon interaction with radiation. The light is then processed in the same manner as in the case of a solid detector, as discussed below.

Both gas and liquid scintillation detectors have low detection efficiency and, therefore, are not used in PET technology. Interaction of radiations with solid scintillation detectors is the basis of radiation detection in PET technology. These solid detectors have the unique property of emitting scintillation or flashes of light after absorbing γ- or X-ray radiations. The light photons are converted to an electrical pulse or signal by a photomultiplier (PM) tube. The pulse is further amplified by a linear amplifier, sorted by a pulse height analyzer (PHA), and then registered as a count. Different types of radiations are detected by different types of detectors. For example, γ-rays or X-rays are detected by sodium iodide crystal containing a trace amount of thallium, NaI(Tl), whereas organic scintillation detectors such as anthracene and plastic fluor are used for β^- particle detection.

G.B. Saha, *Basics of PET Imaging*, DOI 10.1007/978-3-319-16423-6_2

PET is based on the detection of two 511-keV photons in coincidence at 180°. These photons are produced by the annihilation process in which a positron emitted by a positron-emitting radionuclide combines with an electron in the medium and is annihilated. Solid scintillation detectors of different materials have been investigated to detect 511-keV photons. Semiconductor detectors are different kind of solid detectors, which produce electron-hole pairs upon interation with radiations, followed by application of a voltage to produce current. The following is a brief description of the properties and uses of solid detectors in PET imaging.

Solid Scintillation Detectors

Although many scintillation detectors have been investigated, only a few have been widely used in PET technology. The characteristics of different detectors that have application in PET technology are listed in Table 2.1. Note that photon yield from pure detectors is normally poor and so most of them are fabricated with trace amount of a doping element to improve the photon yield. Sodium iodide is doped with a trace amount of thallium (Tl), whereas most others are doped with cerium (Ce). There are

Table 2.1 Properties of different solid scintillation detectors

Detectors	Effective atomic no (Z)	Density (g/cm^3)	Scintillation decay time (ns)	Photon yield (per keV)	Linear attenuation coefficient (cm^{-1}) of 511 keV	Energy resolution (% at 511 keV)
NaI(Tl)	51	3.67	250	38	0.34[a]	7.8
BGO	74	7.13	300	6	0.96	20
BaF_2	54	4.89	0.6	2	0.44	11.4
GSO	59	6.71	50	10	0.67	9.5
Anthracene	–	–	26	30	–	–
LSO	66	7.40	40	29	0.87	10.1
YSO	34	4.53	70	46	0.39	12.5
CsI(Tl)[b]	54	4.51	1000	52	0.483	4.53
LYSO	65	7.2	50	25	0.87	20
YAP	39	5.4	27	18	0.46[c]	2.5
$LaBr_3$	47	5.3	25	61	0.47	5.3

BGO bismuth germanate ($Bi_4Ge_3O_{12}$), *BaF*$_2$ barium fluoride, *LSO* lutetium oxyorthosilicate (Lu_2SiO_5:Ce), *YSO* yttrium oxyorthosilicate (Y_2SiO_5:Ce), *GSO* gadolinium oxyorthosilicate (Gd_2SiO_5:Ce), *LYSO* lutetium yttrium oxyorthosilicate ($LuYSiO_5$:Ce), *YAP* yttrium aluminum perovskite ($YAlO_3$), *LaBr*$_3$ lanthanum bromide ($LaBr_3$:Ce)

[a]The linear attenuation coefficient of 140-keV photons of ^{99m}Tc in NaI(Tl) is 0.155 cm^{-1}

[b]Early P, private communication (2005)

[c]Of 660 keV

several methods of fabrication, but the basic principle is as follows: the detector material and the doping agent in oxide form are mixed in appropriate ratio (e.g., lutetium oxide and cerium oxide) and melted in an iridium crucible, which is heated by a water-cooled induction coil. Crystal growth is initiated on seed crystals which are then pulled out at a controlled rate to form the crystals of desired size.

The choice of a detector is based on several characteristics, namely:

1. Stopping power of the detector for 511-keV photons
2. Scintillation decay time
3. Light output per keV of photon energy
4. Energy resolution of the detector

The stopping power of the detector determines the mean distance the photon travels until complete deposition of its energy and depends on the density and effective atomic number (Z_{eff}) of the detector material. The scintillation decay time arises when a γ-ray interacts with an atom of the detector material, and the atom is excited to a higher energy level, which later decays to the ground state, emitting visible light. Two to sixty light photons are produced per keV of incident energy depending on the type of detector material (Table 2.1). The time of decay is called the scintillation decay time given in nanoseconds (ns) and varies with the material of the detector. The shorter the decay time, the higher the efficiency of the detector at high count rates. A high-light-output detector produces a well-defined pulse resulting in better energy resolution. The intrinsic energy resolution is affected by inhomogeneity in the crystal structure of the detector and random variations in the production of light in it. The energy resolutions at 511 keV in different detectors vary from 2.5 to 20% (Table 2.1), using routine integration time for pulse formation, which runs around a few microseconds. However, in PET imaging, the integration time is a few hundred nanoseconds in order to exclude random coincidences, and the number of photoelectrons collected for a pulse is small, thus degrading the energy resolution. Consequently, the detectors in PET scanners have relatively poorer energy resolution ($\sim$12%) (See later in Table 2.2).

The detection efficiency of a detector is another important property in PET technology. Since it is desirable to have shorter scan times and low tracer activity for administration, the detector must detect as many of the emitted photons as possible. The 511-keV photons interact with detector material by either photoelectric absorption or Compton scattering, as discussed in Chap. 1. Thus, the photons are attenuated (absorbed and scattered) by these two processes in the detector, and the fraction of incident γ-rays that are attenuated is determined by the linear attenuation coefficient (μ) given in Chap. 1 and gives the detection efficiency. At 511 keV, $\mu = 0.92$ cm^{-1} for bismuth germanate (BGO), 0.87 cm^{-1} for lutetium oxyorthosilicate (LSO), and 0.34 cm^{-1} for NaI(Tl) (Melcher 2000). Consequently, to have similar detection efficiency, NaI(Tl) detectors must be more than twice as thick as BGO and LSO detectors.

Sodium iodide: For γ-ray detection, NaI(Tl) detectors are most commonly used, as they provide good light output (30–40 light photons per keV of γ-ray energy)

and energy resolution. They are most widely used in most gamma cameras for planar or single-photon emission computed tomography (SPECT) imaging in nuclear medicine. The NaI(Tl) crystal is hygroscopic and, therefore, hermetically sealed with aluminum foil. It is fragile and needs careful handling. Its major drawback is its poor stopping power, i.e., low density and low linear attenuation coefficient for 511 keV. For this reason, though used in earlier PET scanners, it has not received much appreciation for application in PET technology.

Bismuth germanate: BGO detectors are preferred in some PET cameras because of its highest stopping power (highest density and linear attenuation coefficient). However, it suffers from its longer scintillation decay time (~300 ns) and poor light output. The longer decay time increases the dead time of the detector and limits the count rate that can be detected by the system. The low light output results in poor energy resolution, which is proportional to the square root of the number of scintillation photons and is typically 20% for 511-keV photons. Note that BGO does not contain any doping material.

Lutetium oxyorthosilicate: The three characteristics of cerium-doped LSO, namely, high light output, high stopping power (high-density and large linear attenuation coefficient), and short scintillation decay time (40 ns), have made it a better detector for PET systems. However, owing to its intrinsic property, its energy resolution is poor despite its high light output. A disadvantage of this detector is that it contains a naturally occurring radioisotope of its own, ^{176}Lu, with an abundance of 2.6% and a half-life of 3.8×10^8 years. This radionuclide decays by emission of β^-rays and X-rays of 88–400 keV. However, the activity level is too little to be concerned about radiation exposure from ^{176}Lu, and it does not pose any problem in PET imaging because its photon energy is lower than 511 keV.

Gadolinium oxyorthosilicate: The overall characteristics of cerium-doped gadolinium oxyorthosilicate (GSO) detectors are quite good for application in PET technology. Even though it has lower light output and stopping power than the LSO detector, its better energy resolution has prompted some commercial manufacturers to use this detector in PET technology. Fabrication of GSO detectors requires great care, because the crystals are fragile. GSO detectors collect data faster than other materials and hence are often called “fast crystal.” These detectors can be cut into smaller crystals resulting in improved spatial resolution of the system.

Barium fluoride: Like BGO, BaF_2 too does not contain any doping material. It has the shortest decay time of 0.6 ns and is excellent for time-of-flight scanners. In the past its use was limited due to lack of fast computers. With the introduction of fast electronics and computers, they have been used by some investigators for a limited number of clinical studies.

Lutetium yttrium oxyorthosilicate: A somewhat new detector, yttrium-activated lutetium oxyorthosilicate (LYSO), has the physical properties similar to LSO and has been used in PET scanners by a commercial vendor. Its energy resolution is better than LSO’s.

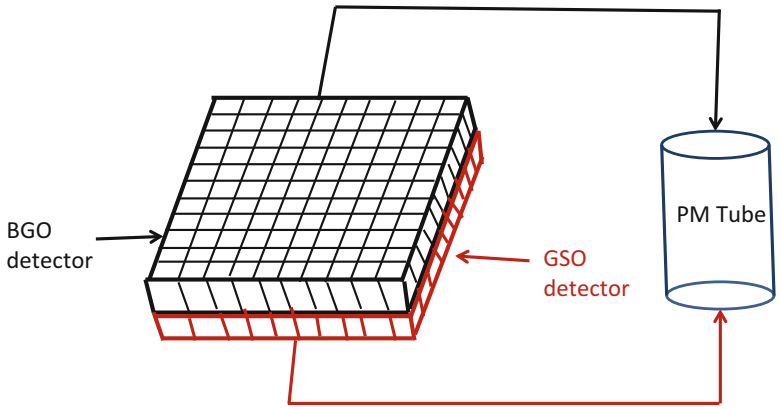

Fig. 2.1 Schematic illustration of phoswich, which is made of two layers of detectors (e.g., BGO and GSO) with different properties

Yttrium oxyorthosilicate: Cerium-doped yttrium oxyorthosilicate (YSO) is a new type of detector, but no commercial manufacturer has yet used it in PET technology.

Lanthanum bromide: Lanthanum bromide (Ce) crystals have high density and hence high stopping power to provide high photon yield upon photon interaction. Also its scintillation decay time is reasonably short (25 ns) to give better energy resolution. All these characteristics make it a potentially good detector for PET scanners. However, there are challenges to its commercial use in PET technology, because it is quite fragile and so difficult to produce large crystals. Furthermore, it is hygroscopic and needs to be hermetically sealed.

Phoswich: For the purpose of increasing spatial resolution in tomographic imaging, two scintillation detectors of different decay times are optically coupled in layers to form a single dual-layered detector, which is connected to a common PM tube (Fig. 2.1). GSO and BGO detectors and NaI(Tl) and LSO detectors have been coupled in this manner for high-resolution scanners. The location of photon interaction is determined from the difference in decay of the pulses from the two detectors, which eliminates the uncertainty in the depth of interaction of the photon thus improving the spatial resolution in images. These detectors can be used in both SPECT and PET scanning by switching between the two detectors.

Semiconductor Detectors

Pure silicon and germanium are semiconductor elements that have been used for photon detection. When a γ-ray strikes these elements, an electron is ejected from the atomic orbital and a positively charged hole is created. If a voltage is applied

between two electrodes placed in the material, the electron–hole pair will move to the respective electrodes producing a current.

The conductivity of pure metals is poor and adding some impurities or dopants (which are typically elements of low atomic number) to them greatly increases the number of electron–hole pairs in the semiconductor material whereby conductivity is enhanced. When dopants such as boron are added to silicon, doped silicon contains mostly free holes and is called "*p*-type" semiconductor. Similarly, "*n*-type" semiconductor possessing more free electrons is obtained by adding dopant like phosphorus to silicon. When these two types of semiconductors are joined together, a unique semiconductor called the PN diode is formed. Since holes and electrons move freely, those at the junction neutralize their charges creating what is called the *depletion* zone and further free flow of electrons and positive holes across the depletion zone is restricted. When an external voltage is applied connecting the positive polarity to the *p*-type side and the negative polarity to the *n*-type side, electron–hole pairs are created and current flows freely and the voltage is called *forward bias*. When the polarity is reversed, electron–hole pairs are drawn away from the depletion zone and no current flows rendering it a sort of resistor. The voltage is called the reverse voltage.

When radiations of sufficient energy strike the PN diode, they create electron–hole pairs in depletion zone. If a voltage of sufficient energy is applied, holes and electrons move to the respective electrodes creating a current that is proportional to the radiation energy deposited in the detector. PN diodes can serve as photodetectors and research is continuing to employ them in preclinical PET imaging, which hopefully will find use in routine clinical studies.

A variation of PN diode is a PIN diode in which a layer of intrinsic material without any dopant is placed at the *p*–*n* junction between the two semiconductors (Fig. 2.2). This increases the depletion region and if a forward bias voltage is applied to the diode, the electron–hole pairs enter the depletion region (including the intrinsic region) and as the two carrier types meet, current starts to flow. Because of the increase in the depletion region with the addition of intrinsic

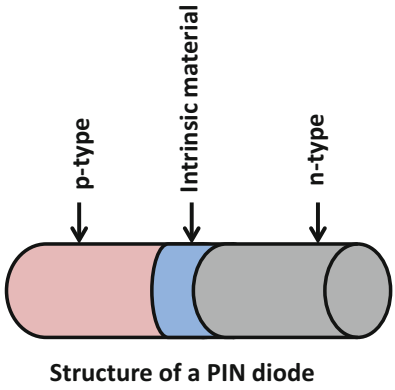

Fig. 2.2 Illustration of the structure of a PIN diode

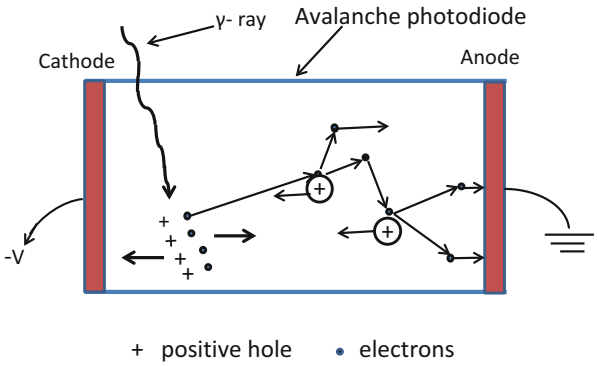

Fig. 2.3 The signal (gain of 1) is formed by the migration of electron–hole pair created by interaction of radiation with semiconductor material and significantly weaker than the PM tube signal (gain of 10^6–10^7). If, however, a reverse bias voltage of sufficient magnitude (200–2000 V) is applied, then the free electron accelerates in the material and can knock out an electron from an atomic orbital creating a second electron–hole pair and the process continues to create an avalanche phenomenon with signal gain of almost 100–1000. Such detectors are called avalanche photodiode (APD)

material and concomitant increase in volume in which light conversion occurs, the performance of the PIN diode in photon detection is much improved.

Because semiconductors are low *Z* material, their stopping power is low. Also, unlike other scintillation detectors, there is no PM tube multiplication (see later) as there is no light photon produced in the semiconductor material, so the signal (gain of 1) is significantly weaker than the PM tube signal (gain of 10^6–10^7). If, however, a reverse bias voltage of sufficient magnitude (200–2000 V) is applied, then the free electron accelerates in the material and can knock out an electron from an atomic orbital creating a second electron–hole pair and the process continues to create an avalanche phenomenon with signal gain of almost 100–1000. These detectors are called avalanche photodiodes (APDs) (Fig. 2.3) and can be produced in a single package or an array.

The APDs have been used in PET/MR scanners (see later), because PET signals from APDs are not affected by the magnetic field. A different variety of APDs are position-sensitive planar APDs (PS-APDs) which use signals from the four corners of the detector to ascertain the location of an event. However, PS-APDs suffer from worse noise. A newer APD is Geiger-mode APD or silicon photomultiplier (SiPM), which is made by connecting a series of micro-APD cells connected to bias voltage via individual resistor in the surrounding silicon. As in a Geiger detector, when photon interacts in the cell, it discharges and then is quenched through the resistor producing a single pulse. When SiPM is coupled to a scintillator, a large number of light photons produced by interaction of radiations from a source strike as many micro-APD cells. This produces an output pulse (gain of 10^5–10^7) as large as in conventional PM tubes. Research is continuing to improve this device.

Another category of semiconductor detectors like cadmium–zinc–tellurium (CZT) and cadmium–tellurium (CdTe) has relatively high stopping power and excellent energy resolution (~5%) and have potential for use in PET scanners. These detectors are fabricated by combining melted Cd and Te (and zinc for CZT) and heating until CdTe or CZT crystals are produced. Sometimes chlorine or indium is added as doping agent to improve the conductivity of detectors thus enhancing the spatial resolution and sensitivity. Although these detectors have been used in SPECT cameras, their use in PET camera is limited due to difficulty in fabricating larger crystals and poor timing performance. However, they are useful for small-animal PET scanner using small crystals providing good resolution of several millimeters. Shiga et al. (2009) made a comparative study between a PET scanner with CdTe detector and one with BGO detector and found better detectability with the former because of high spatial resolution and low scatter noise.

Photomultiplier Tube

As discussed briefly earlier, a PM tube is needed to convert the light photons produced in the detector by γ-ray interaction in the detector to an electrical pulse. The PM tube is a vacuum glass tube containing a photocathode at one end, ten dynodes in the middle, and an anode at the other end, as shown in Fig. 2.4.

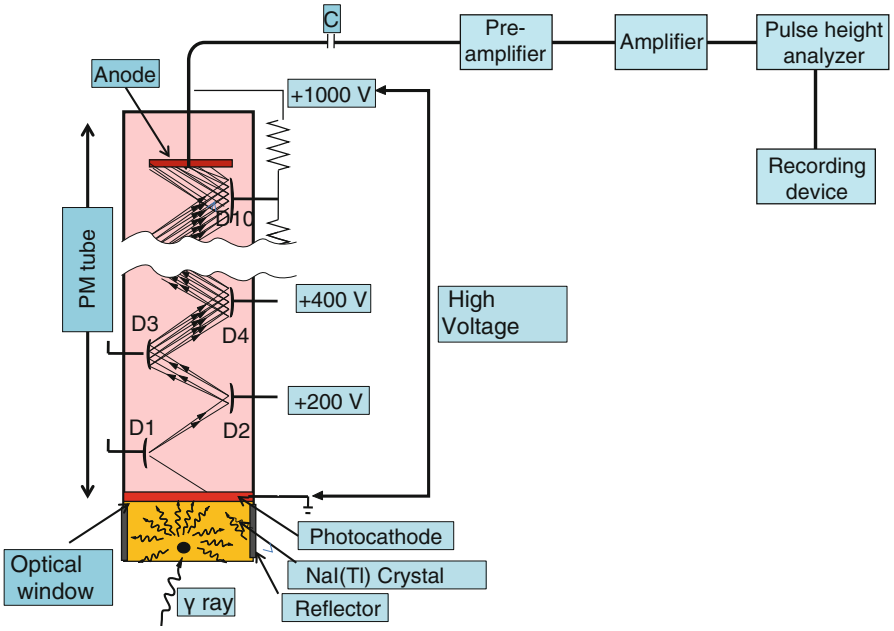

Fig. 2.4 A photomultiplier tube showing the photocathode at one end, several dynodes inside, and an anode at the other end

The photocathode is usually an alloy of cesium and antimony that releases electrons after absorption of light photons. The PM tube is fixed onto the detector by optical grease or optical light pipes.

A high voltage of ~1000 V is applied between the photocathode and the anode, with about 100-V increments between the dynodes. When light photons from the detector strike the photocathode of the PM tube, electrons are emitted, which are accelerated toward the next closest dynode by the voltage difference between the dynodes. Approximately 1–3 electrons are emitted per 7–10 light photons. Each of these electrons is again accelerated toward the next dynode and then more electrons are emitted. The process of multiplication continues until the last dynode is reached and a pulse of electrons is produced, which is attracted toward the anode. The pulse is then delivered to the preamplifier. Next, it is amplified by an amplifier to a detectable pulse, which is then analyzed for its size by the PHA, and finally delivered to a recorder or computer for storage or to a monitor for display. PM tubes are sturdy and expensive and provide fast and strong output pulse.

Pulse Height Analyzer

A PHA is a device that sorts out photons of different energies emitted by photons of the same or different radionuclides or from the scattered photons. Functionally, a PHA is a discriminator with a lower-level and an upper-level setting or with a baseline and a window above the baseline. In either setting, photons of selected energy only are accepted and others are rejected. This type of pulse sorting is essential in nuclear medicine imaging to count mainly unscattered photons that come out of the organ of interest for image formation. The narrower the window of the PHA, the more accurate is the energy discrimination of photons from the sample, but the detection efficiency is reduced. In the case of PET systems, the window of the PHA is centered on 511 keV, with a width of 350–650 keV.

Arrangement of Detectors

In the earlier designs of PET cameras, each detector (normally BGO) was glued to a single PM tube, and a large array of such detectors were arranged in multiple circular rings around the object of imaging. The axial field of view (FOV) is defined by the width of the array of the rings, and the number of detectors per ring varies with the manufacturers. The total number of detectors ranges in thousands, depending on the manufacturer. The larger the number of detectors and hence the more PM tubes per ring, the better the spatial resolution of the system. Although such systems provide good resolution, the cost of using many PM tubes is high, and packaging of a large number of detectors with PM tubes becomes impractical.

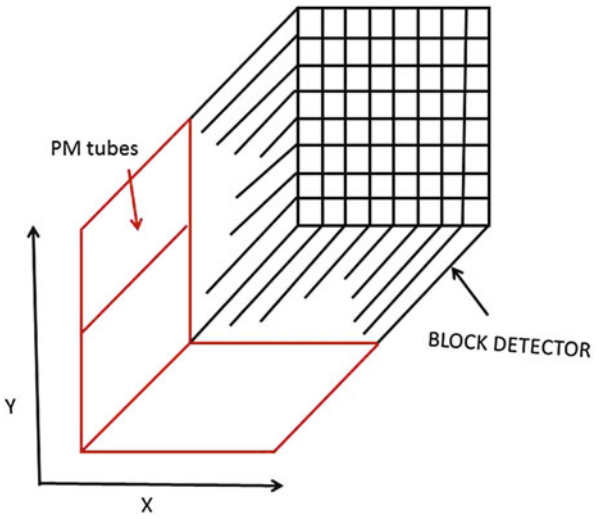

Fig. 2.5 A schematic block detector is segmented into 8×8 elements, and four PM tubes are coupled to the block for pulse formation

In current PET scanners, the *block detectors* are used, in which small detectors are created by partially cutting a large block of detector material and then are attached to a smaller number of PM tubes. Round or square PM tubes of 1–5 cm dimension are commonly used in PET scanners. A schematic block detector is shown in Fig. 2.5. Typically, a block detector of dimension $4 \times 4 \times 3$ cm is grooved into an array of 6×8, 7×8 or 8×8 elements by making partial cuts through the crystal with a saw. The cuts are made at varying depths, with the deepest cut at the edge of the block. The grooves between the elements are filled with an opaque reflective material that prevents optical spillover between elements. Such uneven cutting results in linear sharing of light among PM tubes so that light from photon interaction in the corner element with deep cut will be detected by the PM tube located under that element, whereas the light from the middle interaction will be shared by all PM tubes. The width of the detector elements, among other factors, determines the spatial resolution of the imaging device and is normally 4–5 mm in modern PET scanners (see Chap. 6) The entire block detector is attached to several PM tubes (normally four PM tubes) in the same fashion as in scintillation cameras. BGO block detectors can use up to 16 detector elements per PM tube, whereas LSO block detectors use up to 144 detector elements because of higher intensity of scintillation emission. The detector elements are packed in 3–6 rings in a block. A typical commercial block detector is shown in Fig. 2.6. A PET scanner can contain many block detectors, the number of which varies with the manufacturer. The block detectors are arranged in arrays in full rings or partial rings in different configurations discussed later. The number of rings varies from 18 to 52 depending on the manufacturer. The block detector design has the advantage of reduced dead time compared with those of the scintillation cameras because of the restricted light spread in the former.

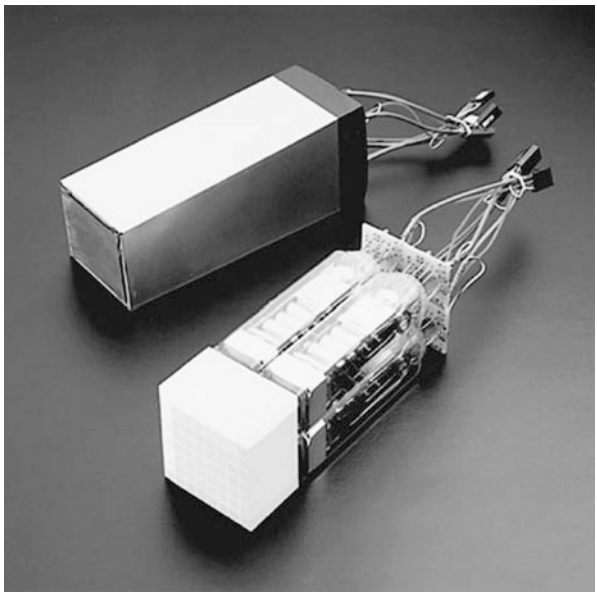

Fig. 2.6 A typical commercial block detector (8×8) attached to four square PM tubes (*bottom*) and a packaged module (*top*), developed and manufactured by Siemens Medical Solutions USA (Courtesy of CPS Innovations, Knoxville, TN, USA, currently Siemens Medical Solutions USA, Inc.)

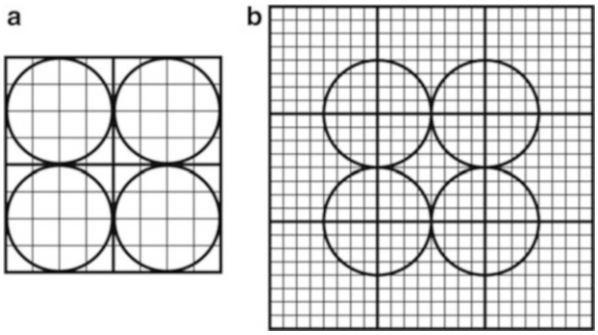

Fig. 2.7 Block detector illustrating the quadrant sharing of PM tubes. (**a**) PM tubes assigned in four quadrants separately. (**b**) Each PM tube shares four quadrants of four block detectors and improves the spatial resolution (Reprinted with the permission of the Cleveland Clinic Center for Medical Art and Photography © 2009. All rights reserved)

A modification of the basic block detector has been made such that each PM tube straddles over four quadrants of four different blocks (Fig. 2.7). The technique of quadrant sharing permits the use of larger PM tubes and reduces the total number of PM tubes used in the PET system. This design improves the spatial resolution relative to the basic design but has the disadvantage of increasing the dead time.

In PET scanners with block detectors, each detector pair is not connected by coincidence circuitry for practical difficulty, so the detectors are grouped together

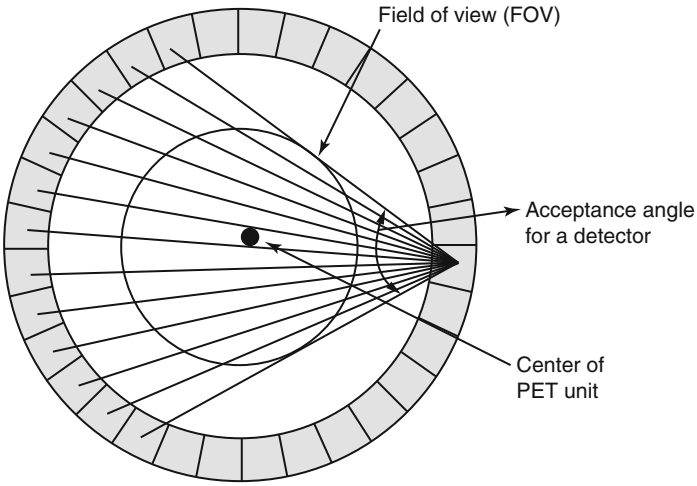

Fig. 2.8 The transverse field of view determined by the acceptance angles of individual detectors in a PET scanner. Each detector is connected in coincidence with as many as half the total number of detectors in a ring, and the data for each detector are acquired in a "fan-beam" projection. All possible fan-beam acquisitions are made for all detectors, which define the FOV as shown in the figure (Reprinted with the permission of the Cleveland Clinic Center for Medical Art and Photography © 2009. All rights reserved)

into banks or sets, which are then connected in coincidence opposite to each other. Essentially each detector in a set is connected by a coincidence circuit with a time window (see next section) to a set of opposite detectors (both in plane and axial). If there are N detectors in a ring, typically each detector can be connected in coincidence with $N/2$ detectors on the opposite side, and, therefore, $N/2$ "fan-beam" projections are available for each detector (Fig. 2.8). These fan-beam projections form for each detector an *angle of acceptance* in the transaxial plane, and these angles of acceptance for all detectors in the ring form the transaxial *field of view (FOV)*. The larger the number of detectors (up to $N/2$) are in multicoincidence with each detector, the larger will be the angle of acceptance and hence the larger transaxial FOV for the PET system.

Coincidence Timing Window

In PET imaging, ideally the two 511-keV annihilation photons should be detected and processed to form coincidence pulses by the detector pair at the same time. In reality, however, a pulse from one photon may be formed in one detector slightly earlier or later than the pulse from the other photon in the opposite detector. This uncertainty in time in coincident counting of the two annihilation photons is called the *coincidence timing window* or *timing resolution* of the PET camera. This timing

resolution results from the statistical variation in light formation in the detector, scintillation decay time of the detector, and fluctuation in gain in PM tube during pulse formation. Also, the difference in distances traveled by the two photons results in delay in their arrival, particularly if the annihilation occurs at the edge of the FOV. For a whole-body scanner with a diameter of 1 m, the maximum distance traveled by one photon can be as large as 1 m, and the other photon travels almost no distance, if the annihilation occurs at the edge. Because the velocity of light is 3×10^8 m/s, the difference in arrival times of the two photons is about 3 ns (time to travel 1 m), which also adds to the delay in pulse formation. All these factors in combination require a time period τ to generate an appropriate pulse to be detected and counted and thus set the minimum limit of the timing window of a PET scanner.

After annihilation of a positron, each 511-keV photon strikes each of the detector pair, and two pulses are produced and further processed by the amplifier, the PHA, and a logic circuit for detection in coincidence. These processes require a definite time period to produce two signals, say, A and B, with a finite time width τ. The value of τ depends on the type of a PET scanner. These time signals are then fed into a coincidence circuitry for analysis of their arrival. Signal B may arrive just τ ahead of (Fig. 2.9a) or τ behind (Fig. 2.9b) the arrival of signal A. As can be seen, they are just touching each other. In these two extreme cases where there is no overlap of the two signals, they will be considered in coincidence and counted as a count. These two scenarios define the minimum limit of coincidence timing window or timing resolution, which is 2τ, twice the width of the time signals. All other coincidence events overlapping within the timing resolution will be counted as coincidence counts (Fig. 2.9c). To include all valid coincident events and not to miss any, the timing window is normally increased more than the minimum limit mentioned above for a given scanner (6–18 ns). The type of detector material influences the value of timing window due to variation in scintillation decay time and light production by photon interaction in the detector. For example, LSO-based PET cameras use a typical timing window of 2–4 ns, whereas a value of 6–12 ns is used in BGO-based cameras. The choice of timing window is very important. If it is too small, many true coincidences will be missed, whereas if it is too large, more random coincidences will be counted.

PET Scanner

PET cameras are horizontally positioned cylinder-shaped units with a cylindrical bore of diameter 80–90 cm along the length and weighing several thousand pounds or kilograms. The critical component of the camera is the block detectors or planar detectors that are arranged in full or partial ring or planar form inside the bore. The detection efficiency is low with a single ring and so several rings or planar detectors are stacked next to each other along the horizontal length of the camera to improve the detection efficiency. The full-ring geometry is realized in a circular or

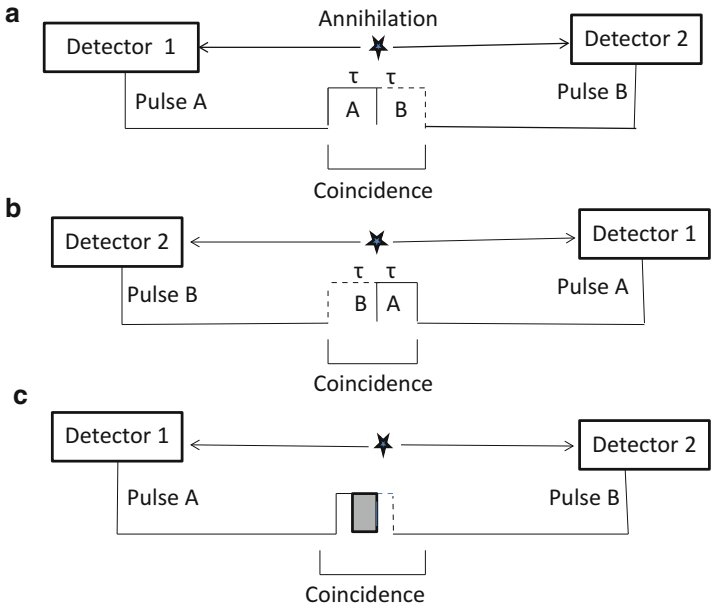

Fig. 2.9 Illustration of coincidence timing window. After positron annihilation, two 511-keV photons strike the two opposite detectors 1 and 2, and two pulses A and B of time width τ are produced after amplification and pulse height analysis. Three scenarios can occur for coincidence counting. (**a**) Pulse B (*dashed line*) just arrives at the coincidence circuit just after the arrival of Pulse A (*solid line*) overlapping only at the edge of the two pulses and they will be counted as a coincidence event. (**b**) Pulse B arrives at coincidence circuit exactly prior to arrival of Pulse A just overlapping at the edge of the two pulses and two events are counted in coincidence. (**c**) Pulses A and B may arrive at coincidence circuit such that both overlap partially or completely depending on their time of arrival resulting in a coincidence event. In order to avoid missing any coincidence event, the minimum time window for coincidence circuit must be 2τ

hexagonal array with either block detectors or large-area planar detectors with built-in position-locating capability. The width of the ring stack or the planar detectors defines the axial FOV and is normally more than 15 cm. The vertical circular plane of the ring perpendicular to the axis of the PET camera defines the transaxial or transverse FOV. Several earlier PET cameras used partial rings of opposite block detectors, and data had to be collected by rotating the rings to fulfill the scanning of the gap areas and also improve the detection efficiency. Three configurations of detectors used by different vendors are shown in Fig. 2.10. Since PET cameras are axially fixed, they are equipped with a computer-controlled horizontal bed for patients to lie on for scanning. The bed along with a patient can be moved to different positions along the axial field in the bore for scanning an organ or a body segment of the patient. The scan length of typical PET cameras varies from 170 to 198 cm depending on the manufacturers. Since this is less than the whole-body length of a typical adult patient, continuous sections of the body are sequentially scanned, which are then adjoined by a software program to give a

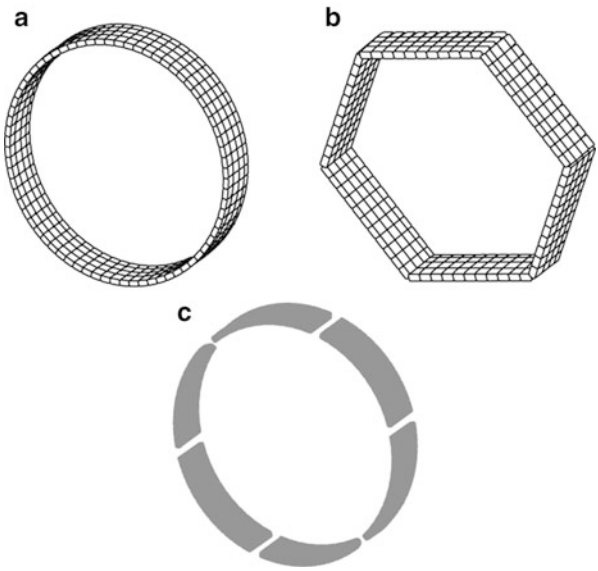

Fig. 2.10 Different configurations of PET scanners. (**a**) A circular full-ring scanner. (**b**) Hexagonal array of quadrant-sharing panel detectors. (**c**) Continuous detectors using curve plates of NaI (Tl) (Reprinted with the permission of the Cleveland Clinic Center for Medical Art and Photography © 2009. All rights reserved)

whole-body image. With the introduction of PET/CT scanners, many manufacturers have shied away from making dedicated PET cameras. However, to have a sense of stand-alone PET cameras, the different features of some earlier PET cameras are given in Table 2.2. Note that some of the features match those of the PET cameras of current PET/CT or PET/MR scanners (see later).

Scintillation Camera for PET Imaging

Conventional scintillation cameras using NaI(Tl) detectors are available in dual-head and triple-head designs to perform planar and SPECT imaging. To utilize them as PET systems, the heads of these cameras are connected with a coincidence circuitry. The coincidence time window is typically set at ~12 ns for dual-head and ~10 ns for triple-head cameras. Data are acquired by rotating the heads without the collimator around the subject. These units are capable of switching between PET and SPECT modes, of course, using the collimator in the latter mode. These scanners are attractive to the community hospitals because of the relatively low cost while providing the scope for PET imaging.

A disadvantage of the coincidence scintillation cameras is that they have low sensitivity due to low detection efficiency of NaI(Tl) crystals for 511-keV photons, which results in a longer acquisition time. To improve the sensitivity, thicker detectors of sizes 1.6–2.5 cm have been used in some cameras, but even then, coincidence photopeak efficiency is only 3–4%. This increase in crystal thickness,

Table 2.2 Features of different PET scanners

Manufacturers→[a]	Philips[b]		Siemens[c]		GE Healthcare[c]	
Models→ Features↓	GEMINI TF Big Bore	GEMINI TF 64 (PET/CT)	Biograph mCT	Biograph TruePoint	Discovery VCT	Discovery PET/CT 600
Number of detectors	28 pixelar modules	28 pixelar modules	192	192	24 rings	24 rings
Number of crystals	28,336	28,336	24,336	24,336	13,440	12,288
			32,448 (TrueV)	32,448 (TrueV)		
Detector material	LYSO	LYSO	LSO	LSO	BGO	BGO
Ring diameter (cm)	90	90	84.2	83	88.6	81
Patient scan range (cm)	190	190	190	190	160	170
Crystal size (mm)	$4 \times 4 \times 22$	$4 \times 4 \times 22$	$4 \times 4 \times 20$	$4 \times 4 \times 20$	$4.7 \times 6.3 \times 30$	$4.7 \times 6.3 \times 30$
Number of PMTs	420	420	4/block	4/block	280	256
Energy resolution (%)	12%	11.7%	12%	12%	–	–
Coincidence window (ns)	5	3.8	4.1	4.5	10	10
Axial FOV (cm)	18	18	16.2/21.6	16.2/21.6	15.7	15.7
Acquisition mode	3D, 4D, TOF	3D, 4D, TOF	3D	3D	D, 3D, 4D	3D, 4D

[a]Reprinted with permission, Copyright 2009, ECRI institute, http://www.ecri.org, 5200 Butler Pike, Plymouth Meeting, PA 19462, USA. 610-825-6000
[b]Data supplied by Philips Healthcare, USA
[c]Reprinted with permission, Copyright 2009, Imaging Technology News (http://www.itonline.net), Scranton Gillette Communications (http://www.scrantongillete.com) 3030 w. Salt Creek Lane, Suite 201, Arlington Heights, IL 60005-5025, USA. Some of Siemens data were provided by Annemarie Grammens, Siemens Medical Solutions, USA

however, compromises the spatial resolution of the system in SPECT mode. Fast electronics and pulse shaping are implemented in modern systems to improve the sensitivity. Also, there is a significant camera dead time and pulse pileups due to relatively increased single count rates in the absence of a collimator in PET mode. Low coincidence count rates due to low detection efficiency of NaI(Tl) detectors for 511-keV photons cause higher background noise that results in low contrast in the reconstructed image with these scanners, compared to dedicated PET scanners. The overall spatial resolution of the dual-head coincidence cameras is poorer than that of the PET scanners.

PET/CT Scanner

In the interpretation of nuclear medicine studies, physicians always prefer to have a comparison between high-resolution anatomical CT or MR images and low-resolution functional PET or SPECT images of a patient for precise localization of lesions. It is very useful to compare the images before and after therapy to assess the effectiveness of treatment. To this end, efforts are made to coregister these two sets of digital images. In coregistration, the matrix size, voxel intensity, and the rotation are adjusted to establish a one-to-one spatial correspondence between the two images. This process is called the coregistration or fusion of images. Several techniques are employed in alignment of images of different modalities, among which the following three are common: in the manual method, the contour of the two sets of images is traced and then the images are aligned; second, in the landmark technique, an external point marker that can be seen on both images is attached to the patient, or an internal marker such as a structure in an organ that is common to both images is chosen; third, in the fully automated method, surfaces or boundaries between organs are chosen by algorithms to define the images for alignment. This technique is useful for rigid body organs such as the brain, whereas it is likely to cause noises and hence errors in registration of the nonrigid, moving organs, such as the heart, abdomen, etc. Another important method of image alignment based on voxel intensities of the two images uses the difference in intensities or the standard deviations of the ratios of image intensities (voxel-by-voxel basis) for proper alignment of the two images. After alignment, the source image or each discrete point in the source image is transformed to the coordinate system of the target image (e.g., CT images transformed to PET images). This is done on a voxel-by-voxel basis. In all cases, algorithms have been developed and employed to achieve coregistration of images of different modalities. Most software is vendor neutral and supports fusion of any combination of functional and anatomical images of different modalities. Some of the common software are Siemens Medical Solutions' Syngo FusionD and TrueD, Philips Healthcare's Syntegra, GE Healthcare's Volemetrix, MIM Vista's MIM, Cedara's PET/CT Workstation, Thinking Systems' MDStation Thin-Client Web Server/Client, and Hermes Medical Solutions' Hermes Workstation.

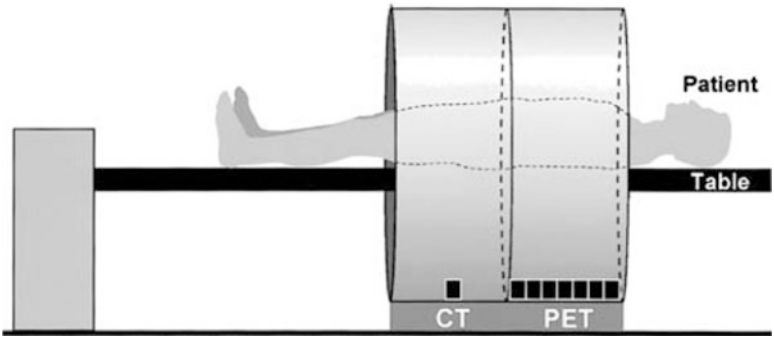

Fig. 2.11 A schematic illustration of a PET/CT system (Reprinted with the permission of the Cleveland Clinic Center for Medical Art and Photography © 2009. All rights reserved)

The coregistered images are displayed side by side with a linked cursor indicating spatial correspondence or may be overlaid or fused using the grayscale or color display. The spatial correspondence by coregistration between the images of two modalities obtained at separate imaging sessions suffers from positional variations of the patient scanned on different equipment and at different times. In addition, patient motion, including involuntary movement of the internal organs, adds to the uncertainty in the coregistration. Even with the most sophisticated algorithm, an error of 2–3 mm in alignment is not uncommon.

To circumvent the problems of positional variations in coregistration of images from different equipment, an integrated system of PET and CT units has been developed by several manufacturers. Similar systems of SPECT/CT and PET/MRI are also available commercially. In a PET/CT system (Fig. 2.11), both units are mounted on a common support with the CT unit in the front and the PET unit in the back next to the CT unit. Both units use the same gantry and a common imaging table. The centers of the scan fields of PET and CT scanners are separated by a fixed distance called the displacement distance. The axial travel range of the scanning table varies from 170 to 200 cm depending on the manufacturers. Because of the displacement between the centers of scan fields of the two systems, the actual scan field is limited by the maximum distance given by the travel range of the table minus the displacement distance.

The CT unit used in the PET/CT system comprises an X-ray producing unit that consists of a cathode filament that emits electrons when a high voltage (kV) is applied to it and a rotating tungsten anode. Electrons from the cathode are focused to impinge on the rotating anode, whereby an intense beam of bremsstrahlung and characteristic *K* X-rays is produced. In a CT scan, the unit transmits a focused beam of X-rays through a patient's body and the transmitted beam is detected by solid detectors composed of materials such as ceramics, gadolinium oxysulfide, gemstone, etc. These detectors emit visible light upon interaction with X-rays, which are processed by the photodiode to produce signal for detection. In some scanners, xenon gas detectors are used in which gas is ionized by X-rays producing current

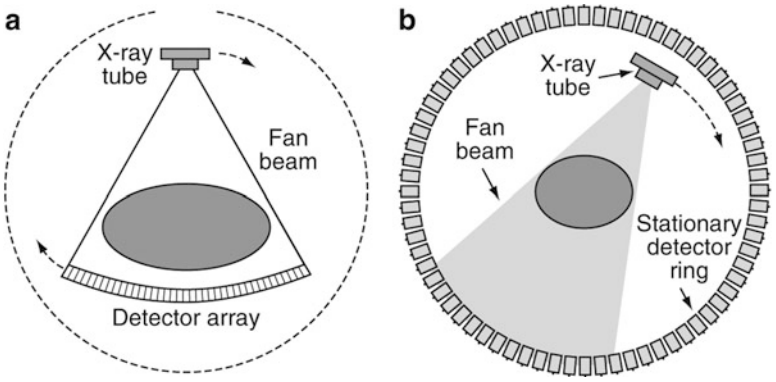

Fig. 2.12 (**a**) A large array of detectors in an arc form are rigidly connected to an X-ray tube. Both rotate around the object at the same speed with the tube transmitting the X-ray beam in a fan-beam projection defined by the arc and the detectors detect the attenuated beam on the opposite side of the object. This configuration is most commonly used. (**b**) Detectors are arranged in a fixed ring and the X-ray tube rotates inside the circular path of the ring (Reprinted with the permission of the Cleveland Clinic Center for Medical Art and Photography © 2009. All rights reserved)

for measurement. The kilovolt (kV) in CT units varies from 100 to 140 kV, and the maximum X-ray energy ranges from 100 to 140 keV. Depending on the design and the manufacturer, a large number of detectors (thousand) are arranged in an arc form or a full ring around the patient. In the arc form, the X-ray tube and the detector arc are mechanically tied in 180° opposition and rotate together inside the gantry during the study (Fig. 2.12a). In full-ring geometry, the detectors are arranged in a fixed 360° ring around the patient, while the X-ray tube only rotates (Fig. 2.12b). In either case, the X-ray tube projects the X-ray beam through the patient's body while rotating fast around the patient, and the detectors opposite to the X-ray tube detect the transmitted photons, which are stored as counts in the computer. The data are then processed to form a CT transmission image (slice). For scanning the entire body length, the scanning table with the patient has to be translated axially after each slice is acquired. The CT scanner can be single slice or multislice collecting data simultaneously for many slices (6, 16, 32, 64, or 128) with the different rotation speeds. In *helical* or *spiral* CT units, the patient table translates or moves while the X-ray tube rotates around the patient during the study. This results in a helical or spiral pattern of the motion of the X-ray tube around the patient, hence the name. The entire time for a conventional CT transmission scan is only a minute at most, and it is much shorter for the helical CT.

When the incident X-ray beam passes through the patient's body, it is attenuated by the tissue. The attenuation of the X-ray beam depends on the density of the body tissue of the patient, giving structural information of different organs. Conventional single-energy CT units provide images of individual organs with different intensities due to differences in attenuation of photons in tissues. These images are obscured by the shadow of adjacent organs or tissues. To have a clear image of an organ of interest, two separate images of the subject are obtained at two different X-ray

energies, and shadow intensity is removed from the intended image by coregistration using software manipulation. A typical example is detection and display of blood vessels and bones in clear contrast to one another. To avoid the difficulty and the inconvenience of two separate CT studies, currently two X-ray tubes operating at separate energies (e.g., 80 and 140 keV) are installed in the same CT unit (e.g., Siemens Somatom), which simultaneously revolve around the patient and collect transmission data. Alternatively, a single X-ray unit is installed (GE Healthcare's Lightspeed) that can be switched between energies and takes two energy images in a fraction of a second. Images at two energies are then processed by coregistration software to separate the tissues of different densities, and the tissue image with shadowing intensity can be removed resulting in clear images of the organ of interest. Dual-energy CTs reduce the scan time and provide high-contrast images and at the same time reduce radiation exposure if contrast agents are used.

An important advantage of a CT transmission scan in the PET/CT system is that the scan data can be used for attenuation correction of PET emission images, obviating the need for a separate lengthy transmission scan in the dedicated PET system. The use of CT scans for attenuation correction reduces the whole-body scan time significantly. CT attenuation correction and fusion of CT and PET images are discussed in detail in Chap. 3.

Prior to the introduction of PET/CT, multimodality images were fused by the algorithm technique that was limited mainly to the brain. In 1999, GE Healthcare introduced the first PET/CT, called the Hawkeye, using a dual-head NaI(Tl) camera and a low-energy CT scanner, followed later in 2001 by the Discovery LS (GE Healthcare). Since then, manufacturers such as Siemens, GE, and Philips have brought a variety of much improved PET/CT units into the market. The physical features of a few current PET/CT scanners are listed in Table 2.3 and a typical commercial PET/CT scanner is shown in Fig. 2.13.

Table 2.3 Specifications of PET/CT scanners from three manufacturers[a]

Company name	GE Healthcare	Philips Healthcare	Siemens Healthcare
Model product name	Optima PET-CT 560	Ingenuity TF	Biograph mCT Flow
Gantry dimensions, $H \times W \times D$, cm	193 × 225 × 146	213 × 225 × 549	204 × 234 × 136
Weight, kg (lb)	4916 (10,834)	4201 (9262)	3980 (8755), w TrueV
Patient port, cm	70	70	78
Attenuation corr.	CT	CT	CT
Vertical travel, cm	2.5–20.5 below isocenter	35.5	53–96
Patient scan range, cm	Standard, 170; option, 200	190	195, w TrueV and Flow Motion
Maximum patient weight, kg (lb)	226 (500)	195 (430)	227 (500)

(continued)

Table 2.3 (continued)

Company name	GE Healthcare	Philips Healthcare	Siemens Healthcare
Acquisition modes	3D, 4D	3D, 4D TOF (respiratory gating)	Static multi-bed, list mode, continuous bed motion
Reconstruction time, 3D mode, 128 × 128, Fore-IT-WLS	45 s frame	<1 min bed w list mode TOF, concurrent	<1 min. per bed
Simultaneous acquisition processing (yes/no)	Yes	Yes	Yes
Attenuation-weighted iterative reconstruction	Yes	Yes	Yes
Number of detectors	24	28 pixelar modules	192 with TrueV
Number of image planes	47	45 or 90	109 with TrueV
Plane spacing, mm	3.27	2 or 4	2
Number of crystals	12,288	28,336	32,448, with TrueV
Ring diameter, cm	88.6	90	84.2
Number of PMTs	1024 (256 quad anode)	420	4 per block
Physical axial FOV, cm	15.7	18	16.2 (standard); 21.6 wTrueV (optional)
Effective axial FOV in whole body, cm—3-D	12.1	NS	21.6 wTrueV and Flow Motion
Detector material	BGO	LYSO	LSO
Crystal size, mm	4.7 × 6.3 × 30	4 × 4	4 × 4 × 20
System sensitivity—3D, kcps/uCi/cc LLD (NEMA 2001)	6.5 cpskBq	19,000 @10 cm with TOF	9.5 435 keV wTrueV
Transverse resolution @ 1 cm, mm (NEMA 2001)	NEMA performance standards, 5.0 mm Vue Point HD, 4.0 mm	4.7	4.4
Transverse resolution @ 10 cm, mm (NEMA 2001)	NEMA performance standards, 5.6 mm Vue Point HD, 4.5 mm	5.2	4.9
Axial resolution @ 1 cm, mm (NEMA 2001)	NEMA performance standards, 5.6 mm Vue Point HD, 5.0 mm	4.7	4.5
Axial resolution @ 10 cm, mm (NEMA 2001)	NEMA performance standards, 6.3 mm Vue Point HD, 5.0 mm	5.2	5.9
Peak noise equivalent count rate, kcps (NEMA 2001)	54 @15 kBq/mL	320 @19 kBq/mL w TOF	NS
Scatter fraction—3D (NEMA 2001)	38%	30%	<34%

(continued)

Table 2.3 (continued)

Company name	GE Healthcare	Philips Healthcare	Siemens Healthcare
Type of detector in CT	Volara DAS	Solid state—GOS	UltraFast Ceramic
Number of elements/ channels fan beam	21,888	43,008 (86,016 effective)	64, 40, or 20 channels, 736 elements row
Gantry dimensions, cm	193 × 225 × 146	Integrated, see above	204 × 234 × 136
CTDI (dose 100 mAs) B 16 cm phant	Axial head, 18.4 mGy, axial body, 9.3 mGy	12.9 mGy 100 mAs	20, 40, 64 slice, 9.6 @100 kV
Standard HC resolution (2% MTF)	8.5 lpcm @0% MTF	13.0 lpcm (at cutoff)	22 lpcm
Scan field, cm	50	Up to 70	78
Number of slices	8 or 16	64 or 128	20, 40, 64
Slice thickness, mm	8 slice, 1.25; 16 slice, 0.62	0.5–12.5	0.4–10 (40 64 slices), 0.6–10 (20 slices)
Topogram length, mm	1700 or 2000	1900	128–2200
DICOM 3.0 PET	Yes	Yes	Yes
DICOM 3.0 CT	Yes	Yes	Yes

[a]Reprinted with permission from the May 2014 issue of *Imaging Technology News (ITN)*, Scranton Gillette Communications. All rights reserved

Fig. 2.13 Siemens Biograph mCT Flow scanner (Copyright Siemens Healthcare 2014. Reprinted with permission)

PET/MR Scanner

In recent years, PET/MR has generated considerable interest as an imaging modality alternative to PET/CT. The primary advantages of PET/MR imaging are that magnetic resonance imaging (MRI) has better soft tissue contrast than CT and also unlike CT, it does not involve any radiation dose to the patient. The following is a concise description of different aspects of MR imaging.

Principles of MR Imaging

Protons and neutrons, collectively called nucleons, in atomic nuclei have magnetic moments due to their angular momentum and they spin or precess randomly about their own axes. Nuclei containing even number of nucleons have zero magnetic moment due to cancelation of their individual momentum, whereas nuclei with odd number of nucleons have a net magnetic moment and direction, which behave like magnets.

A typical example of an odd nucleus is hydrogen nucleus that contains a single proton with a positive magnetic moment. In a living body, there is abundance of hydrogen nuclei or protons (also called spins) from water and tissue content, which have magnetic moment and precess in a random fashion. When the body is placed in a magnetic field, B_0, as in an MR machine, some of these spins will line up parallel to B_0 (low-energy state) and the remainder will be in antiparallel position (high-energy state) because of their randomness (Fig. 2.14). In general, parallel

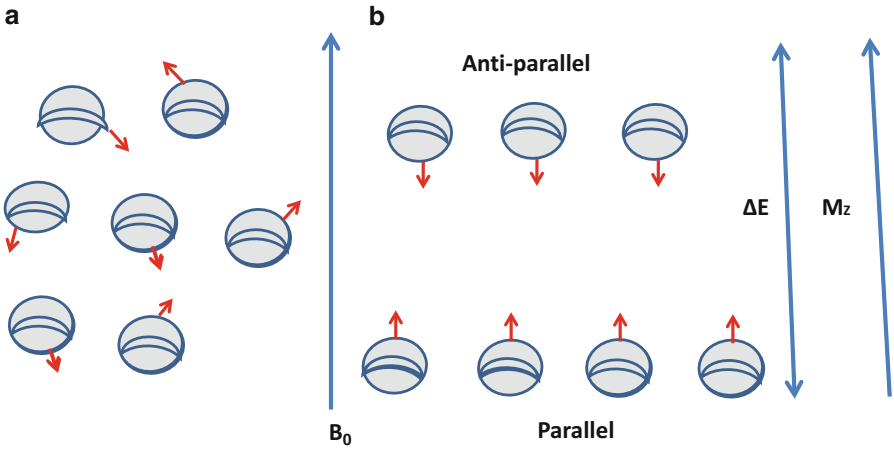

Fig. 2.14 (**a**) Free protons in the body spin randomly and their magnetic moments cancel each other, with a residual magnetic moment due to unpaired proton, if any. (**b**) When a body is placed in an external magnetic field, B_0, protons in the body align themselves in either parallel or antiparallel direction to the applied field, B_0. Normally there is slightly more parallel protons than antiparallel ones, thus resulting in a net magnetic moment M_Z along the direction of B_0. The energy difference between the two groups of protons is ΔE

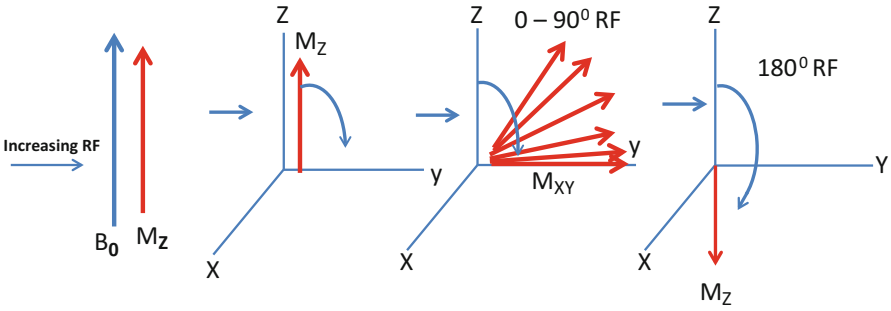

Fig. 2.15 When a radiofrequency pulse (RF) is applied to the M_Z (longitudinal magnetization) created in the presence of B_0, as explained in Fig. 2.13, M_Z flips toward the *X–Y* plane at different flip angles depending on the strength of RF pulse. A 90° RF pulse flips M_Z to the *X–Y* plane producing a transverse magnetization M_{XY} whose value is zero. If a 180° pulse is applied, M_Z becomes $-M_Z$

spins are slightly more in number than antiparallel spins resulting in a net longitudinal magnetization M_Z in the *Z* direction with an energy difference of ΔE. In this state, the spins are considered at equilibrium and the magnitude of M_Z is proportional to the strength of B_0. When a radiofrequency (RF) pulse is applied parallel to the magnetic field, B_0, the equilibrium of longitudinal magnetization (M_Z) is perturbed by absorption of energy from RF pulse, the longitudinal magnetization M_Z will flip toward the *X–Y* plane at different angles (Flip angles, FA) depending on the strength of RF pulse, and all spins remain in excited state. When an RF pulse flips M_Z by 90° on the *X–Y* plane, it is called a 90° RF pulse and M_Z becomes transverse magnetization M_{XY} (Fig. 2.15). Similarly a 180° pulse flips M_Z by 180° in $-Z$ direction and M_Z becomes $-M_Z$. At 90° flipping, all spins are in phase coherence meaning all spins point to the same direction resulting in maximum magnetization.

When the RF pulse is shut off, the spins give off their excitation energy to come to their original state. This process is called relaxation and is accomplished by two mechanisms. In one mechanism, the spins lose their excitation energy by spin–lattice interaction in which spins interact with the molecules in the surrounding tissue (lattice) in the body, whereby transverse M_{XY} reverses exponentially to longitudinal M_Z. This growth of M_Z is characterized by a relaxation time T1 which is defined as the time to grow by 63% of maximum M_Z (Fig. 2.16). The loss of energy appears as a MR signal, which is called T1 signal or pulse. T1 signal describes what happens in the *Z* direction when RF pulse is removed. The strength of the pulse depends on molecular vibrational frequencies and physical characteristics of the tissues such as solid or liquid or stationary or moving.

In the second mechanism, the spins lose their excitation energy by spin–spin interaction. As already mentioned, with the application of RF pulse, M_Z flips to transverse M_{XY} and the spins remain in excited state as well as in phase coherence. When RF pulse is switched off, the phase coherence is lost as the spins interact randomly with one another (spin–spin interaction) losing excitation energy.

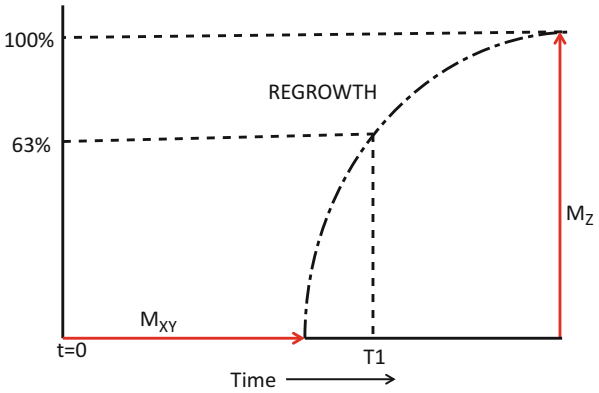

Fig. 2.16 Following a 90° RF pulse, M_{XY} is produced at the *X–Y* plane with zero value, but it returns to equilibrium exponentially over time by spin–lattice interaction in the body. Its regrowth is characterized by a relaxation constant T1, which is the time when 63% of M_Z is recovered

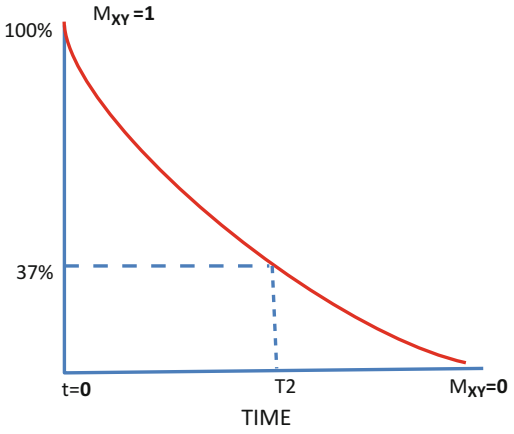

Fig. 2.17 Following a 90° RF pulse M_{XY} produced at the *X–Y* plane loses phase coherence due to spin–spin interaction in the body and inhomogeneity of the external field. The FID signal decays exponentially with a time constant T2, during which the signal decays to 37%

Over time, M_{XY} returns to original longitudinal M_Z. The dephasing of spins is intrinsically caused by micromagnetic inhomogeneity in the structure of the sample, whereby individual spins precess at different frequencies. The loss of energy in dephasing is characterized by an exponential decay, called *free induction decay* (FID), and the lost energy appears as an MR signal. Phase coherence is strong in the beginning but rapidly becomes less with no phase coherence left at the end. The FID decay is characterized by a relaxation time called T2, which is defined by the time that spins take to dephase to 37% (Fig. 2.17) and the signal is called T2 signal or pulse. T2 signal describes what happens in the *X–Y* plane when RF pulse is removed. When inhomogeneity of the external magnetic field, B_0, is also considered, the dephasing is accelerated thus shortening T2 even further, which is designated as T2*.

It should be emphasized that both T1 and T2 relaxations are two independent processes, but they occur simultaneously. So when a receiver coil is placed perpendicular to the magnetic field B_0, either T1 or T2 signal can be detected by the

coil to produce ultimately an image of the tissue in the magnetic field. T1 is normally longer than T2 and both depend on the strength of the magnetic field, B_0, and RF pulse. Their values also vary with the composition of the tissue. For example, fat has shorter T1 and fluid (cerebrospinal fluid) has relatively longer T1; so T1 imaging shows fat as bright and cerebrospinal fluid as dark. Other tissues fall in the range between the two. On the other hand, mobile fluid such as blood has long T2, whereas solid structures such as the bone have shorter T2.

MR signals depend on proton density and T1 and T2 relaxation time constants of different tissues in the body. Tissue contrast is obtained by manipulating these parameters during MR scanning, which is accomplished by a pulse sequence technique that involves timing, order, and repetition of RF pulses and the magnetic field. There are three major pulse sequence techniques, namely, spin echo (SE), inverse recovery (IR) echo, and gradient recalled echo (GRE), the description of which is beyond the scope of this book and readers are referred to books on MR physics. After a 90° RF pulse, M_Z magnetization becomes M_{XY} on the X–Y plane, and following withdrawal of RF pulse, the dephasing starts resulting in stronger to lower MR signal in time. Ideally one would like to have stronger signals, and to achieve it, a 180° pulse is applied after complete dephasing, which causes the spins to rephase leading again to a stronger MR signal. The signal is called an *echo* and the sequence of 90° pulse followed by 180° pulse is called spin-echo sequence. The time between 90° pulse and echo is called time of echo (TE). Spin-echo sequence is repeated many times for formation of an optimal image, and the time between two successive 90° signals is called repetition time (TR). The spin-echo technique takes longer scan time, yet it is widely used in MRI. A spin-echo sequence with a short TR (e.g., 250–1000 ms) and a short TE (less than 25 ms) emphasizes the T1 difference in tissues and is called T1 weighting, whereas a combination of a long TR (~2500–6500) and a long TE (>75 ms) highlights the T2 difference in tissues and hence the T2 weighting.

In the IR sequence, initially a 180° pulse is applied, whereby M_Z flips to $-M_Z$ and there is no M_{XY} and therefore no T2 relaxation (no dephasing). After the RF pulse is switched off, there is only T1 recovery that takes twice as long as M_{XY} would take. During the T1 recovery, at a certain time called inversion time (TI), a normal spin echo is applied to generate the image. In IR sequence, TR is fairly long (~1500 ms) and TE is short (10–30 ms) and image contrast increases with increasing T1.

In the GRE sequence, a gradient magnetic field (with varying FAs) is applied instead of a 180° RF pulse, which makes spins precess at different frequencies and so some spins dephase faster than the others. If the polarity of the gradient is instantaneously reversed after a predetermined time, the spins rephase more rapidly to produce a gradient echo signal. Image contrast of GRE sequence is determined primarily by FA and TE. T1-weighted images are obtained with a short TE and a large FA, whereas a long TE and a small FA will give T2-weighted images. The advantage of the GRE sequence is that it is faster than the spin-echo technique.

Proton density provides a totally different image contrast that depends on the density of protons in the sample and is independent of either T1 or T2. It employs shorter TE to minimize the effect of T1 and longer TR to minimize the effect of T2. Longitudinal magnetization recovery results mainly from the spin-density variations in the sample.

Paramagnetic contrast agents, commonly gadolinium chelates such as Gd-DTPA, when injected intravenously, accumulate in extravascular space over time and shorten both T1 and T2 values. At the optimal concentration of Gd-DTPA, better T1-weighted images are obtained.

MR Scanner

The most commonly used magnets in MR scanners are superconducting electromagnets, which consist of a number of coils made with niobium–titanium alloy embedded in copper and arranged in a cylindrical shape. A schematic cross-sectional view of an MR scanner is illustrated in Fig. 2.18. The coils are immersed in liquid helium in a container, which reduces the temperature low enough to make them superconductive. Further to stabilize the temperature, the helium container is surrounded by containers with liquid nitrogen. The entire set is then placed in a vacuum-sealed vessel. The magnet is attached to a patient support that slides into the bore of the magnet to bring the patient in the magnetic field. A power source is connected to the magnet to supply electric current through the coils, which induces a magnetic field. Gradient coils made of aluminum or copper are placed inside the magnet bore and superimpose a linear magnetic field on the primary magnetic field.

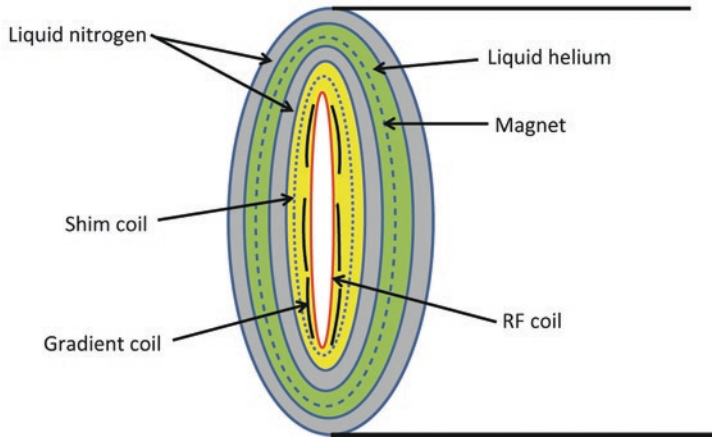

Fig. 2.18 A schematic cross-sectional view of a MR scanner

RF coils usually made of copper are placed within the magnet bore and serve as transmitter coils or as both transmitter and receiver coils. Each RF coil is attached to a power supply to create a magnetic field. Receiver coil receives MR signals. Surface coils and saddle coils are of different sizes and shapes and are used for different applications. Other important components of MR scanners are a signal detector, an amplifier, an analog-to-digital converter (ADC), a computer, and a display monitor. Since MR scanners produce fringe fields affecting signal production and other electronics, they are installed in rooms that are constructed of thick metal walls or electromagnetic system placed in the housing, which significantly reduces the effect of fringe fields.

Commercial PET/MR Scanner

Integration of PET and MR scanners on the same gantry encounters many difficulties, some of which have been overcome to some degree. First, the commonly used PM tubes used in PET scanners are sensitive to the magnetic field of MR scanners, whereby artifacts appear in PET images and so PM tubes cannot be placed inside the MR scanner. To circumvent this problem, PM tubes have been replaced by APD and SiPM tubes, which are not affected by the magnetic field and so can be placed inside the scanner. These tubes have higher quantum efficiency than regular PM tubes. However, PET hardware placed inside the MR scanner reduces the bore size. Second, the PET detectors are affected by the radiofrequency pulse and gradient magnetic field resulting in degradation and loss of PET signals due to reflection and absorption. So electronics and data transmission lines are shielded with reflective materials such as aluminum or copper and absorptive material like mu-metal. Unlike PET/CT where simultaneous data acquisition is not feasible, an integrated PET/MR system offers a unique advantage of simultaneous data acquisition in both modalities, since the radiation signal and the RF pulse do not interfere with each other in a shielded system. This reduces the scanning time significantly. Unlike in CT scanning, there is no X-ray attenuation in MR and so new ways of attenuation correction must be devised. Also, in the absence of radiation in MR, radiation dose to the patient in PET/MR is less than PET/CT.

GE Healthcare, Philips Healthcare, and Siemens Healthcare have manufactured PET/MR units based on different designs but using the same basic principle. The GE unit is a trimodality system consisting of two separate units—PET/CT (Discovery PET/CT 710) and MR (Discovery 3T MR750w)—and the patient is scanned separately on the two systems. The two scans are then fused by algorithm, but the coregistration suffers from alignment inaccuracy due to variation in patient position. This unit gives higher radiation dose to the patient due to CT. An advantage of this unit is that patients can be scanned for clinical purpose in PET/CT separately without the use of MR and vice versa.

Philip Healthcare's Ingenuity TF PET/MR consists of a time-of-flight (TF) PET scanner and a 3T MR scanner placed oppositely at a distance of 2.5 m. A floor-based bed is incorporated between the two scanners that can be rotated around 180° to position the patient in either scanner. The patient is scanned sequentially in the two scanners and images are then fused by algorithm. The time-of-flight technique is used in PET scanning. Since the patient is better positioned on a fixed bed, the alignment is relatively more accurate with this system.

Whole-body Biograph mMR of Siemens Healthcare is a totally integrated system of both PET and MR units in which data acquisition is carried out simultaneously in both units, thus reducing the scanning time significantly. In the PET scanner, APDs are used instead of photomultiplier tubes and are imbedded into the 3T MR coils. The block detectors are placed in cooling system for optimal PET performance, and a special shielding is incorporated in the system to eliminate the radiofrequency interference with the PET data acquisition and processing. In addition, low-attenuation material has been employed in what is called total imaging matrix (TIM) and in the table in MR to minimize the attenuation of PET signals. Simultaneous data acquisition with matching in time and patient position provides most accurate fusion of images. Siemens integrated Biograph mMR is shown in Fig. 2.19.

The specifications of PET/MR scanners from three manufacturers are presented in Table 2.4.

Fig. 2.19 Siemens Biograph mMR scanner (Copyright Siemens Healthcare 2014. Reprinted with permission)

Table 2.4 Specifications of PET/MR scanners from three manufacturers[a]

Company name	GE Healthcare	Philips Healthcare	Siemens Healthcare
Model/product name	Discovery PETCT + MR Discovery 710 and Discovery 3T 750 w	Ingenuity TF PET/MR	Biograph mMR
Integration of PET and MR units	PET and MR data is acquired sequentially in separate rooms	Fully integrated, sequential magnetic shielding	Simultaneous; fully integrated, solid-state, avalanche photodiode; PET-compatible MR coils
PET imaging time of flight or conventional	Time of flight	Time of flight	Conventional
Gantry dimensions, $H \times W \times D$, cm	$193 \times 225 \times 146$	$249.2 \times 261.5 \times 678.4$ cm	$335 \times 230 \times 242$ (finished covers)
Inner bore dimensions, cm	70	PET, 70; MR, 60	60 (D) $\times$ 199 (L)
Weight, kg (lb)	4996 (11,014)	7646	9000
Cooling the PET system	Air-cooling	Air-cooled	Water
Patient scan range, cm	170–200	190	199
Minimum finished bore L–R diameter, cm	NS	PET, 70; MR, 60	60
Table width (moving portion), cm	65	53	54
Acquisition modes (2D, 3D)	3D	PET, 3D; MR, 2D, 3D, spectroscopy	PET, 3D; MR, 2D, 3D, spectroscopy
Simultaneous acquisition/processing	No	Yes	Yes
Measured and automated randoms and scatter corr.	Yes	Yes	Yes
Attenuation-weighted iterative reconstruction	Yes	Yes	Yes
Type of detectors	PMT	Pixelar with continuous light guide	Solid-state, avalanche photo diode
Number of crystals	13,824	28,336	28,672
Detector material	Lu-based scintillator	LYSO	LSO
Crystal size, mm	$4.2 \times 6.3 \times 25$	$4 \times 4 \times 22$	$4 \times 4 \times 20$

(continued)

Table 2.4 (continued)

Company name	GE Healthcare	Philips Healthcare	Siemens Healthcare
Number of photosensors	NA	28 pixelar modular	4032 APDs
Ring diameter, cm	70	90	65.6
Number of PMTs	24	420	NA
Physical axial FOV, cm	15.7	18	26
System sensitivity—3D, kcps/uCi/cc LLD (NEMA 2001)	7.5 cps/KBq	>0.70 kcps/Ci/cc (center), >0.72 kcps/Ci/cc (10 cm)	13.2 cps/kBq
Transverse resolution @ 1 cm, mm (NEMA 2001)	4.0	4.9	4.4
Transverse resolution @ 10 cm, mm (NEMA 2001)	4.5	5.5	5.2
Axial resolution @ 1 cm, mm (NEMA 2001)	5.0	4.9	4.5
Axial resolution @ 10 cm, mm (NEMA 2001)	5.0	5.5	6.7
Peak noise equivalent count rate, cps (TOF)	130 kcps@29.5 kBq/mL	NS	175 kcps
3D	Yes	>91 kcps@16 kBq/mL	175 kcps
Time-of-flight timing resolution	4.9 ns	535 ps	NA
Peak noise equivalent count rate, cps (TOF)	130 kcps@29.5 kBq/mL	NA	NA
3D (TOF)	Yes	0.295 kcps@16 kBq/mL	NA
Scatter fraction—3D (NEMA 2001)	37%	30%	42%
Magnetic field strength, T	3	3	3
Cryogen refill interval, year	Zero boil-off	NA	0
Cooling system	Water-cooled	Liquid	
Reconstruction hardware	VRE 3.0	RapidView reconstructor	Intel Xeon Quad core (Linux 64 bit)
DICOM 3.0 classes supported	Yes	NS	Yes

[a]Reprinted with permission from the October 2013 issue of *Imaging Technology News (ITN)*, Scranton Gillette Communications. All rights reserved

Small-Animal PET/CT and PET/MR Scanner

Drugs are commonly used in animals prior to their clinical use in humans to establish the safety and efficacy of the drug by studying the in vivo biodistribution, pharmacokinetics, and toxicity. However, there are challenges in preclinical imaging research using small animals, because it requires submillimeter spatial resolution to achieve accuracy in images comparable to those of humans, which is difficult to achieve in conventional PET/CT scanners. The scanner must provide high sensitivity with the smaller administered activity in animals allowing dynamic imaging. Furthermore, spatial resolution must be uniform across the FOV. For this reason, small-animal PET/CT cameras have been developed, particularly for drug research using small animals. These scanners are small enough to be installed on a bench.

The first animal PET scanner (Model 713) introduced by Siemens consisted of a single 64-cm diameter ring of 80 BGO block detectors collimated with 7 annular tungsten seta (Cutler et al. 1992). The resolution and sensitivity were not up to expectation. With introduction of LSO detectors and fiber-optic readouts of individually cut crystals, small-animal scanners (PET, PET/CT, or PET/MR) with high resolution have been developed by manufacturers such as TriFoil Imaging, Mediso Medical Imaging Systems, and Sofie Biosciences.

TriFoil Imaging offers PET/CT units in three configurations, LabPET/CT4, LabPET/CT8, and LabPET/CT12, with increasing axial FOV and number of APDs. Phoswich detectors consist of a dual layer of LYSO and LGSO crystals and are connected to APDs in two rings. The XO CT unit employs an advanced digital X-ray detector technology and has a zoom feature to optimize the FOV and spatial resolution.

Mediso's NanoScan PET/CT uses high-density detectors of tightly packed LYSO crystals and thicker crystals for higher sensitivity. Large animals such as monkeys can be imaged with 16-cm bore. The manufacturer claims quantitative accuracy of 97%. The CT unit utilizes an 80-W X-ray source and has zoom capability of 8. It provides helical X-ray scanning due to its large bore size and large detector surface area. Mediso has also introduced a NanoScan PET/MR unit for animal scanning using the same PET characteristics of NanoScan PET/CT unit and a 1T magnet and claimed excellent spatial resolution and sensitivity and better performance characteristics than the NanoScan PET/CT (Nagy et al. 2013).

Sofie Biosciences commercializes a small-animal PET/X-ray scanner Genisys4 that consists of four panels of detectors, each with 24×50 BGO crystals connected to two PM tubes. Attenuation correction is performed using an anatomic reference image that is obtained by a combination of an X-ray projection, a digital mouse atlas, and a photographic image. It also provides highest sensitivity of all (14%) due to its relatively large bore. Siemen Healthcare manufactured and marketed Inveon animal PET/CT scanner in the past, which is being phased out of production.

Different specifications of the small-animal PET/CT scanners from these manufacturers are given in Table 2.5 and a commercial animal scanner is shown in Fig. 2.20.

Table 2.5 Specifications of different small-animal PET/CT and PET/MR scanners

Manufacturer	TriFoil Imaging[a]	Mediso USA[b]	Sofie Biosciences[c]
Model	LabPET/CT	NanoScan PET/CT	G8 PET/CT
Detector material	LYSO/LGSO coupled to APD	LYSO	BGO
Crystal size (mm)	2×2	$1.12 \times 1.12 \times 13$	$1.8 \times 1.8 \times 7$
No. of rings	2	2	4 panels
Bore diameter (cm)	16	16	4.8
Axial FOV (cm)	7.5 (single bed)	10	9.5
Transaxial FOV (cm)	10	12	4.7
Spatial resolution (mm)	<1	0.7	1.4
Sensitivity (%)	2.5	8.1	14

[a]Personal communication with Sean Pitts of TriFoil Imaging, USA
[b]Personal communication with Iles Muller of Mediso, USA
[c]Personal communication with Patrick Phelps of Sofie Biosciences, USA

Fig. 2.20 Mediso's small-animal PET/CT scanner, NanoScan PET/CT (Image courtesy of Mediso Medical Imaging Systems at medisousa.com)

Mobile PET or PET/CT Scanner

For the convenience of hospitals and clinics that do not have a PET scanner, mobile PET scanners are available commercially to provide PET service to these facilities. PET scanners, preferably PET/CT scanners, along with the control console are installed in sturdy mobile vans. These mobile PET/CT vans move to different client's sites to provide PET imaging services. Because of the scanner's weight and heavy electrical requirement, a concrete pad with enhanced electrical connections must be built at the client site to support the weight of the mobile system. This ensures the correct leveled positioning of the van at the site. The power supply (typically 430 V, three-phase at 60 Hz) is provided at the client's site. Also, a generator is installed in the van to run chillers and air conditioning to keep PET scanners at operating temperatures. Currently, only ^{18}F-FDG PET imaging is provided by all mobile PET services.

One must obtain a valid license from the state and/or the Nuclear Regulatory Commission (NRC) to operate a mobile PET or PET/CT system, providing services to different client sites. A requirement for the license is to have a letter of agreement between the licensee and the client signed by the management (chief executive officer or designee) detailing the responsibilities of each. Some states do not allow injection of the radiotracer in the coach, necessitating a separate injection room and a waiting room at the client's site. Many states may require a sink, changing area, specific security considerations, and fire protection in the mobile van. The van must meet Department of Transportation (DOT) overload regulations.

All necessary accessories for PET studies, including a dose calibrator, ^{18}F-FDG storage, a wipe test counter, a survey meter, and so on, are kept in the van. The mobile PET van moves daily to different clients' sites according to the schedule made prior to the day of examination. The patient's PET study is performed and the data are processed in the van, while the interpretation can be made either at the van or at the home site of the mobile PET company.

It requires a great deal of logistics in scheduling PET studies at different sites using a mobile PET scanner. The ^{18}F-FDG must be delivered early in the morning, and enough of it should be available to complete the day's schedule. The mobile PET company may have its own cyclotron and radiochemistry laboratory that supplies ^{18}F-FDG to the van, or it may be purchased from another cyclotron facility.

The timing of the studies must be well coordinated with each client to avoid any overlap of schedules with other clients. Overall, mobile PET provides easy access to PET examinations for many community hospitals that are unable to afford a PET scanner because of the cost. However, during inclement weather, the transportation of the van may be problematic.

Questions

1. Describe the general principles of positron emission tomography.
2. Explain why an LSO detector is better than a BGO detector in PET scanning and NaI(Tl) is least preferred.
3. What are block detectors and why are they preferred to single detectors in a PET scanner?
4. Typical energy resolutions of BGO and LSO detectors in PET scanners are about (a) 10%, (b) 15%, (c) 24%, or (d) 5%.
5. The common number of PM tubes per block detector in a PET scanner is (a) 2, (b) 4, (c) 6, or (d) 8.
6. Positron scanners comprised of BGO or LSO detectors are arranged in full or partial rings, and each detector is connected to a number of opposite detectors in coincidence. If there are N detectors in the scanner, what is the maximum number of fan-beam projections available for coincidence counting?
7. The number of BGO or LSO detectors in common PET scanners is of the order of (a) tens of, (b) thousands of, (c) hundreds of, or (d) only a few detectors.
8. The number of rings in commercial PET scanners varies from (a) 50 to 100, (b) 5 to 10, (c) 18 to 32, or (d) 1 to 5.
9. Semiconductor detectors do not require PM tube. Why?
10. What is the difference between PIN diode and PN diode?
11. Define the mechanism of the operation of an avalanche photodiode.
12. Explain how SPECT scintillation cameras can be used in coincidence counting. Discuss the advantages and disadvantages of these cameras in coincidence counting.
13. Describe the technique of PET/CT imaging. Why is PET/CT better than only PET in detecting various tumors?
14. PET/CT imaging has the advantage over dedicated PET imaging because of:

    (a) shorter scanning time True __; False __.
    (b) higher sensitivity of PET scanner True __; False __.
    (c) better localization of abnormalities True __; False __.

15. If the travel range of the scanning table is 180 cm, and the displacement distance between the centers of the scan fields of CT and PET scanners is 60 cm, what is the maximum body length that can be scanned in this PET/CT scanner?
16. The transverse FOV of PET is defined by (a) the pulse width, (b) the detector material, (c) the angle of acceptance, or (d) the number of PM tubes.
17. What is the basis of dual-energy CT scanners?
18. The good characteristics of PET detectors include (a) high-energy resolution, (b) high light output, (c) high stopping power, and (d) short scintillation decay time. True ____, False _____.

19. Pulse height analyzer is used to (a) increase the count rate, (b) include the scattered radiation, (c) sort the photons of energy of interest, and (d) shorten the scan time.
20. Define free induction decay. What is the relationship between T2 signal and FID?
21. Explain the mechanisms of T1 and T2 relaxation in MR imaging.
22. What are the basic factors that affect the MR signals from the different tissues.
23. What is the effect of Gd-DTPA on T1 and T2 values?
24. Why are avalanche photodiodes (APD) used in integrated PET/MR scanners?

References and Suggested Reading

Blodgett TM, Meltzer CC, Townsend DW. PET/CT: form and function. Radiology. 2007;242:360.

Bushberg JT, Seibert JA, Leidholdt Sr EM, Boone JM. The essential physics of medical imaging. 3rd ed. Philadelphia: Lippincott, Williams and Wilkins; 2011.

Chatziioannou AF, Cherry SR, Shao Y, et al. Performance evaluation of microPET: a high-resolution lutetium oxyorthosilicate PET scanner for animal imaging. J Nucl Med. 1999;40:1164.

Cherry SR, Dahlbom M. PET; physics, instrumentation, and scanners. In: Phelps ME, editor. PET; molecular imaging and its biological applications. New York: Springer; 2004.

Cherry SR, Sorensen JA, Phelps ME. Physics in nuclear medicine. 4th ed. Philadelphia: W.B. Saunders; 2012.

Cutler PD, Cherry SR, Hoffman EJ, et al. Design features and performances of a PET system for animal research. J Nucl Med. 1992;33:595.

Melcher CL. Scintillation crystals for PET. J Nucl Med. 2000;41:1051.

Nagy K, Toth M, Major P, et al. Performance evaluation of the small-animal nanoScan PET/MRI system. J Nucl Med. 2013;54(10):1825.

Patton JA. Physics of PET. In: Delbeke D, Martin WH, Patton JA, Sandler MP, editors. Practical FDG imaging. New York: Springer; 2002.

Shiga T, Morimoto Y, Kubo N, et al. A new PET scanner with semiconductor detectors enables better identification of intratumoral inhomogeneity. J Nucl Med. 2009;50:148.

Turkington TG. Introduction to PET instrumentation. J Nucl Med Technol. 2001;29(1):89.

Chapter 3
Data Acquisition and Corrections

PET Data Acquisition

Positron emission tomography (PET) is based on the detection in coincidence of the two 511-keV annihilation photons that originate from β^+ emitting sources (e.g., the patient). The two photons are detected within an electronic time window (e.g., 12 ns) set for the scanner and must be along the straight line connecting the centers of the two detectors called the line of response (LOR). Since the two photons are detected in coincidence along the straight line in the absence of an absorptive collimator, this technique is called electronic collimation. All coincident events are collectively called prompts, which include true, random, scattered, and multicoincidence events. Examples of these events are illustrated in Fig. 3.1. A true coincident event arises when two 511-keV photons from a single annihilation event are detected by a detector pair along the LOR within the set energy and timing window (Fig. 3.1a). Random coincidences occur when two unrelated 511-keV photons from two separate annihilation events are detected by a detector pair within the same time window (Fig. 3.1b). These events raise the background in the image causing loss of image contrast. Scatter coincidences occur due to Compton scattering of annihilation photons in the patient, and one 511-keV photon and one scattered photon or both scattered photons arising from the same annihilation event may fall within the 511-keV energy window and be detected by a detector pair within the coincidence time window (Fig. 3.1c). Note that two scattered photons from two separate annihilation events falling within the set energy and timing windows will be counted as a random coincident event. Scatter coincidences raise the background of the image and degrades the image contrast. Multicoincidence occurs when more than two unrelated 511-keV photons are detected in coincidence in different detectors within the time window, but these events are discarded because of the difficulty in positioning them. The detailed description of different coincident events is given later.

G.B. Saha, *Basics of PET Imaging*, DOI 10.1007/978-3-319-16423-6_3

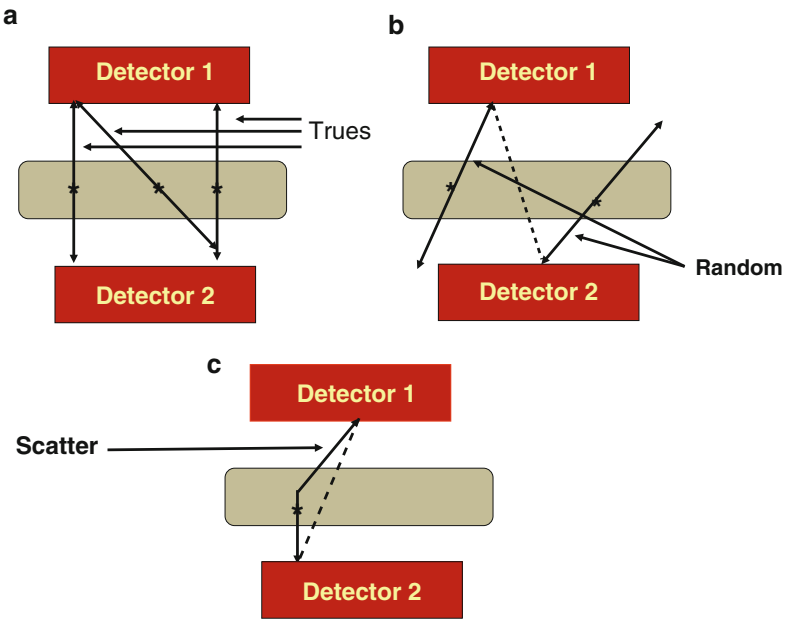

Fig. 3.1 (**a**) True coincident events that result from two 511-keV photons from a single annihilation event and detected along an LOR by a detector pair within the set energy and timing windows. (**b**) Random coincidences occur when photons from two unrelated annihilation events are detected by a detector pair along the LOR (*dotted line*). (**c**) Scattered coincident events result when one or both 511 keV photons from a single annihilation are scattered in the body tissue and one scattered photon and the unscattered 511 keV photon, or both scattered photons, are detected by a pair of detectors along the LOR within the set energy and timing windows

In a full ring system, the data are collected simultaneously by all detector pairs, whereas in partial ring systems, the detector assembly is rotated around the patient in angular increments to collect the data. In acquiring the coincidence events, three steps are followed:

1. The location of the detector pair in the detector ring is determined for each coincident event.
2. The pulse height of the photon detected is checked if it is within the energy window set on 511 keV.
3. Finally, the position of the LOR is determined in terms of polar coordinates to store the event in the computer memory.

As stated in Chap. 2, in a PET scanner, block detectors are cut into small detectors and coupled with four PM tubes, which are arranged in arrays of rings. Each detector is connected in coincidence to as many as $N/2$ detectors, where N is the number of small detectors in the ring. So which two detectors detected a coincidence event within the time window must be determined. Pulses produced in PM tubes are used to determine the locations of the two detectors (Fig. 3.2). As in scintillation cameras, the position of each detector is estimated by a weighted

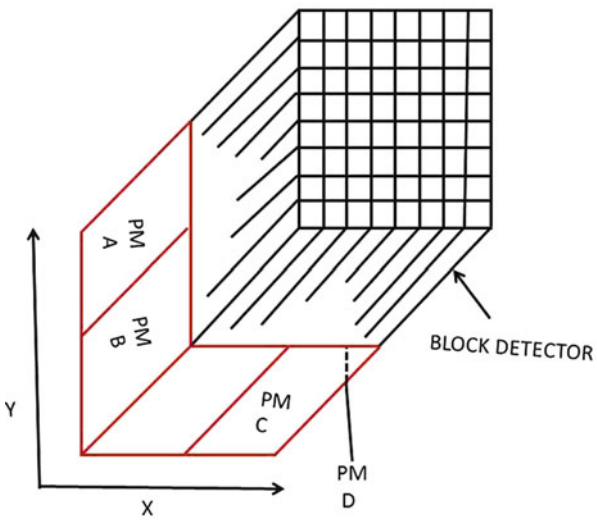

Fig. 3.2 A schematic block detector is segmented into 8×8 elements, and four PM tubes are coupled to the back of the block for pulse formation. The pulses from the four PM tubes (A, B, C, and D signals) determine the location of the element in which 511-keV γ-ray interaction occurs, provided the sum of the four pulses falls within the energy window of 511 keV

centroid algorithm. This algorithm estimates a weighted sum of individual PM tube pulses, which are then normalized with the total pulse obtained from all PM tubes. Similar to scintillation camera logistics, the X and Y positions of the detector element in the ring are obtained as follows:

$$X = \frac{(B + C) - (A + D)}{A + B + C + D}, \tag{3.1}$$

$$Y = \frac{(C + D) - (A + B)}{A + B + C + D}. \tag{3.2}$$

Here A, B, C, and D are the pulses from the four PM tubes as shown in Fig. 3.2.

The four pulses (A, B, C, D) from four PM tubes are then summed up to give a Z pulse, which is checked by the pulse height analyzer (PHA) if its pulse height is within the energy window set for the 511-keV photons. If it is outside the window, it is rejected; otherwise, it is accepted and processed further for storage.

The last step in data acquisition is the storage of the data in the computer. Unlike conventional planar imaging where individual events are stored in an (X, Y) matrix, the coincidence events in PET systems are stored in the form of a sinogram. Consider an annihilation event occurring at the $*$ position in Fig. 3.3a. The coincidence event is detected along the LOR indicated by the arrow between the two detectors. It is not known where along the line of travel of the two photons the event occurred, since photons are accepted within the set time window (say, 12 ns) and their exact times of arrival are not compared. The only information we have is the positions of the two detectors in the ring that registered the event, i.e., the

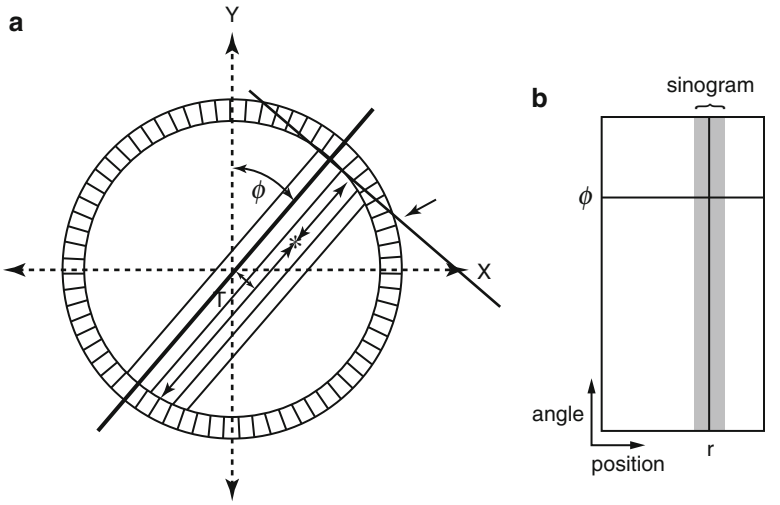

Fig. 3.3 PET data acquisition in the form of a sinogram. Each LOR data is plotted in (r,ϕ) coordinates (**a**). Data for all r and ϕ values are plotted to yield the sinogram indicated by the *shaded area* (**b**). (Only a part of the sinogram is shown.) (Reprinted with the permission of the Cleveland Clinic Center for Medical Art and Photography ©2009. All rights reserved)

location of the LOR is established by the (X, Y) positioning of the two detectors. Many coincidence events arise from different locations along the LOR and all are detected by the same detector pair and stored in the same pixel.

For data storage in sinograms, each LOR is defined by the distance (r) of the LOR from the center of the scan field (i.e., the center of the gantry) and the angle of orientation (ϕ) of the LOR (i.e., the angle between r and the vertical axis of the field). If we plot the distance r on the x-axis and the angle ϕ on the y-axis, then the coincidence event along the LOR (r, ϕ) will be assigned at the cross-point of r and ϕ values (Fig. 3.3b). In a given projection, adjacent detector pairs constitute parallel LORs (at different r values in Fig. 3.3a) at the same angle of orientation. The plot of these LORs will be seen as a horizontal row at angle ϕ. When all projections around the field of view are obtained, the plot of the LORs at different projection angles and r values will result in the shaded area shown in Fig. 3.3b, which is called a sinogram. A sinogram is essentially a matrix of fan-beam projections defined by the angle of acceptance. A typical normal sinogram is shown in Fig. 3.4.

PET data are acquired directly into a sinogram in a matrix of appropriate size in the computer memory. The sinogram is basically a two-dimensional (2D) histogram of the LORs in the (distance, angle) coordinates in a given plane. Thus, each LOR (and hence, detector pair) corresponds to a particular pixel (or element) in the sinogram, characterized by the coordinates r and ϕ. For each coincidence event detection, the LOR is determined, the corresponding pixel in the sinogram is located, and a count is added to the pixel. In the final sinogram, the total counts in each pixel represent the number of coincidence events detected during the counting time by the two detectors along an LOR.

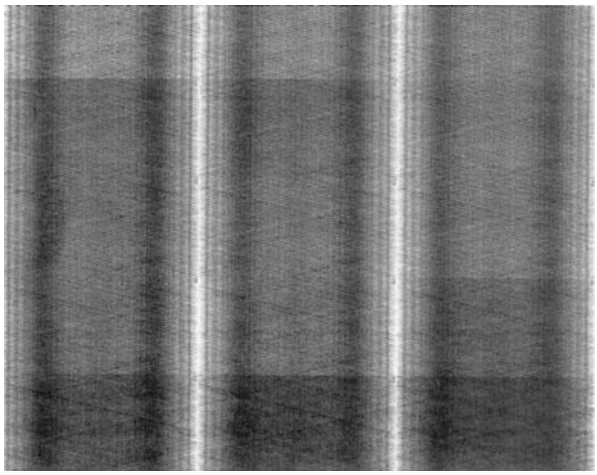

Fig. 3.4 A typical normal sinogram indicating all detectors are working properly

It is of note that comparing raw data acquired in PET with those in SPECT, each projection image in SPECT represents data acquired at that projection angle across all slices, whereas in PET, each sinogram represents the data acquired for a slice across all angles. A set of sinograms from a complete, multislice PET study can be deciphered in the computer to generate a series of projection views that are similar to SPECT raw data.

Data are acquired in either frame mode or list mode. Details of these acquisitions are given in books on physics in nuclear medicine, and the readers are referred to them. Briefly, in frame mode, digitized signals are collected and stored in *X*, *Y* positions in a matrix of given size and depth for a specified time or total number of counts. In list mode, digitized *X*- and *Y*-signals are coded with "time marks" as they are received in sequence and stored as individual events as they occur. After the acquisition is completed, data are manipulated to form images in a variety of ways to meet a specific need. This process is time consuming despite the wide flexibility it provides. In PET studies, while the frame mode acquisition is routinely used, with the introduction of faster computers, the list mode acquisition is now being used more commonly for the newer cameras.

Data can be acquired in both static and dynamic imaging using either list mode or frame mode. In static imaging, a single-frame image is acquired by collecting data over a period of time normally in frame mode. In dynamic imaging, data are collected in multiple frames of sinograms, each of a predetermined period of duration. An example of dynamic imaging is cardiac blood pool gated studies in which the duration of the cardiac QRS cycle is deciphered into nearly 20-ms time segments and list mode data are acquired sequentially for each segment. Acquisition is repeated for many QRS cycles for the data to be statistically meaningful. List mode data are then binned into sinograms and sequential frame mode images are obtained. Whereas static images provide an estimate of gross tracer uptake, dynamic imaging provides the kinetics of tracer uptake in an organ.

How many counts need to be acquired per projection and what size matrix should be chosen for adequate quality of images vary with the different cameras depending on the scatter, random, and extent of smoothing needed. A three-dimensional (3D) scanner would acquire more counts per projection than a 2D scanner because of the more scatter events in the 3D scanner. Typically 250,000–500,000 counts are needed for optimal quality of images. For good-quality images, the pixel size is recommended to be 2–3 mm. If the FOV is of the order of 300 mm acquired in a128 × 128 matrix, then pixel size would be ~2.3 mm indicating the right choice of the matrix for data acquisition.

Since PET systems are axially fixed, whole-body imaging is accomplished by moving a computer-controlled bed with the patient on it along the axial field and collecting data at adjacent bed positions. In whole-body imaging, the total scan time depends on the patient's body length and the effective axial FOV of the scanner per bed position. Since the sensitivity decreases toward the periphery of the FOV, the effective axial FOV is less than the actual FOV and it is necessary to overlap the bed positions in whole-body imaging. A typical overlap of 3–5 cm is common, and an even higher value is used in 3D acquisition, because of the sharper decrease in sensitivity toward the periphery of the FOV. The time for data acquisition at each bed position in whole-body imaging is 5–10 min.

Time-of-Flight Method

The time-of-flight (TOF) PET technique is based on the measurement of time difference in the arrival of the two 511-keV annihilation photons at the detectors, as illustrated in Fig. 3.5. Suppose two detectors are equidistant, x, from the center of

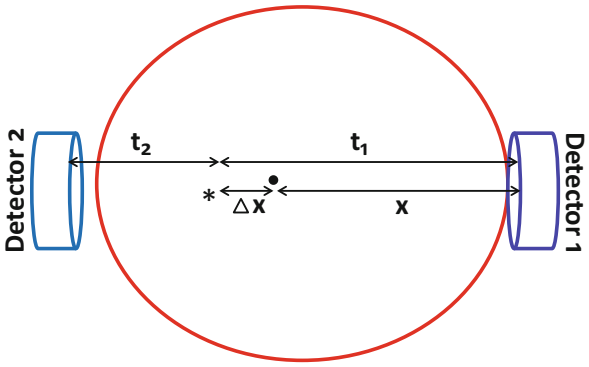

Fig. 3.5 A schematic diagram illustrating the principle of time-of-flight (TOF) technique. The time difference $(t_1 - t_2)$ in the arrival of two photons is related to the difference in distances Δx, traveled by them. Using TOF information, the annihilation point is determined within a spatial range of $\Delta x = (c \cdot \Delta t)/2$, which is stored in the matrix to generate images (Reprinted with the permission of the Cleveland Clinic Center for Medical Art and Photography ©2009. All rights reserved)

FOV (CFOV) and a positron is annihilated in the patient at position $*$ at a distance Δx from the CFOV. One of the 511-keV photons will travel $x + \Delta x$ in time t_1 and the other will travel $x - \Delta x$ in time t_2. Since the photons travel at the speed of light (c), the difference in time of arrival ($\Delta t = t_1 - t_2$) of the two photons at the detectors is $2\Delta x/c$. Note that the photons from the CFOV arrive at the detectors simultaneously ($\Delta x = 0$). The value of x is known but the location of positron annihilation on the LOR is not known. It is determined by the uncertainty in the point of interaction given by $\Delta x = (c \cdot \Delta t)/2$. From the knowledge of the time difference Δt of the photon arrival, Δx is calculated, which is the distance along the LOR away from the midpoint between the two detectors to where the annihilation took place. This localization information is then stored in the computer matrix for image reconstruction later. With faster electronics and improved scintillators, and also shorter time windows, it is possible to measure the time difference Δt fairly accurately by TOF PET scanner and thus to determine the accurate location of the annihilation event providing high-resolution images.

The parameter Δx is usually much smaller than the diameter D of the patient (with good timing resolution). The signal-to-noise ratio (SNR) or sensitivity increases with improved timing resolution and is proportional to $D/\Delta x$, i.e., $2D/(c \cdot \Delta t)$. For a 30-cm subject and a timing resolution of 0.5 ns, the SNR (sensitivity) increases by a factor of 4.

Decades ago, the TOF PET scanners were introduced using fast detector like cesium fluoride (CsF) or barium fluoride (BaF_2) to allow high count rates, but spatial resolution and sensitivity were poorer than those of conventional PET scanners with BGO, because of poor light production. With the advent of improved scintillators like LSO, LYSO, and $LaBr_3$, along with more efficient and reliable PM tubes, TOF is currently adopted in several conventional commercial PET scanners. Philips Healthcare is marketing Big Bore Gemini TF PET scanners based on the TOF technique. Current TOF scanners offer better spatial resolution and sensitivity because of increased light production in the detector material and the shorter timing resolution. Moreover, this technique improves the image quality in heavy patients, compared to the PET scanners that lead to a loss of counts due to attenuation as well as an increase in scattered counts.

Two-Dimensional vs. Three-Dimensional Data Acquisition

Coincidence events detected by two detectors within the time window are termed "prompt" events. The prompts include true, random, and scatter coincidence events. In many PET systems, in an attempt to eliminate random and scatter photons discussed later, annular septa (~1-mm thick and radial width of 7–10 cm) made of tungsten or lead are inserted between rings (Fig. 3.6a). In some scanners, septa are retractable or fixed, while in others, they are not incorporated, depending on the manufacturers. These septa function like the parallel-hole collimators in scintillation camera imaging. Only direct coincidence events between the two paired

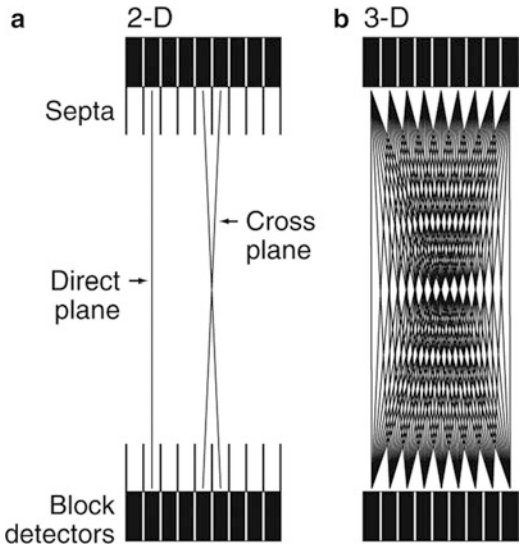

Fig. 3.6 (**a**) 2D data acquisition with the septa placed between the rings so that true coincidence counts are obtained avoiding randoms and scatters. Detectors connected in the same ring give direct plane events. However, detectors are connected in adjacent rings and cross plane data are obtained as shown. (**b**) When septa are removed, the 3D data acquisition takes place, which include random and scatter events along with true events

detectors in a ring are recorded. Such counting is called the 2D mode of data acquisition. In this mode, most of the random and scattered photons from outside the ring are prevented by the septa to reach the detectors, leaving the true coincidences to be recorded (Fig. 3.6a). The use of septa reduces the fraction of scattered photons from 30 to 40% without septa to 10–15%.

Detector pairs connected in coincidence in the same ring give the *direct plane event* (Fig. 3.6a). To improve sensitivity in 2D acquisition, detector pairs in two adjacent rings are connected in coincidence circuit. Coincidence events from a detector pair in this arrangement are detected and averaged and positioned on the so-called *cross plane* that falls midway between two adjacent detector rings (Fig. 3.6a). In current PET scanners, small detectors are used for better resolution but result in low sensitivity in the direct and cross planes. So additional cross planes are included from nearby rings that are connected in coincidence so that the overall sensitivity of the scanner is increased. The acceptable maximum number of rings that are connected in coincidence for cross planes is 5 or 6. Note that for an n-ring system, n direct planes and $n-1$ cross planes can be obtained in 2D acquisition. Thus, a total of $2n-1$ sinograms are generated, each of which produces a transaxial image slice. While the cross planes increase the sensitivity, they degrade the spatial resolution.

The overall sensitivity of PET scanners in 2D acquisition is 2–3% at best. To increase the sensitivity of a scanner, the 3D acquisition has been introduced in which the septa are retracted or they are not present in the scanner (Fig. 3.6b). This mode includes all coincidence events from all detector pairs, thus increasing the sensitivity by a factor of almost 4–8 over 2D acquisitions. If there are n rings in the PET scanner, all ring combinations are accepted and so n^2 sinograms are obtained. However, scattered and random coincidences are increasingly added to the 3D data, thus degrading the spatial resolution as well as requiring more computer memory.

As a trade-off, one can limit the angle of acceptance to cut off the random and scattered radiations at the cost of sensitivity. This can be achieved by connecting in coincidence each detector to a fewer number of opposite detectors than $N/2$ detectors. The sensitivity in 3D mode is highest at the axial center of the field of view and gradually falls off toward the periphery. Three-dimensional data require more storage as they are approximately 10^3 times more than 2D data and so result in time-consuming computation. However, current fast computers have significantly overcome this problem.

Factors Affecting Acquired PET Data

The projection data acquired in the form of sinograms are affected by a number of factors, namely, variations in detector efficiencies between detector pairs, random coincidences, scattered coincidences, photon attenuation, dead time, and depth of interaction. Each of these factors contributes to the sinogram to a varying degree depending on 2D or 3D acquisition and needs to be corrected for prior to image reconstruction. These factors and their correction methods are described below.

Normalization

Current PET scanners can have 10,000–35,000 detectors arranged in blocks and coupled to several hundred PM tubes. Because of the variations in the gain of PM tubes, the location of the detector in the block, and the physical variation of the detector, the detection efficiency of a detector pair varies from pair to pair, resulting in nonuniformity of the raw data. This effect in dedicated PET systems is similar to that encountered in conventional scintillation cameras used for SPECT and PET studies. The method of correction for this effect is termed the *normalization*. Normalization of the acquired data is accomplished by exposing uniformly all detector pairs to a 511-keV photon source (e.g., ^{68}Ge source), without a subject in the field of view. Data are collected for all detector pairs in both 2D and 3D modes, and normalization factors are calculated for each pair by dividing the average of counts of all detector pairs (LORs) by the individual detector pair count. Thus, the normalization factor F_i for each LOR is calculated as

$$F_i = \frac{A_{\text{mean}}}{A_i}, \tag{3.3}$$

where A_{mean} is the average coincidence counts for all LORs in the plane and A_i is the counts in the ith LOR. The normalization factor is then applied to each detector pair data in the acquisition sinogram of the patient as follows:

$$C_{\text{norm},i} = C_i \times F_i, \tag{3.4}$$

where C_i is the measured counts and $C_{\text{norm},i}$ is the normalized counts in the ith LOR in the patient scan. A problem with this method is the long hours (~6 h) of counting required for meaningful statistical accuracy of the counts, and hence overnight counting is carried out. These normalization factors are generated weekly or monthly. Most vendors offer software for routine determination of normalization factors for PET scanners. A difficulty with this method is that scatter and random coincidences require different normalizations from true coincidences, which is difficult to accomplish separately.

A component-based variance reduction method is employed to partially resolve these problems. Normalization factors are calculated as the product of intrinsic crystal efficiencies and geometric factors that account for the variation in crystal efficiency with the position of the crystal in the block and photon incidence angle. Intrinsic efficiencies of individual detectors are determined from the average sum of the coincidence efficiencies between a given detector and all opposite detectors connected in coincidence. The geometric factors are normally determined by the manufacturers using a very high activity source and they presumably remain constant. This reduces the computation from the number of LORs (millions) to the number of detectors (thousands). Even though normalization by the component-based method is less time consuming, residual artifacts in images reconstructed from normalized acquisitions of uniform phantoms have been reported.

Photon Attenuation

Attenuation of annihilation photons occurs due to their absorption and scattering in the body tissue. The extent of attenuation depends on the depth of tissue the photons have to travel before striking the detector. Photons in the center of the body undergo maximum attenuation, because they travel the most depth of the tissue, whereas those at the periphery are least attenuated. Attenuation also occurs when annihilation photons traverse across different organs or tissues. This causes uneven distribution of counts over regions of interest. Therefore, attenuation correction must be applied to the acquired data prior to image reconstruction.

If μ is the linear attenuation coefficient of 511-keV photons in the tissue, and a and b are the tissue thicknesses traversed by the two 511-keV photons along the LOR (Fig. 3.7), then the probability P of coincidence detection is given by

$$P = \mathrm{e}^{-\mu a} \times \mathrm{e}^{-\mu b} = \mathrm{e}^{-\mu(a+b)} = \mathrm{e}^{-\mu D}, \tag{3.5}$$

where D is the total thickness of the body. Equation (3.5) is applicable to organs or tissues of uniform density. All coincident events along the same LOR will have the

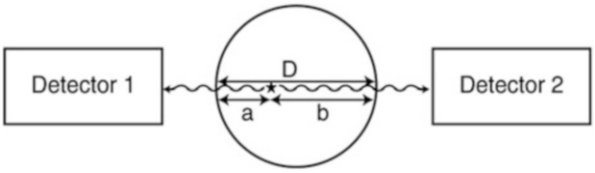

Fig. 3.7 Two 511-keV photons detected by two detectors suffer attenuation after traversing two different tissue thicknesses, *a* and *b*. *D* is equal to the sum of *a* and *b*. Attenuation of 511-keV photons is independent of the location of annihilation and depends on the total dimension of the body as given by Eq. (3.5) (Reprinted with the permission of the Cleveland Clinic Center for Medical Art and Photography ©2009. All rights reserved)

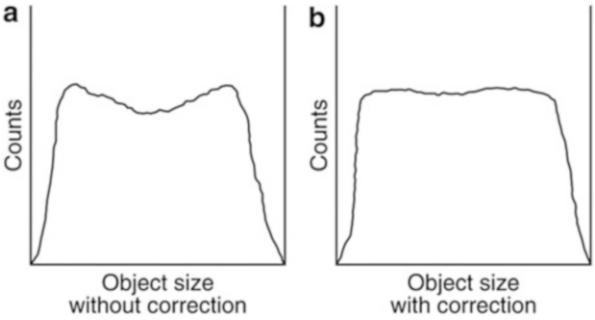

Fig. 3.8 (**a**) Profile of raw acquired data showing depression in activity due to more attenuation at the center. (**b**) The same profile with attenuation correction (Reprinted with the permission of the Cleveland Clinic Center for Medical Art and Photography ©2009. All rights reserved)

attenuation effect given by Eq. (3.5). When photons travel through different organs or tissues with different μ values, then Eq. (3.5) becomes

$$P = e^{-\sum_{i=0}^{n} \mu_i D_i}, \tag{3.6}$$

where μ_i and D_i are the linear attenuation coefficient and thickness of the *i*th organ or tissue, respectively, and n is the number of organs or tissues the photon travels through. Photon attenuation causes nonuniformities in the images (Fig. 3.8), because of the loss of relatively more coincidence events from the central tissues than from the peripheral tissues of an organ and also because the two photons may transverse different organs along the LOR.

Note that the probability P is the attenuation correction factor, which is independent of the location of positron annihilation and depends on the total thickness of the tissue. If an external radiation passes through the body, the attenuation of the radiation will be determined by an effective attenuation coefficient μ (tissues of different μ_i) and the thickness of the body, as expressed by Eq. (3.5). This introduces

the transmission method of attenuation correction, by using an external source of radiation rather than using the patient as the emission source, and the method is described below.

Attenuation Correction Methods

Theoretical Method: A simple theoretical calculation based on Eq. (3.5), also called the Chang method, can be applied for attenuation correction based on the knowledge of μ and the contour of an organ, such as the head, where uniform attenuation can be assumed. However, in organs in the thorax (e.g., heart) and the abdomen areas, attenuation is not uniform due to the prevalence of various tissue structures, and the theoretical method is difficult to apply and, therefore, a separate method such as the transmission method is employed.

Transmission Method Using Radioactive Sources: In the transmission method, typically a thin rod source containing a long-lived positron emitter (e.g., ^{68}Ge, $t_{1/2} = 270$ days) and extending along the axis of the scanner, is attached to the PET scanner gantry. The ^{68}Ge source on the gantry is rotated by an electric motor around the scanner, exposing all detector pairs to radiation uniformly. In some systems, point sources of ^{137}Cs ($t_{1/2} = 30$ years) are used. Two scans are obtained: a blank scan without the patient in the scanner and a transmission scan with the patient positioned in the scanner. Correction factors are calculated for each detector pair (i.e., each LOR) as:

$$\frac{I_0}{I} = e^{\Sigma \mu_i D_i}, \tag{3.7}$$

where I_0 is the blank scan data and I is the measured transmission scan data. These factors are then applied to all individual LOR counts in the sinogram obtained in the subsequent patient's emission study. However, the blank transmission scan need not be taken for every patient, rather a scan taken at the beginning of the day is good for all patients for the day. Note that the patient's transmission scan must be taken at each bed position during whole-body imaging for attenuation correction.

Using currently available rod sources, the above method requires the transmission scan to be taken before the emission scan and obviously requires a long time to acquire enough counts for good accuracy of the measured attenuation correction factors. An alternative to this approach is to collect the transmission scan postinjection immediately after the emission scan without moving the patient from the bed. This method obviates the need for patient repositioning and hence the need for correction for patient motion and misalignment. Although the residual activity is present from the radiopharmaceutical injection, its value along an LOR is

small and the high flux of the transmission source in a small volume along the LOR is enough to mask its effect. However, the detectors must be sufficiently efficient to detect both transmission and emission activities. A further reduction of transmission scan time has been possible by introducing a technique called the segmentation procedure based on the knowledge of prior μ-values of certain tissue types. The measured μ-values from the transmission scans are modified to match the closest allowed known μ-values. This method reduces the transmission scan time to several minutes.

CT Transmission Method: In PET/CT scanning, in addition to its use in fusion of PET and CT images, the CT transmission scan can be conveniently used to make attenuation correction of PET emission data. The CT scan takes a minute at the most, while the ^{68}Ge transmission scan takes as much as 20–40 min depending on the activity level of the ^{68}Ge source. Thus, it obviates the need for a separate lengthy ^{68}Ge transmission scan. Typically, a blank CT scan is obtained without the patient in the scanner, which is stored for subsequent use in the calculation of attenuation correction factors for patients' emission scans for the day. Next, the CT transmission scan of each patient is obtained and the map of the attenuation correction factors is generated from this scan and the blank scan using Eq. (3.7), which are then applied to correct each patient's PET scan.

The attenuation correction factor depends on the energy of the photons, and therefore, correction factors derived from ~70 keV CT X-ray scans must be scaled to the 511-keV photons of the PET by applying a scaling factor defined by the ratio of the mass attenuation coefficient of the 511-keV photons to that of the 70-keV X-ray in a given tissue. Here a mean energy 70 keV of the X-ray beam is assumed as the energy of a monochromatic beam that would give the same μ as the polychromatic beam averaged over all energies. This attenuation factor is assumed to be the same for all tissues that are considered to have the same mass attenuation coefficient except the bone, which has a slightly higher mass attenuation coefficient. The attenuation correction factors are calculated for each pixel and applied to PET emission data. The CT transmission method provides essentially noiseless attenuation correction factors. Figure 3.9 illustrates the effect of attenuation correction using the CT transmission scan on transverse whole-body images at the liver level. Various factors affect the CT attenuation factors that are discussed later in the chapter.

Random Coincidences

As already mentioned, prompt coincidence counts include random or accidental coincidences that raise the background on the images. Random events occur when two 511-keV photons from two separate positron annihilation locations are detected by a detector pair within the set energy and timing window (Fig. 3.1b). They increase with increasing energy window, coincidence timing window, and

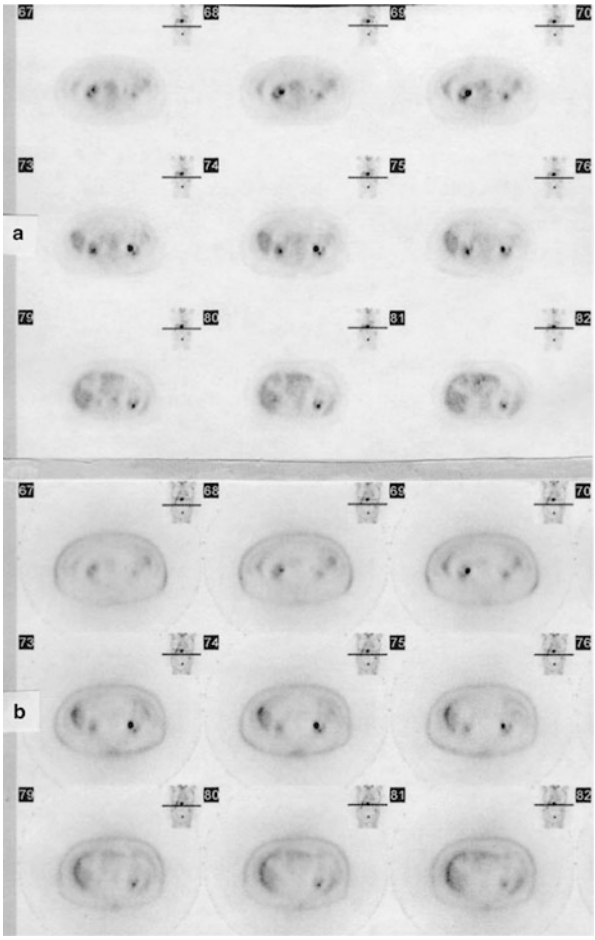

Fig. 3.9 Illustration of attenuation correction by using CT transmission data on transverse whole-body images at the liver level. (**a**) Attenuation-corrected images; (**b**) uncorrected images. Notice that the attenuation correction improves the images significantly showing better contrast and details

increasing activity [varies as the square of activity, see Eq. (3.8) below]. Random events add to the background causing artifacts and loss of image contrast and are more problematic in low-efficiency detectors such as thin NaI(Tl) crystals and in 3D counting.

Random coincidences (R) can be measured in two ways. In one method, the rate of random coincident events is given by

$$R = 2\tau \cdot C_1 \cdot C_2, \tag{3.8}$$

where τ is the time width of the pulses in nanoseconds for the system and C_1 and C_2 are the single count rates in counts/s on each of the two detectors along the LOR. The quantity 2τ is the coincidence timing window discussed in Chap. 2. Thus, one

calculates R by measuring the single count rate on each detector for a given time window and then corrections are made by subtracting it from the prompts between a detector pair. Random events measured by this method are affected by systematic errors associated with electronics in PET scanners. Note that random coincidence events vary with the square of the administered activity, whereas the true coincidence events increase linearly with the administered activity.

Efforts have been made to minimize random events by using the faster electronics and shorter time window, e.g., BGO system (12 ns), GSO and NaI(Tl) systems (8 ns), and LSO system (6 ns). Still, further corrections are needed to improve the image contrast. Note that crystals with shorter scintillation decay time also reduce the random coincidences, e.g., random events are less in LSO (70 ns) than in BGO (300 ns).

The second method of correction for random events is to employ two coincidence circuits—one with the standard time window (e.g., 6 ns for LSO) and another with a delayed time window (say, 50–56 ns) of the same energy window. The counts in the standard time window include both the randoms plus trues, whereas the delayed time window contains only the randoms. For a given source and at a set energy window, the random events in both time windows are the same within statistical variations. Delayed window counts are subtracted from the standard window counts to obtain the true coincidence counts, which are essentially free of any systematic errors associated with the PET scanner because they cancel by subtraction.

Scatter Coincidences

After annihilation of a positron, one or both 511 keV photons may undergo Compton scattering while passing through the body tissue, and because of the high energy most of these scattered radiations move in the forward direction without much loss of energy (Hoffman and Phelps 1986). Both scattered photons or one scattered photon and the unscattered 511 keV photon from the same annihilation event may be detected by the detector pair within the set energy and timing windows (Fig. 3.1c). Note that scattered photons from two separate events falling in the set energy and timing windows will be considered as random coincidences.

These scattered radiations increase the background to the image, thus degrading the image contrast. The scatter contribution increases with the density and depth of the body tissue, the density of the detector material, the activity in the patient, and the window width of PHA for the PET system. Since both scattered and true coincidence rates vary linearly with the administered activity, the scatter-to-true ratio does not change with the activity. Also, this ratio does not change with the width of the time window, because scatter events arise from the same annihilation event and the two similar photons arrive at the two detectors almost at the same time.

The pulse height window cuts off a large fraction of the scattered radiations, which is limited by the width of the window. In 2D acquisition, the use of septa in multiring PET systems removes additional scattered events, whereas in 3D acquisition, they become problematic because of the absence of septa. Typically, the scatter fraction ranges from 15% in 2D mode to more than 60% in 3D mode in modern PET scanners.

Correction for Scatter Coincidences

Correction for scattered events is essential, particularly for 3D acquisition of PET data, because of the loss of contrast and resolution in the image. A review by Zaidi and Koral (2004) provides an extensive account of scatter events in patient imaging and methods to correct them. Several methods have been applied for scatter correction, which are briefly described below.

Dual-Energy Method: In this method, coincidence counts are acquired in 3D mode in two separate energy windows—the photopeak window and a low energy window placed just below the photopeak window. An example of the energy selection is illustrated in Fig. 3.10 with 200–380 keV for the low energy window and 380–680 keV for the photopeak window. In the upper energy window, both scattered and unscattered photons are counted, whereas in the low energy window, mostly scattered photons and only a few unscattered photons are counted. Because there is a difference in counting efficiencies in the two energy windows, a scaling factor is applied to correct the counts. Two scaling factors are derived from

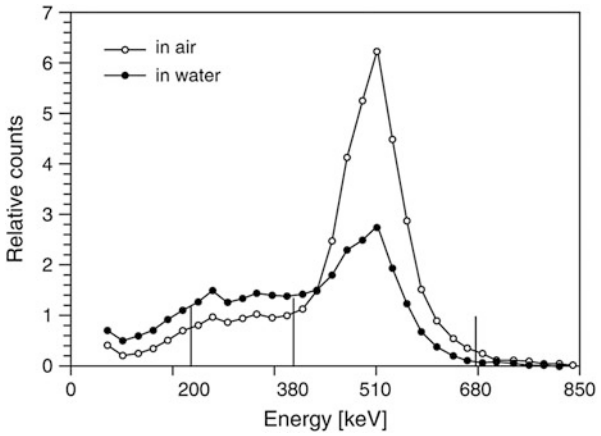

Fig. 3.10 Setting of lower and upper energy windows in the energy spectra of a scanner for a line source in air- (*open circle*) and in a water-filled cylinder (*filled circle*). The energy spectrum from water-filled phantom shows scattering of photons (Reprinted with the permission of the Cleveland Clinic Center for Medical Art and Photography ©2009. All rights reserved)

measurements using a line source (1) in the air at the center of the scanner and (2) in a water-filled brain phantom positioned at the center of the scanner. The ratio of counts in air in the two windows is due to unscattered events, while the ratio in the water-filled phantom is due to scattered events (Fig. 3.10). These two ratios (i.e., scaling factors) are applied to scale the measured data in both windows, and subtraction of the two scaled energy window data results in a distribution of scatter in the upper energy window. The latter is smoothed and then subtracted from the measured upper energy window data to yield scatter-corrected sinogram for reconstruction of PET images. The scaling factors derived from measurements in air- and water-filled phantom should remain constant for all patients, but in reality they vary with the source geometry (e.g., patients of different sizes)—a definite problem in whole-body imaging.

An extension of the dual-energy method is the use of triple windows in which three windows are chosen with two overlapping windows of different width having the same upper energy level located below the lower level of the photopeak, which is centered on 511 keV. Data are obtained for the object and a calibration phantom. A calibration factor is calculated from the ratio of counts in the two lower scatter windows for both the calibration phantom and the object. The scatter contribution to the photopeak is then estimated from the calibration factor and the narrower energy window data. This method works well for a wide range of activity distribution and object sizes.

Fitting to Scatter Outside the Object: In this method, the scatter is estimated by fitting an analytic function (Gaussian or parabolic) to the activity outside the source and interpolating the function to the source. The interpolated scatter contributions are then subtracted from the measured source counts to obtain scatter-corrected data for reconstruction of PET images. This method is based on the assumption that (1) the events outside the source are only scatter events, (2) the scatter distribution is a low-frequency function across the FOV, and (3) they are independent of activity distribution in the source.

Convolution Method: A point source is used to measure the scatter function, which is then used to convolve with the source distribution to give an estimation of scatter data. An iterative method is used so that after each iteration, the scatter estimate is improved. The best estimates of scatter events are scaled and then subtracted from the measured image data. The measured scatter function takes into account its dependence on the location and size of the source, detection angle, etc., and thus improves the scatter estimation. This method is computationally efficient because of the availability of fast algorithms.

Calculation/Simulation Method: In this simulation technique, Monte Carlo calculation is employed to separate the scattered and unscattered events from the measured events. Initially filtered backprojection is applied to the measured emission data to obtain the true reconstructed image of the source. This input image is considered as the 3D source activity distribution for photon tracking in the Monte Carlo simulation, in which the volume planes of the image are stacked and

positioned appropriately in the simulated scanner geometry, assuming a common axis. The algorithm then tracks the interaction of each photon in the scattering medium (e.g., patient) and its detection in the block detectors in a simulated 3D PET acquisition. The distribution of total events and scattered events is calculated and the corresponding sinograms are generated. The scatter data are smoothed and then subtracted from the measured data to give the unscattered data. The unscattered data may contain some random events which need to be corrected separately. This method is the most accurate of all methods, but obviously it does not take into consideration the scatter from outside the source.

Dead-Time Loss

When a 511-keV photon interacts within the detector and is absorbed in the crystal, light photons are produced, which strike the photocathode of the PM tube. A pulse is generated at the end of the PM tube and amplified by an amplifier; the energy and the spatial position of the photon are determined and finally a count is recorded. When two such events are detected by two detectors in the time window, a coincidence event is recorded.

The total time required to complete the above steps is defined as the *dead time* (τ) and is related to the signal integration time that depends on the electronics and the scintillation decay time. During this time the detection system is unable to process a second event, which will be lost. This loss (called the dead-time loss) is a serious problem at high count rates and varies with different PET systems. It is obvious that the dead-time loss can be reduced by using detectors with shorter scintillation decay time and faster electronics in the PET scanners.

Successive pulses during dead time can be processed in two ways: paralyzable and nonparalyzable. In a paralyzable counting system, each event sets its own dead time even if it arrives within the dead time of the previous event and is not counted. The second dead time is added to the previous one thus prolonging the total dead time. This conceivably can make the counting system unresponsive at high count rate. In a nonparalyzable system, however, the instrument cannot process a second event if it arrives within the dead time of the previous event and the dead time remains the same for the system. A subsequent event is counted only after the previous event is processed and counted and the system has recovered. The dead-time loss of counts occurs more rapidly in a paralyzable system than in a nonparalyzable system as illustrated in Fig. 3.11. The following equations represent these two systems:

For paralyzable system,

$$R_t = R_o/(1 - R_o\tau) \tag{3.9}$$

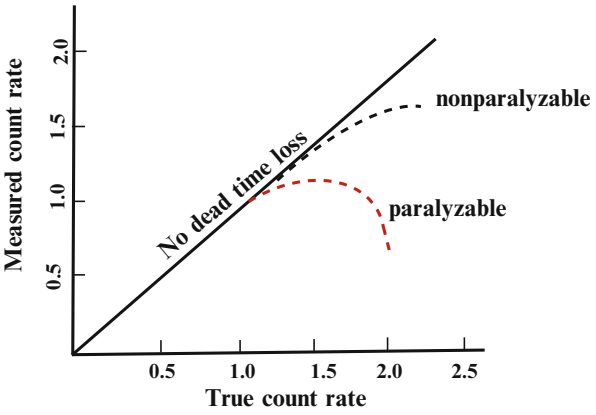

Fig. 3.11 An illustration of paralyzable and nonparalyzable dead-time loss in counting systems. One empirical way to correct for the dead-time loss is to extrapolate the low activity data by a straight line to high activity data (*solid line*) to obtain the true counts

For nonparalyzable system,

$$R_o = R_t e^{-R_t \tau} \tag{3.10}$$

where R_t is true counts, R_o is observed counts, and τ is the dead time of the system. A counting system or its components can have either or both paralyzable and nonparalyzable components.

In a different scenario of scintillation counting, two 511-keV photons may arrive at and be absorbed completely in the detector simultaneously and, therefore, a photopeak of 1.022 MeV will be produced, which will fall outside the energy window of 511-keV photopeak. However, normally the energy window in PET is usually set quite wide. If two Compton scattered photons or one 511-keV and one scattered photon are summed up simultaneously in the detector and the resultant peak falls within the window, then the event will be counted but mispositioned, because of the two unrelated events. These events are called the *pulse pileups*, which cause image distortion at high count rates.

Dead-time correction can be made by empirical measurement of observed count rates as a function of increasing concentrations of activity (Fig. 3.11). From these data, the dead-time loss is compensated by extrapolating the low activity data to obtain the true counts at higher activities, as given by the solid line in Fig. 3.11. Another method uses two radioactive sources of similar activities, which are counted individually and together. From these three measurements, one can calculate the dead time using appropriate equations (see Cherry et al. 2012) and then using it in Eqs. (3.9) and (3.10). Other techniques, such as use of buffers, in which overlapping events are held off during the dead time, use of pulse pileup rejection circuits, and use of high-speed electronics, have been applied to improve the dead-time correction.

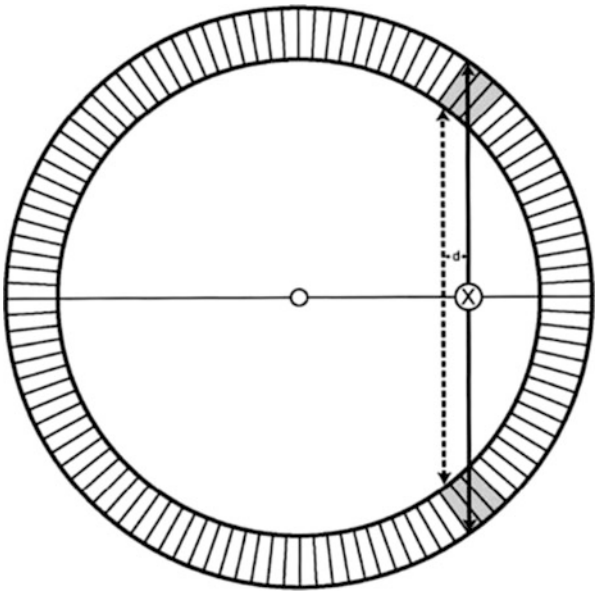

Fig. 3.12 An illustration of depth of interaction effect. An off-center event (*solid line*) strikes the back of the detector pair tangentially. The *X*, *Y* positioning of the detectors (*dash line*) is a distance *d* away from the actual location of the positron annihilation, causing the blurring of the image (Reprinted with the permission of the Cleveland Clinic Center for Medical Art and Photography ©2009. All rights reserved)

Depth of Interaction

Depth of interaction (DOI), also called the detector parallax, occurs when two 511-keV photons originating from an off-centered annihilation event strike tangentially at the backside of the detector pair and are counted as a coincidence event (Fig. 3.12). As can be seen, the photon may cross one or two detectors before it is detected in a final detector. But it is not known how deep in the crystal the event occurred. In conventional PET studies, reconstruction algorithm assigns the interaction positions over all depths in the crystal to a single LOR connecting the centers of interacted detector pair. The apparent location of the LOR is shown by the dashed line, a distance *d* away from the actual LOR (solid line) (Fig. 3.12). The fact that the event can occur deeper anywhere in the crystal and lack of this DOI information causes uncertainty in the exact location of photon interaction and it is incorrectly positioned on an LOR toward the center of the FOV. This degrades the spatial resolution of the image. As can be understood from geometrical considerations, this (DOI) effect worsens significantly with thicker detector and smaller detector ring of the PET scanner, degrading the spatial resolution of the image. A major effort in research is being made to accurately determine the DOI for improvement in the spatial resolution.

Depth of interaction effect can be minimized by several factors such as a larger diameter of the ring, high stopping power of the detector material, and appropriate design of the detector. Larger diameter of the detector ring reduces the probability

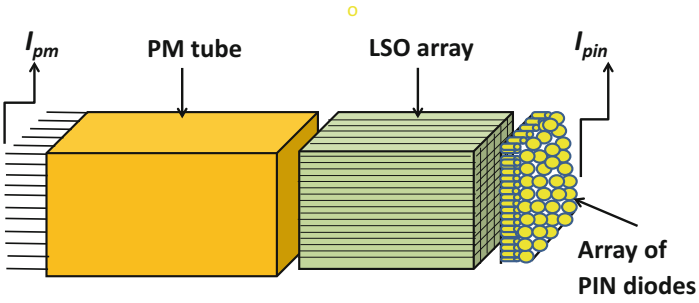

Fig. 3.13 Depth of interaction correction using dual photodetector readout approach. The array of LSO crystals are connected to a PM tube on one end and to an array of PIN diodes on the other. The pulses I_{PM} and I_{PIN} from the two ends are used to calculate the depth of interaction

of tangential crossing of several crystals by the annihilation photons and hence lessens the DOI effect. However, to employ larger diameter rings is a matter of a practical and logistic decision made by the manufacturers. Current detector materials such as LSO, LYSO, $LaBr_3$, etc., with high stopping power have improved the accuracy of detection of the pulse.

The major emphasis for DOI correction is on the design of detector modules for PET scanners. Decades ago, determination of DOI was not possible for various reasons (namely, timing discrimination) and could not be incorporated in PET scanners. Currently several major directions are being pursued for DOI determination, namely, dual photodetector readout, phoswich detectors, and segmented crystals, and readers are referred to two excellent review articles by Humm et al. (2003) and Lewellen (2008) for details. Briefly, in the dual photodetector readout approach, a pixelar array of crystals is coupled to a single-channel PM tube at one end and to an array of PIN diodes at the other. The DOI is calculated from $I_{PIN}/(I_{PIN}+I_{PM})$, where I_{PIN} and I_{PM} are pulses from PIN diodes and PM tubes, respectively (Fig. 3.13).

Phoswich fabricated with two detectors of different scintillation decay times has been described in Chap. 2. Phoswiches have also been made of more than two stacked scintillators of different decay times including BGO, LSO, and GSO, although the latter two are commonly used for reasons of higher photon yield. When 511-keV photons strike the different layers of the phoswich, pulses of varying time widths and heights are produced in different layers, which are then separated by a pulse-shape discriminator to determine the location of interaction (DOI) in a layer.

In another basic approach, similar to the dual photodetector readout method, photosensors are placed at both ends of the crystal, which measure the light produced by the interaction of 511-keV photons in the crystal. The intensities of light at the two ends vary with the depth of the photon interaction in the crystal and the ratio of the light intensities from the two sensors determines the DOI.

PET/CT Data Acquisition

Because of the increased sensitivity, specificity, and accuracy in detecting various tumors, fusion imaging using the PET/CT modality has become the state-of-the-art technique in the imaging field. Because the patient remains in the same position on the bed, the alignment and fusion of the CT (anatomical) and PET (functional) images greatly improve the detection of lesions. For these reasons, PET/CT scanning is widely used in diagnostic oncologic applications. As discussed later, CT scans are also used for attenuation correction of PET emission data.

Data acquisition in PET/CT is performed in two steps: first, CT scan and next, PET scan. In a typical PET/CT protocol, a patient is injected with the PET tracer (normally, ^{18}F-FDG) and allowed to wait for 45–60 min. Waiting for a period shorter than this gives poor target-to-background ratios. After the waiting period, an initial scout scan (topogram) like a conventional X-ray is obtained of the patient during the continuous table motion toward the gantry to define the axial extent of the torso to be imaged. Next, the patient is moved to the CT field of view and a transmission scan is obtained, which takes only a short period of less than a minute. During the CT scan, the patient is asked to hold his breath or, if unable, to breathe in a shallow manner to minimize motion artifact. After the CT scan is completed, the bed with the patient on it is advanced inside the PET scanner and positioned so that the PET scan field matches the CT scan field. During the PET data acquisition, the CT scan data can be concurrently used to calculate the attenuation corrections (see later) and to reconstruct the CT images. After the completion of PET data acquisition, data are corrected for attenuation, and PET images are reconstructed as described in Chap. 4. The CT and PET images are then fused using appropriate algorithms for precise localization of abnormalities. The typical time for the entire protocol for PET scanners using BGO detectors is about 30 min. This is because CT-based attenuation factors can be generated in 30–40 s compared to 30 min for ^{68}Ge transmission scan. This can be further reduced by using faster crystals such as LSO and LYSO and also TOF technique. A typical study involving the fusion of transverse PET and CT images demonstrating non-small cell lung carcinoma is illustrated in Fig. 3.14.

The PET/CT scanning is very useful in equivocal clinical situations, particularly in whole-body imaging for tumor detection. A very small tumor is well detected by PET but can be missed by CT. On the other hand, a large tumor with minimal functional deviations may be seen on a CT image but may not be detected by PET. In both situations, PET/CT would localize the tumor accurately. Overall, accuracy of diagnosis is increased by 20–25% when PET/CT is used instead of either alone. It should be noted that at present, while PET/CT whole-body scanning has been highly successful in detecting various oncologic conditions, the application of PET/CT in cardiac imaging has faced challenges because of the motion of the heart. Sophisticated algorithms, however, have been designed to overcome this difficulty to an extent.

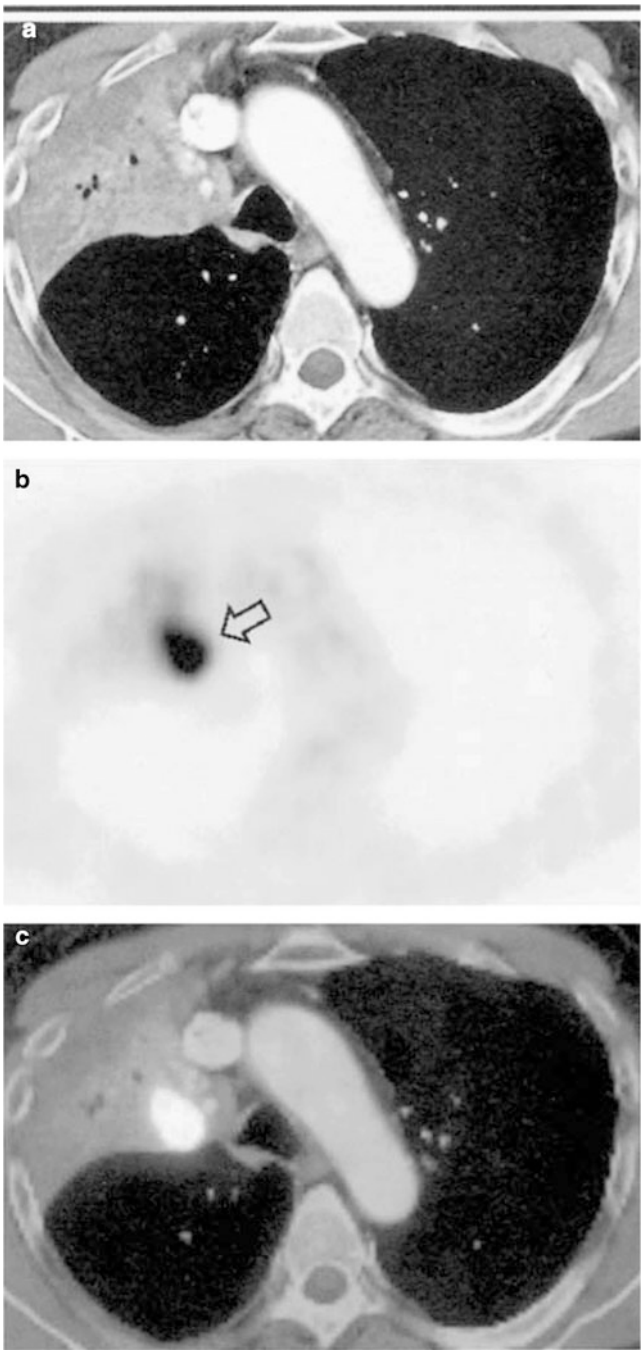

Fig. 3.14 A study showing the fusion of PET and CT images. Transverse (**a**) CT, (**b**) PET, and (**c**) PET/CT fused images showing non-small cell lung carcinoma in the right upper lobe. On PET/CT image, the tumor is accurately demonstrated, which is well differentiated from pulmonary atelectasis (Reprinted with permission from: Antoch G et al (2003) Non-small cell lung cancer: dual modality PET/CT in preoperative staging. Radiology 229:526)

Factors Affecting PET/CT Data

Although PET/CT modality is widely employed for diagnostic purpose, CT data acquired either for fusion of PET and CT images or for photon attenuation correction are affected by several factors that cause artifacts in PET/CT images. The factors include patient positioning, metal objects, CT contrast agents, truncation artifacts, and respiratory movement, which are discussed below.

Positioning of Patient

In patient positioning, questions arise if the patient should raise up or down the arms on the sides. For scanning the thoracic, abdominal, and pelvic areas, the arms are raised to eliminate hardening of the beam and scatter artifacts and also to avoid unnecessary exposure to radiation. But for head and neck scanning, the arms are kept down on the sides to avoid the shadow of the arms in the image of the area. Likewise, the knee should be supported by proper resting aids such as vacuum bags or foam pellets to avoid any artifact.

Metal Object

Metal objects, such as dental fillings, jewelries, prosthesis, etc., cause higher attenuation of photons than tissues showing artifacts in the photopenic areas. This effect is prominent with low-energy X-rays than with high energy 511-keV photons, because of the greater photoelectric absorption of the former in the high Z metals. Mismatch occurs between the CT scans containing such artifacts and the PET scan, and proper fusion cannot be made. If CT data are also used for attenuation correction, the attenuation factors calculated from these scans are overestimated leading to corresponding overestimation of activity in the region and thereby creating a false-positive finding on PET images (Fig. 3.15). Often, it is advisable to omit attenuation correction in these cases as more representative images are obtained without correction. Over the years, reconstruction algorithms have been developed and metal artifacts have been almost eliminated.

Contrast Agent

In recent years, in addition to its use in fusion and attenuation correction, the CT unit in PET/CT systems has been used for diagnostic purposes, and for these CT scans, contrast agents are often recommended for better diagnostic accuracy. When

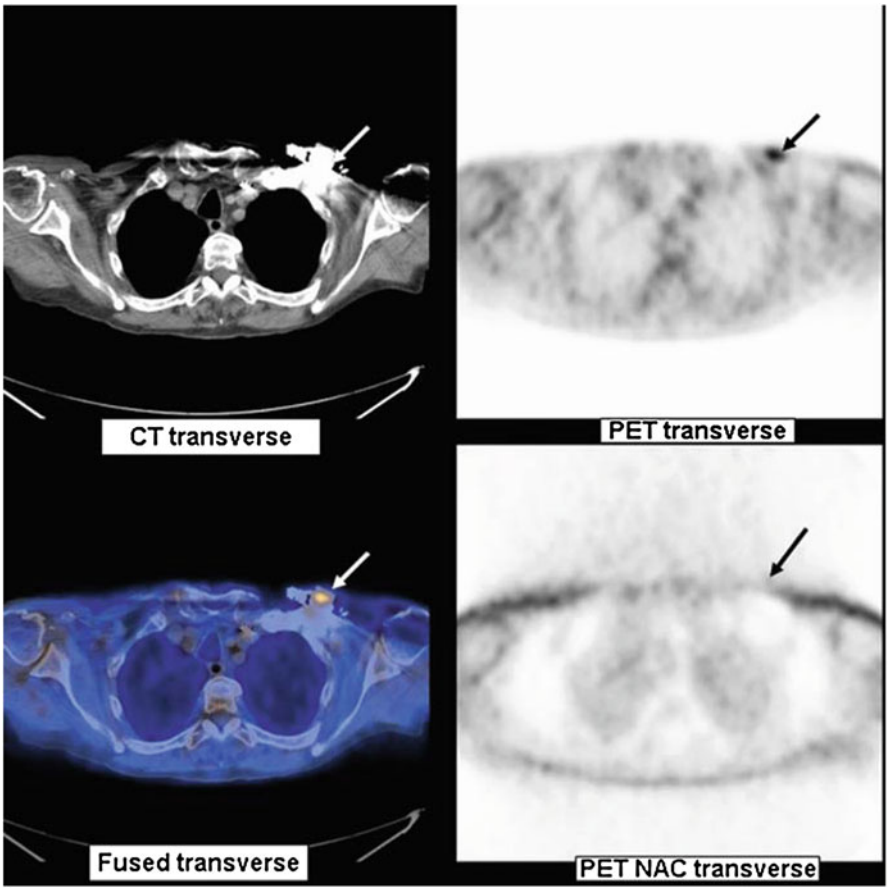

Fig. 3.15 Illustration of overestimation of attenuation due to a pacemaker showing focal uptake in the chest area (Reprinted with permission from Parker et al at the Web site, http://www.jpnm.org)

intravenous or oral iodinated contrast materials are administered for diagnostic CT studies, they accumulate in body tissues or organs, which absorb photons more than in normal tissues or organs causing a greater attenuation in tissues than without the contrast agent and so artifacts are generated. However, such effects are minimal in PET images due to high energy of photons. If these CT scans with contrast agents are used for attenuation correction in PET/CT studies, attenuation correction factors will be overestimated causing an overestimation of activity in the region, thus producing false-positive PET scans (Fig. 3.16). These artifacts, however, depend on the quantity of contrast agent administered, its biodistribution and blood clearance, and time between administration and CT scan. Practically, artifacts due to intravenous contrast agents are found to be insignificant perhaps due to its rapid dispersion in the blood. On the other hand, after administration, the in vivo concentration of oral contrast agents increases due to water reabsorption causing

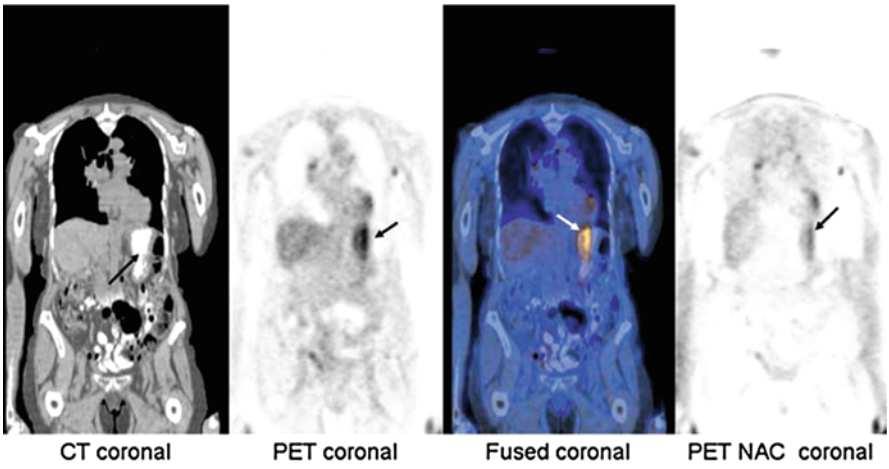

Fig. 3.16 Illustration of the effect of contrast agents on PET/CT scans. Attenuation correction factors are overestimated in tissues where contrast agent localizes and thus results in false-positive scan (Reprinted with permission from Parker et al at the Web site, http://www.jpnm.org)

artifacts. Modified energy scaling methods have been employed in some studies to separate the contrast-enhanced voxels from bone pixels, thus nearly eliminating such artifacts. Some investigators have advocated, and many have followed, to avoid altogether the use of contrast agents in low-dose CT for attenuation correction. Also the use of water-based negative contrast agents has been suggested, which would eliminate such artifacts entirely. It should be pointed out that CT has to be operated at high kV and mAs, where the radiation dose to the patient remains high compared to that in the low-dose CT scan for attenuation correction and localization.

Truncation Effect

Another factor, called truncation factor, arises from the difference in transverse FOV of the CT and PET scanners. CT scans of the abdomen and thorax are acquired with arms raised above the head and neck outside the CT FOV. However, in PET scanning, such holding up of arms for 30–40 min is uncomfortable to patients and so scanning is performed with arms on the side. While the patient port in PET/CT scanners varies from 70 to 85 cm depending on the manufacturer, the transverse FOV of the CT scanner is ~50 cm and that of the PET scanner is ~60 cm. Because of the difference in FOV, in the PET/CT scanning with arms down, some angular CT projections may be truncated. For very large patients, other parts of the body also maybe truncated. As a result, the attenuation correction factors are zero in the region between the edges of CT FOV and PET FOV meaning an underestimation of

the real values. Also there is a streaking artifact (high activity seen as a ring) at the edge of CT image, which results in overestimation of attenuation factor in this region leading to potential misinterpretation of the PET scan.

A simple method of recovering the truncated data is to linearly extrapolate the truncated CT projections to the extent of PET FOV and then setting the values to zero at the edge of the PET FOV. The attenuation correction by this method is adequate to remove the truncation artifacts in PET/CT images (Fig. 3.17). Using the iterative method rather than the filtered backprojection technique also has shown to help eliminate these artifacts.

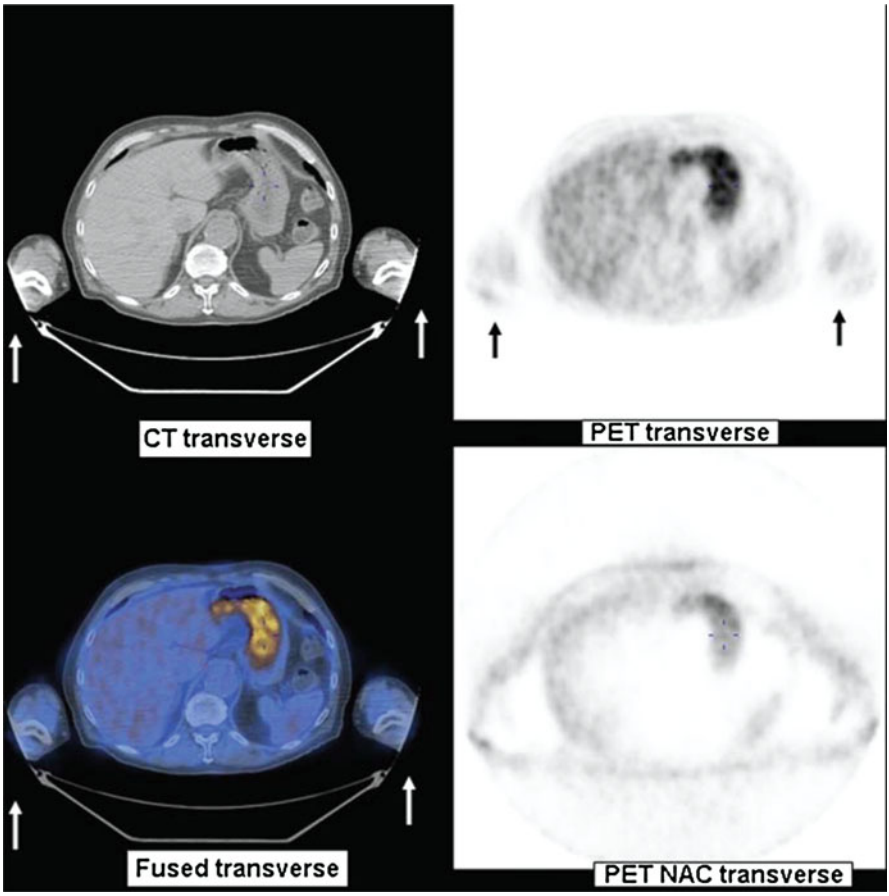

Fig. 3.17 Effect of truncation on attenuation correction due to difference in patient port diameter between CT (~50 cm) and PET (70–85 cm) scanners. CT attenuation factors are extrapolated to the extent of the PET FOV to correct for the truncated area (Reprinted with permission from Parker et al at the Web site, http://www.jpnm.org)

Respiratory Movement

In PET/CT studies, respiratory movement causes mismatch in fusion of CT and PET images in the abdomen or chest areas due to displacement of their positions on the two images. CT scans are normally acquired in short time (less than a minute) with breath hold at full inspiration during which the diaphragm is displaced downward because of the expansion of the lungs and the diaphragm appears to be filled with air. On the other hand, PET scans are acquired over a long time (20–40 min) while the patient is freely breathing. This results in a PET image that represents an average of many breathing cycles and the diaphragm appears in the normal position. The CT attenuation in the diaphragm area is underestimated because air is considered in its place during CT scan, and so attenuation-corrected PET images will show cold spots in this region. The discrepancy in anatomical positions between CT and PET scans caused by respiratory motion results in artifacts in the fused PET/CT image (Fig. 3.18). Several protocols have been advocated to minimize this error, namely, (a) continuous shallow breathing for both CT and PET scans, (b) breath-hold CT with partial inspiration, (c) motion-averaged CT over many respiratory cycles, (d) respiratory-gated CT and PET, and so on. Of all these, shallow breathing for both CT and PET techniques is now widely used to minimize the artifacts. With the inclusion of multidetector CT in PET/CT scanners, respiratory motion artifacts have been greatly reduced, but the exact match of the CT and PET image still remains elusive.

Currently, 4D imaging involving gating of the respiratory cycle, similar to the cardiac-gated technique, has been carried out and a vast improvement in the fusion of PET and CT images has been achieved. In this technique, CT data covering the

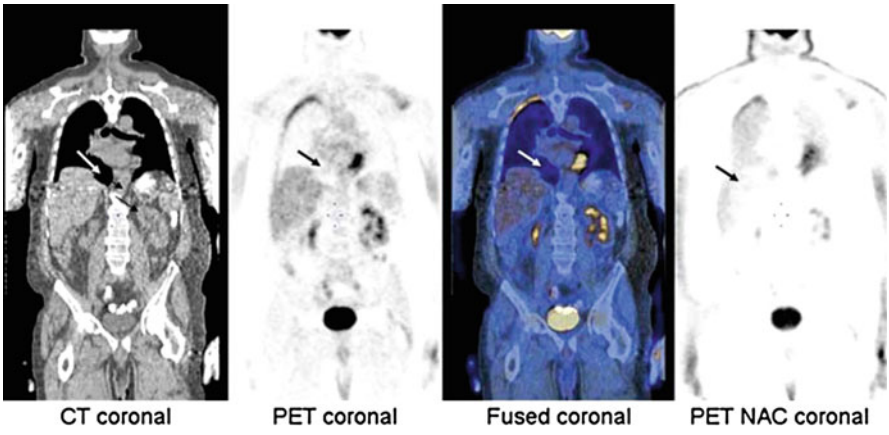

Fig. 3.18 Effect of respiratory movement on fused PET/CT image showing a cold spot due to low attenuation in the area of the displaced diaphragm during breath-hold CT scan (Reprinted with permission from Parker et al at the Web site, http://www.jpnm.org)

whole lung axially are obtained in a "step-and-shoot" manner in a cine mode usually for each breathing cycle at each bed position. Similarly gated PET data are acquired in ten 0.5-s bins for about 10 min. A real-time position management equipment monitors the respiratory cycle and triggers the acquisition at the expiration phase. The time of the trigger and the acquired data are stored in the computer, which are then used for image reconstruction.

PET/MR Data Acquisition

Because of the absence of radiation exposure in MR systems and also better localization of abnormalities in tissues, PET/MR scanners have drawn considerable attention in medical imaging. Data acquisition with hybrid PET/MR scanners depends on the arrangement of the two scanners and is performed in two ways. In sequential imaging, as in GE Healthcare and Philips Healthcare units, PET/CT scanning is first performed followed by MR imaging and hence a longer imaging time is required. On the other hand, in simultaneous imaging as in Siemens Healthcare scanner, both PET and MR data are acquired simultaneously thus reducing the scanning time. In both techniques, a variety of protocols have been developed with respect to the timing, patient positioning, organ or whole-body scanning, duration of scanning, attenuation correction, etc. A thorough understanding of the operation of PET and MR scanners is required prior to the scanning of the patient. Particular attention must be given to the choice of MR pulse sequences appropriate for a given study. With FDG studies, a waiting time of about 40–60 min is required for uptake, which is prudently utilized by having the MR scan done during this time. Hence, patients do not have to stay any longer for PET/MR scanning than for standard PET/CT scanning.

In sequential imaging, MR imaging is first performed on a patient lying on a rotatable table followed by PET imaging of the patient in the same position but with the table rotated to the PET scanner (Philips Healthcare scanner). MR imaging time varies with the choice of pulse sequence and can vary between 30 and 60 min. In GE Healthcare trimodality unit, MR imaging is performed and then PET/CT images are obtained by shuttling the patient to a separate room where the PET/CT unit is installed. In both systems, PET data are collected in sinograms and MR data in matrix format in the computer. Using appropriate algorithms, coregistration of the images are made, but its accuracy suffers from misalignment due to variation in patient position. CT in GE model offers conventional attenuation correction but gives additional radiation dose to the patient.

In simultaneous whole-body PET/MR imaging using FDG, imaging starts after the uptake period of 40–60 min and both MR and PET images are acquired simultaneously. Although PET imaging requires only 20–30 min, MR scan may require much longer time depending on the choice of pulse sequences. Prior to whole-body imaging, MRI localizers, similar to a scout scan or a topogram in

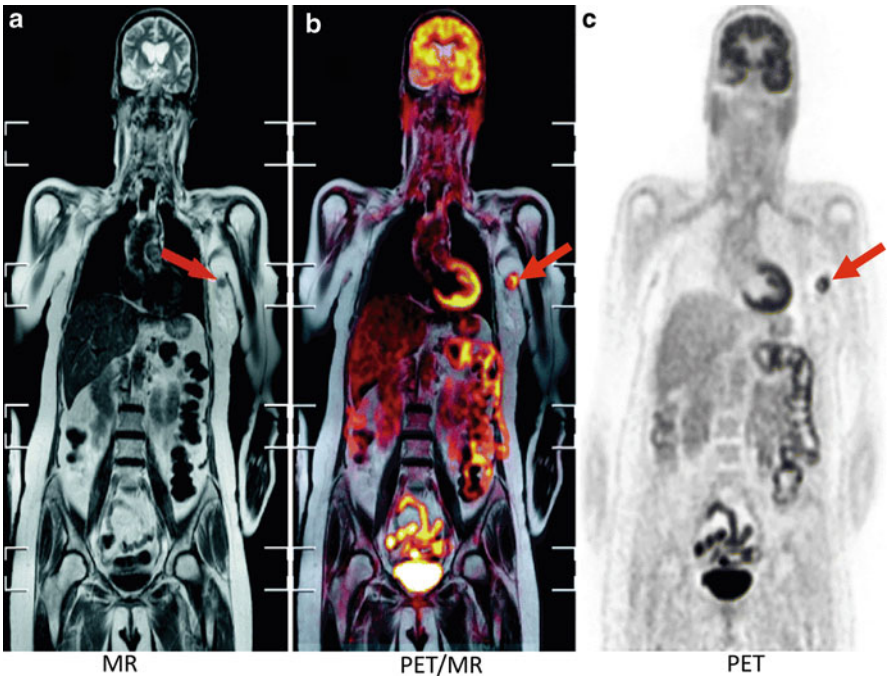

Fig. 3.19 PET/MR image (**b**) obtained by fusion of T2-weighted MR image (**a**) and FDG-PET image (**c**) illustrating the left axillary nodule indicated by *red arrows*. (Fig. 6.5 in Tabouret-Viaud C, Baskin A, Beer AJ et al. Breast cancers. In: Ratib O, Schwaiger M and Beyer T, eds. (2013) *Atlas of PET/MR Imaging in Oncology*. New York, Springer; p. 91. With kind permission from Springer Science and Business Media)

PET/CT, are obtained to define the axial range of scanning. Then the number of bed positions in the axial range and time of scanning for each must be chosen. Typically 2–4 min of data acquisition per bed position is used. Attenuation correction data for PET images are derived from the MR scan and are discussed below. Functional PET and anatomical MR images are then fused for accurate delineation of abnormal lesions. Figure 3.19 illustrates the fusion of PET and MR images of a patient demonstrating the left axillary nodule.

Factors Affecting PET/MR Data

Various factors that affect the PET/CT data discussed above also affect the PET/MR data, because most of them arise from PET scanning. The major artifact arises from attenuation correction (AC) applied to PET data, which is calculated based on MR scans.

Attenuation Correction

Unlike in PET/CT, attenuation correction in PET/MR is a challenging issue because MR units do not have radiation to be attenuated and a transmission source cannot be installed due to space constraint in the MR machine, so different approaches are pursued to apply attenuation correction (AC) to PET data in PET/MR imaging. An excellent review of MR-based ACs has been presented by Bezrukov et al. (2013). All approaches involve the creation of a map of MR-based attenuation correction (MRAC) factors, which are subsequently applied to PET images. Basically three categories of MRAC methods that have drawn considerable attention are template based, segmentation based, and atlas based. Each of these techniques is briefly discussed below.

Template-based MRAC: In this method, the basic principle is to create an attenuation map template and a coregistered MR image template. The attenuation map template is constructed using an average of AC values obtained from several patient transmission scans such as ^{68}Ge-source transmission scans. A T1-weighted MR image is used as the T1-weighted MR template. First, an MR image of the patient under study is obtained, which is warped to the MR template by nonlinear registration to derive the attenuation map. This nonlinear transformation is then applied to the attenuation map template to generate an individualized attenuation map for the PET image of the patient. Investigators have used different numbers of patients in collecting the average transmission scan.

Segmentation-based MRAC: In this method, a T1-weighted MR image is segmented into several tissue regions of importance, and then known linear attenuation coefficients (μ) are assigned to each region to calculate PET attenuation corrections using Eq. (3.5). Segments are categorized as air, brain tissue, soft tissue, lungs, bone, sinus, fat, etc., and two or more of these segments are chosen for a particular study of interest. An MR image, rather than a PET image, is used because it depicts the anatomical features better than the PET image which is more of a functional image. MR images offer excellent delineation of soft tissues, but bone and air cavity produce no appreciable MR signal by conventional MR pulse sequence and are not distinguishable on MR images. However, 511-keV photon attenuation is highest in the bone and almost none in air. So a plausible μ value is assigned to the bone, relative to the air.

Atlas-based MRAC: In this method, the attenuation maps are generated by deforming a single template image to match the patient anatomy or averaging multiple coregistered attenuation template data sets. Often database in the form of an atlas is generated from CT data, which is then used to obtain attenuation maps. Because of the anatomical variability in patients, the atlas approach is more challenging to apply in whole-body imaging than in brain imaging.

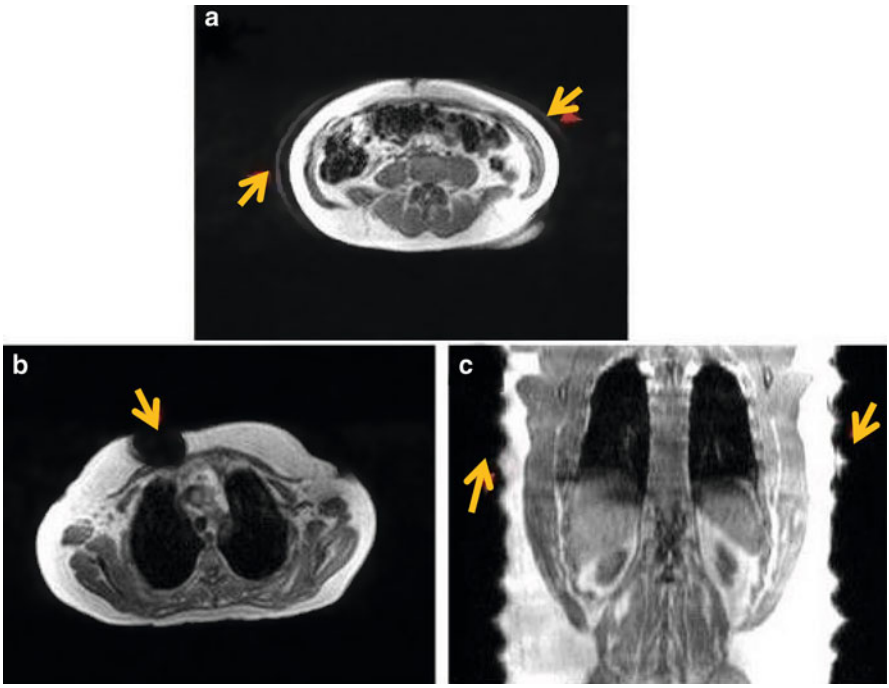

Fig. 3.20 (**a**) Respiration motion effect. (**b**) Presence of metal object. (**c**) Body truncation effect. Defects are indicated by *orange arrows*. (Fig. 6 from David Izquierdo-Garcia; Stephen J. Sawiak; Karin Knesaurek, et al. (2014) Comparison of MR-based attenuation correction and CT-based attenuation correction of whole-body PET/MR imaging. *Eur J Nucl Mol Med Imaging* 41:1574. With kind permission from Springer Science and Business Media)

Respiratory Movement

Although simultaneous acquisition of both PET and MR data essentially nullifies the effects of respiratory motion, occasional motion artifacts are not unusual and the patient should be advised to have continuous shallow breathing during imaging to minimize the effect. A case of respiratory motion effect on an MR image is illustrated in Fig. 3.20a.

Metal Object

MR scans show metallic objects such as dental fillings, implants, etc., as cold spots due to loss of MR signals (Fig. 3.20b). In tissue classification, these areas are assigned as air instead of tissues in MRAC map generation using the segmentation technique described above. AC values calculated using this map are likely to be

underestimated. One needs to keep this information in mind while fusing the two sets of images and interpreting the results.

Truncation Effect

Truncation effect results from the difference in effective transverse FOVs of MR and PET scanners (Fig. 3.20c). This value of MR scanners is much smaller than the patient body cross section. As explained above under "Factors Affecting PET/CT Data," MR scanning will result in truncated images of the body parts, if the patient lies on the table with arms down during scanning, which is commonly done by the patient for comfort. As a result, the alignment of PET and MR images becomes inaccurate, and more importantly, the MR-based attenuation map may be erroneous. Methods of compensating for the truncation effect have been implemented, one of which employs the linear extrapolation of the MR projections up to the edge of the PET FOV where the AC value is assumed to be zero.

Questions

1. Describe how a sinogram is generated in PET data acquisition.
2. Each pixel in a sinogram is represented by:

   (a) r, ϕ coordinates of the coincidence event
   (b) X and Y coordinates of the coincidence event
   (c) (X, Y, Z) coordinates of the coincidence event

3. The location of the LOR is defined by:

   (a) r, ϕ coordinates of the coincidence event
   (b) X, Y positions of the detector pair
   (c) X, Y, Z positions of the coincidence event

4. A sinogram is a (a) file containing individual annihilation events, (b) a matrix of parallel projection data, (c) a matrix of fan-beam projection data, and (d) reconstructed image.
5. A PET scanner has a FOV diameter of 20 cm. If a 64×64 matrix is used for data acquisition, what is the pixel size?
6. In whole-body PET imaging, scanning is performed at 5–7 bed positions to scan the intended axial length of the body. At each bed position, there is an overlap of 3–5 cm between scans of two bed positions. Why?
7. In whole-body PET imaging, the overlap of bed positions is larger in 3D acquisition than in 2D acquisition. True ___; False ___.
8. The 2D PET data acquisition is accomplished in a PET scanner by the use of (a) parallel-hole collimator, (b) lead shield, (c) tungsten septa, or (d) concrete.

9. Explain the direct plane events and cross plane events in 2D data acquisition. What is the total number of sinograms that can be generated in a scanner with *n* rings?
10. The sensitivity in 3D acquisition is 4–8 times more than that in 2D acquisition. What are the disadvantages with these high counts, and how can you overcome them?
11. Explain five important factors that affect fusion imaging by PET/CT. What methods are adopted to mitigate these effects?
12. Attenuation of 511-keV photons in body tissues primarily affects (a) uniformity of the image, (b) spatial resolution of the scanner, and (c) sensitivity of the scanner.
13. Attenuation of the two 511-keV photons arising from positron annihilation in an organ is independent of the location of the annihilation event but depends on the total thickness of tissue the two photons traverse. True ___; False ___.
14. Describe a method of attenuation correction for PET acquisition data.
15. If one of the two 511-keV photons arising from annihilation in an organ traverses through a thickness of 2.2 cm of the organ and the other photon traverses 1.8 cm of the organ, what is the attenuation correction factor? (Linear attenuation coefficient of 511-keV photons in tissue is 0.5 cm^{-1}.)
16. In PET/CT, attenuation correction factors are calculated based on the CT transmission scan that uses ~70 keV X-rays. What is done to correct for attenuation of 511-keV annihilation photons?
17. Attenuation correction in PET is independent of the depth of tissue the two annihilation photons traverse. True___; False ___.
18. FDG images without attenuation correction will show: (a) increased activity at the center, (b) reduced uptake at the center, or (c) uniform activity all over the image.
19. In the time-of-flight technique, calculate the increase in signal-to-noise ratio (sensitivity) for a subject of 50-cm diameter and a timing resolution of 0.6 ns.
20. Contrast agents used in the CT part of PET/CT imaging cause overestimation of attenuation correction in PET images. True ___; False ___ Explain why.
21. Describe the method of normalization of the acquired PET data to correct for nonuniformity due to variations in the gain of PM tube, location of the detector in the block, and physical variation of the detectors.
22. Random events can be reduced A: by (a) narrowing or (b) increasing the coincidence time window; B: by (a) increasing or (b) decreasing the activity administered, C: by (a) widening or (b) narrowing the energy window, and D: by crystals with (a) shorter or (b) longer scintillation decay time.
23. Random events can be reduced by

    (a) increasing the scan time. True_____; False _____
    (b) using a denser crystal. True____; False____

24. Describe the methods of correction for random coincidences and scatter coincidences in the acquired data for PET images.
25. What are the contributing factors for the scatter coincidences in PET images?
26. Indicate how the true, random, and scatter coincidences vary with activity:

    (a) linearly or (b) as square of the activity

27. Explain the depth of interaction effect in PET imaging.
28. Uncertainty in depth of interaction in PET imaging can be improved by

    (a) increasing the ring diameter. True_____ or False_____
    (b) using detector with high stopping power. True_____ or False_____

29. Describe the methods of DOI correction.
30. What are pulse pileup and dead-time loss in PET data acquisition?
31. Briefly describe the methods of attenuation correction of PET images in PET/MR imaging.
32. What are the difficulties encountered in manufacturing the PET/MR system and how are they resolved?

References and Suggested Reading

Bailey DL. Data acquisition and performance characterization in PET. In: Valk PE, Bailey DL, Townsend DW, Maisey MN, editors. Positron emission tomography. New York: Springer; 2003.

Bezrukov I, Mantlik F, Schmidt H, et al. MR-based PET attenuation correction for PET/MR imaging. Semin Nucl Med. 2013;43:5.

Bushberg JT, Seibert JA, Leidholdt Sr EM, Boone JM. The essential physics of medical imaging. 3rd ed. Philadelphia: Lippincott, Williams and Wilkins; 2011.

Cherry SR, Dahlbom M. PET; physics, instrumentation, and scanners. In: Phelps ME, editor. PET; molecular imaging and its biological applications. New York: Springer; 2004.

Cherry SR, Sorensen JA, Phelps ME. Physics in nuclear medicine. 4th ed. Philadelphia: W.B. Saunders; 2012.

Fahey FH. Data acquisition in PET imaging. J Nucl Med Technol. 2002;30:39.

Hoffman EJ, Phelps ME. Positron emission tomography: principles and quantitation. In: Phelps ME, Mazziotta J, Schelbert H, editors. Positron emission tomography and autoradiography: principles and applications for the brain and heart. New York: Raven; 1986. p. 237.

Humm JL, Rosenfield A, Guerra AD. From PET detectors to PET scanners. Eur J Nucl Med Mol Imaging. 2003;30:1574.

Karp JS, Surti S, Daube-Witherspoon ME, et al. Benefits of time-of-flight in PET: experimental and clinical results. J Nucl Med. 2008;49:462.

Kinahan PE, Hasegawa BH, Beyer T. X-ray-based attenuation correction for positron emission tomography/computed tomography scanners. Semin Nucl Med. 2003;33:166.

Lewellen TK. Recent development in PET detector technology. Phys Med Biol. 2008;53:287.

Martinez-Moller A, Elber M, Nekolla S, et al. Workflow and scan protocol considerations for integrated whole-body PET/MRI in oncology. J Nucl Med. 2012;53:1415.

Nehmeh SA, Erdi YE, Pan T, et al. Four-dimensional (4D) PET/CT imaging of the thorax. Med Phys. 2004;31:3179.
Sureshbabu W, Mawlawi O. PET/CT imaging artifacts. J Nucl Med Technol. 2005;33:15.
Townsend DW. Positron emission tomography/computed tomography. Semin Nucl Med. 2008;38:152.
Turkington TG. Introduction to PET instrumentation. J Nucl Med Technol. 2001;29:1.
Zaidi H, Koral KF. Scatter modeling and compensation in emission tomography. Eur J Nucl Med Mol Imaging. 2004;31:761.

Chapter 4
Image Reconstruction

Introduction

Projection data acquired in two-dimensional (2D) mode or three-dimensional (3D) mode are stored in sinograms that consist of rows and columns representing angular and radial samplings, respectively. Acquired data in each row are compressed (summed) along the depth of the object and must be unfolded to provide information along this direction. Such unfolding is performed by reconstruction of images using acquired data. The 3D data are somewhat more complex than the 2D data and usually rebinned into 2D format for reconstruction. After correction for the factors discussed in Chap. 3, the data are used to reconstruct transaxial (transverse) images from which vertical long axis (coronal) and horizontal long axis (sagittal) images are formed. Reconstruction of images is made by two methods: filtered backprojection and iterative methods. Both methods are described below.

Simple Backprojection

In 2D acquisition, activity in a given line of response (LOR) in a sinogram is the sum of all activities detected by a detector pair along the line through the depth of the object. The principle of backprojection is employed to reconstruct the images from these acquired LORs. A reconstruction matrix of a definite size (e.g., 128×128 pixels) is chosen. While the image matrix is in (X, Y) coordinates, the sinogram data are in polar coordinates. An image pixel at (X, Y) position is related to polar coordinates (r, ϕ) (Fig. 3.3a) by

$$r = x \sin \phi + y \cos \phi. \tag{4.1}$$

G.B. Saha, *Basics of PET Imaging*, DOI 10.1007/978-3-319-16423-6_4

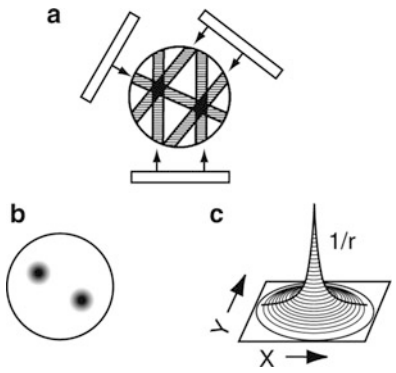

Fig. 4.1 Principle of backprojection in image reconstruction. (**a**) An object with two hot spots (*solid spheres*) is viewed at three projection angles (at 120° angle) and the acquired data are backprojected for image reconstruction; (**b**) when many views are obtained, the reconstructed image represents the activity distribution with "hot" spots, but the activity is blurred around the spots; (**c**) blurring effect described by a $1/r$ function, where r is the distance away from the central point (Reprinted with the permission of The Cleveland Clinic Center for Medical Art & Photography ©2009. All Rights Reserved)

For each image pixel (X, Y) at each projection angle ϕ, r is calculated by Eq. (4.1). The measured counts in the projection sinogram corresponding to the calculated r are added to the (X, Y) pixel in the reconstruction matrix. This is repeated for all projection angles. Thus, the backprojected image pixel $f(X, Y)$ in the reconstruction matrix is given by

$$f(X,Y) = \frac{1}{N}\sum\nolimits_{N=1}^{N} p(r,\phi) \tag{4.2}$$

where $p(r, \phi)$ is the count density in the sinogram element in the acquired matrix and N is the number of projection angles. When all pixels are computed, a reconstructed image results from this simple backprojection (Fig. 4.1).

In another approach of simple backprojection, in the reconstruction matrix of chosen size, the counts along an LOR in a sinogram detected by a detector pair are projected back along the line from which they originated. The process is repeated for all LORs, i.e., for all detector pairs in the PET scanner. Thus, the counts from each subsequent LOR are added to the counts of the preceding backprojected data, resulting in a backprojected image of the original object.

Filtered Backprojection

The simple backprojection has the problem of "star pattern" artifacts (Fig. 4.1a) caused by "shining through" radiations from adjacent areas of increased radioactivity resulting in the blurring of the object (Fig. 4.1b). Since the blurring effect

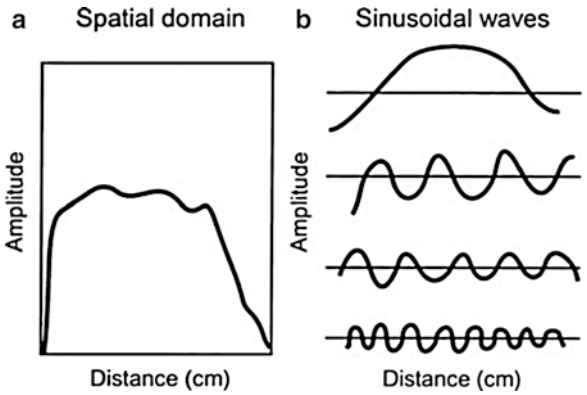

Fig. 4.2 Representation of data in the spatial and frequency domains. The activity distribution as a function of distance in an object (spatial domain) (**a**) can be expressed as the sum of the four sinusoidal functions (**b**)

decreases with distance (r) from the object of interest, it can be described by a $1/r$ function (Fig. 4.1c). It can be considered as a spillover of some counts from a pixel of interest to the neighboring pixels, and the spillover decreases from the nearest pixels to the farthest pixels of different frequencies. The blurring effect is minimized by applying a filter to the acquisition data, and filtered projection data are then backprojected to produce an image that is more representative of the original object. Such methods are called the filtered backprojection and are accomplished by the Fourier method described below.

The Fourier Method

According to the Fourier method, the measured line integral $p(r, \phi)$ in a sinogram is related to the count density distribution $f(X, Y)$ in the object obtained by the Fourier transformation. The projection data obtained in the spatial domain (Fig. 4.2a) can be expressed in terms of a Fourier series in the frequency domain as the sum of a series of sinusoidal waves of different amplitudes, spatial frequencies, and phase shifts running across the image (Fig. 4.2b). This is equivalent to sound waves that are composed of many sound frequencies. The data in each row of an acquisition matrix can be considered to be composed of sinusoidal waves of varying amplitudes and frequencies in the frequency domain. This conversion of data from spatial domain to frequency domain is called the *Fourier transformation* (Fig. 4.3). Similarly the reverse operation of converting the data from frequency domain to spatial domain is termed the inverse Fourier transformation.

In the Fourier method of backprojection, the projection data in each profile are subjected to the Fourier transformation from spatial domain to frequency domain, which is symbolically expressed as

$$F(\nu_x \nu_y) = \mathcal{F} \cdot f(X, Y), \tag{4.3}$$

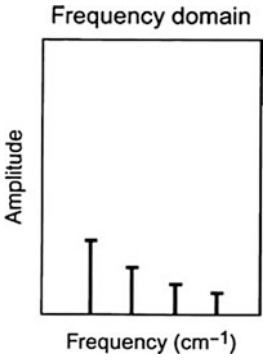

Fig. 4.3 The Fourier transform of this activity distribution is represented, in which the amplitude of each sine wave is plotted at the corresponding frequency of the sine wave

where $F(\nu_x, \nu_y)$ is the Fourier transform of $f(X, Y)$ and $\mathcal{F}$ denotes the Fourier transformation. In essence, the Fourier transform $F(\nu_x, \nu_y)$ of each projection in the sinogram of the 2D projection data is taken prior to backprojection. Straight backprojection of these Fourier projections produces a blurred image because of the oversampling at the center and less sampling at the edge. To reduce blurring (i.e., to improve the signal-to-noise ratio), the Fourier projections must be "filtered" using appropriate filters.

A filter, $H(\nu)$, in the frequency domain is applied to each projection, i.e.,

$$F'(\nu) = H(\nu) \cdot F(\nu), \tag{4.4}$$

where $F'(\nu)$ is the filtered Fourier projection which is obtained as the product of $H(\nu)$ and $F(\nu)$.

Finally, the inverse Fourier transformation is performed to obtain filtered projection data in the spatial domain, which are then backprojected in the same manner as in the simple backprojection. With the use of faster computers, the Fourier technique of filtered backprojection has gained wide acceptance in reconstruction of images in nuclear medicine.

Several factors affect the filtered backprojection. Adequate sampling of projections (both linear and angular projections related to r and ϕ of the sinogram) is needed for accurate backprojection. Data noise, positron range, noncolinearity, scattering, and random events are not taken into consideration in the method. Also in this model, detectors are assumed to be point sources, whereas in reality they have dimensions that cause nonuniform distribution of activity resulting in nonuniform projection.

Types of Filters

A number of Fourier filters have been designed and used in the reconstruction of tomographic images in nuclear medicine. All of them are characterized by a maximum frequency, called the Nyquist frequency, which gives an upper limit to

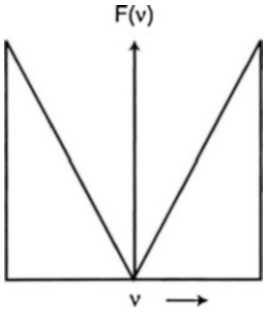

Fig. 4.4 The typical ramp filter in the frequency domain

the number of frequencies necessary to describe the sine or cosine curves representing an image projection. Because the acquisition data are discrete, the maximum number of peaks possible in a projection would be in a situation in which peaks and valleys occur in every alternate pixel, i.e., one cycle per two pixels or 0.5 cycle/pixel, which is the Nyquist frequency. If the pixel size is known for a given matrix, then the Nyquist frequency can be determined. For example, if the pixel size in a 64×64 matrix is 4.5 mm for a given detector, then the Nyquist frequency will be

$$\begin{aligned} \text{Nyquist frequency} &= 0.5\,\text{cycle/pixel} \\ &= 0.5\,\text{cycle}/0.45\,\text{cm} \\ &= 1.11\,\text{cycle/cm}. \end{aligned}$$

A common well-known filter is the ramp filter (name derived from its shape in the frequency domain) shown in Fig. 4.4 in the frequency domain. An undesirable characteristic of the ramp filter is that it amplifies the noise associated with high frequencies in the image even though it removes the blurring effect of simple backprojection. To eliminate the high-frequency noise, various filters have been designed by including a window in them. Such filters are basically the products of the ramp filter with a sharp cutoff at the Nyquist frequency (0.5 cycle/pixel) and a window with amplitude 1.0 at low frequencies but gradually decreasing at higher frequencies. A few of these windows (named after those who introduced them) are illustrated in Fig. 4.5, and the corresponding filters (more appropriately, filter–window combinations) are shown in Fig. 4.6.

The effect of a decreasing window at higher frequencies is to eliminate the noise associated with the images. The frequency above which the noise is eliminated is called the cutoff frequency (ν_c). As the cutoff frequency is increased, spatial resolution improves and more image detail can be seen up to a certain frequency. At a too high cutoff value, image detail may be lost due to inclusion of inherent noise. Thus, a filter with an optimum cutoff value should be chosen so that primarily noise is removed, while image detail is preserved. Filters are selected based on the amplitude and frequency of noise in the data. Normally, a filter with a lower cutoff value is chosen for noisier data as in the case of obese patients and in ^{201}Tl myocardial perfusion studies or other studies with poor count density.

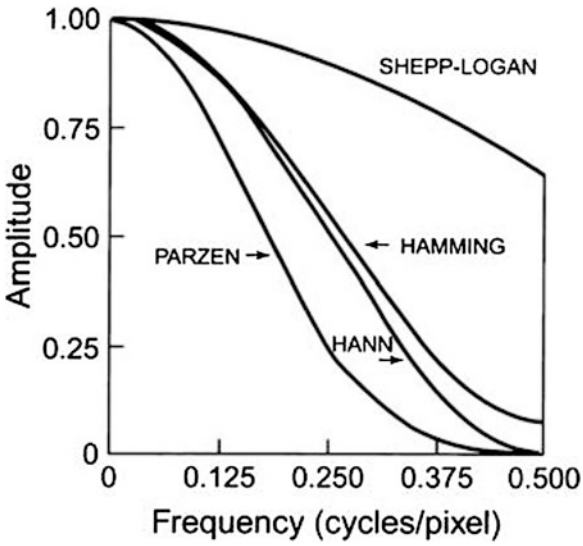

Fig. 4.5 Different windows that are used in combination with a ramp filter to suppress the higher frequency noise in backprojection method

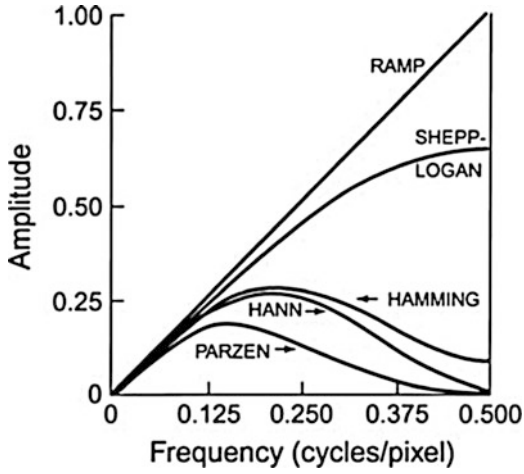

Fig. 4.6 Different filters (filter–window combinations) that are obtained by multiplying the respective windows by the ramp filter with cutoff at Nyquist frequency of 0.5 cycle/pixel

Hann, Hamming, Parzen, and Shepp–Logan filters are all "low-pass" filters, because they preserve low-frequency structures while eliminating high-frequency noise. All of them are defined by a fixed formula with a user-selected cutoff frequency (ν_c). It is clear from Fig. 4.6 that while the most smoothing is provided by the Parzen filter, the Shepp–Logan filter produces the least smoothing.

An important low-pass filter that is most commonly used in nuclear medicine is the Butterworth filter (Fig. 4.7). This filter has two parameters: the critical frequency (f_c) and the order or power (n). The critical frequency is the frequency at which the filter attenuates the amplitude by 0.707, but not the frequency at which it is reduced to zero as with other filters. The parameter, order n, determines how

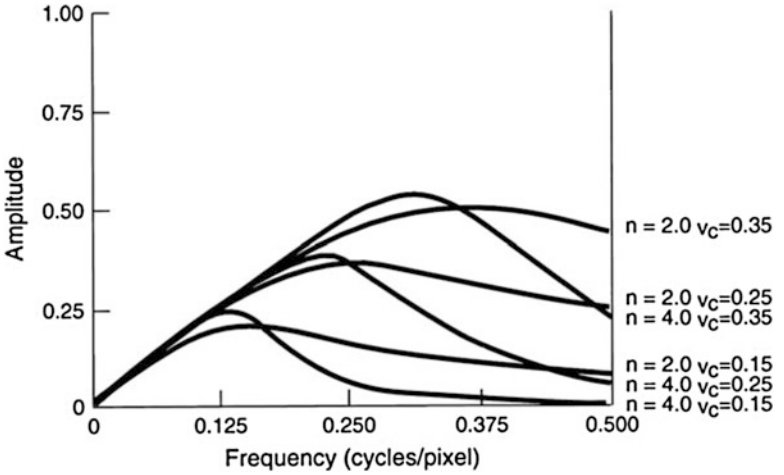

Fig. 4.7 Butterworth filters with different orders and cutoff frequencies

rapidly the attenuation of amplitudes occurs with increasing frequencies. The higher the order, the sharper the fall. Lowering the critical frequency, while maintaining the order, results in more smoothing of the image.

Another class of filters, the Weiner and Metz filters, enhances a specific frequency response.

Many commercial software packages are available, offering a variety of choices for filters and cutoff values. The selection of a cutoff value is important so that noise is reduced, while image detail is preserved. Reducing a cutoff value will increase smoothing and degrade spatial resolution. No filter is perfect, and therefore, the design, acceptance, and implementation of a filter are normally done by trial and error with the ultimate result of clinical utility.

Iterative Reconstruction

In iteration methods of image reconstruction, an initial estimate of image activity is stored in a matrix identical in size to the acquisition matrix. Usually all pixels in the estimate matrix are assigned an initial constant value. A set of simulated projections are unfolded from this estimate for comparison with the acquired projection. It is accomplished by a process called the *forward projection*, as opposed to the backprojection, in which the weighted sum of the activities in all pixels along an LOR is determined to give an estimated projection. After all projections are unfolded, each estimated projection is then compared with the corresponding measured projection. If there is a difference between the two, a weighted correction is applied to all pixels in each estimated projection. All corrected projections are backprojected to obtain an updated image, which is then entered into the algorithm as the estimated image for the next iteration. Iterations are continued until an

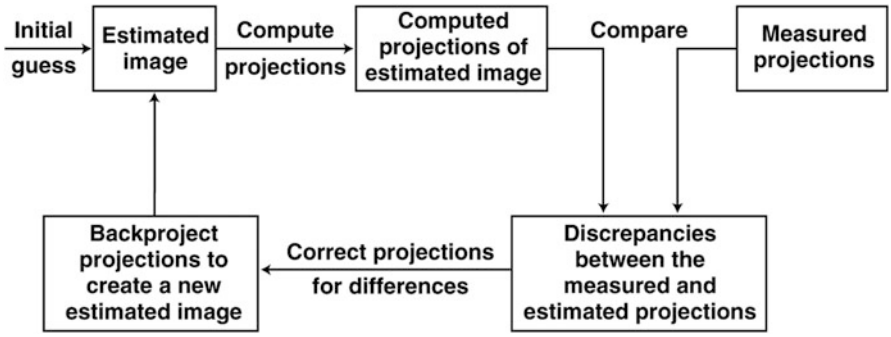

Fig. 4.8 Conceptual steps in iterative reconstruction methods (Reprinted with permission of the Cleveland Clinic Center for Medical Art & Photography ©2009. All rights reserved)

acceptable agreement between the two sets of projections is achieved. The concept of iterative reconstruction techniques is illustrated in Fig. 4.8. Several algorithms have been developed for iterative methods. They differ primarily in the manner in which the projections are computed from the estimated image, the order in which the corrections are applied, and the type of error corrections to be applied to the estimated projections.

Let us consider a transverse section of a body with a distribution of radioactivity, which is perpendicular to the axis of the PET scanner. We can simulate the transverse section as a matrix in which activity is distributed in its pixels that reflect the actual image of the transverse section, which we do not know and which we want to reconstruct from the acquired data in the sinogram. It is understood that the measured count p_i in each pixel of the sinogram is the sum of all coincidence counts arising from pixels of the transverse section matrix along an LOR and detected by two opposite detectors.

Now let us assume that a 5×5 matrix represents the transverse section of the body mentioned above and the pixels containing varied amount of activity are shown in Fig. 4.9a. For simplicity, only three measured projections A, B, and C obtained at different angles and each having five bins are shown in the figure. The bins are essentially the pixels in a row of the acquisition matrix (i.e., sinogram). Since all pixels on an LOR do not contribute equally, the weighted sum of the contributions from each pixel makes up the measured activity p_i in the ith bin. Thus,

$$p_i = \sum_{j=1}^{m} a_{ij}\, q_j \tag{4.5}$$

where q_j is the counts in the jth pixel, m is the number of pixels along the LOR, and a_{ij} is the weighting factor which is given by the fraction of activity in the jth pixel

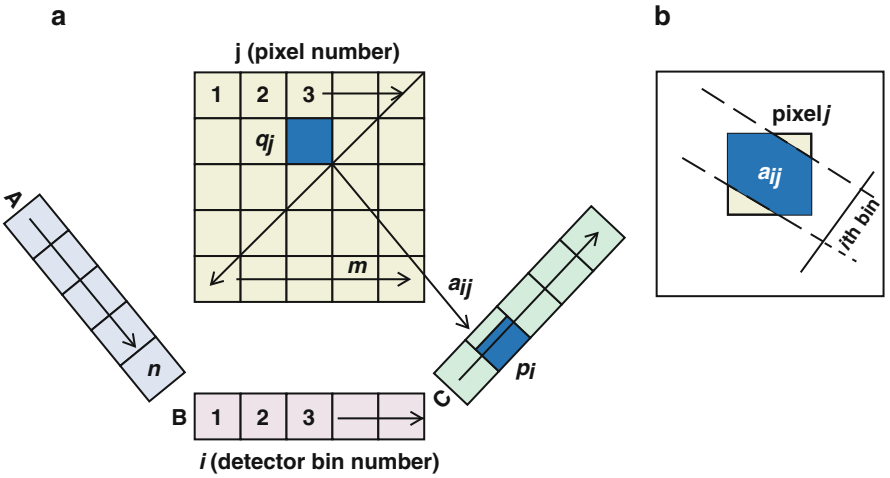

Fig. 4.9 (**a**) Three projections A, B, and C each with five bins taken of a 5×5 matrix. Counts p_i is the weighted sum of counts from all pixels along the LOR projected by the ith bin. (**b**) Concept of weighting factor a_{ij} (Fig. 12.13 on p. 182, *Image reconstruction,* in: Gopal B Saha (2013), *Physics and Radiobiology of Nuclear Medicine*, Springer; with kind permission from Springer Science and Business Media)

out of the total activity along the ith LOR. The concept of a_{ij} is illustrated by the shaded area of pixel j in the ith bin (Fig. 4.9b).

It is understood that in Fig. 4.9 the measured p_i is known, but q_j values are not known and will be determined by the iterative method for reconstruction of the image of the transverse section we started with. Let us consider only one measured projection, say, projection C in the figure. Initially some arbitrary positive values q_j (0, 1, and so on) are assigned to each pixel in the 5×5 matrix. Then the q_j values are summed up along an LOR to give an estimated value, say, q_i, that is compared to the measured p_i. This is performed for all LORs at the same projection angle to give an estimated projection C′ to compare with the measured projection C. If there is no acceptable agreement between the two projections, corrections based on the ratio of p_i/q_i or the difference $(p_i - q_i)$ are applied to each pixel in the 5×5 matrix (backprojection) to obtain an updated projection C″ to compare with measured C. This is repeated for all projections (such as A, B, etc., obtained at different angles) to complete one iteration. Many iterations are performed until a satisfactory agreement is achieved between the estimated and measured projections. The final estimated projections yield a reconstructed image of the transverse section we are looking for. The method of corrections using the ratio p_i/q_i is called the *maximum_likelihood expectation maximization* (MLEM) and the correction using the difference $(p_i - q_i)$ method is called the *additive simultaneous iterative reconstruction technique* (ASIRT).

For MLEM:

$$q_j^{k+1} = \frac{q_j^k}{\sum_i^n a_{ij}} \sum_i^n \frac{a_{ij} p_i}{\sum_j^m a_{ij} q_j^k} \tag{4.6}$$

For ASIRT:

$$q_j^{k+1} = q_j^k + \frac{1}{\sum_i^n a_{ij}} \sum_i^n \frac{\left(p_i - \sum_j^m a_{ij}\, q_j^k\right) a_{ij}}{\sum_j^m a_{ij}} \tag{4.7}$$

where k is the iteration number and n is the number of bins (pixels) in a given projection.

A flowchart of sequential steps of the iterative method is shown in Fig. 4.10.

The MLEM method is commonly applied as the iterative method to reconstruct the image. The main feature of the MLEM algorithm is to update the image during each iteration using Eq. (4.5) and Eq. (4.6). In the method, estimation of an image, unfolding of projections, comparison of estimated and measured projections, updating of projections for the difference, and backprojection of corrected projections to form the estimated image are all applied. It requires many iterations (as many as several hundreds) to achieve an acceptable agreement between the estimated image and the measured image. With many iterations, the inherent noise due to low photon counting systems causes variance on the image and often some smoothing is applied to reduce overall noise levels. This method, however, demands a lengthy computation time.

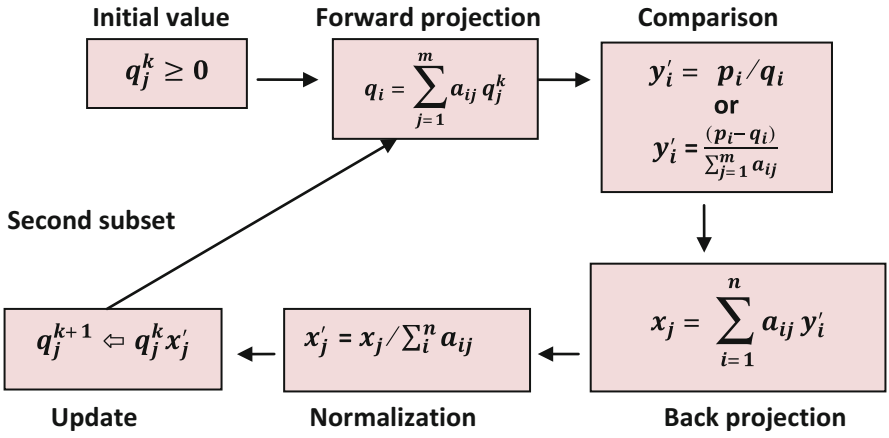

Fig. 4.10 A flowchart of sequential steps in iterative construction algorithm (Fig. 12.14 on p. 182, *Image reconstruction,* in Gopal B Saha (2013), *Physics and Radiobiology of Nuclear Medicine*, Springer; with kind permission from Springer Science and Business Media)

To reduce the computation time, the *ordered subset expectation maximization* (OSEM) algorithm has been introduced, which is a modification of the MLEM, in that angular projections are grouped into subsets, and an MLEM iteration is performed on each subset rather than each projection in it. Suppose there are 32 projections acquired at 32 equal angular intervals around the object and they are grouped into 8 subsets. Then each subset contains four projections:

Subset 1: projections 1, 9, 17, 25
Subset 2: projections 2, 10, 18, 26
. . . . . .
Subset 8: projections 8, 16, 24, 32

Standard MLEM is applied to each subset, using the rows of the estimated matrix corresponding to the LORs in the measured subset. The resulting reconstruction is then used as the starting value for the next subset. A single iteration is considered complete when all eight subsets in the above example are processed. Use of eight subsets in OSEM, as in this example, accelerates convergence by nearly a factor of 8 compared with that in standard MLEM, thus shortening the computation time. Additional iterations can be performed for better agreement by repeating the process on the same ordered subsets, always using the estimated reconstruction of the previous iteration as the starting estimated image for the next.

It would be appropriate to make a practical illustration of the OSEM method as given in Fig. 4.11. In the figure, we assume that a 2×2 matrix represents the true image of an object, the pixel values of which are not known and need to be determined. The measured p_i values at 4 projection angles (8 and 12 at 0°, 10 at 45°, 6 and 14 at 90°, and 10 at 135°) are known. In the OSEM method, an estimated reconstruction matrix of the same 2×2 size is assumed and for the first estimate, arbitrary positive values of 4 are assigned to each of the 4 pixels. One could choose any other values instead of 4. At 0° projections, the pixel data from each of the two vertical columns are summed up to give q_j values of 8 and 8. The corresponding measured p_i values are 8 and 12. The ratios, p_i/q_i, are calculated as $8/8 = 1$ and $12/8 = 1.5$ and these correction ratios are applied to the pixel data in each column of the estimate, $4 \times 1 = 4$, $4 \times 1 = 4$, $4 \times 1.5 = 6$, and $4 \times 1.5 = 6$, resulting in the first subset. Next, q_i values for the estimated 90° projection is calculated by adding the pixel values in each row, that is, $4 + 6 = 10$ and $4 + 6 = 10$, and the p_i/q_i ratios are $6/10 = 0.6$ and $14/10 = 1.4$, which are then applied to the pixel values in the first estimate to give the second subset: $4 \times 0.6 = 2.4$, $6 \times 0.6 = 3.6$, $4 \times 1.4 = 5.6$, and $6 \times 1.4 = 8.4$. The diagonal values at 45° and 135° of the second subset are added to obtain the q_i values, the p_i/q_i ratios are calculated, and the correction is applied to the pixel values in the second subset to obtain the third subset. This is the end of the first iteration and many iterations can be made for better agreement. The detailed description of the method is given by Hudson and Larkin (1994) and Shepp and Vardi (1982).

For noiseless projections, it has been shown that if there are n subsets of projections, an OSEM estimate based on a single iteration of all n subsets approaches to an MLEM estimate obtained by n iterations of all projections

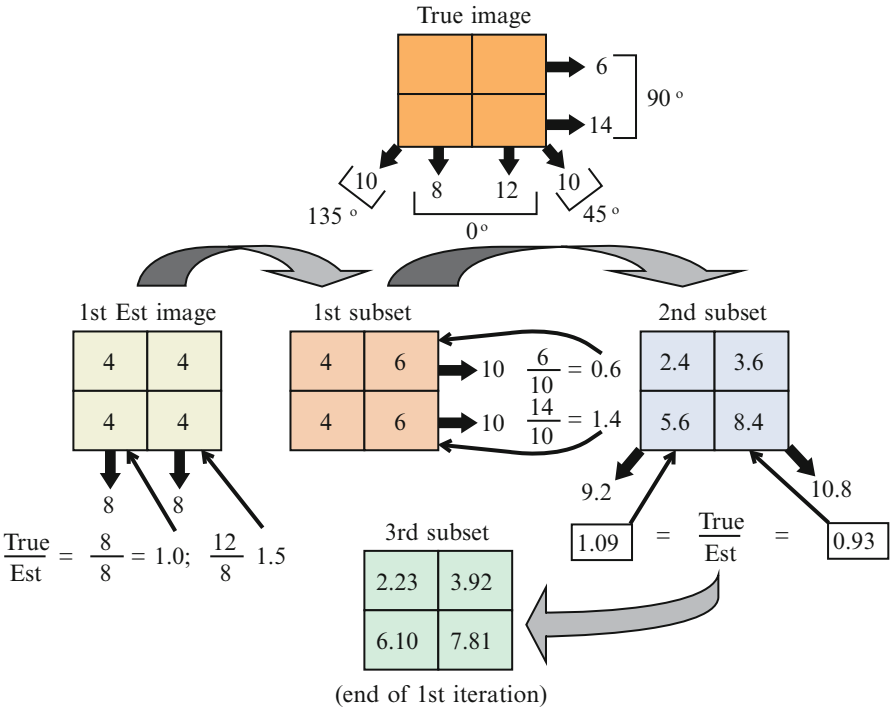

Fig. 4.11 Illustration of iterative reconstruction of an image represented by a 2×2 image. Known are *i*th bin values (sum), 8 and 12 at 0° projection, 10 at 45° projection, 14 and 6 at 90° projection, and 10 at 135° projection. Initially an estimate of the image in a 2×2 matrix is assumed with arbitrary values of 4 in each pixel. From these values, the estimated *i*th bin values are calculated for a given projection, e.g., 8 and 8 at 0° projection. The ratios of true to estimated values are calculated as 1.0 and 1.5, which are then applied to update the estimated image which becomes the first subset. The estimated *i*th bin values are calculated for a next projection (90° projection) and the ratios are calculated and applied to generate the next subset. When comparison of all bin values of all projections is made, an iteration is complete. Iterations are repeated until an acceptable agreement is achieved between the estimated image and measured image (Fig. 12.15 on p. 183, *Image reconstruction,* in Gopal B Saha (2013), *Physics and Radiobiology of Nuclear Medicine*, Springer; with kind permission from Springer Science and Business Media)

(Hudson and Larkin 1994). It is this feature of the OSEM that accelerates the computation process, and in general, the computation time is shortened with decreasing number of subsets (i.e., with more projections in each subset). However, there is a tendency of having more image variance with increasing number of subsets when compared to the MLEM. So an optimum number of subsets need to be chosen.

While corrections for detection efficiency, variation, noise component, random coincidences, scatter coincidences, and photon attenuation are made prior to reconstruction in the FBP method, in the MLEM and OSEM methods, these factors are included in the estimated image and also applied to the 3D reconstruction yielding better images. The latest development of the method, "high-definition (HD)" PET,

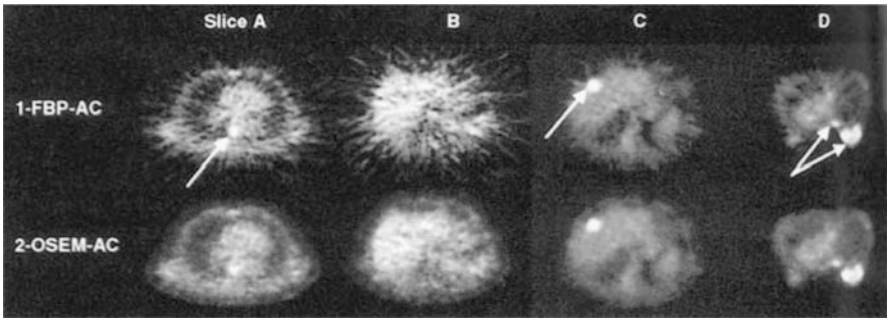

Fig. 4.12 Comparison of filtered backprojection (FBP) and iterative (OSEM) methods with attenuation correction: the (**a**) lungs, (**b**) normal liver, (**c**) liver with tumor, and (**d**) breast. FBP images with attenuation corrections are noisier than OSEM images with attenuation correction (Reprinted by permission of the Society of Nuclear Medicine from: Riddell C et al (2001) Noise reduction in oncology FDG PET images by iterative reconstructions: a quantitative assessment. J Nucl Med 42:1316)

includes the point-spread function (PSF), which varies throughout the field of view (FOV), because of the depth of interaction (photons striking the detector obliquely). By appropriately modeling the PSF with measured activity distribution across the FOV, uniform spatial resolution has been achieved and much improved images have been obtained. Despite many improvements in image quality by the OSEM method, the effect of obese patients on image quality is still a challenge to resolve. In general, iterative reconstruction methods do not produce artifacts observed with FBP methods and provide a better signal-to-noise ratio in regions of low tracer uptake (Fig. 4.12). Overall, the MLEM and OSEM iterative methods reduce noise providing high-quality images and are currently included in many PET and SPECT systems.

Another algorithm, the row-action maximum-likelihood algorithm (RAMLA), has been proposed as a special case of OSEM requiring sequences of orthogonal projections, which leads to faster convergence than OSEM itself.

In the time-of-flight (TOF) technique, the sinogram is divided into time bins, where each time bin contains the counts registered with time difference Δt. The image estimation is made by simulating the time bins and then the iterative method is applied to match a sinogram simulated from a prototype image with the real sinogram. Reconstruction of TOF images by iterative methods provide better images than those without TOF information.

3D Reconstruction

Reconstruction of images from 3D data is complicated by a very large volume of data, particularly in a multiring scanner. In a multiring scanner having N rings, a full 3D acquisition would generate N direct (perpendicular to the axis of the scanner)

and $N(N-1)$ oblique sinograms (N^2 total) in the absence of septa, compared to $2N-1$ in the case of 2D acquisition. Processing and storage of such a large amount of data are challenging for routine clinical applications. Furthermore, in 3D acquisition, there is more activity measured at the center of the scanner axis than at the edge causing spatial variance that in turn leads to complication in the reconstruction of the images.

The filtered backprojection can be applied to 3D image reconstruction with some manipulations. The 3D data sinograms are considered to consist of a set of 2D parallel projections, and the FBP is applied to these projections by the Fourier method. The iteration methods also can be generally applied to the 3D data. However, the complexity, large volume, and incomplete sampling of the data due to the finite axial length of the scanner are some of the factors that limit the use of the FBP and iterative methods directly in 3D reconstruction. To circumvent these difficulties, a modified method of handling 3D data is commonly used, which is described below.

A common method of 3D reconstruction involves the rebinning of the 3D acquisition data into a set of 2D equivalent projections. Rebinning is achieved by assigning axially tilted LORs to transaxial planes intersecting them at their axial midpoints. This is equivalent to collecting data in a multiring scanner in 2D mode, and the technique is called the *single-slice rebinning* algorithm (SSRB). The method works well along the central axis of the scanner but steadily becomes worse with increasing radial distance. This is true with smaller objects and as long as the axial acceptance angle is relatively narrow. Otherwise, views along the vertical and horizontal long axes become blurred. In another method, called the *Fourier rebinning* (FORE) algorithm, rebinning is performed by applying the 2D Fourier method to each oblique and transverse sinogram in the frequency domain. This method is more accurate than the SSRB method because of the more accurate estimate of the axial location of the source. After rebinning of 3D data into 2D data sets, the FBP or iterative method is applied. This method amplifies statistical noise slightly compared with SSRB but results in significantly less distortions.

In a 2D ring scanner, complete uniform transverse projections are obtained regardless of the position of the source inside the scanner's FOV, whereas in a 3D cylindrical scanner, this situation would occur only in a spherical sphere. In a typical cylindrical scanner of finite length, the projections are truncated toward the outer axial extent of the scanner (Fig. 4.13) that had to be restored prior to reconstruction for better signal-to-noise ratios. A practical method of 3D PET image reconstruction called the three-dimensional reprojection (3DRP) algorithm is employed to correct for truncation of the projections at the outer extent of the scanner. In this method, the 3D data are deciphered into conventional 2D sinograms. An initial 3D volume estimate is made of the object image by applying the Fourier 2D filtered backprojection to only direct plane projections (which are not truncated) and then reconstructing the image. Then unmeasured oblique projections that are truncated (Fig. 4.13a) are estimated by numerical *forward* projection or *reprojection* of the estimated image. In essence, the activity from the estimated image is numerically added to the missing LORs, which are then summed

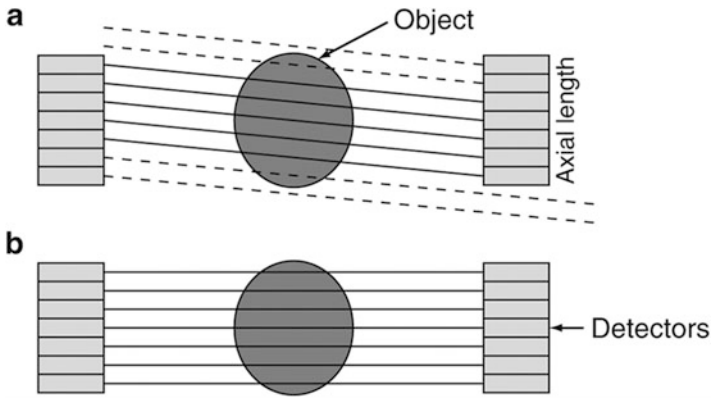

Fig. 4.13 (**a**) LORs that are not sampled beyond the scanner length in the 3D acquisition are shown by *dashed line*. (**b**) A 3D image is estimated by applying 2D filtered backprojection to the 3D data and from the estimated image activity is added to the truncated LORs, which are then added to form the missing sinograms (Reprinted with the permission of The Cleveland Clinic Center for Medical Art & Photography ©2009. All Rights Reserved)

to give the missing sinogram (Fig. 4.13b). This method significantly improves the signal-to-noise ratio but is very time consuming because of the complexity of computation and a large volume of data to handle.

Partial Volume Effect

In PET imaging, the reconstructed images should depict the radiotracer distribution uniformly and accurately throughout the FOV. However, because of the limit of the spatial resolution of current PET scanners, "hot" spots (structures) relative to a "cold" background that are smaller than twice the resolution of the scanner show partial loss of intensity, and the activity around the structure appears to be smeared over a larger area than it occupies in the reconstructed image. While the total counts are preserved, the object appears to be larger and to have a lower activity concentration than it actually has. Similarly, a cold spot relative to a hot background would appear smaller with high activity concentration. Such underestimation and overestimation of activities around smaller structures in the reconstructed images is called the partial volume effect (Fig. 4.14), and this reduces the contrast between high- and low-uptake regions. However, this effect also contains the so-called spillover effect due to contamination of activity from the neighboring tissues to these hot or cold areas.

Corrections need to be applied for overestimation or underestimation of activities to these smaller structures in the reconstructed images. A correction factor, called the recovery coefficient (RC), is the ratio of the reconstructed count density to the true count density of the region of interest that is smaller than twice the spatial

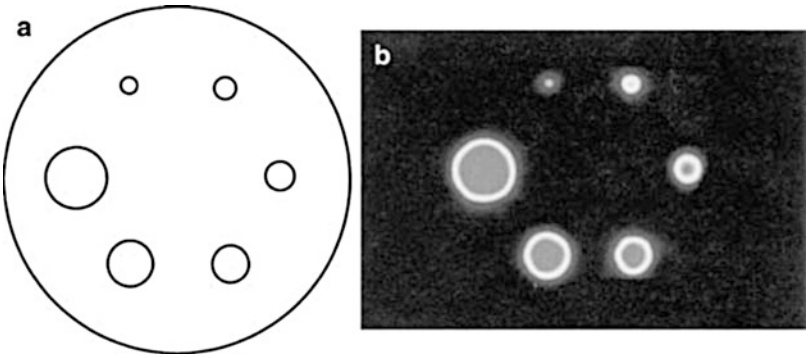

Fig. 4.14 An illustration of partial volume effect. (**a**) Cross section of a sphere phantom with six different spheres; (**b**) PET images of the spheres demonstrating partial volume effect (Reproduced with permission from Rota Kops E, Krause BJ (2000) Partial volume effects/corrections. In: Wieler HJ, Coleman RE (eds) PET in Oncology. Springer, Darmstadt)

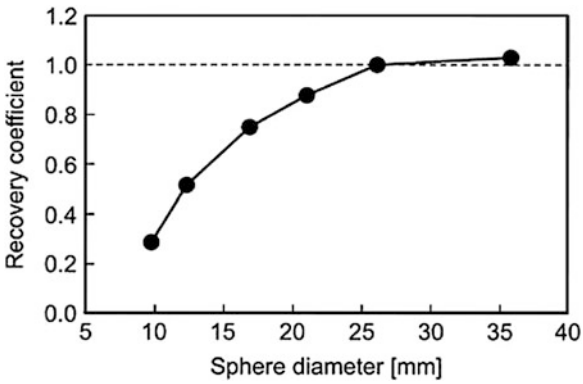

Fig. 4.15 Recovery coefficients as a function of object size (Reproduced with permission from Rota Kops E, Krause BJ (2000) Partial volume effects/corrections. In: Wieler HJ, Coleman RE (eds) PET in oncology. Springer, Darmstadt)

resolution of the system. The recovery coefficient is determined by measuring the count density of different objects containing the same activity but with sizes larger as well as smaller than the spatial resolution of the system. Normally, the recovery coefficients would be 1 for larger objects (Fig. 4.15). These RC values are then applied to the images of small structures for partial volume corrections. However, the sizes of the in vivo structures are not precisely known, and so the phantom RC data may not be accurate for these structures. Other methods using point-spread functions of the activity distribution around the object have been investigated with limited success.

Questions

1. Discuss the methods and merits and disadvantages of filtered backprojection and iterative methods.
2. Why are filters used in reconstruction of PET images by backprojection?

3. What is the common initial step that is taken in the reconstruction of 3D data?
4. When do you apply various corrections (e.g., detection efficiency variations, noise components, random and scatter coincidences, attenuation) in the FBP and iterative methods of image reconstruction?
5. What is the partial volume effect and how do you correct it?
6. The OSEM method is slower in computation than the MLEM method. True____; False____.
7. Both OSEM and MLEM methods reduce image noise compared to filtered backprojection. True____; False____.
8. 3D reprojection method is commonly used in 3D reconstruction because of (a) less time consuming in computation, (b) correction for the loss of projections at the edge of the scan axis, and (c) improvement in noise reduction on images.
9. What is the major advantage of the OSEM over the MLEM method?
10. Compared to the FBP, the OSEM reduces artifacts in the image. True ____, False____.

References and Suggested Reading

Bacharach SL. Image analysis. In: Wagner Jr HN, Szabo Z, Buchanon JW, editors. Principles of nuclear medicine. Philadelphia: W.B. Saunders; 1995. p. 393–404.

Cherry SR, Dahlbom M. PET; physics, instrumentation, and scanners. In: Phelps ME, editor. PET; molecular imaging and its biological applications. New York: Springer; 2004.

Cherry SR, Sorensen JA, Phelps ME. Physics in nuclear medicine. 3rd ed. Philadelphia: W.B. Saunders; 2003.

Defrise M, Townsend DW, Clack R. Three-dimension image reconstruction from complete projections. Phys Med Biol. 1989;34:573.

Defrise M, Kinahan PE, Christian M. Image reconstruction algorithms in PET. In: Valk PE, Bailey DL, Townsend DW, Maisey MN, editors. Positron emission tomography. New York: Springer; 2003.

Dreyer KJ, Mehta A, Thrall JH. PACS: a guide to the digital revolution. New York: Springer; 2002.

Hoffman EJ, Phelps ME. Positron emission tomography; principles and quantitation. In: Phelps ME, Mazziotta J, Schelbert H, editors. Positron emission tomography and autoradiography: principles and application for the brain and heart. New York: Raven; 1986. p. 237.

Hudson HM, Larkin RS. Accelerated image reconstruction using ordered subsets of projection data. IEEE Trans Med Imaging. 1994;13:601.

Shepp LA, Vardi Y. Maximum likelihood reconstruction for emission tomography. IEEE Trans Med Imaging. 1982;MI-1:113.

Chapter 5
Storage, Display, and PACS

Introduction

Completion of a nuclear medicine procedure involves many steps that are intertwined with one another. A referring physician orders a nuclear medicine study for a patient after clinical examination. The patient reports to the nuclear medicine department for the study according to the schedule. The study is performed according to the established protocol using specific equipment. The data are processed and used to construct images which are then stored for display on monitors as needed. The nuclear physician retrieves the images from storage and interprets them to diagnose the patient's diseases. The report on the diagnosis is dictated into a computer, which can be retrieved along with images by the referring physician for making a clinical decision for the patient. The entire sequence of operations in the procedure is depicted by the term *workflow* that represents each operation much like flowcharts. Workflow software has been developed by various vendors to implement all sequential operations of a procedure in an integrated form. The advantage of workflow lies in the management of large imaging data in multiple formats along with the capability of interrelating among different operations. Below is given a description of storage and display of image data in nuclear medicine and the concept of workflow involving multiple operations to complete a study.

Storage

Reconstructed digital PET images are stored in the computer in the format of a matrix. The images are characterized by two quantities: matrix size and pixel depth. In PET studies, the computer memory approximates the FOV as a square matrix of a definite size that can range from 64×64 to 512×512 with a total of

G.B. Saha, *Basics of PET Imaging*, DOI 10.1007/978-3-319-16423-6_5

1026 (1 K) to 262,144 (262 K) picture elements, called pixels, respectively. The matrix size depends on the type of study and is chosen by the operator. Since the FOV is approximated to the matrix size, the pixel size is calculated by dividing the length of FOV by the number of pixels across the matrix. For example, if an image of 250×250 mm FOV is stored in a 128×128 matrix, then the pixel size would be $250/128 \approx 2$ mm. The spatial resolution of an image is improved by decreasing the pixel size but is limited by the spatial resolution of the scanner. Pixel size smaller than one-third the spatial resolution of the PET system does not improve the image resolution any more. Thus, for a 6-mm spatial resolution, choosing pixel size smaller than 2 mm does not add to the improvement of the image resolution.

How many counts can be stored in a pixel depends on the depth of the pixel, which is represented by a byte or a word. Digital computers operate with *binary* numbers using only 2 digits, 0 and 1, as opposed to 10 digits, 0–9, in the decimal system. The basic unit of the binary system is a *bit* (binary digit) that is either 0 or 1. In computer nomenclature, a byte of memory is equal to 8 bits that can store up to 2^8, i.e., 0–255 units of information. Similarly, a word of memory consists of 16 bits or 2 bytes and can store up to 2^{16}, i.e., 0–65,535 units of information. The color levels or gray shades on the displayed images are affected by pixel depth. Currently 32-bit and 64-bit processors have been introduced, allowing storage capacity of 2^{32} and 2^{64} units of information in computers.

After completion of a PET study, the images are archived in long-term storages, which are available in a variety of hardware accessories. In the past the scope of PET imaging was limited and the digital images could be stored in the hard drive of the local computers with capacity of several gigabytes. As the technology expanded and PET imaging grew tremendously, demand for larger storage became enormous. External storage like optical disk, magnetic tape, spinning media, etc., was utilized for storage with more capacity. For reasons of natural disasters, terrorism, viruses, etc., electronic data vaulting was accepted as a plausible merging technique for off-site data storage, which provides a means for geographically distant storage and retrieval of data as needed. The distant storage, however, requires strict security of the storage facility to ward off any natural calamity and criminal attack.

Nowadays the prolific growth of PET modality has prompted the need for storage capacity of tens to hundreds of terabytes (TB). Vendors have developed a unique system called picture archiving and communication system (PACS) (described later) for storage of massive volume of PET images. PACS utilizes magnetic hard drives with capacity of several hundred terabytes and they are managed by secure and reliable software. The PACS software includes provision for disaster recovery, backup, and replication. Various features of PACS are discussed in detail later.

Recently, internet-based cloud-computing has drawn enormous attention in medical imaging because of its vast storage capacity and ease of exchange of stored information among institutions and individuals on-site and remotely in real time (Kagadis et al. 2013). Faster network communication and decreasing cost has made

cloud computing very attractive in archiving medical information. Vendors now are introducing cloud-based PACS taking advantage of versatile features of cost-effective storage capacity and easy data interchange over the internet. It can be accessed from any location, provided an internet connection is available. Clinical information and diagnostic images stored in cloud can be shared among physicians and medical institutions, which improves the patient care. However, strict cyber security and data encryption are challenges in cloud computing and must be implemented meticulously.

Display

Images are displayed on video monitors after the conversion of digital images into analog images by digital-to-analog conversion (DAC) at the video interface between the computer and the monitor. Two common video monitors are cathode ray tubes (CRTs) or flat panel-type liquid crystal display (LCD) monitors. These monitors are characterized by parameters such as spatial resolution, contrast resolution, aspect ratio, luminance, persistence, refresh rate, and dynamic range. These properties are described in standard physics books on imaging and are not discussed here. It should be noted that the spatial resolution and luminance of LCD monitors are far superior to those of CRTs. These monitors are set in what is called the *workstation*, where practitioners manipulate, view, and interpret images using the computer attached to the workstation.

Display can be in either grayscale (black and white) or color-scale format. Grading of scale in either case is dictated by the pixel values (number of counts in the pixel) in the digital image. The number of counts in a pixel defines the brightness level of the pixel. Thus, in a digital image, the grayscale can be applied to delineate areas of contrast, and when comparing separate images, the grayscale should be kept the same for all images.

Color display of digital images can be obtained by assigning color hues to different pixel values corresponding to counts stored in the individual pixels. In a common color scale, blue, green, yellow, and red colors from the visible spectrum are in order assigned to pixels with increasing counts: blue color to the pixels with the lowest counts and red color to the pixels with the highest counts. Edges of color bands are blended to produce a gradual change over the full range of the color scale. As with the grayscale, the color scale provides contrasts between areas of different pixel counts and thus a means to discriminate between normal and abnormal areas on the images. Conventionally, PET functional images are displayed in color, and CT anatomical images are shown in grayscale. On fusion of the two images, the combination of color and grayscales is quite effective in differentiating the abnormal areas.

Often a grayscale or color-scale bar is shown on the side of the image so that the interpreter can easily differentiate the contrast on the image. The regions of interest (ROIs) can be chosen from sequential images, and time–activity curves can be

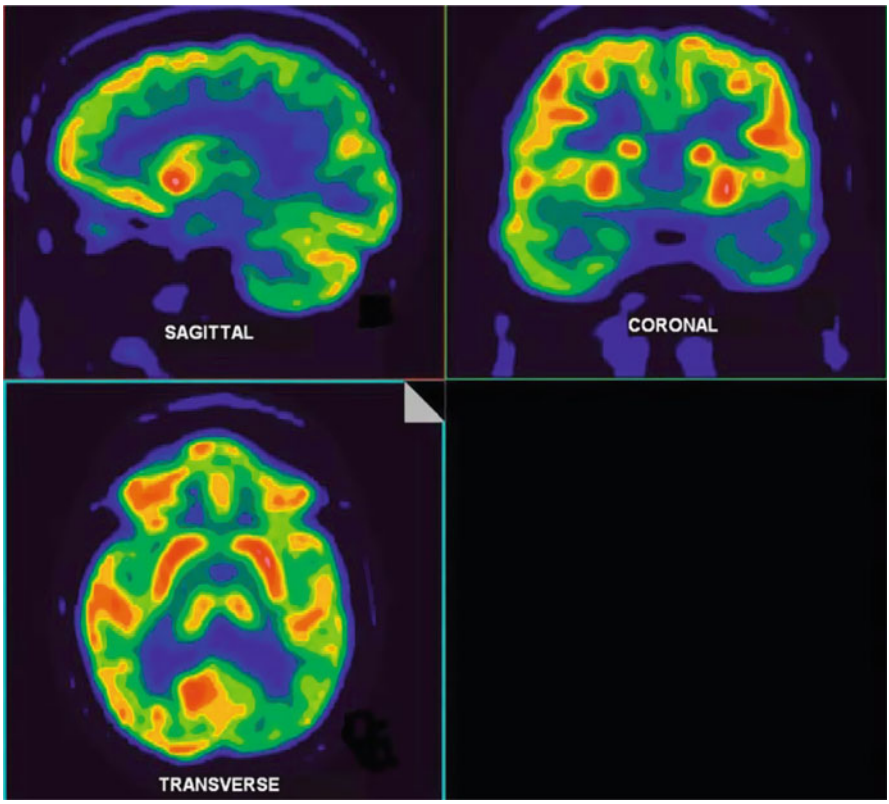

Fig. 5.1 Simultaneous display of PET images of the brain in transaxial, coronal (*horizontal long axis*), and sagittal (*vertical long axis*) orientation

obtained by plotting counts in ROIs against the corresponding time. Images can be subtracted from one another or can be superimposed, as needed.

PET images can be displayed in transaxial, coronal (horizontal long axis), or sagittal (vertical long axis) views separately or simultaneously on the same screen (Fig. 5.1). On a simultaneous display, a point within an image of the object is chosen using the cursor and three images that pass through that point are displayed. New sets of images are obtained by moving the cursor to a different point along the image. Such sequential screening of images is helpful in delineating the abnormal areas in patients on images.

Angular projections around an object can be computed from the three-dimensional (3D) tomographic data and then displayed in continuous rotation. This results in the presentation of the image data in a movie or cinematographic (or cine) mode whereby a rotating 3D image is seen on the screen. The relative location of a lesion in an organ with respect to other organs in the body can be easily identified in these movie presentations of PET images.

Software and DICOM

Commercial vendors provide software for acquisition, processing, storage, and display of images specially designed for their scanners. Such software is either developed by the vendor or acquired from a third-party software developer. These types of software use a proprietary format for each vendor, and it is difficult to transfer, store, and display images on equipment from different vendors.

This problem can be partially solved by using equipment all from the same vendor in an institution. To overcome this difficulty, the American College of Radiology (ACR) and the National Electrical Manufacturers Association (NEMA) jointly sponsor a standard format for software called Digital Imaging and Communications in Medicine (DICOM) to facilitate the transmission and usage of medical images and related data among different imaging equipment. DICOM consists of a standard image format as well as a network communication protocol and specifies standard formats for operations such as Patients, Studies, Storage, Query/Retrieve, Verification, Print, Study, etc.

Currently, all vendors provide software conforming to the DICOM standard and agree to a commitment to that effect to all customers. Compliance with this standard establishes a common format for imaging systems connecting hardware and software components and allows interoperability for transfer of images and associated information among multiple vendors' devices. The DICOM standard is particularly useful in the implementation of PACS, which is discussed below.

Picture Archiving and Communication Systems

The PACS is a system for storage of images and transferring images between computers in different facilities through networks. This system consists of devices to produce and store digital images electronically, workstations to view and interpret images, and a network linking computers from different sites. Appropriate PACS software allows the interpreter to manipulate images as needed, at his own location, by retrieving images from other locations via PACS. The introduction of PACS has eliminated the use of X-ray films or Polaroid films for routine interpretation of images, making the imaging centers filmless.

A PACS connects different computers through a high-speed network to share information. This connection can be in a single department using a local area network (LAN), in a hospital using the intranet, or outside the hospital via the Internet. In radiology, it is often desirable to compare CT, MRI, and ultrasound images with those of nuclear medicine studies. A PACS is helpful to provide such comparative studies among different imaging modalities via Web protocols without physically moving to and from different locations of the department. Similar transfer of images can occur through a PACS to other parts of the hospital, to different parts of the country, or even to other countries.

In a radiology department, the Radiology Information System (RIS) is implemented to maintain all aspects of the workflow within the department, from

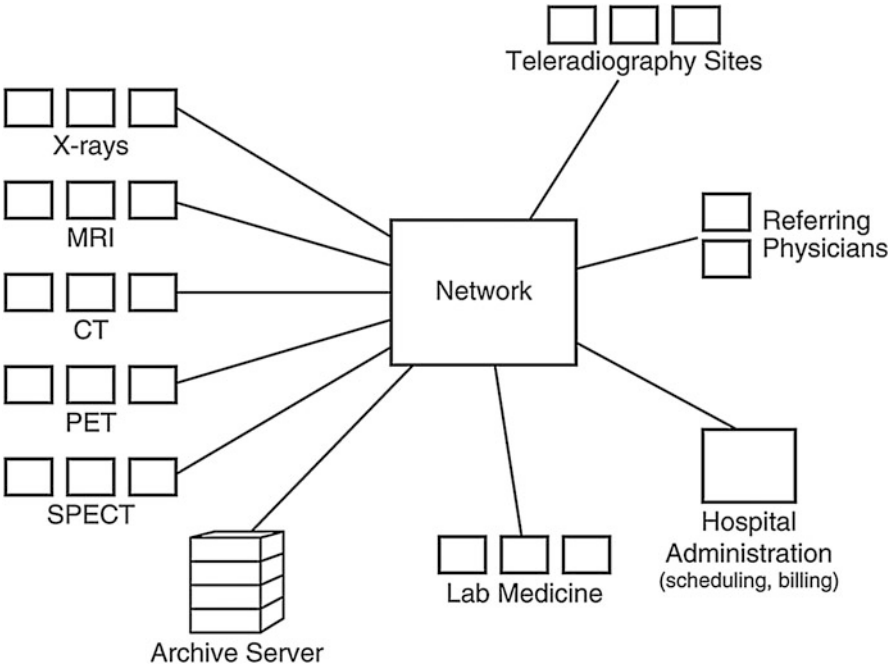

Fig. 5.2 A schematic PACS integrating RIS and HIS (Reprinted with the permission of the Cleveland Clinic Center for Medical Art and Photography ©2009. All rights reserved)

scheduling to billing to reporting. Similarly, hospitals have the Hospital Information System (HIS) that maintains information on patients regarding their demographic data, clinical history, laboratory data, medication, and again, scheduling, tracking, billing, and reporting. A PACS can integrate both RIS and HIS for broader exchange of information among healthcare personnel that will save time and money in healthcare operations. In an integrated system, a referring physician can call in an image of a patient on his computer connected to the PACS, rather than waiting for the hard copy from the imaging department. He can then correlate the clinical findings with the images in the same sitting with considerable saving of time. A schematic integrated PACS is shown in Fig. 5.2.

A PACS is maintained by a server that provides storage, informatics, etc., for communication among members of the PACS and also as many workstations as necessary to connect to the server. As already mentioned, at workstations one can retrieve reports and images of patients from the PACS and manipulate them to interpret as needed. A PACS is run by software designed for a particular operating system, such as Windows, Mac OS, Unix, or Linux, although most PACS workstations run on a PC platform. All PACS software can perform some standard functions, but ease of operation may vary. They differ at times in limitation of the number of the patient studies that can be displayed on a monitor screen. The software provides different protocols to access the PACS at the workstation. For example, a protocol may be based on a modality and body part combination, such as

"CT abdomen/pelvis," or on a secondary descriptor such as "gallbladder stone protocol," or on a subspecialty such as "nuclear medicine." A PACS software should be able to present and interact with all pertinent information for a given patient from different systems, such as the hospital system, the radiology system, and the dictation system.

PACS software must address four issues: confidentiality, integrity, reliability, and availability. From the legal point of view mandated by various federal and state regulations, these issues are paramount in the operation of a healthcare institution.

Confidentiality refers to how well private information is kept private, regardless of whether it is a patient, employee, or corporation. Information is available only to authorized persons, and none will be divulged to unauthorized individuals. This invokes the concept of security in the information system. In most cases, security is maintained in the system by introducing an appropriate "user's ID and password" format for each eligible user. Implementation of a federal law, the Hospital Insurance Portability and Accountability Act (HIPAA), has made it mandatory to insure stricter confidentiality measures in the healthcare system. A PACS should strictly meet this requirement.

Integrity refers to the correctness and completeness of patient information. An error in demographic data or patient medication regimen may result in a fatal condition, which can provoke a legal action. A PACS should provide maximum integrity to maintain a reliable information system.

Reliability refers to the stability of the PACS—meaning the downtime of the system should be nil. If a PACS falters in its operation and encounters frequent failures, it will seriously disrupt the healthcare operation, leading to adverse financial loss. The software should be well written and user friendly to avoid unnecessary failures of the system.

Availability refers to the timely access to patient information, which can affect the quality of care. Patient data should be entered into the computer on time by the healthcare personnel, as delays can have adverse effects on patient care. Computers and networks must have no or minimal downtime to avoid delays in patient management. A PACS software should address this issue faithfully to maintain an efficient system.

PACS software is evolving over time to meet the challenging demands of healthcare professionals and usually is up for upgrade every 6–12 months. Since a variety of factors are involved in the implementation of PACS in a facility, a caveat is in order for purchasing a PACS from a vendor. One should make a thorough assessment of the software prior to purchase. Even though trade shows and demonstrations at professional meetings may offer a reasonable background on the system, one should not hesitate to ask for a visit to sites that have the actual systems that are up and running before making a decision to purchase.

Almost three dozens of PACS software are available commercially in the market from different vendors. Each of these systems is sold as a package consisting of the software and a Web-based server. There are software companies, such as Siemens Healthcare, GE Healthcare, Philips Healthcare, Agfa, Fujifilm, Infinitt, Medweb, Sectra, and Voyager, to name a few, which market the PACS packages that are universally compatible with most imaging systems. The specifications of four commercially available PACS are shown in Table 5.1. Vendors often

Table 5.1 Specifications of four commercial PACS systems[a]

Company	Fujifilm	GE Healthcare	Philips Healthcare	Siemens Healthcare
Product name	Synapse Radiology PACS	Centricity PACS-IW	IntelliSpace PACS	syngo.plaza
Proprietary software integrated with PACS	Integrates well with all systems that support DICOM, HL7, IHE, HTML, and APIs	EMRRISAdvVis VR ortho mammo peer review	Any DICOMHL7IHE compliant	3D, RIS and DICOMHL7, IHE-based connectivity, film scanning
Turnkey solutions, software only or both	Both	Both	Turnkey solutions	Both
Primary system design (Web based, client server, etc.)	Web based	Web based	Client server with HTML5 zero footprint	Web-enabled client server
Primary OEM hardware providers	HP, Dell, IBM, VMWare	HP; Del; multiple storage vendors such as EMC, Nexsan, Assureon	IBM	Customer decides based on Siemens specs
Storage: DAS (direct-attached storage), NAS (network-attached storage), SAN (storage area network), etc.	EMC, Hitachi, HP, Netapp, Nexsan	DAS, NAS, SAN	SAN with data always online and automated off-site disaster recovery	DAS, NAS, SAN, etc.
Number of upgrades/year	1–2	2–3	Few/year	1–2
RIS and HIS interface with PACS; specific vendor systems on which PACS has been validated	Epic Radiant, MEDITECH, Cerner, McKesson, GE, Siemens, and many more. Any RIS that integrates using HL7 will be supported	Typically integrate interface to third-party RIS systems through an open API or desktop integration; interfaces are typically HL7 and open for passing orders and results	Interface with any RIS vendors through HL7 standard	HL7-capable RIS vendors
DICOM encapsulation to attach non-DICOM files: (PDF, JPEG, TIFF)	Yes	JPEG, TIFF	Yes	Yes

Images are stored/compressed/uncompressed	Images are stored with lossless and lossy compression	Compressed, JPEG 2000	Images stored in iSyntax format, using lossless 2.5:1 compression	Both, configurable
Local archive: server level archive level	Yes, both	Server level	Server level	SAN, DAS
Long-term archiving	Local, data replication for disaster recovery, cloud-based DR	Onsite remote cloud based	SAN with data always online and automated off-site disaster recovery	NAS, DICOM LTA, VNA
Seamless system interface with electronic medical records (EMRs); specific vendor systems on which PACS has been validated	Yes, multiple, Epic, Cerner, and others	Yes	Yes, through industry standards	OEM call UP-based integration (api)
Capture of static color images; dynamic color images (30 fps); cine playback	Yes	Static color, cine playback	Yes	Yes
Document scanning is supported (yes/no)	Yes	Yes	Yes	Yes
Dictation/voice automation compatible	Yes	Yes	Yes	Yes, Siemens RIS
Web-enabled viewer: PACS, RIS, mammography	Yes	Yes	Yes	Yes
3D viewing, advanced visualization software	Yes	Yes	Yes	Yes
Monitors supported	6	6	5	6
Security features	Supports AD for user authentication, URL encryption, SSL, and VPN	NS	VPN, SSL, HTTPS, lightweight device access protocol (LDAP), 128-bit SSL	Supports AD, HIPAA enabling technology

[a]Reprinted with permission from the April 2014 issue of *Imaging Technology News (ITN),* Scranton Gillette Communications. All rights reserved

customize the software to meet the specific need of a customer. All vendors claim their software to be robust, reliable, and user friendly, with an uptime of more than 99.9%. Even though many PACS versions are applicable to imaging equipment of different manufacturers, it is not uncommon to encounter a few glitches in implementing the PACS of one vendor into a system of a different vendor.

The use of PACS has become universally common in all hospitals to maintain a stable electronic health record (EHR). According to a study in 1999 by the Institute of Medicine (IOM), an estimated 98,000 Americans die each year due to medical errors. These deaths could be prevented by having PACS because of the quick and easy access by the healthcare providers to reliable and comprehensive patient information. The IOM is strongly recommending hospitals and physicians to adopt electronic record keeping, a measure that could save thousands of Americans. The US Congress is planning on legislation to implement mandatory electronic record keeping of patients' health information. This would need a more uniform standard for PACS software. To have such a standard, the medical community and perhaps the federal government should come up with a consensus policy similar to DICOM so that PACS can be instituted universally for all concerned.

Electronic Health Record

Currently healthcare industry is strongly encouraged to implement EHR or sometimes called electronic medical record (EMR) to document patient data replacing handwritten hard copies. It contains digital documentation of demographics, patients' health information, immunization, etc., which helps reduce the errors in handwritten copies arising from poor eligibility and often from missing forms. The Center for Medicare and Medicaid Services (CMS) currently offers a financial incentive to eligible hospitals and physicians for implementing meaningful EHR for patient management. Hospitals around the country are increasingly adopting it in patient care, but overall adoption in the USA is somewhat slow. An advantage of the EHR is that physicians can access the data from distant phones on their smartphone using mobile apps.

Information in EHR is protected by HIPAA regulations and vigilant monitoring is required for this protection. However, its compliance with HIPAA has become a challenge due to cyber attack and identity theft that can plague the Web services. Despite the stringent safeguard required by the HIPAA, access to the patient data by unauthorized personnel can occur compromising the patient information in EHR. Web-based information exchange is prone to hacking. Exchange and sharing of patient data between healthcare providers by e-mails lack sufficient encryption. However, the lately introduced online and cloud-based data storage Web sites are well encrypted with sufficient protection and offer easy access and availability almost everywhere with mobile apps. But healthcare providers must be on constant watch to maintain the perpetual security and integrity of the cloud system, as it is the responsibility of the providers to ensure the safety of patient information and data theft.

Cost effectiveness of EHR is a debatable concern, because any cost saving from implementation of EHR tends to be offset by increase in cost for the need for Internet technology. Large healthcare facilities may benefit from EHR, while the office-based physicians may not.

Teleradiology

A patient's diagnostic images obtained at one location can be transferred to different locations by PACS through computer networks. This system is termed *teleradiology* in parallel with telemedicine. Nowadays the practice of nuclear medicine has spread over different geographical regions, and nuclear physicians cover many hospitals and clinics, reading patient scans from distant locations. It is time consuming and impractical for these practitioners to commute to different distant hospitals to read scans. Teleradiology offers a great advantage to these practitioners, because they can read patients' reports and scans from different hospitals at their own locations using teleradiology. For example, on-call nuclear physicians can read scans at home using a computer connected to the teleradiology network through a cable modem, ISDN or DSL connection, or using Wi-Fi (wireless) technology using mobile apps provided by the telecommunications company. Teleradiology has advanced greatly, so much so that interstate teleradiology and worldwide intercountry teleradiology are quite common in modern medical practice.

Teleradiology communication is accomplished in several ways. The classical technique involves the use of two workstations directly connected to each other via TCP-IP protocol with built-in data security and teleconferencing capability. Mail servers in the Internet can serve efficiently to communicate images via e-mails provided they are fast and dedicated to avoid transmission delays. Web-based servers offer a convenient way of submitting and receiving patient data over the Internet. Different combinations of these methods are often made to customize individual preferences. For example, radiologists can use their own computers for acquisition and reporting while transmitting images via an established gateway using available standard protocols such as DICOM and HL7. The gateway performs all necessary steps such as data security, compression, etc., for passage through WAN and send the data to many locations or even to different countries.

By virtue of teleradiology, the radiology business groups in the USA are in the global practice of radiology by outsourcing, for example, qualified radiologists in India to interpret imaging scans performed in the USA. This provides a great deal of financial benefit because Indian radiologists are paid less than one-third the pay that their US counterparts get.

Questions

1. LCD monitors are superior to CRT monitors for image display. Explain why.
2. What are the major media for the storage of image information in radiology?

3. What is the standard format used in software for transmission of images and related data among different imaging equipment?
4. PACS has become the most efficient means of exchanging patients' data among physicians and medical institutions. Specify some important features and advantages of PACS to justify such a unique status.
5. What are the important issues of PACS one should consider in purchasing a PACS software?
6. How many ways teleradiology can be accomplished via the Internet?
7. What is the benefit of having electronic health record of a patient?

References and Suggested Reading

Dreyer KJ, Mehta A, Thrall JH. PACS: a guide to the digital revolution. New York: Springer; 2002.

Huang HK. PACS and imaging informatics: basic principles and applications. Hoboken: Wiley; 2004.

Kagadis GC, Uloukinas C, Moore K et al. Cloud computing in medical imaging. Med Phys. 2013; 40: 070901.

Kohn LT, Corrigan JM, Donaldson MS, editors. To err is human: building a safer health system. Washington, DC: National Academy Press; 1999.

Chapter 6
Performance Characteristics of PET Scanners

Introduction

In PET/CT and PET/MR imaging, PET images are of primary interest, whereas CT and MR images complement PET images by attenuation correction and fusion of images for better delineation of lesions. So we will discuss the performance parameters of only PET scanners. However, quality control tests for all three scanners are presented. A major goal of the PET studies is to obtain a good-quality and detailed image of an object by the PET scanner, and so it depends on how well the scanner performs in image formation. Several parameters associated with the scanner are critical to good-quality image formation, which include spatial resolution, sensitivity, noise, scattered radiations, and contrast. These parameters are interdependent, and if one parameter is improved, one or more of the others are compromised. A description of these parameters is given below.

Spatial Resolution

The *spatial resolution* of a PET scanner is a measure of the ability of the device to faithfully reproduce the image of an object, thus clearly depicting the variations in the distribution of radioactivity in the object. It is empirically defined as the minimum distance between two points in an image that can be detected by a scanner. A number of factors discussed below contribute to the spatial resolution of a PET scanner.

Detector size: One factor that greatly affects the spatial resolution is the intrinsic resolution of the scintillation detectors used in the PET scanner. For multidetector PET scanners, the intrinsic resolution (R_i) is related to the detector size d. R_i is normally given by $d/2$ on the scanner axis at midposition between the two detectors and by d at the face of either detector (Fig. 6.1). Thus, it is best at the center of the

G.B. Saha, *Basics of PET Imaging*, DOI 10.1007/978-3-319-16423-6_6

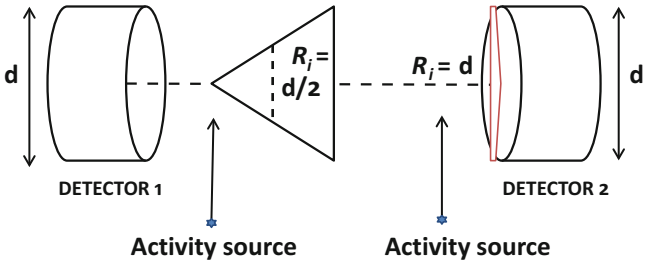

Fig. 6.1 Illustration of spatial resolution R_i of a PET camera, the detector size of which is d. The R_i at any position along the LOR between the two detectors is given by the full width at half maximum (FWHM) of the activity distribution profile obtained by counting a point source of activity across the detector face at the position. The R_i is $d/2$ at the center of the FOV determined by the FWHM from a triangular profile, while it is d at the edge of the FOV (i.e., the face of the detector) indicated by the red-lined near-rectangular box

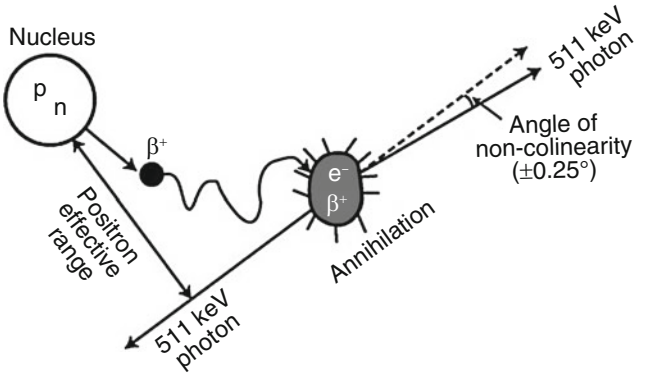

Fig. 6.2 Positrons travel a distance before annihilation in the absorber and the distance increases with positron energy. Since positrons with different energies travel in zigzag directions, the effective range is the shortest distance between the nucleus and the direction of 511-keV photons. This effective range degrades the spatial resolution of the PET scanner (Reprinted with the permission of the Cleveland Clinic Center for Medical Art and Photography ©2009. All rights reserved)

FOV and deteriorates toward the edge of the FOV. For a 6-mm detector, the R_i value is ~3 mm at the center of the FOV and ~6 mm toward the edge of the FOV. For continuous single detectors, however, the intrinsic resolution depends on the number of photons detected, not on the size of the detector, and is determined by the full width at half maximum (FWHM) of the photopeak.

Positron range: A positron with energy travels a distance in tissue, losing most of its energy by interaction with atomic electrons and then is annihilated after capturing an electron (Fig. 6.2). Thus, the site of β^+ emission differs from the site of annihilation as shown in Fig. 6.2. The distance (range) traveled by the positron increases with its energy but decreases with the tissue density.

Since the positrons are deflected after interaction with electrons resulting in a zigzag trajectory, the positron range is essentially an effective range, which is given by the shortest (perpendicular) distance from the emitting nucleus to the positron annihilation line. Furthermore, positrons are emitted with a distribution of energy, which also affects the effective range. The effective positron ranges in water for ^{18}F $\left(E_{\beta^+,\max} = 0.64\,\text{MeV}\right)$ and ^{82}Rb. $\left(E_{\beta^+,\max} = 3.35\ \text{MeV}\right)$ are 2.2 and 15.5 mm, respectively (Table 1.2). Since coincidence detection is related to the location of annihilation and not to the location of β^+ emission, an error (R_p) occurs in the localization of true position of the positron emission thus resulting in the degradation of spatial resolution. This contribution (R_p) to the overall spatial resolution is determined from the FWHM of the positron count distribution, which turns out to be 0.2 and 2.6 mm for ^{18}F and ^{82}Rb, respectively (Tarantola et al. 2003).

Noncolinearity: Another factor of concern is the noncolinearity that arises from the deviation of the two annihilation photons from the exact 180° position. That is, two 511-keV photons are not emitted at exactly 180° after the annihilation process (Fig. 6.3), because of some small residual momentum of the positron at the end of the positron range. The maximum deviation from the 180° direction is ±0.25° (i.e., 0.5° FWHM). Thus, the observed LOR between the two detectors does not intersect the point of annihilation, but is somewhat displaced from it, as illustrated in Fig. 6.3. This error (R_a) degrades the spatial resolution of the scanner and deteriorates with the distance between the two detectors. If D is the distance in cm between the two detectors (i.e., detector ring diameter), then R_a can be calculated from the point-spread function (PSF) as follows:

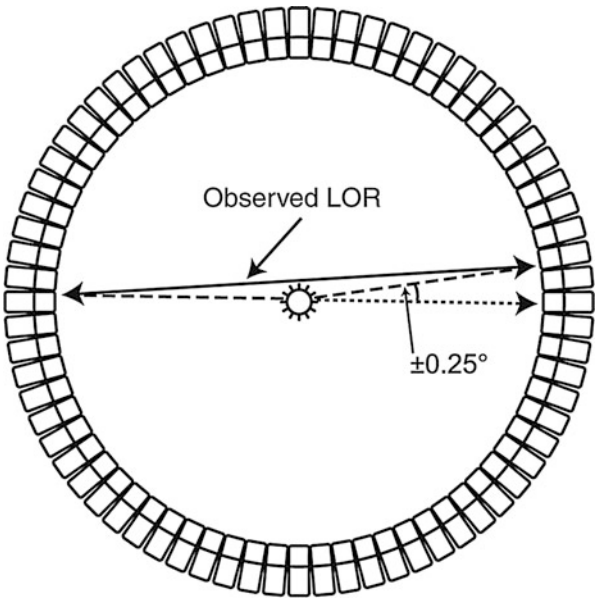

Fig. 6.3 Noncolinearity of 511-keV annihilation photons. Because there is some residual momentum associated with the positron, the two annihilation photons are not emitted exactly at 180° but at a slight deviation from 180°. Two detectors detect these photons in a straight line, which is slightly deviated from the original annihilation line. The maximum deviation is ±0.25° (Reprinted with the permission of the Cleveland Clinic Center for Medical Art and Photography ©2009. All rights reserved)

$$R_a = 0.0022D. \tag{6.1}$$

The contribution from noncolinearity worsens with larger diameter of the ring, and it amounts to 1.8–2 mm for currently available 80–90-cm PET scanners.

Reconstruction method used: Choice of filters with a selected cutoff frequency in the filtered backprojection reconstruction method may introduce additional degradation of the spatial resolution of the scanner. For example, a filter with a too high cutoff value introduces noise and thus degrades spatial resolution. An error (K_r) due to the reconstruction technique is usually a factor of 1.2–1.5 depending on the method (Huesman 1977).

Localization of detector: The use of block detectors instead of single detectors causes an error (R_ℓ) in the localization of the detector by X, Y analysis and it may amount to 2.2 mm for BGO detectors (Moses and Derenzo 1993). However, it can be considerably minimized by using better light output scintillators, such as LSO.

Combining the above factors, the overall spatial resolution R_t of a PET scanner is given by

$$R_t = K_r \times \sqrt{R_i^2 + R_p^2 + R_a^2 + R_\ell^2}. \tag{6.2}$$

In whole-body scanners, the detector elements are normally large, and therefore, $R_i(d$ or $d/2)$ is large so that the contribution of R_p is negligible for ^{18}F-FDG $\left(E_{\beta^+,\max} = 0.64\,\text{MeV}\right)$ whole-body imaging. For ^{18}F-FDG studies using a 90-cm diameter PET scanner with 6-mm detectors, $R_a \sim 2$ mm, and assuming $R_p = 0$, $R_\ell = 2.2$ mm, and $K_r = 1.5$, $R_t = 1.5 \times \sqrt{3^2 + (2.2)^2 + 2^2} = 6.3\,\text{mm}$ at the center of FOV and $R_t = 1.5 \times \sqrt{6^2 + (2.2)^2 + 2^2} = 10.0\,\text{mm}$ at the edge of FOV of the scanner. However, the contribution of R_p may be appreciable for high-energy positron emitters (e.g., ^{82}Rb; $E_{\beta^+,\max} = 3.35\,\text{MeV}$) and small-animal PET scanners (e.g., microPET system) having smaller detectors.

The detailed method of measuring the spatial resolution of a PET scanner is given later in this chapter. The spatial resolutions of PET scanners from different manufacturers are given in Table 6.1.

Sensitivity

The sensitivity of a PET scanner is defined as the number of counts per unit time detected by the device for each unit of activity present in a source. It is normally expressed in counts per second per microcurie (or kilobecquerel) (cps/μCi or cps/kBq). Sensitivity depends on the geometric efficiency, detection efficiency,

Table 6.1 Performance data of different PET scanners

Manufacturers→[a]	Philips[b]		Siemens[c]		GE[c]	
Models→	GEMINI TF	GEMINI TF	Biograph	Biograph	Discovery	Discovery
Features↓	Big Bore	64 (PET/CT)	mCT	TruePoint	VCT	PET/CT 600
Sensitivity – 3D (cps/kBq/cc)	7.2	7.2	9.5	7.6	9.1	9.1
Transverse Resol. at 1 cm (mm)	4.7	4.7	4.4	4.2	5.0 (2D) 5.0 (3D)	5.1
Transverse Resol. at 10 cm (mm)	5.2	5.2	5.8	4.8	5.4 (2D) 5.4 (3D)	5.6
Axial resol. at 1 cm (mm)	4.7	4.7	4.5		5.0 (2D) 5.0 (3D)	5.6
Axial resol. at 10 cm (mm)	5.2	5.2	4.8	5.5	5.6 (3D)	6.3
Peak noise Equivalent Count rate (kcps) (3D)	94	110	100	165 170 (TrueV)	78	76
Scatter fraction (%)	31	30	<36	<36	36	38

[a]Reprinted with permission, Copyright 2009, ECRI institute, http://www.ecri.org, 5200 Butler Pike, Plymouth Meeting, PA 19462. 610-825-6000
[b]Data supplied by Philips Healthcare, USA
[c]Reprinted with permission, Copyright 2009, Imaging Technology News (http://www.itonline.net), Scranton Gillette Communications (http://www.scrantongillette.com) 3030 W. Salt Creek Lane, Suite 201, Arlington Heights, IL 60005-5025. Some of Siemens data were provided by Annemarie Grammens, Siemens Medical Solutions, USA

PHA window settings, and dead time of the system. The detection efficiency of a detector depends on the scintillation decay time, density, atomic number, and thickness of the detector material that have been discussed in Chap. 2. Also, the effect of PHA window setting on detection efficiency has been discussed in Chap. 2. The effect of the dead time on detection efficiency has been described in Chap. 3. In the section below, only the effects of geometric efficiency and other related factors will be discussed.

The geometric efficiency of a PET scanner is defined by the solid angle projected by the source of activity at the detector. The geometric factor depends on the distance between the source and the detector, the diameter of the ring, and the number of detectors in the ring. Increasing the distance between the detector and the source reduces the solid angle and thus decreases the geometric efficiency of the scanner and vice versa. Increasing the diameter of the ring decreases the solid angle subtended by the source at the detector, thus reducing the geometric efficiency and in turn the sensitivity. Also the sensitivity increases with increasing number of rings in the scanner.

Based on the above factors discussed, the sensitivity S of a single-ring PET scanner can be expressed as (Budinger 1998)

$$S = \frac{A \cdot \varepsilon^2 \cdot e^{-\mu t} \cdot 3.7 \times 10^4}{4\pi r^2} (\text{cps}/\mu\text{Ci}), \tag{6.3}$$

where A = detector area seen by a point source to be imaged, ε = detector's efficiency, μ is the linear attenuation coefficient of 511-keV photons in the detector material, t is the thickness of the detector, and r is the radius of the detector ring. The proportionality to ε^2 arises from the two detectors with efficiency ε, i.e., $\varepsilon \times \varepsilon$. So if the single-detector efficiency is reduced by half, the coincidence detection efficiency is $\varepsilon/2 \times \varepsilon/2 = \varepsilon^2/4$.

Equation (6.3) is valid for a point source at the center of a single-ring scanner. For an extended source at the center of such scanners, it has been shown that the geometric efficiency is approximated as $w/2r$, where w is the axial width of the detector element and r is the radius of the ring (Cherry et al. 2003). Thus, the sensitivity of a scanner is highest at the center of the axial FOV and gradually decreases toward the periphery. In typical PET scanners, there are also multiple rings and each detector is connected in coincidence with as many as half the number of detectors on the opposite side in the same ring as well as with detectors in other rings. Thus, the sensitivity of multiring scanners will increase with the number of rings.

Note that the sensitivity of a PET scanner increases as the square of the detector efficiency, which depends on the scintillation decay time and stopping power of the detector. This is why LSO, LYSO, and GSO detectors are preferred to NaI(Tl) or BGO detectors (see Table 2.1). In 2D acquisitions, system sensitivity is compromised because of the use of septa between detector rings, whereas these septa are retracted or absent in 3D acquisition, and hence the sensitivity is increased by a factor of 4–8. However, in 3D mode, random and scatter coincidences increase significantly, the scatter fraction being 30–40% compared to 15–20% in 2D mode. The overall sensitivities of PET scanners for a small-volume source of activity are about 0.2–0.5% for 2D acquisition and about 2–10% for 3D acquisition, compared to 0.01–0.03% for SPECT studies (Cherry et al. 2003). The greater sensitivity of the PET scanner results from the absence of collimators in data acquisition.

Sensitivity is given by volume sensitivity expressed in units of kcps/μCi/cc or cps/Bq/cc. It is determined by acquiring data in all projections for a given duration from a volume of activity (uniformly mixed) and dividing the total counts by the duration of counting and the concentration of the activity in the source. Manufacturers normally use this unit as a specification for the PET scanners. The detailed method of determining volume sensitivity is described under acceptance tests in this chapter. The volume sensitivities of PET scanners from different manufacturers are given in Table 6.1.

Noise Equivalent Count Rate

Image noise is the random variation in pixel counts across the image and is given by $\left(1/\sqrt{N}\right) \times 100$, where N is the counts in the pixel. It can be reduced by increasing the total counts in the image. More counts can be obtained by imaging for a longer period, injecting more radiopharmaceutical, or improving the detection efficiency of the scanner. All these factors are limited by various conditions, e.g., too much activity cannot be administered because of increased radiation dose to the patient, random coincidence counts, and dead-time loss. Imaging for a longer period may be uncomfortable to the patient and improving the detection efficiency may be limited by the design of the imaging device.

The image noise is characterized by a parameter called the noise equivalent count rate (NECR) which is given by

$$\mathrm{NECR} = \frac{T^2}{T + S + R}, \tag{6.4}$$

where T, R, and S are the true, random, and scatter coincidence count rates, respectively. This value is obtained by using a 20-cm cylindrical phantom of uniform activity placed at the center of the FOV and measuring prompt coincidence counts. Scatter and random events are measured according to methods described later in this chapter. The true events (T) are determined by subtracting scatter (S) and random (R) events from the prompt events. From the knowledge of T, R, and S, the NECR is calculated by Eq. (6.4). The NECR is proportional to the signal-to-noise (SNR) ratio in the final reconstructed images and, therefore, serves as a good parameter to compare the performances of different PET scanners. The 3D method has a higher NECR at low activity. However, the peak NECR in the 2D mode is higher than the peak NECR in the 3D mode at higher activity. Image noise can be minimized by maximizing NECR.

Another type of image noise arises from nonrandom or systematic addition of counts due to imaging devices or procedural artifacts. For example, bladder uptake of ^{18}F-FDG may obscure the lesions in the pelvic area. Various "streak"-type artifacts introduced during reconstruction may be present as noise in the image.

Scatter Fraction

The scatter fraction (SF) is another parameter that is often used to compare the performances of different PET scanners. It is given by

$$\mathrm{SF} = \frac{C_\mathrm{s}}{C_\mathrm{p}}, \tag{6.5}$$

where C_s and C_p are the scattered and prompt count rates. The lower the SF value, the better the performance of a scanner and better the quality of images. The method of determining SF is given later in this chapter. Comparative SF values for different PET scanners are given in Table 6.1.

Contrast

Contrast of an image arises from the relative variations in count densities between adjacent areas in the image of an object. Contrast (C) gives a measure of the detectability of an abnormality relative to normal tissue and is expressed as

$$C = \frac{A - B}{A}, \tag{6.6}$$

where A and B are the count densities recorded in the normal and abnormal tissues, respectively.

Several factors affect the contrast of an image, namely, count density, scattered radiations, type of film, size of the lesion, and patient motion. Each contributes to the contrast to a varying degree. These factors are briefly discussed here.

Statistical variations of the count rates give rise to noise that increases with decreasing information density or count density (counts/cm^2) and are given by $\left(1/\sqrt{N}\right) \times 100$, where N is the count density. For a given image, a minimum number of counts are needed for a reasonable image contrast. Even with adequate spatial resolution of the scanner, lack of sufficient counts may give rise to poor contrast due to increased noise, so much so that lesions may be missed. This count density in a given tissue depends on the administered dosage of the radiopharmaceutical, uptake by the tissue, length of scanning, and detection efficiency of the scanner. The activity of a dosage, scanning for a longer period, and the efficiency of a scanner are optimally limited, as discussed above under NECR. The uptake of the tracer depends on the pathophysiology of the tissue in question. Optimum values for a procedure are obtained from the compromise of these factors.

Scattered radiations increase the background in the image and thus degrade the image contrast. Maximum scatter radiations arise from the patient. Narrow PHA window settings can reduce the scatter radiations, but at the same time the counting efficiency is reduced.

Image contrast to delineate a lesion depends on its size relative to system resolution and its surrounding background. Unless a minimum size of a lesion

develops larger than system resolution, contrast may not be sufficient to appreciate the lesion, even at higher count density. The effect of lesion size depends on the background activity surrounding it and on whether it is a "cold" or "hot" lesion. A relatively small-size "hot" lesion is easily well contrasted against a lower background, whereas a small-size "cold" lesion may be missed against the surrounding background of increased activities.

Film contrast is a component of overall image contrast and depends on the type of film used. The density response characteristics of X-ray films are superior to those of Polaroid films and provide the greatest film contrast, thus adding to the overall contrast. Developing and processing of exposed films may add artifacts to the image and, therefore, should be carried out carefully.

Patient motion during imaging reduces the image contrast. This primarily results from the overlapping of normal and abnormal areas due to movement of the organ. It is partly alleviated by restraining the patient or by having the patient in a comfortable position. Artifacts due to heart motion can be reduced by using the gated technique. Similarly, breath holding may improve the thoracic images.

Quality Control of PET Scanner

In the image formation of an object using PET scanners, several parameters related to the scanners play a very important role. To ensure high quality of images, several quality control tests must be performed routinely on the scanner. The frequency of these tests is either daily or weekly or even at a longer interval depending on the type of parameter to be evaluated.

Daily Quality Control Tests

Sinogram (*uniformity*) *check*: Sinograms are obtained daily using a long-lived ^{68}Ge or ^{137}Cs source mounted by brackets on the gantry and rotating it around the scan field without any object in the scanner. It can also be done by using a standard phantom containing a positron emitter at the center of the scanner. All detectors are uniformly exposed to radiations to produce homogeneous detector response and hence a uniform sinogram. A malfunctioning detector pair will appear as a streak in the sinogram.

Typically, the daily acquired blank sinogram is compared with a reference blank sinogram obtained during the last setup of the scanner. The difference between the two sinograms is characterized by the value of the so-called average variance, which is a sensitive indicator of various detector problems. It is expressed by the square sum of the differences of the relative crystal efficiencies between the two scans weighted by the inverse variances of the differences. The sum divided by the total number of crystals is the average variance. It is essentially an χ^2 value. If the

average variance exceeds 2.5, recalibration of the PET scanner is recommended, whereas for values higher than 5.0, the manufacturer's service is warranted (Buchert et al. 1999). In Fig. 3.4, the average variance between the two scans is 1.1, indicating all detectors are working properly.

Weekly Quality Control Tests

In the weekly protocol, system calibration and plane efficiency are performed by using a uniform standard phantom filled with radioactivity, and normalization is carried out by using a long-lived radionuclide rotating around the field of view or a standard phantom with radioactivity placed at the center of the scanner.

System calibration: A system calibration scan is obtained by placing the standard phantom containing a positron emitter in a phantom holder at the center of the FOV for uniform attenuation and exposure. The reconstructed images are checked for any nonuniformity. A bad detector indicates a decreased activity in the image and warrants the adjustment of PM tube voltage and the discriminator settings of PHA.

Normalization: As discussed in Chap. 3, normalization corrects for nonuniformities in images due to variations in the gain of PM tubes, the location of the detector in the block, and the physical variation of the detector. This test is carried out by using a rotating rod source of a long-lived radionuclide (normally ^{68}Ge) mounted on the gantry parallel to the axis of the scanner or using a standard phantom containing a positron emitter at the center of the scanner. The activity used in the source is usually low to avoid dead-time loss. Data are acquired in the absence of any object in the FOV. The source activity exposes all detectors uniformly. The multiplication factor for each detector is calculated by dividing the average of counts of all detector pairs by each individual detector pair count (i.e., along the LOR) Eq. (3.3). These factors are saved and later applied to the corresponding detector pairs in the acquired emission data of the patient Eq. (3.4). Normalization factors normally are determined weekly or monthly. To have better statistical accuracy in individual detector pair counts, several hours of counting is necessary depending on the type of scanner, and therefore, overnight acquisition of data is often made.

Dose calibration of PET scanner: Standard uptake values (SUV) and other parameters of PET images are often calculated that require the knowledge of absolute activity in regions of interest (ROI). The counts (corrected for randoms, dead time, scatter, and attenuation) in individual pixels of the ROI are converted to absolute activity by using calibration factors. To calculate the calibration factor, *CF*, a cylindrical phantom (normally 20 cm long and 20 cm in diameter) containing a known amount of positron-emitter activity (e.g., ^{68}Ge or ^{18}F) in a known volume is scanned, and an image is obtained. The calculated concentration of activity (A_{cal}) is given by

$$A_{\text{cal}} = \frac{A}{V} \times N \times \exp\left[-0.693t/t_{1/2}\right], \tag{6.7}$$

where A is the activity (Bq or μCi) in the phantom measured in a dose calibrator, V is the volume of the phantom (mL), N is the branching ratio of positron decay of the radionuclide, t is the time delay from initial measurement to the start of the scan, and $t_{1/2}$ is the half-life of the radionuclide used. Some investigators determine the activity by measuring an aliquot of the sample in a well counter whose counting efficiency is known.

Images are reconstructed using the scan data of the phantom after correction for scatter, randoms, and attenuation. Using a large ROI on each of the central image slices, the mean ROI activity (Bq/pixel *or* μCi/pixel) for each slice is calculated, from which an average measured activity A_{measured} is calculated using the ROIs of all slices. The calibration factor CF is then given by

$$CF = \frac{A_{\text{measured}}}{A_{\text{cal}}}. \tag{6.8}$$

CF is applied to the measured activity in each voxel of the ROI of interest of the patient scan (by dividing) to calculate the absolute activity, which is then multiplied by the area of the ROI to obtain SUV. Note that if the radionuclide in the patient study is different from the calibration source radionuclide, the branching ratio N of the radionuclide must be taken into calculation. This calibration of PET scanners should be performed at installation, after major service or at least annually.

Quality Control of CT Scanner

Like PET scanners, CT scanners need daily QC testing to check if they are performing within acceptable limits of operational parameters. Most of the daily tests are automatic and less rigorous. These tests include tube voltage, mA setting, and detector response, which are available as system-ready messages. Operator-based daily QC tests include the evaluation of image uniformity, accuracy of CT numbers of water (given in Hounsfield unit HU), tube voltage, and image noise measured at commonly used voltages. The uniformity is assessed by observing the display of a CT image of a phantom. Water CT numbers and standard deviations are measured by using a water phantom in the scan plane and should be within 0 ± 5 HU. All these measurements are mostly menu driven initiated by the manufacturers' software, and the final result is often given in the form of PASS/FAIL display. Other parameters such as slice thickness, spatial resolution, contrast resolution, linearity, and laser alignment are assessed monthly or quarterly as recommended by the manufacturers.

An important parameter, CT dose index (*CTDI*, defined as the cumulative dose along the patient's axis for a single tomographic image), should be evaluated at least semiannually at different values of kVp and mA. It is measured by using an ionization chamber or thermoluminescent dosimeters placed in a tissue-equivalent acrylic phantom simulating the head or body. ACR (2015)[1] recommends reference doses (CTDI) of 7.5 mrad (75 mGy) for adult head, 2.5 rad (25 mGy) for adult abdomen and 3.5 rad (35 mGy) for pediatric (1-yr old) head. The details of these measurements are available in standard CT physics books.

Quality Control of MR Scanner

The American College of Radiology (ACR) mandates that like other imaging devices, quality control (QC) tests are performed on MR scanners to obtain better images of patients, especially for accreditation of an institution. In order to perform these tests, the ACR has introduced short cylindrical phantoms made of acrylic plastic with specific dimensions, which are called ACR phantoms and has two sizes—small and large. Inside the phantoms, there are several complex structures to generate suitable images for quantitative or qualitative analysis. Specifications and frequencies of the tests to be performed are given by the ACR. Some tests are performed daily and some others weekly or annually. The common routine QC tests for optimum operation of MR scanners are listed below:

1. *Geometric efficiency*: It measures the lengths on the images between locations in the phantom and compares them with the true values of those lengths. Affected by miscalibrated gradient and inhomogeneity in magnetic field (daily or weekly).
2. *High-contrast spatial resolution*: It is a measure of how well the MR scanner can delineate the structures on the images and determined by the spatial resolution of the holes inside the phantom. It is specific but not sensitive and also affected by the poor gradient and inhomogeneity in magnetic field (daily or weekly).
3. *Uniformity*: It indicates the constant signal response throughout the image obtained of the phantom filled with water. It is calculated in percent from the high and low signals from an ROI on the phantom image as $\% = [(1 - (\text{high} - \text{low})/(\text{high} + \text{low}))]$.
4. *Slice thickness*: The accuracy of slice thickness is assessed by comparing the measured and assigned slice thicknesses (annually).

[1] Data used with permission of the American College of Radiology (ACR). No other representation of this material is authorized without expressed, written permission from the ACR. Refer to the ACR website at www.acr.org (Computed Tomography Accreditation) for the most current and complete information.

5. *Slice position accuracy*: It is measured by the difference between the assigned and actual positions of specific sites using 45° cross wedges in the ACR phantom, which appear as bars on the image (annually).
6. *Percent signal ghosting*: These are artifacts caused by a faint copy (ghost) of the imaged object appearing superimposed on the image, displaced from its true location, and essentially result from signal instability between pulse cycle repetitions.
7. *Low-contrast detectability*: This test assesses how low-contrast objects are delineable in the image obtained by using the ACR phantom that contains a set of low-contrast objects of various sizes and contrast. The low-contrast detectability is determined by contrast-to-noise ratios in the image and is affected by artifacts like ghosting.

For most tests the ACR phantom filled with water solution of various paramagnetic ions such as manganese, copper, and nickel is used and positioned at the center of the magnet. Scanning is performed for all tests with preset scan parameters such as pulse sequence, timing parameters (T1, T2, TR, TE, etc.), flip angle, matrix size, field of view, RF power setting, slice thickness, number of acquisition, and other relevant parameters. Some tests can be performed by technologists, whereas others must be performed by certified medical physicists, as required by the ACR. The details of these tests are available from acr.org and also the American Association of Physicists in Medicine (AAPM 2010).

Acceptance Tests for PET Scanner

Acceptance tests are a battery of quality control tests performed to verify various parameters specified by the manufacturer for a PET scanner. These are essentially carried out soon after a PET scanner is installed in order to establish the compliance of specifications of the device. The most common and important specifications are transverse radial, transverse tangential, and axial resolutions; sensitivity; scatter fraction; and count rate performance. It is essential to have a standard for performing these tests so that a meaningful comparison of scanners from different manufacturers can be made.

In 1991, the Society of Nuclear Medicine (SNM) established a set of standards for these tests for PET scanners (Karp et al. 1991). Afterward, in 1994, the National Electrical Manufacturers Association (NEMA) published a document, NU 2-1994, recommending improved standards for performing these tests, using a 20 × 19-cm phantom (NEMA 1994) (Fig. 6.4a). This phantom was useful for earlier scanners, in which the FOV was less than 17 cm and data were acquired in 2D mode, because of the use of septa. Modern whole-body PET scanners have FOVs as large as 25 cm and employ 3D data acquisition in the absence of septa. The coincidence gamma cameras have typical FOVs of 30–40 cm. Because of larger FOVs and high count rates in 3D mode, the NU 2-1994 phantom may not be accurately applied for some

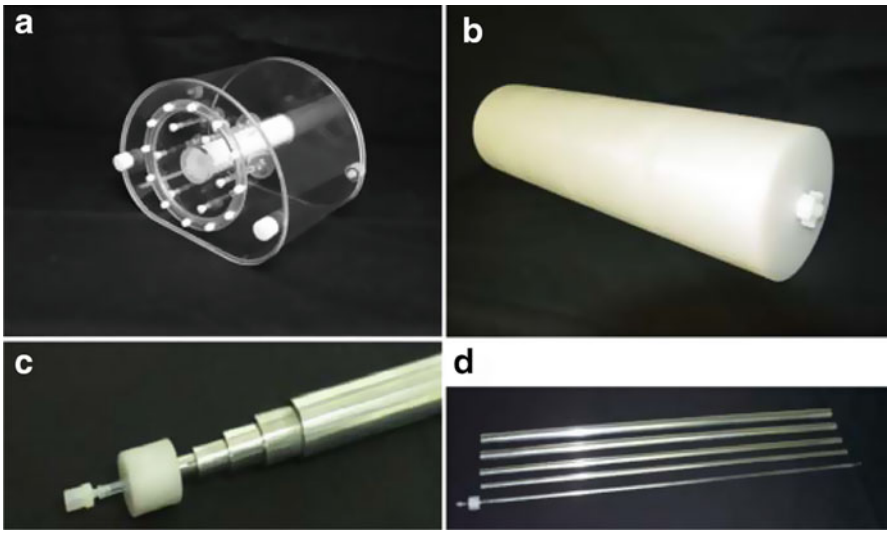

Fig. 6.4 NEMA phantoms for PET performance tests. (**a**) This NEMA body phantom is used for evaluation of the quality of reconstructed images and simulation of whole-body imaging using camera-based coincidence imaging technique. (**b**) This phantom is used for measuring scatter fraction, dead time, and random counts in PET studies using the NEMA NU 2-2007 standard, (**c**) closeup end of the sensitivity phantom, (**d**) set of six concentric aluminum tubes used in phantom (**c**) to measure the sensitivity of PET scanners (Courtesy of Data Spectrum Corporation, Hillborough, NC)

tests in some scanners, and a new NU 2-2001 standard has been published by NEMA in 2001 (NEMA 2001) and corresponding new phantoms have been introduced.

Currently most PET scanners use the LSO or LYSO detectors composed of natural lutetium (Lu) that has a 2.6% radioisotopic content of ^{176}Lu ($t_{1/2} = 4.0 \times 10^{10}$ years). This isotope emits β^- particle and a cascade of high-energy γ- and X-rays. These intrinsic radiations cause errors in the performance parameters of a scanner such as the sensitivity, count losses, random events, etc. To correct for the contribution of this intrinsic activity, Watson et al. (2004) have recommended modifications in the performance tests and accordingly, NEMA has introduced the NEMA NU 2-2007 (2007) standard for these tests of PET scanners with Lu-based detectors. Many features of this standard have been kept the same as those of the NU 2-2001 standard, with some modifications for the sensitivity, count losses, and random events.

NEMA has recently published NU 2-2012 (2012) with minor changes to the 2007 version to make the tests reproducible and easy to carry out. No publication using this model for validation of commercial PET scanners has been reported in the literature as of this writing. Daube-Witherspoon et al. (2002) reported the methods of performing these tests based on the NEMA NU 2-2001 standard. The following is a brief description of these tests based on this article and the article of

Watson et al., and NEMA NU 2-2007, and NEMA NU 2-2012 standard has been alluded to, wherever needed. Refer to these publications for further details.

Spatial Resolution

The spatial resolution of a PET scanner is determined by the FWHM of PSFs obtained from measurement of activity distribution from a point source. The spatial resolution can be transverse radial, transverse tangential, and axial, and these values are given in Table 6.1 for scanners from different manufacturers.

The spatial resolution is measured by using six-point sources of ^{18}F activity contained in glass capillary in a small volume of less than 1 cm^3 (Daube-Witherspoon et al. 2002). *NEMA NU 2-2012 suggests an activity source contained in a capillary of 1 mm inner diameter and 2 mm length*. For axial resolutions, two positions—at the center of the axial FOV and at one-fourth of axial FOV from the center—are chosen (Fig. 6.5), *whereas NEMA NU 2-2012 suggests the latter position at three-eighth of the axial FOV from the center*. At each axial position, three point sources are placed at $x = 0$, $y = 1$ cm (to avoid too many sampling of LORs); $x = 10$, $y = 0$ cm; and $x = 0$, $y = 10$ cm. Data are collected for all six positions and from reconstructed image data, PSFs are obtained in X, Y, and Z directions for each point source at each axial position. The FWHMs are determined from the width at 50% of the peak of each PSF, totaling 18 in number.

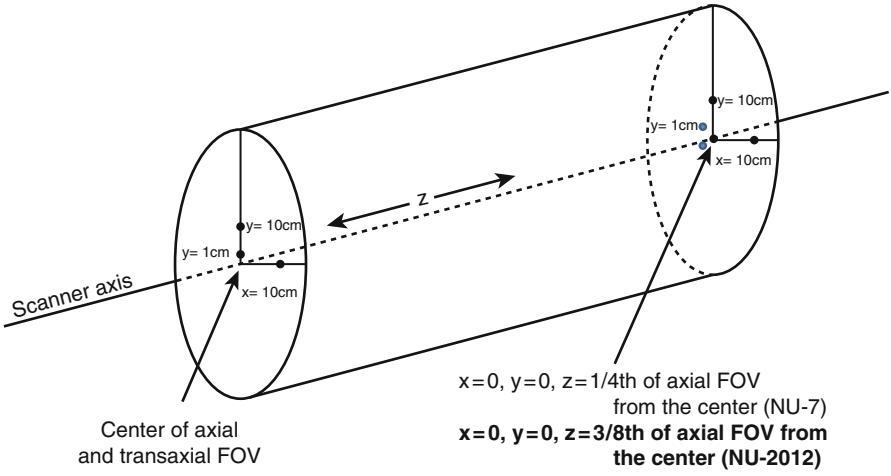

Fig. 6.5 Arrangement of six-point sources in the measurement of spatial resolution. Three sources are positioned at the center of the axial FOV and three sources are positioned at one-fourth of the axial FOV (NEMA 7) or three-eighth of the axial FOV (NEMA 12) away from the center. At each position, sources are placed on the positions indicated in a transverse plane perpendicular to the scanner axis (Reprinted with the permission of the Cleveland Clinic Center for Medical Art and Photography ©2009. All rights reserved)

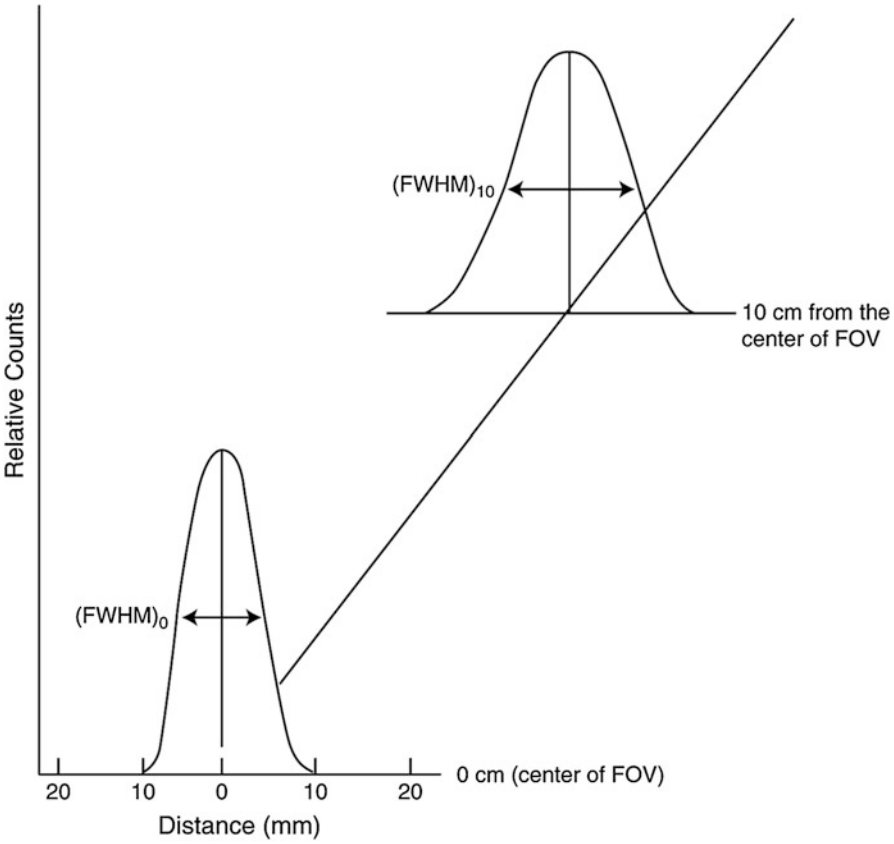

Fig. 6.6 Point-spread functions (PSF) at 0 and 10 cm from the FOV. The transverse resolution (FWHM) is best at the center and worsens radially across the FOV (Reprinted with the permission of the Cleveland Clinic Center for Medical Art and Photography ©2009. All rights reserved)

Related FWHMs are combined and then averaged for the two axial positions to give the transverse radial, transverse tangential, and axial resolutions. Transverse resolution worsens as the source is moved away from the center of the FOV (Fig. 6.6), i.e., the resolution is best at the center and deteriorates toward the periphery of the scanner.

Scatter Fraction

Scattered radiations add noise to the reconstructed image, and the contribution varies with different PET scanners. Normally the test is performed with a very high activity source counted over a period of time, from which high activity data are used for determination of random events and count losses (see later) and low activity

data for scatter fraction. A narrow line source made of 70-cm-long plastic tubing and filled with high activity of ^{18}F is inserted into a 70×20-cm cylindrical polyethylene phantom through an axial hole made at a radial distance of 4.5 cm and parallel to the central axis of the phantom (Fig. 6.4b). NEMA NU 2-2012 recommends similar parameters for the test. The phantom is placed at the center both axially and radially on the scan table such that the source is closest to the patient table, since the line source and the bed position affect the measured results.

Data acquisition is recommended in two ways based on whether random events are estimated separately for scanners with Lu-based detectors or they are assumed negligible as in scanners with non-Lu detectors. If the random events are to be estimated independently for Lu-based scanners, then data are acquired over time using two windows—a peak window and a delayed window—until both dead-time count losses and random events are reduced to less than 1% of the true rates. For PET scanners with non-Lu detectors, data acquisition is continued with only a peak window until the random-to-true ratio is less than 1% (NEMA 2007). The data are used to form both random and prompt sinograms, which are basically 2D representation of projection rays versus angle. Oblique projections are assigned to the slice where they cross the scanner axis using single-slice rebinning. The sinogram profile of an extended diameter of 24 cm (4 cm larger than the phantom) is generated, because the FOV varies with different scanners. Each projection in the sinogram is shifted so that the peak of the projection is aligned with the center of the sinogram (line source image). This produces a sum projection with a count density distribution around the maximum counts (peak) at the center of the sinogram (NEMA 2001, 2007). It is arbitrarily assumed that all true events including some scatter lie within a 4-cm-wide strip centered in each sinogram of the line source and that there are no true events but scatter events beyond ± 2 cm from the center of the sinogram. Thus, the total count C_T is the area under the peak in prompt sinogram that includes true events plus scatter and random events. In the case of PET scanners with non-Lu detectors, C_T will contain only the true plus scatter events.

For Lu-based PET scanners, random counts are estimated from the delayed window sinograms for all projections in a slice to give C_R for the slice, which is then applied to calculate true and scatter events. For non-Lu scanners, random events are negligible and not measured separately.

Scattered events under the peak are estimated by taking the average of the pixel counts at ± 2-cm positions from the center, multiplying the average by the number of pixels (obtained by interpolation) along the 4-cm strip and finally adding the product to the counts in pixels outside the strip. This gives total scatter events (C_S) for the slice. Using the values of C_T, C_R, and C_S, the true count for a slice is calculated as

$$C_{\text{true}} = C_T - C_R - C_s \tag{6.9}$$

and for PET scanners with non-Lu detectors, the true count is

$$C_{\text{true}} = C_{\text{T}} - C_{\text{s}}. \tag{6.10}$$

The scatter fraction SF_i for the slice is given by Eq. (6.5) as

$$\text{SF}_i = C_{\text{s}}/(C_{\text{true}} + C_{\text{s}}). \tag{6.11}$$

The system scatter fraction SF is calculated from the weighted average of the SF_i values of all slices. These values are given in Table 6.1 for several PET scanners.

Note that counting rates for each component are calculated by dividing the respective counts by time of acquisition to give total count rate R_{T}, true count rate R_{True}, random count rate R_{R}, and scatter count rate R_{S}.

Sensitivity

Sensitivity is a measure of counting efficiency of a PET scanner and is expressed in count rate (normally, cps) per unit activity concentration (normally, MBq or μCi per cc).

According to NEMA NU 2-2001 and NEMA NU 2-2007 standards, a 70-cm-long plastic tube filled with a known amount (A_{cal}) of a radionuclide is used (Fig. 6.4c, d) (Daube-Witherspoon et al. 2002). The level of activity is kept low so as to have random rate less than 5% of the true counts and count loss less than 1% (*<5% according to NEMA NU 2-2012*). The source is encased in metal sleeves of various thicknesses and suspended at the center of the transverse FOV in parallel to the axis of the scanner in such a way that the supporting unit stays outside the FOV.

Successive data are collected in sinograms using five metal sleeves. Duration of acquisition and total counts in the slice are recorded for each sleeve, from which the count rate is calculated. Count rates are corrected for decay to the time of calibration of radioactivity and then summed for all slices to give the total count rate for each sleeve. Next, the natural logarithm of the measured total count rate (R_{T}) is plotted as function of sleeve thicknesses. After fitting of the data by linear regression, the extrapolated count rate (R_0) with no metal sleeve (no attenuation) is obtained. For non-Lu scanners, the random rate ($R_{\text{R}} = C_{\text{R}}/T_{\text{acquisition}}$) is negligible. Scatter count rate determined by the method described previously is subtracted from R_0 to give the true count rate (R_{true}) for the system. Thus,

$$R_{\text{true}} = R_0 - R_{\text{S}}. \tag{6.12}$$

For Lu-based scanners, there is an intrinsic activity as well as possible intrinsic random events due to ^{176}Lu, which need to be subtracted from the total count rate.

These can be measured with the plastic tubing in place in the scanner but without any activity in it. Both prompt and delayed acquisitions are made of the tubing as described in the section on Scatter Fraction, from which intrinsic prompt rate and intrinsic random rate are calculated. The true intrinsic count rate R_{int} is obtained by subtracting the random rate from the prompt rate in all sinograms. Thus, for Lu-based scanners, true count rate R_{true} is given as

$$R_{\text{true}} = R_0 - R_{\text{S}} - R_{\text{R}} - R_{\text{int}}. \tag{6.13}$$

The system sensitivity is calculated as

$$S = R_{\text{true}}/A_{\text{cal}}, \tag{6.14}$$

where A_{cal} is the calibrated activity added to the tubing. The sensitivity is given in either cps/μCi/cc or cps/kBq/cc. The measurement of sensitivity is repeated with the source placed radially at 10 cm from the center of the transverse FOV. The system sensitivity of commercial PET scanners is given for both 0- and 10-cm positions and the values for some scanners at the center of FOV are given in Table 6.1.

Count Rate Loss and Random Coincidence

To characterize the count rate behavior of a PET scanner at high activity, random events, NECR, and dead-time loss are determined as a function of activity. The activity source is the same as described above under Scatter Fraction in this chapter. A high activity source of ^{18}F is used to acquire the sinogram, and data are collected until the activity level is low enough to consider random events and dead-time count losses to be negligible. The total counts are obtained from each high activity sinogram, which comprise true, random, and scatter events. The total count rate R_{T} is obtained by dividing the total counts by the duration of acquisition. As in scatter fraction experiment, the low activity data are used to calculate the scatter fraction SF_i and the true count rate R_{true} for each slice Eqs. (6.9)–(6.11). The random count rate R_{R} at high activity acquisition for each slice is then calculated according to Daube-Witherspoon et al. (2002) as

$$R_{\text{R}} = R_{\text{T}} - [R_{\text{true}}/(1 - SF_i)]. \tag{6.15}$$

The system random count rate is calculated by summing R_{R} values for all slices.

The NECR for each slice is computed by Eq. (6.4) as

$$(\text{NECR}) = (R_{\text{true}})^2/R_{\text{T}}. \tag{6.16}$$

The system NECR is computed as the sum of NECRs for all slices. These values for some PET scanners are shown in Table 6.1.

The percent dead-time count loss (%DT) as function of activity is calculated by

$$\%\text{DT} = \left(1 - R_{\text{true}}/R_{\text{extrap}}\right) \times 100, \tag{6.17}$$

where R_{extrap} is the count rate extrapolated from the low activity data to the activity at the time when the total count rate R_{T} is measured.

Questions

1. The typical transaxial resolution at 1 cm of a PET scanner ranges between (a) 14 and 16 mm, (b) 3 and 4 cm, or (c) 4 and 7 mm.
2. What are the common factors that affect the spatial resolution of a PET scanner? Out of these, which one is most predominant?
3. The transverse resolution is worse at the center of the FOV than away from the center. True _____; False _____.
4. The axial resolution of a scanner is its ability to differentiate two points on an image along the axis of the scanner. True _____; False _____.
5. If the detector size is 8 mm, what is the expected approximate spatial resolution for ^{18}F-FDG PET images at the center of the FOV?
6. The maximum positron energy for ^{18}F is 0.64 MeV and for ^{82}Rb is 3.35 MeV. Which radiopharmaceutical would provide better spatial resolution?
7. Noncolinearity is a factor that affects the spatial resolution of a PET scanner. How is it affected by the diameter of the detector ring? For a 90-cm diameter detector ring, what is the value of the noncolinearity component in the overall spatial resolution?
8. Describe the method of measuring transverse radial, transverse tangential, and axial spatial resolutions of a PET scanner.
9. Define the sensitivity of a PET scanner and discuss the important parameters that affect the sensitivity.
10. Scanner 1 has twice the ring diameter of scanner 2. The ratio of sensitivities of scanner 1 to scanner 2 is:

    (a) 0.75
    (b) 0.67
    (c) 0.25

11. The sensitivity in 3D acquisition is four to eight times higher than in 2D acquisition. Why?
12. The overall sensitivities of PET scanners in 2D mode are:

    (a) 1–2%
    (b) 3–5%
    (c) 0.2–0.5%

    and in 3D mode:

    (a) 2–10%
    (b) 0.5–1%
    (c) 15–20%

13. Scanner 1 has the detectors of size 3 mm, and scanner 2 has the detectors of size 6 mm. Assuming that all detectors are squares and all other parameters are the same, the sensitivity of scanner 1 is: (a) half, (b) one-tenth, or (c) one-fourth of scanner 2.
14. Describe the methods of daily and weekly quality control tests for PET and CT scanners.
15. Explain why and how normalization of PET acquisition data is carried out.
16. What are acceptance tests? Describe the methods of determining sensitivity and scatter fraction for a PET scanner.
17. The NECR is proportional to the signal-to-noise ratio in the reconstructed image. True _____; False _____.
18. The sensitivity of a scanner increases with (a) the size of the detector in the ring True _____; False _____ and (b) with the diameter of the detector ring True _____; False ____.
19. Scanner 1 has the individual detector size of 36 mm^2 and scanner 2 has the detector size of 60 mm^2. Scanner 1 has (a) 30%, (b) 60%, or (c) 1.7 times the sensitivity of scanner 2.
20. Define contrast of an image. Elucidate the different factors that affect the contrast.
21. Increasing administered activity increases the spatial resolution. True _____; False ___.
22. Increasing administered activity increases the contrast resolution. True _____; False _____.
23. The daily QC check of CT scanner includes (a) laser alignment, (b) CT number of water, (c) tomographic uniformity, or (d) tomographic image noise.
24. Define CTDI.
25. Elucidate different parameters that are measured in the quality control of MR scanner.
26. What type of phantoms are used in MR quality control tests.

References and Suggested Reading

AAPM. Report no 100. Acceptance testing and quality assurance procedures for magnetic resonance imaging facilities. 2010.

Brix G, Zaers J, Adam LE, et al. Performance evaluation of a whole-body PET scanner using the NEMA protocol. J Nucl Med. 1997;38:1614.

Buchert R, Bohuslavizki UH, Mester J, et al. Quality assurance in PET: evaluation of the clinical relevance of detector defects. J Nucl Med. 1999;40:1657.

Budinger TF. PET instrumentation: what are the limits? Semin Nucl Med. 1998;28:247.

Cherry SR, Sorensen JA, Phelps ME. Physics in nuclear medicine. 3rd ed. Philadelphia: Saunders; 2003.

Daube-Witherspoon ME, Karp JS, Casey ME, et al. PET performance measurement using the NEMA NU 2-2001 standard. J Nucl Med. 2002;43:1398.

Huesman RH. The effects of a finite number of projection angles and finite lateral sampling of projections on the propagation of statistical errors in transverse section reconstruction. Phys Med Biol. 1977;22:511.

Karp JS, Daube-Witherspoon ME, Hoffman EJ, et al. Performance standards in positron emission tomography. J Nucl Med. 1991;32:2342.

Kearfott K. Sinograms and diagnostic tools for the quality assurance of a positron emission tomograph. J Nucl Med Technol. 1989;17:83.

Keim P. An overview of PET quality assurance procedures: part 1. J Nucl Med Technol. 1994;22:27.

Moses WW, Derenzo SE. Empirical observation of performance degradation in positron emission tomographs utilizing block detectors. J Nucl Med. 1993;34:101P.

National Electrical Manufacturers Association. NEMA Standards Publications NU 2-1994. Performance measurements of positron emission tomographs. Washington, DC: National Electrical Manufacturers Association; 1994.

National Electrical Manufacturers Association. NEMA Standard Publication NU 2-2001. Performance measurements of positron emission tomographs. Rosslyn: National Electrical Manufacturers Association; 2001.

National Electrical Manufacturers Association. NEMA Standard Publication NU 2-2007. Performance measurements of positron emission tomographs. Rosslyn: National Electrical Manufacturers Association; 2007.

National Electrical Manufacturers Association. NEMA Standard Publication NU 2-2012. Performance measurements of positron emission tomographs. Rosslyn: National Electrical Manufacturers Association; 2012.

Tarantola G, Zito F, Gerundini P. PET instrumentation and reconstruction algorithms in whole-body applications. J Nucl Med. 2003;44:756.

Watson CC, Casey ME, Eriksonn L, et al. NEMA NU2 performance tests for scanners with intrinsic activity. J Nucl Med. 2004;45:822.

Zanzonico P. Routine quality control of clinical nuclear medicine instrumentation: a brief review. J Nucl Med. 2008;49:1114.

Chapter 7
Cyclotron and Production of PET Radionuclides

Introduction

Nearly 3700 nuclides are known to exist, of which approximately 280 are stable and the remainder are radioactive. The majority of radionuclides are artificially produced in the cyclotron and reactor. In PET technology, only positron-emitting radionuclides are required, and only a few positron emitters of all radionuclides have been suitably utilized in clinical studies. These radionuclides include ^{11}C, ^{13}N, ^{18}F, ^{15}O, etc., and are produced in the cyclotron. The operation of a cyclotron and the production of useful positron emitters are described below.

Cyclotron Operation

In a cyclotron (Fig. 7.1), charged particles (S) are accelerated in circular paths within the two D-shaped hollow metallic electrodes called the *dees* (A and B) under vacuum by means of an electromagnetic field. Charged particles can be either positive ions (e.g., proton, deuteron, α particle) or negative ions (e.g., negatively charged hydrogen atom, H^-). The following is a description of a cyclotron to accelerate H^- particles (negative ion cyclotrons).

The ions are obtained from an ion source (S) positioned at the center of the cyclotron. The ion source is a small chamber located between two negative high-voltage (V) (1–3 kV) tantalum cathodes. The hydrogen gas flows (4–10 mL/min) into the chamber. Electrons emitted from the cathodes and constrained by the magnetic field of the main magnet interact with the hydrogen atoms to form a plasma in the chamber that consists of three entities: protons, negatively charged hydrogen atoms H^-, and neutral hydrogen atoms. In some cyclotrons, the gas is ionized by applying 20 kV DC, producing proton and H^-. Protons or negative

G.B. Saha, *Basics of PET Imaging*, DOI 10.1007/978-3-319-16423-6_7

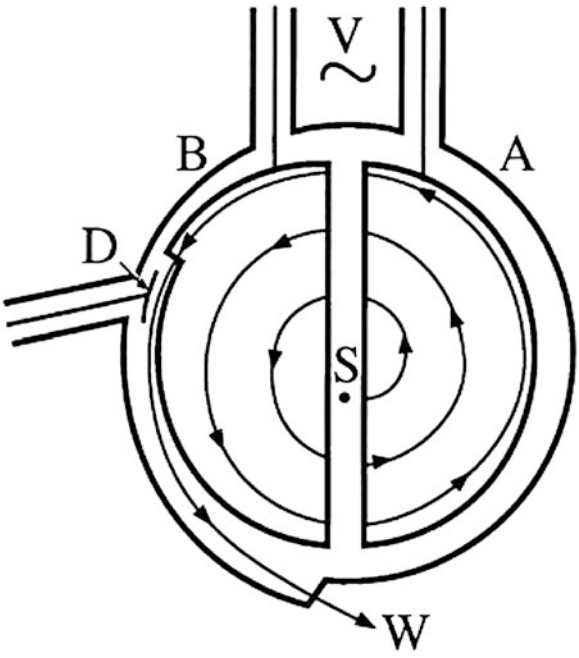

Fig. 7.1 A schematic illustration of a cyclotron: *V* alternating voltage, *S* ion source, *A* and *B* dees under vacuum, *D* carbon foil stripper, *W* window

hydrogen ions (H^-) are pulled out of the ion source chamber through a narrow slit by the electrostatic force depending on the polarity of the dees.

The two dees (A and B) are half-pie-shaped, troughlike, hollow copper structures connected to an alternating high-voltage (30 kV) oscillator operating at radiofrequencies of 20–30 MHz and are positioned between the two poles of an electromagnet. In some cyclotrons, there are four dees, which look like a quarter of a pie. The inside of the dees is kept at extremely high vacuum (10^{-6} mtorr for positive ions and 10^{-7} mtorr for negative ions). Since H^- can lose its electrons on interaction with any molecule inside the dee, such high vacuum is essential in negative ion cyclotrons, which is tenfold higher than in positive ion cyclotrons. Charged ions are attracted toward a dee with an opposite charge during the cycle of oscillating radiofrequency voltage waveforms and pass into the hollow dee, while in the dee, ions do not experience any electrical field, but are subjected to a magnetic field provided by a large electromagnet (up to 2 T). Under the magnetic field, the path of the ions bends such that as the ions reach the edge of the dee, the polarity of the dee is changed. At this moment, the ions are repelled by the dee and also attracted toward the opposite dee, thus gaining more kinetic energy to accelerate. The radiofrequency is so synchronized that every time the ions cross the dee intersection, the polarity of the dee is changed and the ions gain energy and travel in a larger trajectory in the dee. For a particular cyclotron, the energy of the ions depends on the radius of the cyclotron, magnetic field, and charge and mass of the ion. Thus, the kinetic energy (KE) of the ion is given by

$$\mathrm{KE} = \frac{(qMr)^2}{2m}, \tag{7.1}$$

where q is the charge of the particle, M is the magnetic field in gauss, r is the radius of the cyclotron, and m is the mass of the particle.

Since negative H^- ions do not interact with the nuclei of the target and positive ions do, a 2- to 5-μm-thick and <4 cm in diameter carbon foil (D) is inserted vertically inside the cyclotron just ahead of the target position to strip two electrons to produce positive ions (i.e., protons), which then can cause nuclear reactions in target nuclei. The carbon foils are loaded in a carousel, and multiple such carousels (e.g., 2–6) are placed in appropriate locations near the exit inside the cyclotron. The carousels are spun under computer control providing multiple beam lines as needed. The negative ion cyclotron offers the scope of dual bombardments where two targets can be irradiated simultaneously. A carousel containing the carbon-stripping foil is inserted in the path of the beam in such a way that only a part of the beam passes through it producing a positive ion beam that is steered out to the beam line leading to a target for radionuclide production. The remainder of the beam is intercepted by a carbon foil in another carousel further down the orbit to produce a second positive ion beam aimed at another target. Two separate targets can be used for the production of two different radionuclides (e.g., ^{18}F and ^{13}N) or two same targets may be used to produce a larger quantity of the same radionuclide. The kinetic energy of the accelerated particles can vary from a few MeV to several hundred MeV depending on the size and design of the cyclotron. For a given cyclotron, the external beam energy remains constant, whereas the internal beam energy varies radially inside the cyclotron. Various particles, namely, α particle, proton, deuteron, ^3He, and a few heavy ions can be accelerated depending on the design of the cyclotron. The operation of cyclotrons is mostly automatic with minimal manual input and is controlled by the computer.

There are several features that make the negative ion cyclotron operationally more advantageous than the positive ion cyclotron. Beam extraction in a positive ion cyclotron is accomplished by steering the beam along a relatively long channel under the application of an electrostatic force with an extraction efficiency of ~80%. The remaining 20% of the positron beam is lost inside the cyclotron inducing radioactivity in the housing. This obviously warrants more shielding around the cyclotron unit. In contrast, beam extraction in a negative ion cyclotron by carbon foil stripping is a simple method. Because of the short path of extraction and an extraction efficiency of almost 100%, cyclotron housing is not activated by negative ions and shielding requirement is less than in positive ion cyclotrons. In a negative ion cyclotron, the particle beam can be split into several beam lines providing the scope of irradiating several targets simultaneously. On the other hand, a positive ion cyclotron is limited to only a single beam line because of the large size of the electrostatic deflector. However, since H^- can lose the electrons by an encounter with any molecule producing positive ions, the vacuum inside the negative ion cyclotron needs to be extremely high compared to the positive ion cyclotron.

A point of consideration for the positive ion cyclotron is that the internal beam of positrons of variable energy can be utilized for radionuclide production by placing a probe with the target at different radial positions. The negative ion cyclotron does not have this provision.

Medical Cyclotron

Medical cyclotrons are compact cyclotrons that are primarily used to produce short-lived, positron-emitting radionuclides used for PET imaging. Most of the clinically useful positron emitters are formed by nuclear reactions with low-energy particles and hence the compact cyclotrons. These are commercially available and can be installed in a relatively small space. Moreover, in medical cyclotrons, negative hydrogen ions (H^-) are commonly accelerated, because unlike in positive ion cyclotrons, the housing of the cyclotron does not become radioactive in negative ion cyclotrons. Also, the beam can be split by two carbon-stripping foils so that two targets can be irradiated simultaneously. Whereas the particle energy may be in the range of a billion electron volts in high-energy cyclotrons, the typical energy of the protons or H^- particles in medical cyclotrons ranges between 10 and 30 MeV. In some medical cyclotrons, both deuterons and H^- particles can be accelerated interchangeably by switching the ion sources between deuterium and hydrogen. Shielding is a major concern for cyclotron installation. Whereas, in high-energy cyclotrons, shielding is achieved mostly by thick concrete walls and with large separation between the walls and the cyclotron, medical cyclotrons are mostly self-shielded with lead blocks because of their compact nature. The shielding commonly consists of four lead block quadrants supported on casters that wheel in and out for closing and opening of the quadrants for easy access to the cyclotron for maintenance. The operation of a medical cyclotron is a turnkey type and computer controlled, and a technologist with appropriate training can operate it without difficulty. A typical medical cyclotron is shown in Fig. 7.2. The cyclotrons from different manufacturers are listed in Table 7.1.

Nuclear Reaction

When targets of stable elements are irradiated by placing them in the external beam or in the internal beam of accelerated particles at a given radius inside a cyclotron, the particles interact with the target nuclei and nuclear reactions take place. Depending on the kinetic energy, the incident particle may be completely absorbed, depositing all its energy, or may leave the nucleus after interaction with one or more nucleons, leaving part of its energy. Nuclear reactions involving very high-energy particles are called spallations, in which many nucleons are ejected from the nucleus by the direct interaction of the incident particle. In either case, an excited nucleus is

Fig. 7.2 A commercial cyclotron, ECLIPSE HD, manufactured by Siemens Medical Solutions USA (Courtesy of Siemens Medical Solutions USA, Inc.). The features of this cyclotron are given in Table 7.1

Table 7.1 Features of medical cyclotrons from different manufacturers

Company	Model	Beam type	Proton particle energy (MeV)	Proton beam current (μA)	No. of target positions	Simultaneous irradiation of targets
IBA	Cyclone 11 Cyclone 18/9	H^- H^-/d^-	11 18/9	60 80/35	8 8	2 2
Siemens	Eclipse	H^-	11	60/40	4	2
GE	PETtrace 840 Minitrace	H^-/d^- H–	16.5 9.6	75 60	8 8	2 2
Advanced Cyclotron Systems	TR 30 TR 14–19	H^-/d^- H^-/d^-	15–30 14–19	1000 300	8 16	2 2
Best Cyclotron Systems, Inc.	BCSI 15p	H^-	15	400	4	2
Sumitomo	Cypris HM-12	H^-/d^-	12	90	8	2

formed, and the excitation energy is disposed of by the emission of protons and neutrons, provided it is energetically allowed. Particle emission is followed by a cascade of γ-ray emissions when the former is no longer energetically possible. Depending on the energy deposited, several nucleons may be emitted resulting in the production of different radionuclides. The larger the energy deposited, the more particles are emitted, and a variety of radionuclides are produced. A simple nuclear reaction induced by a proton p on a target ${}^{A}_{Z}X$ can be given by

$$ {}^{A}_{Z}X(p,n)_{Z+1}{}^{\mathrm{A}}Y, $$

where n is the neutron emitted and ${}_{Z+}{}^{A}_{1}Y$ is the radionuclide formed.

After irradiation, the target is transferred to a specially constructed containment unit called "hot cell" by a pneumatic tube system. The hot cell is built with thick lead wall encased in stainless steel sheets for radiation protection. It has a lead glass window to view inside and is equipped with two robotic arms, also termed manipulators, to maneuver the different operations such as transferring, pouring, lifting, heating, etc., of containers and materials inside the hot cell. It is exhausted through a HEPA filter for clean air environment to comply with good manufacturing practice (GMP) and kept under negative air pressure. The hot cell is equipped with water supply, purified air, lighting, electrical outlets, and other gases needed for various chemical procedures. A typical hot cell is shown in Fig. 7.3. Solid targets are dissolved in an appropriate solvent and radionuclides are separated from the target material by appropriate chemical methods such as solvent extraction, precipitation, chromatography, ion exchange, and distillation. Liquid and gas targets are specially designed, and appropriate methods are adopted to separate radionuclides. A dose calibrator is installed in the hot cell to measure the radioactivity produced.

Whereas the synthesis of some radiopharmaceuticals is carried out in the hot cell, many radiopharmaceuticals are synthesized in a step-down compact unit called *minicell* that is a smaller version of a hot cell and is commonly used for handling low level of activity (Fig. 7.4). A synthesis box of radiopharmaceuticals is placed inside the minicell, which is kept in GMP compliance and negative pressure. Water supply, air, exhaust, lighting, electrical outlets, and other essential accessories are provided in the mincell. In many cases, the minicell is seamlessly attached next to the hot cell and the separated radionuclide is transferred from the hot cell to the minicell by remote control via a side door. The features of a commercial synthesis box are described in Chap. 8.

Cyclotron-produced radionuclides are typically proton rich, i.e., neutron deficient and, therefore, decay by β^{+} emission or electron capture. Also, the radionuclides, which are different from the target nuclides, do not contain any stable (or "cold") atoms and are called *carrier-free*. Another term for these preparations is *no-carrier-added* (NCA), because no cold atoms have been intentionally added to the preparations.

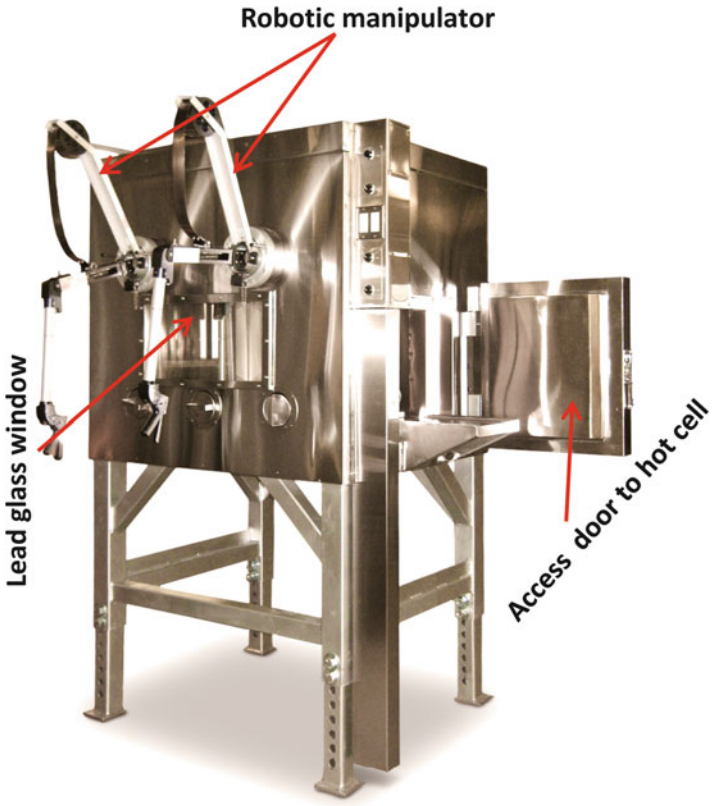

Fig. 7.3 A commercial hot cell whose features are described in the text. *Red arrows* indicate the robotic manipulators, the lead glass window, and the door to access the hot cell (picture provided by Radiation Shielding, Inc.)

Target and Its Processing

Excessive heat is generated in the target during irradiation with charged particles at a beam current of 50–1000 μA, and the temperature can rise, exceeding 1000 °C. This is because only 0.1% of the incident particles react with the nucleus and the rest interact with the atomic electrons producing intense heat. If proper precautions for heat dissipation are not taken, the target may be burned or melted. The most common method is to cool the probe to which the target is attached by using circulating water, helium gas, or other coolants. Also, the targets are designed in the form of a foil to maximize heat dissipation.

The common form of target is the metallic foil, but metals melt at high temperature caused by high beam intensity of the particles. Other forms are oxides, carbonates, nitrates, etc., contained in the aluminum tubes, which are flattened after loading to maximize heat loss. The choice of aluminum is owing to its high melting point. The target material for irradiation must be pure and preferably

Fig. 7.4 Four commercial minicells, inside each of which a synthesis box for synthesis of PET radiopharmaceuticals is installed (picture provided by Radiation Shielding, Inc.)

monoisotopic or at least isotopically enriched to minimize the production of extraneous radionuclides.

Liquid targets are used in the production of many PET radionuclides, particularly ^{18}F and ^{13}N. Fluorine-18 is produced by using a liquid target of ^{18}O-enriched water and so is ^{13}N by using 5-nM ethanol in water. The target volume is small in the range of 3–15 mL under high pressure. Since ^{18}O-water is expensive, it is customary to recover it for subsequent irradiation and the method of recovery is described in the later section.

Gas targets are used for some PET radionuclides such as ^{11}C and ^{15}O. A mixture of $^{14}N_2$ gas and (1%) $^{16}O_2$ gas is used to produce ^{11}C, and a mixture of enriched $^{15}N_2$ gas and 2.5% $^{16}O_2$ is used for the production of ^{15}O. The gas targets are maintained at high pressure.

Equation for Production of Radionuclides

The amount of activity produced by irradiation of a target material with a charged particle beam can be quantitated by

$$A = In\sigma\left(1 - e^{-\lambda t}\right), \tag{7.2}$$

where A, the activity in disintegration per second of the radionuclide produced; I, intensity of irradiating particles (number of particles/cm^2 s); n, number of target atoms; σ, formation cross section (probability) of the radionuclide (cm^2); it is given in units of "barn," which is equal to 10^{-24} cm^2; λ, decay constant of the radionuclide given by $0.693/t_{1/2}$ (s^{-1}); and t, time of irradiation in seconds.

Equation (7.2) indicates that the quantity of radionuclides increases with time of irradiation, intensity, and energy of the particles (related to σ) of the incident particle, and the amount of target material. The term $(1–e^{-\lambda t})$ is called the saturation factor, which approaches to unity when t is five to six half-lives of the radionuclide in question. At that time, the yield of the radionuclide is maximum, and its rates of production and decay become equal, indicating that there is no gain in activity by further irradiation. For irradiation for five to six half-lives of the daughter, Eq. (7.2) then becomes

$$A = In\sigma. \tag{7.3}$$

A graphical representation of Eqs. (7.2) and (7.3) is shown in Fig. 7.5.

The values of I are measured by various techniques, the description of which is beyond the scope of this book, but they are available from the cyclotron operators.

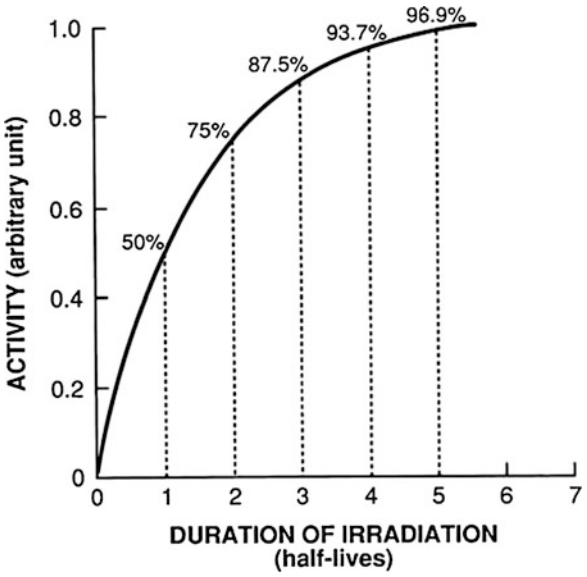

Fig. 7.5 Production of radionuclides in a cyclotron. The amount of activity produced reaches a maximum (saturation) in five to six half-lives of the radionuclide

The values of σ also have been determined for various nuclear reactions and are available in literature. The number of atoms N of the target is given by

$$N = \frac{W \times K}{A_w} \times 6.02 \times 10^{23}, \tag{7.4}$$

where W is the weight of the target, A_w and K are the atomic weight and natural abundance of the target element, and 6.02×10^{23} is the Avogadro's number.

Note that 1 ampere (A) is equal to 1 Coulomb (C)/s, and 1 C equals to 6.25×10^{18} protons, so in a cyclotron where protons or H^- are accelerated, the beam intensity is conventionally expressed in μA/cm^2-h. The yield of the radionuclide is then expressed in MBq or mCi per μAh.

Problem 7.1
Calculate the activity of ^{18}F produced when 1 g of 70% enriched $H_2{}^{18}O$ is irradiated for 1 h with a proton beam of 30 μA/cm^2 in a cyclotron. The half-life of ^{18}F is 110 min and the cross section for the $^{18}O(p, n)^{18}F$ reaction is 300 mb (1 b = 10^{-24} cm^2).

Answer:
Since 1 A is equal to 1 C/s and 1 C equals 6.25×10^{18} protons, the number of protons in 30 μA/cm^2 is

$$I = 30 \times 10^{-6} \times 6.25 \times 10^{18} = 1.875 \times 10^{14} \text{protons}/(\text{cm}^2 \cdot \text{s})$$
$$\sigma = 0.3 \times 10^{-24} \text{cm}^2.$$

Effective molecular weight of enriched water is $0.3 \times 18 + 0.7 \times 20 = 19.4$.

$$N = \frac{0.7 \times 1}{19.4} \times 6.02 \times 10^{23} = 2.17 \times 10^{22} \text{ atoms}^{18}O$$
$$\lambda = \frac{0.693}{110 \times 60} = 1.05 \times 10^{-4} \text{s}^{-1}$$
$$t = 1 \times 60 \times 60 = 3600 \text{ s}$$

Using Eq. (7.2)

$$\begin{aligned} D\,(\text{dps}) &= 1.875 \times 10^{14} \times 2.17 \times 10^{22} \times 0.3 \times 10^{-24} \\ &\quad \times \left[1 - \exp\left(-1.05 \times 10^{-4} \times 3600\right)\right] \\ &= 1.22 \times 10^{12} \times 0.3148 \\ &= 3.84 \times 10^{11} \text{ dps} (384 \text{ GBq}) \\ A &= \frac{3.84 \times 10^{11}}{3.7 \times 10^{10}} \\ &= 10.4 \text{ Ci} \end{aligned}$$

Specific Activity

Specific activity of a sample is defined as the radioactivity per unit mass of a radionuclide or a labeled compound. If a 50-mg sample contains 100 mCi (370 MBq), then the specific activity of the sample is given as $100/50 = 2$ mCi/mg or 74 MBq/mg. One should not confuse the specific activity with the concentration, which is given in mCi/mL or MBq/mL. The specific activity is at times expressed in units of mCi/mol (MBq/mol) or mCi/μmol (MBq/μmol).

The specific activity of a carrier-free radionuclide can be calculated by

$$\text{Specific activity (mCi/mg)} = \frac{3.13 \times 10^9}{A \times t_{1/2}}, \tag{7.5}$$

where A is the mass number of the radionuclide and $t_{1/2}$ is the half-life in hours of the radionuclide.

The specific activity is an important parameter to consider in radiolabeling and in vivo biodistribution of tracers. Cold molecules in low-specific-activity radiopharmaceuticals compete with radioactive molecules and lower the uptake of the tracer in tissues. Similarly, low-specific-activity radionuclides yield poor radiolabeling.

Production of Positron-Emitting Radionuclides

Since only a limited number of short-lived radionuclides are useful for PET imaging, production of those in routine clinical use and a few with potential for future clinical use are described here. A few essential long-lived positron emitters are also included. The different characteristics of these radionuclides are summarized in Table 7.2.

Fluorine-18

Fluorine-18 ($t_{1/2} = 110$ min) decays by 97% β^+ emission and is commonly produced by the $^{18}O(p, n)^{18}F$ reaction on a $H_2{}^{18}O$ target using 11–18 MeV protons in medical cyclotrons. ^{18}O-O_2 gas target also has been used as the target for ^{18}F production, but has not received wide acceptance because of the low yield. $H_2{}^{18}O$ (85–99% enriched) is isotopically enriched target material in liquid form and is available from commercial vendors (e.g., Isotec, Inc., Miamisburg, OH, USA). A metal target holder (e.g., silver, titanium, nickel, copper, and stainless steel) with cavities of 0.1–4 cm^3 volume is used to contain $H_2{}^{18}O$. Target design varies widely with the type and energy of the cyclotron. Since the ^{18}O-water target is quite expensive, and also only one in million target atoms is consumed in the nuclear reaction, bulk of the

Table 7.2 Production and characteristics of common positron emitters

Nuclide	Physical half-life ($t_{1/2}$)	Mode of decay (%)	γ-ray energy (keV)	Abundance (%)	Common production method
$^{11}_{6}C$	20.4 min	β^+ (100)	511	200	$^{10}B(d, n)^{11}C$ $^{14}N(p, \alpha)^{11}C$
$^{13}_{7}N$	10 min	β^+ (100)	511	200	$^{12}C(d, n)^{13}N$ $^{16}O(p, \alpha)^{13}N$ $^{13}C(p, n)^{13}N$
$^{15}_{8}O$	2 min	β^+ (100)	511	200	$^{14}N(d, n)^{15}O$ $^{15}N(p, n)^{15}O$
$^{18}_{9}F$	110 min	β^+ (97) EC (3)	511	194	$^{18}O(p, n)^{18}F$
$^{62}_{30}Zn$	9.3 h	β^+ (8) EC (92)	41 550	25 56	$^{63}Cu(p, 2n)^{62}Zn$
$^{62}_{29}Cu$	9.7 min	β^+ (97) EC(3)	511	194	^{62}Zn–^{62}Cu generator
$^{62}_{29}Cu$	12.7 h	β^+ (18) β^- (39) EC (43)	511	36	$^{64}Ni(p, n)^{64}Cu$
$^{68}_{31}Ga$	68 min	β^+ (89) EC(11)	511	178	$^{68}Ge-^{68}Ga$ generator $^{68}Zn(p, n)^{68}Ga$
$^{68}_{32}Ge$	270.8d	EC(100)	–	–	$^{66}Zn(\alpha, 2n)^{68}Ge$
$^{94m}_{43}Tc$	52 min	β^+ (70) EC(30)	511 871 1521 1868	140 94 4.5 5.7	$^{94}Mo(p, n)^{94m}Tc$
$^{124}_{53}I$	4.2 d	β^+ (23) EC(77)	511 603 1691	46 61 10.4	$^{124}Te(p, n)^{124}I$
$^{82}_{37}Rb$	75 s	$\beta+$(95) EC(5)	511 777	190 13.4	$^{98}Mo \xrightarrow{\text{spallation}} {}^{82}Sr$ $25.6d \downarrow$ ^{82}Rb
$^{86}_{39}Y$	14.7 h	β^+(33) EC (67)	511 many γ-rays	66	$^{86}Sr(p, n)^{86}Y$
$^{89}_{40}Zr$	78.1 h	β^+ (100)	511 909	200 100	$^{89}Y(p, n)^{89}Zr$

target material is routinely recovered for reuse. After irradiation, the target mixture is loaded on a column of carbonate ion-exchange resin, and $H_2{}^{18}O$ is forced out of the column by neon gas and reused as the target. $^{18}F^-$ ion is recovered by eluting the column with potassium carbonate solution. Greater than curie (GBq) amount of ^{18}F-fluoride is easily produced in an 11-MeV cyclotron after bombardment for an hour. The NCA specific activity of ^{18}F-fluoride is in the order of about 1×10^4 Ci/mmol (3.7×10^5 GBq/mmol). ^{18}F-Fluoride has been used for labeling deoxyglucose to

produce ^{18}F-fluorodeoxyglucose (^{18}F-FDG) and other ^{18}F-labeled radiopharmaceuticals for PET imaging (discussed later).

Some compounds such as L-dopa need the precursor fluorine-18 gas [^{18}F] F_2 instead of $^{18}F^-$ ion for electrophilic labeling. It is produced by the ^{18}O(p, n)^{18}F reaction on an ^{18}O gas target contained in aluminum tubing. After irradiation, the ^{18}O gas target is recovered cryogenically in a stainless steel cylinder cooled in liquid nitrogen and ^{18}F gas remains adsorbed on the target wall. The latter is then recovered by flashing with 1% nonradioactive fluorine gas mixed with krypton or neon with a recovery efficiency of about 50%.

Carbon-11

Carbon-11 has a half-life of 20.5 min and decays by 100% β^+ emission. It can be produced by ^{10}B(d, n)^{11}C, ^{11}B(p, n)^{11}C, and ^{14}N(p, α)^{11}C reactions in the cyclotron. In the first two reactions, B_2O_3 is the target and nitrogen gas in the third. Both ^{11}CO and $^{11}CO_2$ are produced in boron targets by using 10–12 MeV protons, which are then flushed out by neutral gases. Either ^{11}CO is oxidized to have all the gas in $^{11}CO_2$ form or $^{11}CO_2$ is reduced to have all the gas in ^{11}CO form. Both ^{11}CO and $^{11}CO_2$ are commonly used as precursors in the preparation of various clinically useful compounds, such as ^{11}C-palmitate for myocardial metabolic imaging by PET.

The most common method of ^{11}C production is the ^{14}N(p, α)^{11}C reaction with 10–12 MeV protons. When the pure ^{14}N target is mixed with traces of oxygen, both ^{11}CO and $^{11}CO_2$ are produced. $^{11}CO_2$ is recovered by initially trapping $^{11}CO_2$ in a liquid nitrogen trap and later removing it by flushing with helium or heating the trap. The yield can be in curie (GBq) range with 99.9% purity.

The ^{14}N(p, α)^{11}C reaction is carried out by bombardment of a mixture of N_2 and H_2 to give ^{11}C, which reacts with N_2 to produce ^{11}CN, followed by hydrolysis of ^{11}CN to give $^{11}CH_4$ (95–100% radiochemical yield). Carbon-11-methane is often allowed to react with NH_3 over platinum at 1000 °C to give a 95% overall yield of H^{11}CN. Various biological molecules such as aliphatic amines, amino nitriles, and hydantoins have been labeled with ^{11}C using H^{11}CN or $^{11}CH_4$ as a precursor. A frequently employed precursor for ^{11}C labeling is ^{11}C-methyl iodide or ^{11}C-ethyl iodide, which are prepared by either converting ^{11}C-CO_2 to ^{11}C-methoxide or ^{11}C-ethoxide respectively, followed by reaction with hydroiodic acid, or by a gas phase reaction where ^{11}C-CH_4 or ^{11}C-C_2H_6 is reacted with iodine.

Nitrogen-13

Nitrogen-13 has a half-life of 10 min and decays by 100% β^+ emission. It is commonly used as NH_3. It is produced by the ^{12}C(d, n)^{13}N reaction by bombarding

Al_4C_3 or methane with 6–7 MeV deuterons or by the $^{16}O(p, \alpha)^{13}N$ or $^{13}C(p, n)^{13}N$ reaction. However, the $^{16}O(p, \alpha)^{13}N$ reaction is the most common method of ^{13}N production, and a target of pure water contained in a titanium holder is used for irradiation with 11–12 MeV protons. The major chemical species are nitrates, nitrites, ammonia, and hydroxylamine, of which the nitrate has the highest yield and is separated by the ion-exchange method. The nitrates and nitrites are reduced to give $^{13}NH_3$ which is swept by helium into saline. $^{13}NH_3$ in the form of NH_4^+ ion is primarily used for myocardial perfusion imaging by PET. $^{13}NH_3$ is also used to label glutamine and asparagine for assessment of viability of tissues.

Oxygen-15

Oxygen-15 has a half-life of 2 min and decays by 100% β^+ emission. It is produced by the $^{14}N(d, n)^{15}O$ reaction by 8–10 MeV deuteron irradiation of gaseous nitrogen or by the $^{15}N(p, n)^{15}O$ reaction by 10–12 MeV proton bombardment of enriched ^{15}N gas target contained in an aluminum alloy container. Pure ^{15}O gas is used for bolus and steady-state metabolic studies. $^{15}O_2$ is passed over activated charcoal heated at 1000 °C to convert it to $C^{15}O$ and $C^{15}O_2$, which are then used for labeling hemoglobin in clinical investigations of pulmonary and cardiac malfunctions. Oxygen-15-labeled water is obtained by heating a mixture of ^{15}O and hydrogen gas and is useful for cerebral and myocardial perfusion studies.

Iodine-124

Iodine-124 has a half-life of 4.2 days and is produced by the $^{124}Te(d, 2n)^{124}I$ or $^{124}Te(p, n)^{124}I$ reaction using 10–18 MeV protons and a 96% enriched ^{124}Te target in the form of oxide. While it has the advantage of having a long half-life to produce suitable iodinated PET tracers, its low positron abundance (only 23%) and complex decay scheme involving high-energy photons cause difficulty in PET imaging.

Strontium-82

Rubidium-82 ($t_{1/2} = 75$ s) is available from the ^{82}Sr–^{82}Rb generator (supplied by Bracco Diagnostics, Inc., under the brand name, CardioGen-82). ^{82}Sr ($t_{1/2} = 25.6$ days) is produced by the $^{85}Rb(p, 4n)^{82}Sr$ reaction using the high-energy proton beam on a ^{85}Rb target or by the spallation reaction of ^{99}Mo target with very high-energy protons, the latter being the preferred reaction. The ^{82}Sr radionuclide is separated from the target by the ion-exchange method. The purified ^{82}Sr in amounts of 90–150 mCi (3.33–5.55 GBq) is loaded on a stannic oxide column in the

generator. ^{82}Rb is eluted as chloride with 0.9% sodium chloride solution from the ^{82}Sr–^{82}Rb generator by using an infusion pump (see Chap. 14). The major impurities in the ^{82}Sr sample are ^{85}Sr ($t_{1/2} = 65$d) and ^{83}Sr ($t_{1/2} = 32$ h). However, ^{83}Sr is not a concern, because having a short half-life it decays to a negligible quantity by the time ^{82}Sr is loaded on the generator column. While ^{85}Sr contamination can be as much as five times the ^{82}Sr activity in the range of 400–700 mCi (14.8–25.9 GBq) when produced using the ^{98}Mo target, it is significantly less when produced by the ^{85}Rb(p, 4n)^{82}Sr reaction. The method of determination of ^{85}Sr contamination is given in Chap. 14.

Technetium-94m

Technetium-94m ($t_{1/2} = 52$ min) is produced by the ^{94}Mo(p, n)^{94m}Tc reaction using an enriched ^{94}Mo target and 11–12 MeV protons. ^{94m}Tc is separated from ^{94}Mo by steam distillation. It is an attractive positron emitter since it can be substituted for ^{99m}Tc in many SPECT radiopharmaceuticals for use in PET imaging.

Germanium-68

Germanium-68 ($t_{1/2} = 270.8$ days) decays 100% by electron capture and remains in equilibrium with ^{68}Ga ($t_{1/2} = 68$ min). It is produced by the ^{66}Zn(α, 2n)^{68}Ge reaction or the 40-MeV proton bombardment of a gallium target ^{69}Ga(p, 2n)^{68}Ge and ^{71}Ga(p, 4n)^{68}Ge reactions or the spallation reactions in a molybdenum target with high-energy protons. It is separated in HCl solution. It is mainly used as a sealed source for transmission scan and quality control studies in PET imaging. It is also used in the ^{68}Ge–^{68}Ga generator to provide easy supply of ^{68}Ga. The generator is made by adsorbing ^{68}Ge on tin oxide (SnO_2) or titanium dioxide (TiO_2) contained in a polyethylene tube and ^{68}Ga is eluted with HCl. It is available in quantities of 10–50 mCi. The ^{68}Ge breakthrough in the eluate is normally negligible. The generator is supplied by IDB-Holland in Europe, but it is not FDA approved in the USA.

Gallium-68

Gallium-68 ($t_{1/2} = 68$ min) decays by 89% β^+ emission and 11% electron capture. It is obtained by eluting the abovementioned ^{68}Ge–^{68}Ga generator with 0.1 M HCl. Recently, several octreotides have been labeled with ^{68}Ga–DOTA chelating agent, which are primarily used to diagnose the neuroendocrine tumors.

Copper-64

Copper-64 ($t_{1/2} = 12.7$ h) decays by 18% by positron emission to ^{64}Ni, 39% by beta decay to ^{64}Zn, and 43% by electron capture to ^{64}Ni. It is abundantly produced by the ^{64}Ni(p, n)^{64}Cu reaction using an enriched ^{64}Ni target and low-energy protons in a medical cyclotron. ^{64}Cu is separated from the target material by ion-exchange chromatography and obtained in HCl solution. It has been used in the preparation of ^{64}Cu-ATSM for use in measurement of hypoxia in tumors. Several antibodies and nanoparticles have been labeled with ^{64}Cu for tumor imaging.

Copper-62

Copper-62 ($t_{1/2} = 9.7$ min) is available from the ^{62}Zn–^{62}Cu generator supplied by Proportional Technologies, Inc. Zinc-62 ($t_{1/2} = 9.3$ h) is produced by the ^{63}Cu(p, 2n)^{62}Zn reaction by irradiation with 25–30 MeV protons using a 99% pure copper-63 foil target (Green et al. 1990). The typical yield is about 4.5 mCi (166.5 MBq) per mAh at EOB. ^{62}Zn is taken up in 2 N HCl and loaded on a Dowex 1 × 8 anion-exchange column to provide the ^{62}Zn–^{62}Cu generator. ^{62}Cu is eluted with 2 N HCl for use in the synthesis of ^{62}Cu-PTSM, which is useful for measurement of perfusion in the heart, kidneys, and brain.

Yttrium-86

Yttrium-86 has a half-life of 14.2 h and decays 33% by β^+ emission and 67% by EC. It has many high-energy γ-rays having energy higher than 1.0 MeV. It is produced by 11 MeV proton irradiation of enriched ^{86}Zr via the ^{86}Sr(p, n)^{86}Y reaction. It is separated from the target material by electrochemical method or ion-specific resin chromatography. It is primarily used to label various antibodies by the chelating method. It is not approved by the US FDA for human use.

Zirconium-89

Zirconum-89 ($t_{1/2} = 78.1$ h) decays by 23% positron emission and 77% EC. It has a high-energy gamma ray of 909 keV (100%). It is produced by the ^{89}Y(p, n)^{89}Zr reaction in a cyclotron by 11 MeV proton irradiation of natural ^{89}Y target. The target is dissolved in hydrochloric acid and ^{89}Zr is separated by the ion-exchange method. The final solution is obtained in 1 M oxalic acid. It is commercially available from BV Cyclotron VU University Medical Center. Its radionuclidic

purity is 99.9% and it is available in concentrations of 20–50 mCi/mL (740–1850 MBq/mL). It has been used in labeling antibodies by the chelating method described later for PET imaging of various diseases. ^{89}Zr is not approved for human use and used only for research and animal studies.

Questions

1. Describe the principles of the operation of a cyclotron.
2. What is the major advantage of a negative ion cyclotron over a positive ion cyclotron?
3. Why is the higher vacuum required in a negative ion cyclotron than in a positive ion cyclotron?
4. Describe the production of the following radionuclides in a cyclotron: (a) ^{13}N, (b) ^{11}C, (c) ^{18}F, and (d) ^{15}O.
5. Radionuclides produced in a cyclotron are typically carrier-free or NCA. True _____; False _____.
6. Calculate the activity of ^{18}F when 700 mg of 85% enriched $H_2{}^{18}O$ is irradiated for 1 h with a proton beam of 20 μA/cm^2 in a cyclotron. The half-life of ^{18}F is 110 min and the cross section for the ^{18}O(p,n)^{18}F reaction is 200 mb (1 b = 10^{-24} cm^2).
7. In producing a radionuclide with $t_{1/2} = 3$ h in a cyclotron, what is the duration of irradiation after which there is no more gain in additional activity?
8. What are the chemical forms of ^{18}F that are obtained at the end of bombardment to be used for further chemical synthesis?
9. The specific activity of a radioactive sample decreases with the increasing cold atoms. True _____; False _____.
10. What are the expected contaminants in the ^{82}Sr sample in a ^{82}Sr–^{82}Rb generator?
11. Calculate the specific activity of a carrier-free ^{18}F sample.
12. Negative ion cyclotrons are more advantageous than positive ion cyclotrons, because the negative ion beam is easily extracted. True _____; False _____.
13. Describe the structure and feature of a hot cell and a minicell.

References and Suggested Reading

Friedlander G, Kennedy JW, Miller JM. Nuclear and radiochemistry. 3rd ed. New York: Wiley; 1981.

Green MA, Mathias CJ, Welch MJ, et al. Copper-62 labeled pyruvaldehyde Bis(N^4-methylthiosemicarbazonato) Copper (II): synthesis and evaluation as a positron emission tomography tracer for cerebral and myocardial perfusion. J Nucl Med. 1990;31:1989.

McCarthy TJ, Welch MJ. The state of positron emitting radionuclide production in 1997. Semin Nucl Med. 1998;28:235.

Saha GB. Fundamentals of nuclear pharmacy. 6th ed. New York: Springer; 2010.
Saha GB, MacIntyre WJ, Go RT. Cyclotrons and positron emission tomography for clinical imaging. Semin Nucl Med. 1992;22:150.
Silvester DJ, Waters SL. Radionuclide production. In: Sodd VJ, Allen DR, Hoogland DR, Ice RD, editors. Radiopharmaceuticals II. New York: Society of Nuclear Medicine; 1979. p. 727.
Stöcklin G, Pike VW. Radiopharmaceuticals for positron emission tomography. Dordrecht: Kluwer; 1993.

Chapter 8
Synthesis of PET Radiopharmaceuticals

Introduction

PET radiopharmaceuticals are uniquely different from SPECT radiopharmaceuticals in that the former have radionuclides that are positron emitters and the majority of them have short physical half-lives. The most common PET radionuclides are ^{11}C, ^{15}O, ^{13}N, ^{18}F, and ^{82}Rb, which are short-lived (see Table 7.2) and put limitations on the synthesis time for PET radiopharmaceuticals and their clinical use. The attractive advantage of PET radiopharmaceuticals, however, is that the ligands used in radiopharmaceuticals are common analogs of biological molecules and, therefore, often depict a true representation of biological processes after in vivo administration. For example, ^{18}F-fluorodeoxyglucose (FDG) is an analog of glucose used for cellular metabolism and $H_2^{15}O$ for cerebral perfusion.

Automated Synthesis Device

Conventional manual methods of synthesis of radiopharmaceuticals using a high level of radioactivity are likely to subject the personnel involved in the synthesis to high radiation exposure. This is particularly true with short-lived positron emitters such as ^{11}C, ^{13}N, ^{15}O, and ^{18}F, because the quantity of these radionuclides handled in the synthesis is very high. To minimize the level of exposure, automated modules have been devised for the synthesis of PET radiopharmaceuticals.

The automated synthesis device, often called the *black box*, is a unit controlled by microprocessors and software programs to carry out the sequential physical and chemical steps to accomplish the entire synthesis of a radiolabeled product. The unit consists of templates or vials prefilled with required chemicals attached to the apparatus via tubings that are connected to solenoid valves to switch on and off as needed. Most black boxes are small enough to be placed in a space of

G.B. Saha, *Basics of PET Imaging*, DOI 10.1007/978-3-319-16423-6_8

$20 \times 20 \times 20$ in. and are capable of self-cleaning. In some units, disposable cassettes (cartridges) are employed so that new cassettes can be used for each new synthesis, thus minimizing contamination and radiation exposure. Various parameters for synthesis such as time, pressure, volume, and other requisites are all controlled by a remote computer using appropriate software. The unit has a graphic display showing the status of the ongoing process. After the synthesis, a report with the date and start and end time of the radiosynthesis and the calculated yield is printed out. Technologists can operate these units very easily. Automated synthesis modules for ^{18}F-FDG, ^{13}N-NH_3, ^{11}C-CH_3I, ^{11}C-HCN, ^{11}C-acetate, and a few other PET tracers are commercially available. Versatile automated modules are commercially available to use for the synthesis of a variety of PET tracers in the single module. This is accomplished by simple exchange or modification of various segments inside the unit to suit the specific product synthesis. To minimize radiation exposure, often the synthesis box is placed inside a minicell (see Chap. 7). After each synthesis, the product is passed through a high-performance liquid chromatography (HPLC) described later to achieve a high-purity finished product. A schematic diagram of a black box for ^{18}F-FDG synthesis is shown in Fig. 8.1. Often the synthesis box is placed inside a minicell to minimize radiation exposure. An automated multi-synthesis module (FASTlab2) for the synthesis of different PET radiopharmaceuticals marketed by GE Healthcare is shown in Fig. 8.2. Other vendors include Siemens Medical Solutions, Inc. (Explora), IBA (Synthera), and Eckert & Ziegler (FDG-Plus).

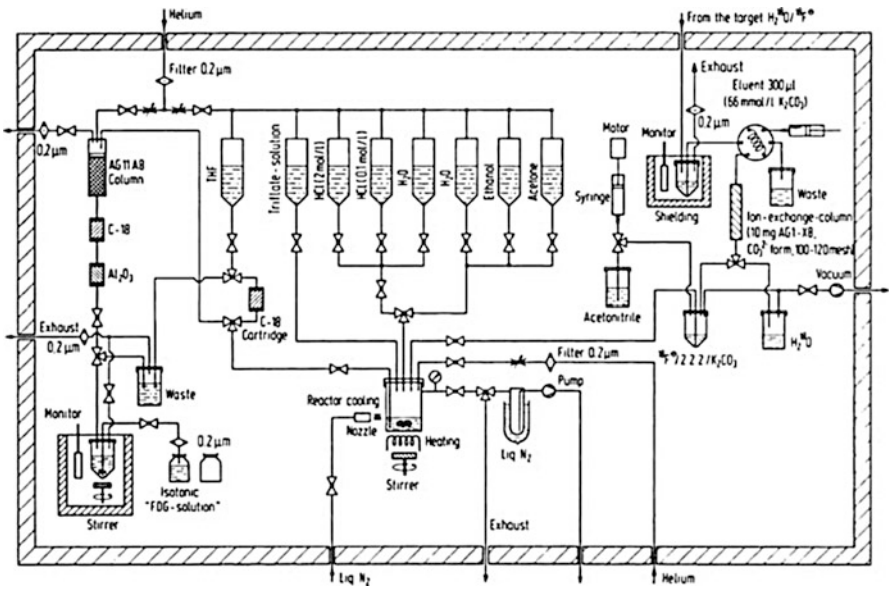

Fig. 8.1 A schematic block diagram showing different components in the ^{18}F-FDG synthesis box (Reproduced with kind permission of Kluwer Academic Publishers from Crouzel C et al. (1993) Radiochemistry automation PET. In: Stöcklin G, Pike VW (eds) Radiopharmaceuticals for positron emission tomography, Kluwer Academic, Dordrecht, the Netherlands, p 64. Fig. 9)

Fig. 8.2 Automated synthesis box, FASTlab2, from GE Healthcare (Courtesy of GE Healthcare)

PET Radiopharmaceuticals

Many radiopharmaceuticals have been used for PET imaging; however, only a few are routinely utilized for clinical purposes. Almost all of them are labeled with one of the four common positron emitters: ^{11}C, ^{13}N, ^{15}O, and ^{18}F. Of the four, ^{18}F is preferred most, since it has a relatively longer half-life ($t_{1/2} = 110$ min) that allows its supply to relatively remote places. In all cases, a suitable synthesis method is adopted to provide a stable product with good labeling yield, high specific activity, high purity, and, most importantly, high in vivo tissue selectivity. The following is a description of the syntheses of the common clinically used PET radiopharmaceuticals and a few with potential for future use.

^{18}F-Sodium Fluoride

Fluorine-18 ($t_{1/2} = 110$ min) is produced by irradiation of ^{18}O-water with 10–18 MeV protons in a cyclotron and recovered as ^{18}F-sodium fluoride by passing the irradiated water target mixture through a carbonate-type anion-exchange resin column. The water is forced out of the column with neon gas, whereas $^{18}F^-$ is retained on the column, which is recovered by elution with potassium carbonate solution. Its pH should be between 4.5 and 8.0. While ^{18}F-sodium fluoride is most commonly used for the synthesis of FDG, it is also used for other ^{18}F-labeled PET radiopharmaceuticals.

The US FDA has approved it for bone scintigraphy, since it localizes in bone by exchanging with PO_4^- ion in the hydroxyapatite crystal.

^{18}F-Fluorodeoxyglucose

^{18}F-2-fluoro-2-deoxyglucose (2-FDG) is normally produced in places where a cyclotron is locally available. Its molecular formula is $C_8H_{11}{}^{18}FO_5$ with molecular weight of 181.3 Da. ^{18}F-2-FDG can be produced by electrophilic substitution with ^{18}F-fluorine gas or nucleophilic displacement with ^{18}F-fluoride ions. The radiochemical yield is low with the electrophilic substitution, so the nucleophilic displacement reaction has become the method of choice for ^{18}F-FDG synthesis. Deoxyglucose is labeled with $^{18}F^-$ by nucleophilic displacement reaction of an acetylated sugar derivative followed by hydrolysis (Hamacher et al. 1986). In nucleophilic substitution, a fluoride ion reacts to fluorinate the sugar derivative. A solution of 1,3,4,6-tetra-*O*-acetyl-2-*O*-trifluoromethane-sulfonyl-*β*-D-mannopyranose in anhydrous acetonitrile is added to a dry residue of ^{18}F-fluoride containing aminopolyether (Kryptofix 2.2.2) and potassium carbonate (Fig. 8.3). Kryptofix 2.2.2 is used as a catalyst to enhance the reactivity of the fluoride ions. The mixture is heated under reflux for about 5 min. The solution is then passed through a C-18 Sep-Pak column, and acetylated carbohydrates are eluted with tetrahydrofuran (THF), which are then hydrolyzed by refluxing in hydrochloric acid at 130 °C for 15 min. ^{18}F-2-fluoro-2-deoxyglucose (2-FDG) is obtained by passing the hydrolysate through a C-18 Sep-Pak column. The yield can be as high as 60%, and the preparation time is approximately 50 min. The final solution is filtered through a 0.22-μm filter and diluted with saline, as needed. According to USP specifications, it should have pH of 4.5–7.5 and a specific activity of more than 1 Ci (37 GBq)/μmol. The chemical purity is limited to 50 μg/mL of Kryptofix 2.2.2 and 1 mg of 2-chloro-2-deoxy-D-glucose per total volume. Radiochemical purity should be >90%, as determined by the TLC method

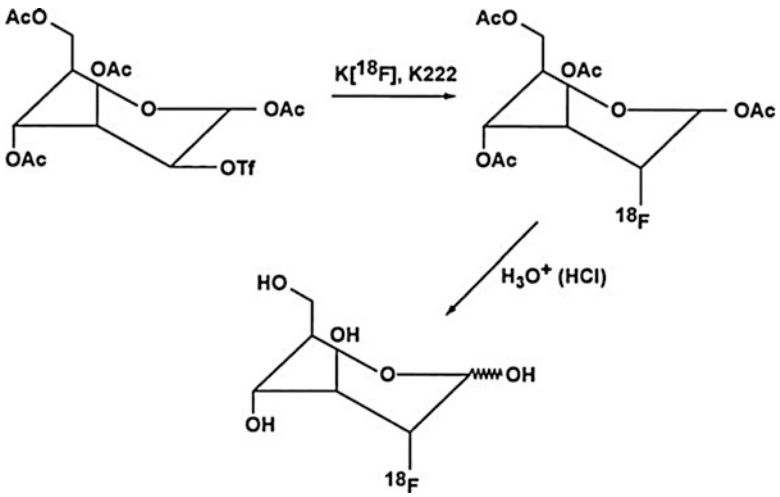

Fig. 8.3 Schematic synthesis of ^{18}F-2-fluoro-2-deoxyglucose (FDG) (Reprinted with the permission of the Cleveland Clinic Center for Medical Art and Photography ©2009. All rights reserved)

using activated silica gel as the solid phase and a mixture of acetonitrile and water (95:5) as the liquid phase.

Since Kryptofix 2.2.2 is toxic causing apnea and convulsions, modifications have been made to substitute it with tetrabutylammonium hydroxide or bicarbonate, which have been adopted by many commercial vendors. Also, in some other methods, the C-18 Sep-Pak column separation has been eliminated so as to carry out the acidic hydrolysis in the same vessel. In methods where Kryptofix 2.2.2 is still used, several Sep-Pak columns are used to separate Kryptofix 2.2.2 and reduce it to practically a negligible quantity.

The FDA has approved ^{18}F-2-FDG for many clinical uses such as the metabolism in the brain and heart and the detection of epilepsy and various tumors. In metabolism, ^{18}F-2-FDG is phosphorylated by hexokinase to 2-FDG-6-phosphate which is not metabolized further. It should be noted that 3-fluorodeoxyglucose (3-FDG) is not phosphorylated and hence is not trapped and essentially eliminated rapidly from the cell. This is why 3-FDG is not used for metabolic studies. Detailed protocols of ^{18}F-FDG usage in humans are given in Chap. 13.

Because of the relatively longer half-life of ^{18}F among the PET radionuclides, commercial and institutional facilities having cyclotrons produce ^{18}F-FDG in bulk quantities and supply to nearby clinics and hospitals as needed. Supply can be made as far as 200 miles away with a loss of activity, which can be compensated by adding more activity. The details of ^{18}F-FDG distribution is given in Chap. 10.

6-^{18}F-L-Fluorodopa

Like ^{18}F-2-FDG, 6-^{18}F-L-fluorodopa is also produced in places where a cyclotron is available locally. There are several methods of synthesizing 6-^{18}F-fluoro-3,4-dihydroxyphenylalanine (6-^{18}F-L-fluorodopa), of which the method of fluorodemetallation using electrophilic fluorinating agents is most widely used. Electrophilic reactions involve the reaction of fluorine in the form of F^+ with other molecules. Only the L-isomer of dopa is important, because the enzymes that convert dopa to dopamine, which is targeted by the radiopharmaceutical, are selective for this isomer. Initially, a suitably protected organomercury precursor (*N*-[trifluoroacetyl]-3,4-dimethoxy-6-trifluoroacetoxymercuriophenylalanine ethyl ester) of dopa is prepared. [^{18}F]-labeled acetylhypofluorite prepared in the gas phase is then allowed to react with the mercury precursor in chloroform or acetonitrile at room temperature. Other precursors using metals such as tin, silicon, selenium, and germanium have been reported. Acid hydrolysis with 47% HBr provides a relatively high yield (10–12%) of 6-^{18}F-L-fluorodopa (Luxen et al. 1992) compared with other available methods. Substitution at position 6 is most desirable, because this does not alter the behavior of dopa, whereas substitutions at 2 and 5 do. It is sterilized by filtering through a 0.22-μm membrane filter and is supplied at pH between 6 and 7. Normally EDTA and ascorbic acid are added to the final preparation for stability. Its specific activity should be more than 100 mCi (3.7 GBq)/mmol and radiochemical purity >95% as

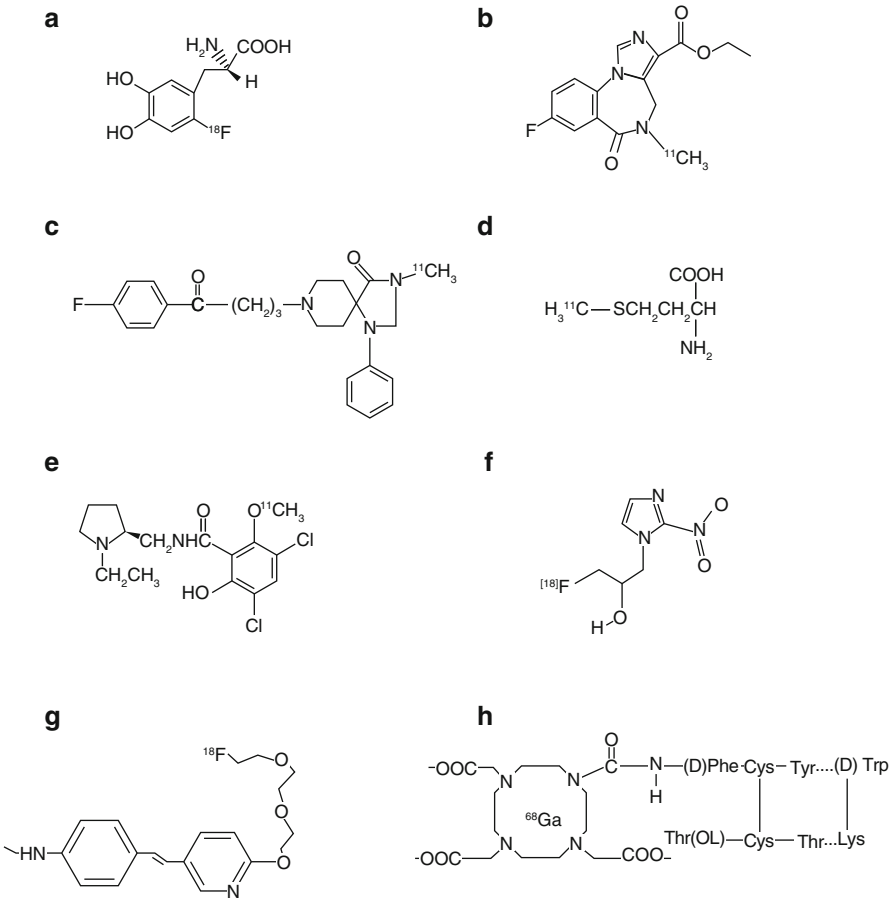

Fig. 8.4 Molecular structures of (**a**) 6-^{18}F-L-fluorodopa, (**b**) ^{11}C-flumazenil, (**c**) ^{11}C-methylspiperone, (**d**) ^{11}C-L-methionine, (**e**) ^{11}C-raclopride, (**f**) ^{18}F-fluoromisonidazole, (**g**) ^{18}F-florbetapir, and (**h**) ^{68}Ga-DOTATOC (Reprinted with the permission of the Cleveland Clinic Center for Medical Art and Photography©2009. All rights reserved)

determined by HPLC. Mercury is the major chemical impurity (toxic) that originates from organomercuric precursor used in the synthesis, and its USP limit is 0.5 μg/mL of L-dopa solution. The molecular structure of 6-^{18}F-L-fluorodopa is shown in Fig. 8.4a.

It is particularly useful for the detection of Parkinson's disease.

^{18}F-Fluorothymidine

^{18}F-Fluorothymidine (FLT) is prepared by nucleophilic reaction between ^{18}F-sodium fluoride and a precursor, 2, 3′-anhydro-5′-*O*-benzoyl-2′-deoxythymidine, which is prepared by standard organic synthesis (Machula et al. 2000). ^{18}F-Sodium fluoride is added to a mixture of Kryptofix 2.2.2 and potassium carbonate in acetonitrile, and the mixture is dried to a residue by heating at 120 °C for 5 min. The precursor in dimethyl sulfoxide (DMSO) is added to the dried residue and heated at 160°C for 10 min. Hydrolysis of the 5′-0-protecting group is performed with sodium hydroxide. ^{18}F-FLT is isolated by passing through alumina Sep-Pak and further purified by using high-performance liquid chromatography (HPLC). The overall yield is about 45% and the radiochemical purity is more than 95%. The synthesis time is about 60 min.

Since thymidine is incorporated into DNA and provides a measure of cell proliferation, ^{18}F-FLT is commonly used for in vivo diagnosis and characterization of tumors in humans.

^{18}F-O-(2-Fluoroethyl)-L-Tyrosine

The synthesis of ^{18}F-O-(2-fluoroethyl)-L-tyrosine (FET) is carried out in two steps (Wester et al. 1999): First, ethylene glycol-1,2-ditosylate in acetonitrile is reacted with dry ^{18}F-containing Kryptofix 2.2.2 and potassium bicarbonate at 90°C for 10 min. The product is purified by absorbing it on a polystyrene cartridge and then eluting with dimethyl sulfoxide. Second, the eluate is mixed with dipotassium sodium salt of L-tyrosine and heated at 90°C for 10 min. The mixture is purified by HPLC and cation exchange to obtain ^{18}F-FET. The radiochemical yield is about 40–45% with purity between 97 and 99%.

^{18}F-FET is used as a PET tracer for the detection of a variety of tumors.

^{18}F-Fluoromisonidazole

^{18}F-Fluoromisonidazole (FMISO) is synthesized in one-step reaction between the protected precursor, 1-(2′-nitro-1′-imidazolyl)-2-*O*-tetrahydropyranyl-3-*O*-toluenesulfonyl-propanediol (NITTP) and ^{18}F-containing Kryptofix 2.2.2 in acetonitrile solution (Kamarainen et al. 2004). The labeled product is hydrolyzed with acid to give ^{18}F-FMISO, which is further purified by column chromatography using a Sep-Pak cartridge. From automated synthesis, the radiochemical yield is 34% at EOS after a synthesis time of 50 min. HPLC shows a radiochemical purity of 97%. The molecular structure of ^{18}F-FMISO is shown in Fig. 8.4f.

^{18}F-FMISO is a specific tracer used for detection of hypoxic tissues by PET.

^{18}F-1-(5-Fluoro-5-Deoxy-α-Arabinofuranosyl)-2-Nitroimidazole

^{18}F-1-(5-Fluoro-5-deoxy-α-arabinofuranosyl)-2-nitroimidazole (FAZA) is synthesized by nucleophilic substitution reaction between the precursor 1-(2,3-di-*O*-acetyl-5-*O*-tosyl-α-D-arabinofuranosyl)-2-nitroimidazole in DMSO solution and ^{18}F-fluoride containing mixture of Kryptofix 2.2.2 and potassium carbonate at 100°C for 5 min (Reischl et al. 2005). The product is hydrolyzed with NaOH solution at 20°C for 2 min, and the solution is neutralized with NaH_2PO_4. It is further purified by HPLC and sterilized by 0.22-μm filtration. The radiochemical yield is about 61%.

^{18}F-FAZA is used for the detection of tissue hypoxia by PET.

^{18}F-Florbetapir

^{18}F-Florbetapir (brand name ^{18}F-AV-45 or Amyvid) has the molecular structure of (E)-4-(2-(6-(2-(2-(2-([^{18}F]-fluoroethoxy)ethoxy)ethoxy)pyridin-3-yl)vinyl)-*N*-methylbenzenamine. It is prepared by nucleophilic substitution reaction between ^{18}F-containing mixture of Kryptofix 2.2.2 and potassium carbonate in acetonitrile solution and the precursor (E)-2-(2-(2-(2-tosyloxyethoxy)ethoxy)ethoxy)-5-(4-(tertbutoxycarbonyl (methyl)amino)styryl)pyridine (-OTs derivative) in DMSO solution at 115 °C for 10 min (Liu et al. 2010). The product is hydrolyzed by hydrochloric acid solution followed by neutralization with a solution of NaOH and ammonium acetate solution. The solution is loaded on a Sep-Pak C18 column, and unreacted $^{18}F^-$ is removed by rinsing with deionized water, and ^{18}F-florbetapir is eluted with acetonitrile. ^{18}F-Florbetapir is purified by HPLC and finally taken up in ethyl alcohol for clinical use. The radiochemical yield is 34% and the radiochemical purity is nearly 95%.

^{18}F-florbetapir binds to amyloid plaques in Alzheimer's disease (AD) and other dementia-related conditions and has been approved by the FDA for the detection of these diseases in patients. The molecular structure of ^{18}F-florbetapir is shown in Fig. 8.4g.

^{15}O-Water

^{15}O-Oxygen ($t_{1/2} = 2$ min) is produced in the cyclotron by the ^{15}N(p, n)^{15}O reaction, or the ^{14}N(d, n)^{15}O reaction, and the irradiated gas is transferred to a [^{15}O] water generator in which ^{15}O is mixed with hydrogen and passed over a palladium/charcoal catalyst at 170 °C (Meyer et al. 1986; Welch and Kilbourn 1985). The $H_2{}^{15}O$ vapor is trapped in saline, and the saline solution is filtered through a 0.22-μm

membrane filter. The sample is then passed through a radiation detector for radioassay and ultimately injected online into a patient in a very short time.

$H_2{}^{15}O$ is commonly used for myocardial and cerebral perfusion studies.

n-^{15}O-Butanol

n-^{15}O-Butanol is prepared by the reaction of ^{15}O-oxygen, produced by the ^{15}N(p, n)^{15}O reaction, with tri-*n*-butyl borane loaded onto an alumina Sep-Pak cartridge (Kabalka et al. 1985). Carrier oxygen at a concentration of about 0.5% is added to the ^{15}N target in order to recover ^{15}O. After the reaction, *n*-^{15}O-butanol is eluted from the cartridge with water. It is further purified by passing through C-18 Sep-Pak and eluting with ethanol–water.

n-^{15}O-Butanol is used for blood flow measurement in the brain and other organs. It is a better perfusion agent than ^{15}O-water, because its partition coefficient is nearly 1.0 compared to 0.9 for water.

^{13}N-Ammonia

Nitrogen-13-labeled ammonia ($t_{1/2} = 10$ min) is produced by reduction of ^{13}N-labeled nitrates and nitrites that are produced by proton irradiation of water in a cyclotron. The reduction is carried out with titanium chloride in alkaline medium. $^{13}N\text{-}NH_3$ is then distilled and finally trapped in acidic saline solution. Wieland et al. (1991) has used a pressurized target of aqueous solution of acetic acid and ethanol, in which ethanol acts as a hydroxyl free radical scavenger to improve the yield of $^{13}N\text{-}NH_3$. The mixture is passed through an anion-exchange resin to remove all anion impurities. It is filtered through a 0.22-μm membrane filter and its pH should be between 4.5 and 7.5. The radiochemical purity is greater than 95% as determined by HPLC.

The US FDA has approved it for measurement of myocardial and cerebral perfusion.

^{11}C-Sodium Acetate

^{11}C-Sodium acetate is produced by the reaction of the Grignard reagent, methylmagnesium bromide in diethyl ether, with cyclotron-produced ^{11}C-carbon dioxide at −15 °C (Oberdorfer et al. 1996). After reaction, the product is allowed to react with O-phthaloyl dichloride to produce ^{11}C-acetyl chloride, which is then hydrolyzed to ^{11}C-acetate with saline. The solution is filtered through a 0.22-μm

membrane filter. ^{11}C-Acetate has been found to be stable at pH between 4.5 and 8.5 for up to 2 h at room temperature. The overall yield is about 10–50%.

It is used for the measurement of oxygen consumption (oxidative metabolism) in the heart, since acetyl CoA synthetase converts ^{11}C-acetate to acetyl coenzyme A after myocardial uptake, which is metabolized to ^{11}C-CO_2 in the tricarboxylic acid cycle.

^{11}C-Flumazenil

^{11}C-Flumazenil is commonly labeled at the *N*-methyl position by *N*-methylation with ^{11}C-iodomethane, which is prepared from ^{11}C-CO_2, and using the freshly prepared Grignard reagent, methylmagnesium bromide (Maziere et al. 1984). The specific activity is very important for this product and therefore is purified by HPLC to give an optimum value between 0.5 and 2 Ci/μmol (18.5–74 GBq/μmol). It remains stable for up to 3 h at room temperature at pH 7.0. The molecular structure of ^{11}C-flumazenil is shown in Fig. 8.4b.

Since it is a benzodiazepine receptor ligand, ^{11}C-flumazenil is primarily used for the neuroreceptor characterization in humans.

^{11}C-Methylspiperone

^{11}C-Methylspiperone (MSP) is prepared by *N*-methylation of commercially available spiperone with ^{11}C-methyl iodide in the presence of Grignard reagent, methylmagnesium bromide, using different solvents and bases (Mazière et al. 1992). Since spiperones are sensitive to bases and to radiolysis at high level of activity, the yield of ^{11}C-MSP has been variable for different investigators. Cold spiperone present in the preparation reduces its specific activity and should be controlled. Specific activity should be around 10–50 GBq/mol (270–1350 mCi/mol). High specific activity ^{11}C-MSP undergoes autodecomposition in saline due to radiation, and a hydroxyl radical scavenger (e.g., ethanol) is added to prevent it. The final preparation is filtered through a 0.22-μm membrane filter and its pH is adjusted to 7 ± 1 with a suitable buffer. The molecular structure of ^{11}C-methylspiperone is shown in Fig. 8.4c.

^{11}C-Methylspiperone is primarily used to determine the dopamine-2 receptor density in patients with neurological disorders, because of its high affinity for D-2 receptors in the brain.

^{11}C-L-Methionine

^{11}C-L-Methionine has ^{11}C at its methyl position and has two forms: L-[1 – ^{11}C] methionine and L-[*S*-methyl-^{11}C] methionine. The former is obtained by the reaction between ^{11}C-CO_2 precursor and carbanion produced by a strong base added to the respective isonitrile, followed by hydrolysis with an acid. The latter is the common method and obtained by alkylation of the sulfide anion of L-homocysteine with ^{11}C-iodomethane or ^{11}C-methyl triflate (Långström et al. 1987). The product is purified by HPLC yielding a purity of >98% and further filtered through a 0.22-μm membrane filter. The pH should be between 6.0 and 8.0 and it is stable for 2 h at room temperature. The molecular structure of ^{11}C-L-methionine is shown in Fig. 8.4d.

This compound is used for the detection of different types of malignancies, reflecting the amino acid utilization (transport, protein synthesis, transmethylation, etc.).

^{11}C-Raclopride

Raclopride is labeled with ^{11}C either by *N*-ethylation with [1-^{11}C] iodoethane or by *O*-methylation with [^{11}C] iodomethane, although the latter is more suitable for routine synthesis. Production of ^{11}C-labeled iodoethane and iodomethane are described in Chap. 7. A recent efficient method of synthesis of ^{11}C-raclopride utilizes a loop chemistry in which the precursor (raclopride) is dissolved in a small quantity of ethanol and loaded in an HPLC loop. ^{11}C-Methy triflate is then passed through the HPLC loop for 3 min, whereby reaction occurs to produce ^{11}C-raclopride (Shao et al. 2013). The product is purified by HPLC giving a purity of greater than 98%. The specific activity should be in the range of 0.5–2Ci/μmol (18.5–74GBq/μmol). The product at pH between 4.5 and 8.5 remains stable for more than 1 h at room temperature. The molecular structure of ^{11}C-raclopride is shown in Fig. 8.4e.

^{11}C-Raclopride is primarily used to detect various neurological and psychiatric disorders, such as schizophrenia, Parkinson's disease, etc.

^{11}C-Choline

^{11}C-Choline is prepared by the reaction between the precursor ^{11}C-methyl iodide and dimethylaminoethanol at 130 °C for 5 min (Hara and Yuasa 1999). The reaction mixture is evaporated to remove the precursors leaving behind the residue of ^{11}C-choline, which is dissolved in water and further purified by the cation exchange

method. The final product is available as ^{11}C-choline chloride with a radiochemical yield of ~43% at the end of synthesis.

^{11}C-Choline is a highly specific PET tracer used for the detection of various tumors, specifically prostate cancer, and has been approved by the FDA for clinical use in some specific prostate cancer patients.

^{62}Cu-Pyruvaldehyde-Bis(N^4-Methylthiosemicarbazonato) Copper(II)

^{62}Cu-Pyruvaldehyde-bis(N^4-methylthiosemicarbazonato) copper(II) (PTSM) is prepared by mixing H_2(PTSM) in ethanol and ^{62}Cu acetate solution at room temperature for 2–3 min (Green et al. 1990). The mixture is passed through C_{18} Sep-Pak column, and finally ^{62}Cu-PTSM is eluted from the column with ethanol followed by filtration through a 0.2-μm filter. The radiochemical yield is nearly 50% (without decay correction).

^{62}Cu-PTSM is used for measurement of myocardial perfusion by PET.

^{68}Ga-DOTA-Peptides

^{68}Ga-labeled peptides such as octreotide (DOTATOC) and octreotate (DOTATATE) are obtained by mixing the DOTA-peptides in 0.01 M acetic acid solution and $^{68}GaCl_3$ solution with 1.25 M Na-acetate in a small volume (Breeman et al. 2005). The reaction is allowed in a temperature-controlled heating block at a pH of 4. HPLC is employed to purify the labeled peptide, which is then filtered through a 0.22 μm Millipore filter for sterilization. The molecular structure is shown in Fig. 8.4g.

^{68}Ga-DOTATOCand ^{68}Ga-DOTATATE are used for PET imaging of neuroendocrine tumors and more advantageous than ^{111}In-octreotide because imaging time with the former is only a few hours compared to 2–3 days with the latter. The FDA has recently approved ^{68}Ga-DOTATOC as an orphan drug for specific use in neuroendocrine tumor imaging. An orphan drug is stipulated in relatively rare diseases that affect less than 200,000 people or for limited clinical use. This will ultimately lead to final approval for routine clinical use.

^{82}Rb-Rubidium Chloride

^{82}Rb-Rubidium chloride is available from the ^{82}Sr–^{82}Rb generator, which is manufactured and supplied monthly by Bracco Diagnostics, Inc. The activity in

the column is typically 90–150 mCi (3.33–5.55 GBq) ^{82}Sr at calibration time. ^{82}Rb is eluted with saline and must be checked for ^{82}Sr and ^{85}Sr breakthrough daily before the start of its use for patient studies. The allowable NRC limit for ^{82}Sr is 0.02 μCi/mCi or 0.02 kBq/MBq of ^{82}Rb and the limit for ^{85}Sr is 0.2 μCi/mCi or 0.2 kBq/MBq of ^{82}Rb. Measurement of ^{82}S and ^{85}Sr breakthrough is described later in Chap. 14. Since ^{82}Rb has a short half-life of 75 s, it is administered to the patient by an infusion pump (see Chap. 14). The administered activity is the integrated activity infused at a certain flow rate over a set time, which is provided on the printout from a printer. The generator is supplied with calibrated activity enough for a month's or 6 weeks' study with ^{82}Rb. Because of the long half-life of ^{82}Sr, the generator can be shipped to remote places.

The FDA approved it in 1989 for clinical use. Now ^{82}Rb is routinely used for myocardial perfusion imaging to delineate ischemia from infarction. A detailed protocol for its clinical use in patients in the USA has been included in Chap. 13.

Quality Control of PET Radiopharmaceuticals

The FDA mandates that synthesis of all PET radiopharmaceuticals including those described above for human administration must be carried out in sterile and clean environment, following recommendations given in FDA 21CFR212, which is described in detail in Chap. 9. All PET radiopharmaceuticals must undergo a set of quality control tests prior to human administration, which are described below. US Pharmacopeia (USP) 35 Chapter <823> provides the recommended methods for all these tests to ensure drug identity, strength, quality, purity, and patient safety. Because of the short half-lives of positron emitters used in PET imaging, some quality control tests have been grouped into two categories: those with nuclides with $t_{1/2} > 20$ min and those with nuclides with $t_{1/2} < 20$ min. In the case of the former, each production on a given day is considered a batch and all quality control tests must be performed for the batch; while in the latter group, a batch is defined as all related subbatches of PET radiopharmaceuticals compounded on a given day. The first subbatch (for $t_{1/2} < 20$ min) is designated as the *initial quality control subbatch* for the day, which is considered good for all quality control tests for all subsequent subbatches.

(a) The following quality control tests must be performed for all PET radiopharmaceuticals prior to release for human use:

- Visual inspection.
- pH.
- Radionuclidic purity.
- Radiochemical purity.
- Chemical purity.
- Specific activity.
- Isotonicity.

- Limits for residual solvents or toxic chemicals.
- A bubble point test or filter integrity test to check the structural integrity of the membrane filter immediately after filtration but prior to release of the product. (This is done by applying air pressure through the filter until the validated bubble point is reached. Filter integrity is indicated by the absence of a steady stream of bubbles. Maximum pressure to be applied is specified on the filter.)
- A 20-min endotoxin test on each batch ($t_{1/2} > 20$ min) or quality control subbatch ($t_{1/2} < 20$ min).
- Sterility tests on each individual batch ($t_{1/2} > 20$ min) or quality control subbatch ($t_{1/2} < 20$ min) initiated within 24 h (USP 35 Chapter <823>) or 30 h (FDA 21CFR 212) of sterility filtration.
- Toxicity.

(b) Written procedures for each quality control test must be established.
(c) Verification testing of all equipment (e.g., dose calibrator) and procedures must be carried out to comply with the acceptance limit. The results must be recorded, signed, and dated by the individual carrying out the test.

Methods of Quality Control

In this section, the methods of quality control tests for these products are briefly described below. Since PET radiopharmaceuticals are short-lived, some lengthy tests cannot be performed prior to release for human use and are performed within a short time after the release.

The quality control tests can be divided into two categories: physicochemical tests and biological tests. Refer to Saha (2010) for detailed description of these methods. These tests are briefly outlined below.

Physicochemical tests. Physicochemical tests include the tests for the physical and chemical parameters of a PET radiopharmaceutical, namely, physical appearance, isotonicity, pH, radionuclidic purity, chemical purity, and radiochemical purity.

Physical appearance. Physical appearance relates to the color, clarity, or turbidity of a PET radiopharmaceutical and should be checked by visual inspection of the sample.

pH. The pH of a PET radiopharmaceutical for human administration should be ideally 7.4, but both slightly acidic and basic pH values are tolerated due to the buffer capacity of the blood. The pH can be adjusted by adding appropriate buffer to the solution.

Isotonicity. Isotonicity is the ionic strength of a solution, which is mainly adjusted by adding appropriate electrolytes. Normally PET radiopharmaceuticals have appropriate isotonicity for human administration.

Radionuclidic purity. The radionuclidic purity of a radiopharmaceutical is the fraction of total activity in the form of the desired radionuclide in the sample. These impurities primarily arise from the radionuclides produced by various nuclear reactions in a target as well as the impurities in the target material. Using a multichannel spectrometer, one can determine the level of impurities in a sample of a positron-emitting radionuclide produced by a specific nuclear reaction in a cyclotron. Using highly pure target material and appropriate chemical separation techniques, the radionuclidic impurity can be minimized to an acceptable level. Short-lived radionuclides can be allowed to decay to have a pure long-lived radionuclide in question. Even though the impurities in the routine preparations of PET radionuclides do not vary significantly from batch to batch, periodic checkup is recommended to validate the integrity of the method of production. The radionuclidic impurities must be established in ^{11}C, ^{13}N, ^{15}O, and ^{18}F radionuclides, prior to their use in the synthesis of radiolabeled compounds.

Chemical purity. Chemical purity is the fraction of a radiopharmaceutical in the desired chemical form, whether all of it is radiolabeled or not. The presence of extraneous stable atoms may cause adverse reactions and is not desirable in a PET radiopharmaceutical. These impurities arise from the incomplete synthesis, addition of extraneous ingredients during the synthesis, and so on. Chemical methods such as the spectrophotometric method, ion exchange, solvent extractions, chromatography, etc., are applied to measure the level of these chemical impurities. Again, these tests can be performed a priori in many dry runs and thus the level of chemical impurities can be established, prior to human administration.

Radiochemical purity. The radiochemical purity of a radiopharmaceutical is defined as the fraction of the total activity in the desired chemical form in the sample. These impurities arise from incomplete labeling, breakdown of the labeled products over time due to instability, and introduction of extraneous labeled ingredients during synthesis. These impurities cause altered in vivo biodistribution after administration, resulting in an unnecessary radiation dose to the patient. For these reasons, the USP and the US Food and Drug Administration have set limits on the impurities in various radiopharmaceuticals, and these limits must not be exceeded in clinical operations.

Since most PET radiopharmaceuticals are produced on site daily, the radiochemical purity must be checked for each batch. For very short-lived radionuclides, however, the methodology must be validated beforehand by carrying out many dry runs so that the radiochemical purity of the product remains within the limit set for human administration.

Several analytical methods are employed to establish the radiochemical purity of PET radiopharmaceuticals. The most common method is HPLC, which gives separation of components with high resolution. The general principle of HPLC involves forcing a sample at high pressure (6000 psi) by a pump through a column (15–30 cm long and 2–5 mm inner diameter) of special packing material by an electric pump, whereby various components pass out of the column at different rates depending on their molecular weights. The eluate is passed through a sensitive ultraviolet

(UV) detector to identify different components, which are then quantitated by the UV absorbance peaks. Alternatively, fractions of the eluate are collected and the activity in each fraction is measured in a gamma counter.

Another common method of determining the radiochemical purity is the thin-layer chromatography (TLC). In this method, a drop of the radiopharmaceutical sample is spotted on a solid-phase paper strip (e.g., silica gel, Whatman), and then the paper is placed vertically in a small vial containing a small amount of an appropriate solvent, taking care that the spotted area remains above the solvent. The solvent flows along the paper strip, and different components of the sample will flow at different rates along the strip depending on their solubility in the solvent. The ratio of the distance traveled by a component to the distance traveled by the solvent front is called the R_f value. When the solvent front reaches the top of the strip, the strip is removed and scanned with radiochromatographic scanner for the distribution of components along the strip. Alternatively, the strip is cut into several segments (e.g., ten segments), and the activity in each segment is measured in a gamma counter. From the counts of the segments, the radiochemical purity can be calculated.

Biological tests. Biological tests include sterility testing, pyrogen testing, and toxicity testing.

Sterility. Sterility indicates the absence of any viable bacteria or microorganisms in a radiopharmaceutical preparation. All radiopharmaceuticals must be sterile prior to administration to humans, and it is normally accomplished by filtering the product through a 0.22-μm membrane filter or heating the sample to 120°C for 20 min at a pressure of 18 psi. PET radiopharmaceuticals are normally sterilized by filtration because of their short half-life.

Sterility tests are normally performed by incubating the sample with fluid thioglycollate medium at 30–35°C for 14 days or with soybean–casein digest medium at 20–25°C for 14 days. The sample volume should be as large as that for human dosage. If bacterial growth is observed in either test, the preparation is considered asterile. For PET radiopharmaceuticals, these tests must be started within 24 h (per USP 35 Chapter <823>) or 30 h (per FDA 21CFR212) after the release of the product.

Pyrogenicity. Pyrogens are bacterial endotoxins consisting of polysaccharides or proteins produced by the metabolism of microorganisms, and upon administration they cause undue symptoms such as fever, flushing, chill, sweating, malaise, etc. These symptoms typically set in 30 min to 2 h after administration and are rarely fatal. There are no specific methods of making a preparation pyrogen-free, and the only way to avoid pyrogens is to strictly follow the method of preparation employing meticulous aseptic technique so that microbes are not introduced into the sample.

Tests for pyrogens include a rabbit test, in which rabbits are administered with the radiopharmaceutical and their rectal temperatures are monitored. From the rise in temperature in the rabbits, pyrogenicity of a sample is determined. However, a

simpler and quicker method is the so-called limulus amebocyte lysate (LAL) test, also called the bacterial endotoxin test (BET). In this test, the lysate of amebocytes from the blood of the horseshoe crab (*Limulus polyphemus*) is mixed with the sample and incubated at 37°C. An opaque gel is formed within 15–60 min depending on the concentration of pyrogens.

Toxicity. The toxicity of a radiopharmaceutical causes alteration in the histology or physiologic functions of an organ or even death of a species after in vivo administration. It is commonly characterized by $LD_{50/60}$, which is defined as the quantity of a sample that kills 50% of the species within 60 days after administration. For a radiopharmaceutical, it must be established at least in two species (e.g., rats and rabbits) before human administration, and the dosage for the humans is decided by a large safety factor. Toxicity arises from the pharmaceutical part and most PET radiopharmaceuticals are not toxic for human administration.

Questions

1. Describe in detail the method of ^{18}F-FDG synthesis.
2. Describe the method of synthesis of (a) 6-^{18}F-L-fluorodopa, (b) ^{18}F-fluorothymidine, and (c) ^{11}C-L-methionine.
3. What is the difference between the nucleophilic and electrophilic reaction?
4. What are the clinical uses of ^{18}F-FDG, ^{18}F-FLT, 6-^{18}F-L-fluorodopa, ^{15}O-water, ^{13}N-ammonia, ^{11}C-sodium acetate, ^{18}F-florbetapir, and ^{11}C-methylspiperone?
5. Describe the operational principles of an automated synthesis box.
6. Define (a) radionuclide purity, (b) radiochemical purity, and (c) chemical purity of a radiopharmaceutical.
7. Describe the method of determining the radiochemical purity of an ^{18}F-FDG sample.
8. Describe the methods of sterilizing radioactive samples.
9. Describe the methods of sterility tests and pyrogen tests.
10. A sterile sample is always pyrogen-free. True _____; False _____.
11. A LAL test is required for every batch prior to release of PET radiopharmaceuticals ($t_{1/2} < 20$ min) for human use. True _____; False _____.
12. Sterility test of PET radiopharmaceuticals must begin (a) prior to release, (b) within 24 h of release, (c) anytime after release, or (d) is not required.

References and Suggested Reading

Breeman WA, de Jong M, de Blois E, et al. Radiolabelling DOTA-peptides with ^{68}Ga. Eur J Nuc Med Mol Imaging. 2005;32:478.

Green MA, Mathias CJ, Welch MJ et al. [62Cu]-labeled pyruveldehyde bis (N4-methylthiosemicarbazonato) copper(II): synthesis and evaluation as a positron emission tomography tracer for cerebral and myocardial perfusion. J Nucl Med 1990; 31:1989.

Hamacher K, Coenen HH, Stöcklin G. Efficient stereospecific synthesis of no-carrier-added 2-[18F]-fluoro-2-deoxy-D-glucose using aminopolyether supported nucleophilic substitution. J Nucl Med. 1986; 27:235.

Hara T, Yuasa M. Automated synthesis of [^{11}C] Choline, a positron-emitting tracer for tumor imaging. Appl Radiat Isot. 1999;50:531.

Kabalka GW, Lambrecht RM, Fowler JS, et al. Synthesis of ^{15}O-labelled butanol via organoborane chemistry. Appl Radiat Isot. 1985;36:853.

Kamarainen EL, Kyllonen T, Nihtila O, et al. Preparation of fluorine-18 labeled fluoromisonidazole using two different synthesis methods. J Labeled Comp Radiopharm. 2004;47:37.

Långström B, Antoni G, Gullberg P, et al. Synthesis of L- and D-[Methyl-^{11}C]Methionine. J Nucl Med. 1987;28:1037.

Liu Y, Zhu L, Plossl K, et al. Optimization of automated radiosynthesis of [^{18}F]AV-45: a new PET imaging agent for Alzheimer's disease. Nucl Med Biol. 2010;37:917.

Luxen A, Guillaume M, Melega WP, et al. Production of 6-[^{18}F]fluoro-L-dopa and its metabolism in vivo—a critical review. Int J Rad Appl Istrum B. 1992;19:149.

Machula HJ, Blocher A, Kuntzch M, et al. Simplified labeling approach for synthesizing 3′-deoxy-3′-[^{18}F]fluoro-thymidine [^{18}F]FLT. J Radioanal Nucl Chem. 2000;243:843.

Maziere M, Hantraye P, Prenant C, et al. Synthesis of ethyl-8-fluoro-5,6-dihydro-5-[^{11}C]-methyl-6-oxo-4H-imidazo[1,5][1,4] benzodiazepine-3-carboxylate (R_0-151788-^{11}C): a specific radioligand for the in vivo study of central benzodiazepine receptors by positron emission tomography. Int J Appl Radiat Isot. 1984;35:973.

Mazière B, Coenen HH, Haldin C, et al. PET radioligands for dopamine receptors and re-uptake sites: chemistry and biochemistry. Nucl Med Biol. 1992;19:497.

Meyer GJ, Ostercholz A, Handeshagen H. ^{15}O-water constant infusion system for clinical routine application. J Label Comp Radiopharm. 1986;23:1209.

Oberdorfer F, Theobold A, Prenant C. Simple production of [1-carbon-11] acetate. J Nucl Med. 1996;37:341.

Reischl G, Ehrlichmann W, Bieg C, et al. Preparation of the hypoxia imaging PET tracer [^{18}F] FAZA: reaction parameters and automation. Appl Radiat Isot. 2005;62:897.

Saha GB. Fundamentals of nuclear pharmacy. 6th ed. New York: Springer; 2010.

Shao X, Schnau PL, Fawaz M, et al. Enhanced radiosyntheses of [^{11}C] Raclopride and [^{11}C] DASB using ethanolic loop chemistry. Nucl Med Biol. 2013;40:109.

Stöcklin G, Pike VW, editors. Radiopharmaceuticals for positron emission tomography. Dordrecht: Kluwer; 1993.

US Federal Registrar 21CFR212. Current good manufacturing practice for positron emission tomography; 2011.

U.S. Pharmacopeia 35 & National Formulary 30. United States pharmaceutical convention, Rockville, MD. Chapter <823> Positron emission tomography drugs for compounding, investigational, and research uses; 2012.

Welch MJ, Kilbourn MR. A remote system for the routine production of oxygen-15 radiopharmaceuticals. J Label Comp Radiopharm. 1985;22:1193.

Wester HJ, Herz M, Weber W, et al. Synthesis and radiopharmacology of O-2-[^{18}F] fluoroethyl-L-tyrosine for tumor imaging. J Nucl Med. 1999;40:205.

Wieland D, Bida G, Padgett H, et al. In-target production of [^{13}N] ammonia via proton irradiation of dilute aqueous ethanol and acetic acid mixtures. Appl Radiat Isot. 1991;42:1095.

Chapter 9
FDA Regulations for PET Radiopharmaceuticals

Food and Drug Administration

Since 1975, the clinical use of all radiopharmaceuticals in humans has been regulated by the US Food and Drug Administration (FDA). The FDA regulates them in two major ways: for investigational purposes, submission of a *Notice of Claimed Investigational Exemption for a New Drug* (*IND*) by a sponsor (an individual or a commercial manufacturer) or submission of a *New Drug Application* (*NDA*) by a manufacturer for marketing. However, under special circumstances and specific conditions, Exploratory IND (*e*IND), Radioactive Drug Research Committee (RDRC) IND, and Expanded Access IND (*ea*IND) are permitted. Furthermore, physicians and technologists are required to have sufficient training and experience to practice in PET imaging. The FDA has provided specific contents for these training and experience.

In Chap. 8, we have described the methods of production of PET radiopharmaceuticals useful for clinical applications. For human use, these must be produced under strict environmental and procedural conditions and undergo a battery of quality control tests (e.g., stability, biological safety, efficacy, etc.), which are mandated by the FDA. The following is a brief description of different regulations for the synthesis of PET radiopharmaceuticals and their use in humans. Only the important points of regulations are presented.

Investigational New Drug

An IND for a PET radiopharmaceutical is approved by the FDA for human use following a submission by a sponsor of the preliminary data of the radiopharmaceutical in humans and animals, technical details of the project, the clinical protocol, and the credential of the sponsor. There are three phases in the IND

G.B. Saha, *Basics of PET Imaging*, DOI 10.1007/978-3-319-16423-6_9

clinical investigation of a radiopharmaceutical. In Phase I, only pharmacologic and biodistribution data of the radiopharmaceutical are obtained in a limited number of humans and no therapeutic and diagnostic evaluation can be made. In Phase II, clinical effectiveness of the radiopharmaceutical is evaluated for a specific disease only in a limited number of patients. In Phase III, a large number of patients involving many trial centers are included in the clinical trial to establish the safety and clinical effectiveness of the radiopharmaceutical for a specific disease. Annual reports must be submitted on the progress of the project. Any serious adverse reaction from the product must be reported immediately to the FDA.

New Drug Application

After a radiopharmaceutical is proven by clinical trials under an IND to be safe and efficacious for a specific clinical indication, an NDA is submitted with all clinical data by a commercial vendor to the FDA for approval to market it. Many clinical trial centers are sponsored by the vendor to collect the data, which are then submitted in the application. After scrutiny of the data, if the FDA is convinced of the safety and efficacy of the radiopharmaceutical for a clinical indication, it approves the product for marketing. It takes a long time (at times, a couple of years) from an IND to an NDA for approval of a particular radiopharmaceutical for clinical use in humans.

PET radiopharmaceuticals are uniquely different from conventional radiopharmaceuticals because they are short lived and are produced on site at the cyclotron facility. Synthesis of these tracers by radiolabeling with positron emitters is accomplished in automated synthesis boxes. Several lengthy quality control tests are often performed on an "after-the-fact" basis. The production methods and their technical details may vary from facility to facility. For these reasons, the FDA treats PET radiopharmaceuticals somewhat differently and attempts to standardize the techniques employed in all PET facilities. In the mid-1990s, the FDA published the regulations and guidelines for the manufacture of PET radiopharmaceuticals in the Federal Register. These regulations provided guidance for submission of NDAs and abbreviated NDAs (ANDAs) to the FDA for PET radiopharmaceuticals, and the guidelines gave details of the current good manufacturing practice (CGMP) to follow in the manufacture of PET radiopharmaceuticals.

However, the above regulations and guidelines were considered too costly and burdensome by the nuclear medicine community, particularly the commercial vendors. Also, other radiopharmaceuticals and conventional drugs were subjected to strict scrutiny by the FDA, resulting in a very long waiting time for marketing approval. Following strong lobbying by the nuclear medicine community, drug manufacturers, and other stakeholders, the US Congress enacted the FDA Modernization Act (FDAMA) (Public Law 105–115) in 1997 to overhaul several aspects of the drug manufacturing industry, which took effect on November 21, 1997. Under

the Act, the existing regulations regarding PET radiopharmaceuticals were retracted and new provisions were introduced.

In the FDAMA, PET radiopharmaceuticals are categorized as positron-emitting drugs compounded by, or on the order of, a licensed practitioner following the state's regulations and meeting the specifications of the official monographs of the US Pharmacopeia (USP). The FDAMA directed the FDA to develop approval procedures and guidance for the manufacture of PET radiopharmaceuticals within a time frame of 4 years. In this 4-year time line, all PET tracer-producing facilities in the USA were to be registered as drug manufacturers. In the first 2 years, the FDA was to consult with patient advocacy groups, professional associations, manufacturers, physicians, and scientists who prepare or use PET drugs, in developing approval procedures and CGMP for PET radiopharmaceuticals. The remaining 2 years were allowed for all PET radiopharmaceutical manufacturing facilities to comply with the new PET drug CGMP and register as manufacturers. During these 4 years, the FDAMA prohibited the FDA to require the submission of NDAs or ANDAs for PET radiopharmaceuticals produced according to the USP specifications. However, voluntary submissions of NDAs or ANDAs were not prohibited.

Based on the literature survey of PET data, the FDA concluded that certain PET radiopharmaceuticals, when produced under specific conditions, are safe and effective for certain clinical indications. Based on this survey, three PET radiopharmaceuticals, ^{18}F-sodium fluoride for bone imaging, ^{18}F-FDG for use in oncology and for assessment of myocardial viability, and ^{13}N-NH_3 for evaluation of myocardial blood flow, were approved by the FDA in 2000. ^{82}Rb-rubidium chloride was approved by the FDA for evaluation of myocardial perfusion in 1989. Recently ^{18}F-florbetapir has been approved for amyloid-plaque imaging in AD and ^{11}C-choline for prostate cancer.

The FDA also published in the Federal Register a draft guidance for industry entitled, "PET Drug Applications—Content and Format for NDAs and ANDAs" (March 10, 2000; 65 Fed.Reg. 13010), citing the safety and effectiveness of ^{18}F-FDG, ^{18}F-soodium fluoride, and ^{13}N-ammonia. It is intended to assist manufacturers of these radiopharmaceuticals in submitting ANDAs, instead of full NDAs, simply referring to this guidance for product information. Following a period of comments from various stakeholders, the final rule was adopted. The guidance gives the details on the criteria for when to apply for an NDA or an ANDA and what to include in the application. In addition, this 2000 Federal Register addressed user fees against the applicants of NDAs for the application, manufacturing facilities, and drug products.

Exploratory IND

A traditional Phase I IND requires a very comprehensive and detailed application for any human research protocol for evaluation of a drug. In 2006, the FDA has instituted a new approach, called the "Exploratory IND," or "*e*IND," to ease the

application process as well as expedite the research progress. An *e*IND is a clinical trial that is conducted early in Phase I, involves a limited radiation exposure, and has no therapeutic or diagnostic intent.

It usually involves the use of a very limited dosage of the drug (microdosage) in research subjects for a limited time (e.g., 7 days). Through *e*IND, an investigator can assess (a) the mechanism of action, (b) the pharmacokinetics, and (c) the therapeutic potential of a drug from a group of candidates, and explore (d) the biodistribution using a variety of imaging techniques.

An *e*IND containing the following information must be submitted to the FDA:

(a) *A clinical development plan*: It entails the rationale for the drug in question, a single-dosage or multiple-dosage study, and pharmacologic and/or pharmacodynamic end points.
(b) *Chemistry, manufacturing, and control*: It includes a summary report for each drug on the following: physicochemical and biological properties of the drug, dosages to be administered, route of administration, grade and quality of all ingredients in the manufacture of the drug, and name and address of the manufacturer, if different from the sponsor; method of manufacture of the drug; composition of the drug; tests performed to ensure the identity, strength and quality, and purity and potency of the drug; stability of the drug; and results of sterility and pyrogen tests.
(c) *Pharmacology and toxicology information regarding the drug*: This information can be obtained from animal studies using increasing dosages of the drug, but the needed information may be less than that required in a traditional IND.
(d) Previous human experience with the investigational product, if any.

It should be noted that an *e*IND is meant for quick assessment of pharmacokinetics, pharmacological effects, and mechanism of action of a drug for its potential clinical use. For pharmacokinetics study, microdosages of the product are used not to induce any pharmacological effect. A microdosage is defined as less than 1/100th of the dosage calculated to yield a pharmacological effect of a test product with a maximum dosage of $\leq$100 μg. Microdosage studies performed in animals for pharmacokinetics are acceptable to the FDA for extrapolation to human studies. For pharmacological studies, toxicity of the test product is established in animals (e.g., rats) by repeated administration of the product over a 7-day period and observing the pathological changes in tissues. The study can be extended to a 2-week repeat study. The aim of the experiment is to establish the starting dosage and the maximum dosage of the test product for safety and efficacy in the clinical trial. The dosage and the dosing regimen determined in the animal experiments for pharmacokinetics and pharmacologic effects are extrapolated to the human clinical trial to establish the mechanism of action for a given target. The study must be withdrawn after the completion of the proposed protocol. Readers are referred to "Guidance for Industry, Investigators and Reviewers Exploratory IND Studies" at http://www.fda.gov/cder/guidance for further information.

Radioactive Drug Research Committee

In order to expedite research investigations of new radiopharmaceuticals, in 1975 the FDA allowed institutions to form the so-called *Radioactive Drug Research Committee* (RDRC) (21CFR 361.1), which functions like a mini-FDA. The committee is composed of at least five members—a nuclear physician, a radiochemist or radiopharmacist competent to formulate radioactive drugs, a person with experience in radiation safety and dosimetry, and at least two more individuals of other disciplines. Additional members of diverse disciplines are recommended in the committee. The RDRC is normally formed in medical institutions having sufficient experts, but a joint RDRC also can be established with more than one institution to achieve a high level of diversity and experience. The proposed committee membership with a designated chairman is submitted to the FDA, and upon satisfactory review the FDA approves it. The committee is primarily charged with the approving and monitoring of protocols involving the research use of radiopharmaceuticals to study the kinetics, distribution, localization, biochemistry, physiology, etc., in humans, but not for immediate therapeutic or diagnostic purpose nor to determine the safety and effectiveness of the drug as in a clinical trial.

The radiation dose to the critical organs (effective dose, dose to the lens and blood-forming organ) of a patient cannot exceed 3 rem (0.03 Sv) from a single dosage and a sum of greater than 5 rem (0.05 Sv) per year during the entire study. Only 30 patients over the age of 18 are allowed for study per protocol, and a special summary report must be submitted to the FDA, if the number exceeds 30 and the age is greater than 18. The pregnant women are not allowed to participate in the study under the RDRC.

An investigator in an institution formally submits a research protocol to its RDRC with detailed description of the study, but prior to submission, the protocol must be approved by the Institutional Review Board. The RDRC meets at least quarterly if active research is pursued, with at least 50% membership present. Members with conflict of interest in a protocol must excuse themselves from voting on the protocol. Based on the critical review of the protocol, the study may be or may not be approved by the RDRC. If approved, the study will be regularly monitored by the committee on the progress. Any adverse effects encountered during the study must be immediately reported to the FDA. The chairman of the RDRC is the primary contact person with the FDA and must submit an annual report on all projects. Also any change in the membership must be reported to and approved by the FDA.

Difference Between RDRC and Exploratory IND

The following major differences between the two processes are noted:

1. The study under the RDRC is a basic research protocol investigating the pharmacokinetics, pharmacology, biodistribution, etc., of a radioactive drug in

patients, whereas an *e*IND is a clinical protocol to study the safety and efficacy of a drug using small dosages with maximally tolerable pharmacologic effect.
2. While an *e*IND protocol is approved and monitored directly by the FDA, the RDRC studies are approved and monitored by the committee itself in an institution and the FDA monitors it only indirectly.
3. The number of subjects is normally limited to 30 in the RDRC, whereas there is no limit on the number of patients in an *e*IND, although it should be small.
4. In the RDRC, if subjects of age less than 18 or more than 30 subjects are used, a special summary report must be submitted to the FDA. Also women of child-bearing age must declare in writing the absence of pregnancy to participate in the RDRC study. Under an *e*IND, no such restriction exists except that each case is individually evaluated.
5. The RDRC limits the radiation doses to subjects, whereas in an *e*IND there is no such limit.

Expanded Access IND for PET Radiopharmaceutical

Expanded Access IND (*ea*IND) has been designed by the FDA to provide access to investigational drugs on an emergency basis for serious or life-threatening diseases. Pursuant to the FDAMA, 1997, specific provision for the *ea*INDs was included in a final rule on CGMP published in 2009 (see below). Although *eaI*ND drugs were meant for therapeutic drugs, the FDA has included the diagnostic PET radiopharmaceuticals in *ea*IND groups because of the short half-lives and difficulty in commercial production.

An *ea*IND can be applied for an individual patient, a small group of patients, or a large group of patients. *ea*INDs are most useful for individual patients and the submission of an application to the FDA is simplistic. The required information for application includes pharmacology data, previous experience, evidence from literature, etc. For an individual patient, only direct cost can be recovered, whereas for a larger group, both direct cost and indirect cost (e.g., administrative costs) can be charged to the patients. PET *ea*INDs do not pose any potential risk, because of the diagnostic nature of the ingredients. *ea*INDs are not applicable to FDA-approved drugs such as ^{18}F-FDG and ^{13}N-ammonia.

Compounding of PET Radiopharmaceuticals

The FDA has recognized for many years that compounding and dispensing of drugs for human use based on physician's order falls under the regulations of medical and pharmacy practices in individual states in the USA. A noncommercially available drug, if ordered in a prescription by a physician, can be compounded by a pharmacist or some qualified individuals authorized and supervised by the physician using

US Pharmacopeia (USP) guidelines under the regulations of practice of medicine and pharmacy. Because PET radiopharmaceuticals are short lived and produced daily in the cyclotron on the order of a prescription by a physician, their production for human use is considered compounding and falls under the USP guidelines. The physicians and pharmacists who compound (or oversee the compounding of) PET radiopharmaceuticals must be well trained and responsible for the strength, quality, and integrity of the product for compounding and dispensing.

On November 27, 2013, the Drug Quality and Security Act was signed into law, which recommends drug compounding facilities to register with the FDA as outsourcing facilities and encourages healthcare providers to utilize only the registered facilities for their supply of compounded drugs. It is not mandatory to register, but unregistered facilities must follow drug and labeling requirements of the FDA. The FDA can inspect the registered facilities on a risk-based schedule. IND and RDRC holders are not required to register.

As mandated by the FDAMA, since 1999, the FDA issued a couple of draft regulations and guidance for CGMP for PET drugs, each successive one being revised with FDA responses to comments from the public and stakeholders. A draft guidance for PET CGMP was issued in 2005 [PET Drug Products—Current good manufacturing practice (CGMP). September, 2005] and the final guidance in 2009 (PET Drugs—Current good manufacturing practice (CGMP), December, 2009) was published. Readers are referred to http://www.fda.gov/cder/fdama for details.

The final guidance issued in 2009 was published in title 21 of Code of Federal Regulations part 212 (21CFR212) regarding the current good manufacturing practice (CGMP) in the manufacture of PET drugs for their safety and quality assurance. It became effective December 12, 2011, and all manufacturers must be compliant with these regulations. In parallel, the USP 35 Chapter <823> gives detailed procedures for safety and quality assurance of PET radiopharmaceuticals. Many elements are common in both 21CFR212 and USP35 Chapter <823>, but the former supersedes the latter in terms of authority. In many situations, the FDA does not object to manufacturers following USP35 Chapter <823>. The following is a summarized outline of requirements of 21CFR212 and USP35 Chapter <823>.

Personnel

Personnel working in PET drug synthesis must be well trained in different aspects of synthesis, labeling, and dispensing at different stages. The number of personnel depends on the size of the facility, and their training must be documented. The training should be comprehensive enough for an individual to perform efficiently in a PET laboratory. One person may be able to operate in a small PET laboratory.

Facility and Equipment

Sterile procedures must be employed following the International Organization for Standardization (ISO) Class 5 environment with use of HEPA filters, and aseptic techniques must be applied throughout the facility including equipment, and during all stages of synthesis. All equipment must be calibrated with precision, and calibration must be validated and recorded.

Components, Materials, and Supplies

Under this category, specifications of components, materials, and supplies used for compounding of PET tracers must be established in writing for the following:

(a) Identity, purity, and quality of components (chemicals, targets, gases, etc.), containers and closures, analytical supplies (chromatography columns, TLC papers etc.), and sterility and pyrogen testing agents must be established.
(b) Sterility testing of PET drugs must be initiated within 24 h according to USP 35, Chapter <823>, or within 30 h according to 21CFR212. Longer wait time is allowed if it can be shown that the drug remains stable that long.
(c) Storage conditions (heat, light, humidity, etc.) in a controlled area for the above materials must be known or established.
(d) Records of lot number, quantity, manufacturer, date of receipt, and expiration date of all the above materials must be kept.
(e) Verification of each lot of the above material complying with the required specifications must be made.

Compounding Procedure Verification

(a) Acceptance limits for the identity, purity, and quality of each compounded radiopharmaceutical must be set in writing.
(b) A written procedure for compounding of each PET radiopharmaceutical including sterilization by filtration (0.22 μm for parenteral administration and 0.45 μm for inhalation). These procedures need to be routinely updated, reviewed, and verified at least once a year.
(c) The use of computer and related automated equipment must undergo strict controls for their accuracy, operation, and upgrade instituted by authorized personnel only.
(d) A verification method must be established to verify that all the above steps have met the set acceptance criteria. Prior to human use of a new or modified PET tracer, three consecutive batches of the product must be compounded and verified for the acceptance limit.

(e) Expiration date and storage conditions must be established and recorded.
(f) Failure of a product must be investigated thoroughly and the cause of failure must be determined and remedied.

Dispensing of PET Radiopharmaceuticals

The following general rules are recommended for dispensing PET radiopharmaceuticals:

(a) All compounding and dispensing must be done in sterile clean area using aseptic technique.
(b) Label all components for identity and traceability.
(c) The label on PET radiopharmaceutical containers must contain: name of the radiopharmaceutical, lot or batch number, radioactive symbol, total activity and concentration at calibration time, and time and date of expiration.
(d) Records of all the above information and the percent yield of the final product must be maintained in writing for each batch of the PET tracer.
(e) The qualified individual compounding a batch must initial the record attesting to the accurate current compounding procedure used.
(f) The overall responsible individual must sign and date the record attesting to compliance to the verified compounding procedure.

Aseptic Technique

(a) Equipment and components used in compounding PET radiopharmaceuticals must be clean and sterile supported by a verification method.
(b) Work must be done in clean areas, e.g., a Class 100 aseptic hood like laminar flow hood or ISO Class 5 environment.
(c) Sterile conditions of space and equipment must be monitored regularly by microbial testing.
(d) Clean garb and sterile gloves must be worn during compounding.
(e) Vial septum should be sterilized by swabbing with 70% alcohol before inserting the content into or withdrawing it from the vial.

Legal Requirements for Practicing PET

Because PET radiopharmaceuticals are used in humans, the FDA has implemented specific regulations for synthesis and strict quality assurance of these products mentioned above. Rules for preliminary trial with investigational drugs (IND) and for new drug application (NDA) have been established. Physicians and

technologists are required to have adequate training and experience to practice in PET imaging. Specific criteria for licensing, training, and experience for physicians and technologists have been outlined by the FDA. Also, PET facilities must meet the requirements of accrediting agencies to be accredited to perform PET studies. The following is a description of these requirements.

License or Registration

Facilities. The PET center and/or the cyclotron facility must be registered or licensed by the state for the manufacture of PET radiopharmaceuticals. However, the use of PET radiopharmaceuticals is regulated by the NRC or Agreement States for their radiation aspects. The license for medical use of radiopharmaceuticals is called the radioactive material (RAM) license, which a licensee obtains by applying to the NRC or the Agreement State. The RAM license specifies the type, the chemical form, and the possession limit of the radionuclides to be used, depending on the scope of the operation at the applicant's facility. While a PET center may be approved for a few hundred millicuries (GBq) of ^{18}F-FDG in its RAM license, the cyclotron facilities may be approved in the license for curie amounts for commercial distribution. Note that the ^{82}Sr–^{82}Rb generator typically is supplied with a strength of 80–150 mCi (2.96–5.55 GBq) of ^{82}Sr, but it also contains ^{85}Sr, which may be as much as five times the amount of ^{82}Sr. Although ^{85}Sr is not used clinically but is contained as a contaminant in the generator, a licensee must include in the RAM license the maximum possible amount of ^{85}Sr as the possession limit in addition to those of ^{82}Sr and ^{82}Rb. These licenses are issued for a certain number of years (e.g., 1 year, 3 years, etc.) and renewed after the period, if needed. The licensee agrees in the license application to strictly follow all the terms and regulations implemented by the NRC or Agreement State.

A cyclotron is required to be registered with both the FDA and the state since it produces radionuclides. A dedicated PET scanner may or may not be required to be registered in a state depending on the state's statutes on this matter. Some states may require a *certificate of need* (CON) prior to the purchase of a PET scanner, a mobile PET, a PET/CT scanner, or a PET/MR scanner. A PET/CT scanner is required to be registered with the state because of the CT unit, since all states require registration of radiation-generating machines.

Physicians. Physicians are required to be licensed by the NRC or the Agreement State as authorized users for the medical use of byproduct materials in humans. Accredited board certifications or minimum hours of training and experience are required to qualify as authorized users. As required by the NRC, 700 h of training and experience, which include 80 h of classroom and laboratory training in radiation science and 620 h of work experience in radionuclide handling, are needed to qualify as an authorized user for imaging and localization studies using

PET radiopharmaceuticals (10CFR35.290). In addition to these requirements, a preceptor's certification as to the competence of the individual is required. The specialty boards that meet the requirements of the above hours of training and work experience are eligible for the authorization for PET studies.

For interpretation of PET or PET/CT studies, the Joint Commission on Accreditation of Healthcare Organizations (JCAHO) requires that every hospital must have a definite policy in place to offer privileges to staff members to practice their discipline but does not spell out any specific qualifications for any particular privilege. So all privileges that include interpretation of diagnostic images are hospital specific and normally are granted based on the standards of competency set forth by respective professional organizations. The Society of Nuclear Medicine, the American College of Nuclear Physicians, and the American College of Radiology set these standards for various diagnostic imaging modalities. For body PET interpretation, physicians should meet the following requirements: certification by the American Board of Nuclear Medicine (ABNM) or American Board of Radiology (ABR); interpretation of 150 PET and/or PET/CT examinations under the direct supervision of an ABNM- or ABR-certified physician who has interpreted 500 PET and/or PET/CT examinations; 8 h of continuing medical education (CME) in PET and/or PET/CT studies for physicians with ABNM certification or ABR certification with nuclear radiology subspecialty; or 35 h of CME for other ABR-certified physicians. The continuation of privilege requires interpretation and reporting of 100 PET and/or PET/CT studies per year.

For interpretation of CT part in PET/CT studies, ABR-certified diagnostic radiologists are privileged by virtue of their training, whereas ABNM-certified physicians should have training in CT that include 100 h of continuing education incorporating the physics of diagnostic radiology and interpretation of 500 CT examinations including a distribution of the neck, chest, abdomen, and pelvis, under the supervision of a qualified radiologist. The continuation of privilege requires interpretation and reporting of 100 PET/CT studies per year.

Technologists. To work in nuclear medicine in the USA, a nuclear medicine technologist is required to be certified by the Nuclear Medicine Technology Certification Board (NMTCB) or the American Registry of Radiologic Technologists (ARRT) with specialty in nuclear medicine technology. Many states require healthcare technologists to be licensed to practice their profession in the state. At present, 26 states in the country require licensing for nuclear medicine technologists; 38 states require licensure for radiographers; and 33 states require licensure for radiation therapists. Congress is considering the passage of the Consumer Assurance of Radiologic Excellence (CARE) bill to establish uniform educational and credentialing standards for all personnel in the USA who perform medical imaging and radiation therapy procedures. The nuclear medicine technology licensure is given based on the NMTCB certification and work experience. The duration of the license varies among the states, but they are renewable on the accrual of required CME credits.

PET Certification for Technologists

Currently nuclear medicine technologists can work as PET technologists at the entry level; however, many consider PET technology to be a unique modality and hence see a need for a separate certification for the PET technologists. The NMTCB introduced a PET specialty examination starting in 2004 for nuclear medicine technologists and also now offers it to registered radiographers and radiation therapy technologists. The certification is valid for 7 years, after which the technologists must be recertified after taking the PET examination. Also, the education and training must be complemented by annual continuing education (CME) of certain hours to keep up with the changes in the technology.

CAMRT(RT), CAMRT(RTT), ARRT(R), or ARRT(T) certificants are eligible to sit for the PET examination if they meet all the three of the following requirements:

1. Active CAMRT(RTR), CAMRT(RTT), ARRT(R), or ARRT(T) certification
2. Seven hundred hours of documented clinical experience performing all aspects of PET imaging including radiopharmaceutical handling, injection, and imaging under supervision of a nuclear medicine physician or a radiologist and direct supervision of a certified NMTCB, ARRT(N), or CAMRT(RTNM) technologist
3. Satisfactory completion of a minimum of 15 contact hours of coursework each in radiopharmacy, nuclear medicine instrumentation, and radiation safety (for a total of 45 h)

CT Certification for Technologists

The PET/CT units involve the use of two modalities—PET using radionuclides and CT using X-ray radiations—thus complicating the issue of personnel as to who will operate them for a given patient study. Ideally, technologists credentialed in both CT and nuclear medicine technology should operate PET/CT units. However, regulations vary from state to state regarding the operation of PET/CT. Some states require dual certification of the technologists in nuclear medicine and radiography or require two technologists—one certified in nuclear medicine and the other in radiography. However, CT in PET/CT scanners is mainly used for fusion of CT and PET images and attenuation correction for PET images and is considered less complex than in diagnostic CT tests. Cross-training programs are offered by different groups in the USA, which include several descriptive modules of course materials on CT technology. Nuclear medicine technologists take these courses online or by correspondence and then pass a test. These cross-trained technologists then take limited CT clinical training at the employment site or elsewhere to be qualified to perform the CT part in PET/CT studies for the purpose of fusion of images and attenuation correction only. Often, PET/CT facilities use the CT for diagnostic purpose as an additional service involving administration of contrast agents as needed. Cross-trained nuclear medicine technologists cannot perform

these CTs, and registered radiographers with CT experience are required to perform them. With a shortage of trained technologists, staffing in PET/CT for CT operation often becomes difficult.

Based on these circumstances, the Society of Nuclear Medicine Technologists' Section (SNMTS) and the American Society of Radiologic Technologists (ASRT) jointly issued two consensus statements that were published in the *Journal of Nuclear Medicine Technology*, 2002;30:201. The first statement says in part, "*Any registered radiographer with the credential RT* (*R*), *registered radiation therapist with the credential RT* (*T*), *or registered nuclear medicine technologist with the credential RT* (*N*) *or CNMT may operate PET/CT equipment after obtaining appropriate additional education or training and demonstrating competency*. . ." A task force has been appointed by the ASRT and SNMTS to outline and recommend a formal course of study for PET/CT technologists. The second consensus statement says in part, "*States that license radiographers*, *nuclear medicine technologists*, *or radiation therapists are encouraged to amend their regulations to permit any of these individuals to perform PET/CT examinations after they have received appropriate additional education or training and demonstrate competency*. *States that do not currently license radiographers, nuclear medicine technologists, or radiation therapists are encouraged to adopt laws that regulate education and credentialing of these individuals*. . ."

In 2008, the ASRT published a consensus statement on the practice of CT based on a conference held in 2007 attended by all stakeholders (ASRT 2008). It calls for increased continuing education in CT and also for a basic CT certification examination. One of the many recommendations pertinent to the PET/CT technologists calls for a solely separate CT examination for fusion imaging. It encourages flexibility in state regulations for CT operation. Following these recommendations and consensus statements, the ARRT offers CT certification for PET/CT operation to nuclear medicine technologists certified by the ARRT or NMTCB. Beginning 2014, NMTCB has started offering CT certification to those who are already certified by CNMT, AART, and CAMRT and successfully passed the CT examination. To qualify for sitting for the CT examination, the candidate must have 500 hundred hours of clinical experience with CT (PET/CT, SPECT/CT, or CT) plus 35 contact hours of didactic or continuing education.

As it stands now, in states requiring dual certification, two technologists—one certified in CT and the other in PET—must be employed to perform the PET/CT procedure, unless the technologist is certified in both modalities. In other states, a registered nuclear medicine technologist should be able to perform both PET and CT as long as the technologist is competent in both modalities.

MR Certification for Technologists

A similar but more complicated situation exists for the technologists to perform in PET/MR hybrid modalities. While PET (NMTCB) and MR (ARRT) certifications at the entry level are available separately and each modality includes a limited

amount of information on the other, a combined program for entry level is not available yet. There is no established regulation as to how and who can perform PET/MR imaging. Currently a PET technologist and an MR technologist are needed to perform PET/MR imaging, each performing the individual modality, causing burden on the manpower. To address this situation, the Society of Nuclear Medicine and Molecular Imaging-Technology Section (SNMMI-TS) and the Society of Magnetic Resonance Technologists (SMRT) published a PET/MR Imaging Consensus Paper (Gilmore et al. 2013) with advisory recommendations to adopt. The major recommendation stipulates to create a master's level PET/MR program beyond the entry level of either modality, with more advanced competency requirements and syllabus contents that would include didactic, clinical, and technical education to qualify a candidate for registry/certification in PET/MR. A part of the consensus was to cross-train a technologist certified in one modality (e.g., NMT) for additional two terms with advanced education in the other specialty (e.g., MR). The report also advocates licensing of the technologists by the states, if required, in each modality, and establishing a number of CME credits in PET and MR.

The ACR currently recommends two MR imaging technologists to be present during MR scanning, which is quite burdensome in PET/MR imaging. The consensus statement recommends that until certified PET/MR technologists are available, one PET-certified technologist and one MR-certified technologist performing the PET/MR are acceptable. As suggested above, the ideal solution would be to introduce an advanced level of education and training in all aspects of both PET and MR technologies to certify PET/MR technologists, who would then be able to perform PET/MR imaging skillfully and without undue harm to the patient. SNMMI-TS and SMRT should come together to develop a definite pathway for the technologists to perform this unique hybrid imaging technology.

Accreditation of PET Facility

For the purpose of reimbursement for imaging services and to improve patient care, the Center for Medicare and Medicaid Services (CMS) mandated that all healthcare facilities including PET centers must be accredited by professional accrediting organizations. Following the CMS, private insurers like Blue Cross and Blue Shield, United Health, etc., also demand such accreditation of imaging facilities for reimbursement for patient care. In the USA, the Intersocietal Accreditation Commission (IAC) and the American College of Radiology (ACR) are two accrediting organizations, which set the standards and criteria for accreditation. To be accredited, PET centers, institutional or stand alone, must meet these standards and criteria and apply online to one of these organizations with required information, supporting data and applicable fees. If the application is complete and satisfactory, accreditation is granted to the PET center.

The goal of IAC and ACR is to improve patient care by continuous monitoring of the facilities' upkeep, optimal functioning of the equipment,

appropriate procedures, maintenance of records, and continuing education and training of physicians and personnel working in the facility. Although most criteria are similar for both organizations, there are some important differences in their requirements that are briefly outlined below.

IAC: PET centers providing patient care must be accredited by submitting an online application to the IAC providing required information available on the IAC Web site: www.intersocietal.org/nuclear. The IAC has a set of *standards*, which detail the minimum requirements for a PET center to provide high-quality patient care, and also set terms and conditions for accreditation, which must be agreed to, signed, and submitted along with the application.

The application must contain the following information:

1. An overview of physical setup of the facility
2. An organizational chart of physicians, technologists, and supporting staff and description of their roles and responsibilities
3. Number of procedures performed annually
4. NRC/Agreement States Radioactive Material License, with citations, if any, and corresponding responses
5. Board certifications and medical licenses of all physicians, technologists, nurses etc., along with their verifications by issuing agencies
6. 15 CME credits obtained every 3 years
7. Number of PET, PET/CT, and/or PET/MR scanners with manufacturer and model number
8. Policies and protocols for patient identification, patient complaint, pregnancy/breast feeding, radiopharmaceutical dosage administration, imaging protocols, quality control images, biannual preventive maintenance, and plan and meeting on quality control improvement
9. Five PET studies performed within one year of submission of application (including images and interpretation) in the category (cardiac, brain, and/or cancer) for which accreditation is requested, which must be submitted via traceable carriers (not e-mail or fax)

Initially, the IAC checks online the pre-submission application for any errors and missing information, which the applicant, on notification, corrects and submits the final application. Once the application is complete and satisfactory, the IAC grants the PET center accreditation for 3 years, which is renewable upon making a new application with required information. During the accreditation period, the IAC can make site visit and audit the activities of the PET center to monitor if it is in compliance with the terms of the accreditation.

ACR: The requirements of the ACR are similar in many ways to those of the IAC with some specific differences and are available on their Web site: www.ACR.com. The following are some of the major ACR requirements for accreditation of PET facilities:

1. Physicians and technologists working at the center must be certified by their respective boards or board eligible as specified by the ACR or must have

ACR-approved hours of training and experience including didactic lessons. Also they must be licensed by the state in which they are practicing.
2. A specific requirement of the ACR is a medical physicist who is board certified in medical physics or meets specific requirements of having a graduate degree in medical physics or any physical sciences along with course work in biological science and having clinical experience in a PET facility. Note that the IAC does not require a medical physicist for accreditation.
3. NRC or agreement license must be submitted with citations, if any, and corresponding responses.
4. All personnel involved in patient care must have hours of CME specified by the ACR.
5. The ACR requires at least semiannually, preferably quarterly, quality control performance of all PET imaging equipment using an ACR-designated phantom, which is the Jaszczak Deluxe Flangeless ECT phantom with spheres removed (available from Data Spectrum, North Carolina). Quality control data from phantom studies must be reviewed by the medical physicist and included in the annual physics survey report for the ACR review.
6. Linearity and accuracy of dose calibrators must be tested quarterly and documented.
7. For accreditation purpose, the ACR has categorized the PET images into three modules: oncology, brain and cardiac. A PET center can apply for accreditation for any or all modules, as necessary. For each module, two studies—one normal and one abnormal—must be submitted in a format given in the ACR Practice Guidelines and Technical Standards, along with the physician's interpretation report, and the images must be properly labeled for orientation and identification.

The above is a summary of essential requirements of the ACR accreditation for a PET center, and additional information is available at www.acr.org. The ACR application process entails two steps. The first step includes the submission of an application with all information mentioned above except the phantom data and case studies. Once the initial application is found complete and satisfactory, the PET center is asked to submit the phantom data and case studies. On review, if the latter are found acceptable and satisfactory, the ACR grants accreditation to the PET center for three years, which is renewable on submitting a new application. The ACR reserves the right to visit and audit the facility any time during or after the accreditation process, to verify the information submitted in the application, and to monitor the compliance with accreditation standards.

Facilities having PET/CT and PET/MR scanners have to fulfill additional requirements for CT and MR scanners, which are essentially similar in contents. The Web sites of these two organizations provide details of these requirements for all imaging equipment.

Questions

1. If a radiopharmaceutical is not approved by the FDA for clinical use, but the clinician wants to use it for investigation, what is needed from the FDA for such a situation?
2. What different aspects of PET radiopharmaceuticals are controlled by the FDA?
3. Does a vendor need a license from the state for interstate distribution of ^{18}F-FDG?
4. What are the requirements for nuclear medicine technologists to do the CT in PET/CT studies for fusion and attenuation correction?
5. Why is accreditation of a PET facility needed?
6. What are the differences between the RDRC and the Exploratory IND?
7. When is an Expanded Access IND needed?
8. What are the limitations and advantages of the RDRC?

References and Suggested Reading

American Society of Radiologic Technologists. Computed tomography in the 21st century—changing practice for medical imaging and radiation therapy professionals. Albuquerque: American Society of Radiologic Technologists; 2008.

Consensus Conference. Fusion imaging: a new type of technologist for a new type of technology. J Nucl Med Technol. 2002;30:201.

Gilmore CD, Comeau CR, Alessi AM, et al. PET/MR imaging consensus paper: a joint paper by the society of nuclear medicine and molecular imaging technologist section and the section for magnetic resonance technologists. J Nucl Med Tech. 2013;41:1.

Schwarz SW, Dick D, VanBrocklin HF, et al. Regulatory requirements for PET drug production. J Nucl Med. 2014;55:1132.

SNM Practice Standard Committee. Conjoint statement of the SNM and the American College of Nuclear Physicians and delineation of privileges for CT performed in conjunction with body PET or SPECT, Reston; 2006.

US Food and Drug Administration. Drug quality and security act; 2013.

US Federal Registrar. 65: 13010; 2000.

US Federal Registrar. 21CFR212—current good manufacturing practice for positron emission tomography; 2011.

U.S. Pharmacopeia 35& National Formulary 30. United States Pharmaceutical Convention, Rockville. Chapter <823> Positron emission tomography drugs for compounding, investigational, and research uses; 2012.

US Food Drug Administration. Food and drug administration modernization act of 1997. Rockville: US Food Drug Administration; 1997.

US Food Drug Administration. PET drug products—current good manufacturing practice (CGMP). Rockville: US Food Drug Administration; 2005.

US Food Drug Administration. Guidance for industry, investigators, and reviewers. Exploratory IND studies. Rockville: US Food Drug Administration; 2006.

US Food Drug Administration. PET DRUGS—current good manufacturing practice (CGMP). Rockville: US Food Drug Administration; 2009.

Chapter 10
NRC Regulations for Radiation Protection in PET

NRC Regulations for PET Radiopharmaceuticals

Until 2005, the Nuclear Regulatory Commission (NRC) regulated only by-product materials that were produced in reactors, whereas all natural and accelerator-produced radionuclides were regulated by the state agencies such as the Health Department, Environmental Protection Department, etc. The US Congress passed a law in 2005 to include all naturally occurring and accelerator-produced radionuclides as by-product material and authorized the NRC to regulate them. Now all radionuclides, irrespective of the source of production, are regulated by the NRC. At the time of this writing, 37 of the 50 states in the USA have entered into agreement with the NRC to have the authority to regulate all by-product materials. These states are called Agreement States and implement the NRC regulations for the use of by-product material including PET radiopharmaceuticals. Regulations vary among 50 states, but the basic principles of regulations are the same in all states. However, state regulations can be stricter but not less strict than NRC regulations. In Nonagreement States, the NRC is responsible for regulations of PET radiopharmaceuticals. Given below are the highlights of some important and pertinent regulations concerning the clinical and research use of PET radiopharmaceuticals.

Because radiation causes damage in living systems, international and national organizations have been established to set guidelines for safe handling of radiations. The International Committee on Radiological Protection (ICRP) and the National Council on Radiation Protection and Measurement (NCRP) are two such organizations. They are composed of experts in the subject of radiation and set guidelines for working with radiation and limits of radiation exposure and dose to the radiation workers as well as the general public. The NRC or the state agencies adopt these recommendations and implement them into radiation protection programs in the USA. NRC regulations for PET radiopharmaceuticals are given in 10CFR20 for

G.B. Saha, *Basics of PET Imaging*, DOI 10.1007/978-3-319-16423-6_10

radiation protection and 10CFR35 for medical use. The following is a brief outline of these regulations.

Definitions

Roentgen (R) is a measure of external exposure to radiations and is defined by the amount of γ- or X-ray radiation that produces 2.58×10^{-4} Coulomb(C) of charge per kilogram of air. This unit applies only to air and γ- and X-ray radiations of energy less than 3 MeV.

Rad is a universal unit and is defined as

$$1\,\text{rad} = 100\,\text{ergs/gm absorber} = 10^{-2}\,\text{J/kg absorber}.$$

In System Internationale (SI) units, it is termed *gray* (Gy) and given by

$$1\,\text{gray (Gy)} = 100\,\text{rad} = 1\,\text{J/kg absorber}.$$

Rem is the unit of dose equivalent and accounts for the differences in effectiveness of different radiations in causing biological damage. It is denoted by H_r and has the unit of rem. Thus,

$$H_r\,(\text{rem}) = \text{rad} \times W_r,$$

where W_r is the radiation weighting factor for radiation type r. W_r is related to linear energy transfer of the radiation and reflects the effectiveness of the radiation to cause biological damage.

In SI units, the dose equivalent H_r is given by *sievert* (Sv).

$$1\,\text{sievert (Sv)} = 100\,\text{rem}.$$

The values of radiation weighting factors W_r for different radiations are given in Table 10.1. These were called quality factors.

Table 10.1 Radiation weighting factors (W_r) (quality factors) of different radiations

Type of radiation	W_r
X-rays, γ-rays, β^- particles	1.0
Neutrons and protons	10.0
α-particles	20.0
Heavy ions	20.0

Table 10.2 Tissue weighting factors, W_T, of different tissues

Tissue	W_T[a]
Gonads	0.25
Breast	0.15
Red bone marrow	0.12
Lungs	0.12
Thyroid	0.03
Bone surfaces	0.03
Remainder	0.30
Total body	1.00

[a]From 10CFR20

Committed dose equivalent ($H_{T,50}$) is the dose equivalent to organs or tissues of reference (T) that will be received from an intake of radioactive material by an individual during the 50-year period following the intake.

Committed effective dose equivalent ($H_{E,50}$) is the sum of the products of the tissue weighting factors (W_T) applicable to each of the body organs or tissues that are irradiated and the committed dose equivalent to the corresponding organ or tissue ($H_{E,50} = \Sigma W_T \times H_{T,50}$). W_T accounts for the tissue sensitivity to radiation, and their values are given in Table 10.2. Note that this is due to committed dose equivalent from only internal uptake of radiation. This quantity is referred to as the effective dose.

Effective dose equivalent (H_E) is the sum of the products of the dose equivalent to the organ or tissue (H_T) and the weighting factors (W_T) applicable to each of the body organs or tissues that are irradiated ($H_E = \Sigma W_T H_T$).

Deep-dose equivalent (H_d), which applies to the external whole-body exposure, is the dose equivalent at a tissue depth of 1 cm (1000 mg/cm^2).

Shallow-dose equivalent (H_S), which applies to the external exposure of the skin or an extremity, is the dose equivalent at a tissue depth of 0.007 cm (7 mg/cm^2) averaged over an area of 1 cm^2.

Total effective dose equivalent (TEDE) is the sum of the effective dose equivalent (for external exposure) and the committed effective dose equivalent (for internal exposure). This is also called the total effective dose.

Radiation area is an area in which an individual could receive from a radiation source a dose equivalent in excess of 5 mrem (0.05 mSv) in 1 h at 30 cm from the source.

High radiation area is an area in which an individual could receive from a radiation source a dose equivalent in excess of 100 mrem (1 mSv) in 1 h at 30 cm from the source.

Very high radiation area is an area in which an individual could receive from radiation sources an absorbed dose in excess of 500 rad (5 Gy) in 1 h at 1 m from the source.

Restricted area is an area of limited access that the licensee establishes for the purpose of protecting individuals against undue risks from exposure to radiation and radioactive materials.

Unrestricted area is an area in which an individual could receive from an external source a maximum dose of 2 mrem (20 μSv)/h, and access to the area is neither limited nor controlled by the licensee.

Controlled area is an area outside of the restricted area but inside the site boundary, access to which is limited by the licensee for any reason.

Caution Signs and Labels

Specific signs, symbols, and labels are used to warn people of possible danger from the presence of radiations in an area. These signs use magenta, purple, and black colors on a yellow background. Some typical signs are shown in Fig. 10.1.

Fig. 10.1 Radiation caution signs and labels. (Fig. 16.1 on page 304, *Radiation Regulations and Protection*, in: Gopal B Saha (2013), Physics and Radiobiology of Nuclear Medicine, Springer; With kind permission from Springer Science and Business Media)

Caution: Radiation Area: This sign must be posted in radiation areas.

Caution: High Radiation Area or Danger: High Radiation Area: This sign must be posted in high radiation areas.

Caution: Radioactive Material or Danger: Radioactive Material: This sign is posted in areas or rooms in which ten times the quantity or more of any licensed material specified in Appendix C of 10CFR20 are used or stored. All containers with quantities of licensed materials exceeding those specified in Appendix C of 10CFR20 should be labeled with this sign. These labels must be removed or defaced prior to disposal of the container in the unrestricted areas.

Radiation Safety Officer

Large institutions employ radiation safety officers (RSOs) to implement and monitor various regulations for the use of radioactive materials. Smaller facilities such as clinics and stand-alone units often appoint authorized users as RSOs and hire an outside firm, which advises and monitors the radiation safety program at the facility. In these facilities, a Radiation Safety Committee (RSC) is not needed. The duties of an RSO include investigations of accidents, spills, losses, thefts, misadministrations, unauthorized receipts, uses, and transfers of radioactive materials and instituting corrective actions. In larger institutions, in addition to the RSO, an RSC is required, which is composed of individuals experienced in radiation safety and oversees the overall radiation protection program at the institution. The RSO works with the recommendations of the RSC in setting the policies and procedures for the purchase, receipt, storage, transfer, and disposal of the radioactive materials. The RSO conducts periodic checks of calibration of survey instruments, dose calibrators, and surveys of radiation areas and keeps records of all activities related to the use of radiation at the facility.

Occupational Dose Limits

The annual occupational dose limit to an adult radiation worker is the more limiting of (1) total effective dose of 5 rem (0.05 Sv) or (2) the sum of deep-dose equivalent and the committed dose equivalent to any individual organ or tissue, other than the lens of the eye, being equal to 50 rem (0.5 Sv).

The limit on the annual occupational dose to the lens of the eye is 15 rem (0.15 Sv).

The limit on the annual occupational dose to the skin and other extremities is the shallow-dose equivalent of 50 rem (0.5 Sv).

The annual occupational effective dose limit for the minor (<18 years working with radiation) is 0.5 rem (5 mSv). The occupational dose limit to the embryo/fetus

during the entire gestation period of a declared pregnant radiation worker is 0.5 rem (5 mSv) with a monthly limit of 0.05 rem (0.5 mSv).

The effective dose to an individual member of the public is limited to 0.1 rem (1 mSv) per year.

Personnel Monitoring

Personnel monitoring is required when an occupational worker is likely to receive an excess of 10% of the annual dose limit from radiation sources and for individuals entering high or very high radiation areas. Monitoring is accomplished by using film badges or thermoluminescent dosimeters (TLD).

The film badge is the most common method of personnel monitoring because of its cost effectiveness. It gives reasonably accurate readings of exposure from β^-, γ-, and X-ray radiations. The film badge consists of radiation-sensitive film held in a holder. Filters of different materials (aluminum, copper, and cadmium) are attached to the holder in front of the film to differentiate the exposures from radiations of different energies and types. The density of the film changes with exposure to radiation and is measured after development by a densitometer. The measured density is proportional to the exposure from the radiation. The film badges are changed monthly and therefore give integrated radiation dose to the worker for every month.

The TLD consists of inorganic crystals of lithium fluoride (LiF) or manganese-activated calcium fluoride (CaF_2:Mn) held in holders and is commonly used for finger exposures. TLDs exposed to radiations emit light when heated at 300–400 °C and the amount of light emitted is proportional to radiation energy absorbed, thus giving the exposure value. The TLD readings are reasonably accurate.

Receiving and Monitoring of Radioactive Packages

All packages carrying radioactive material are required to be monitored for possible radioactive contamination. The regulations described in 10CFR20 of the NRC are the plausible guide for monitoring the received radioactive packages, and states normally follow this guide. Monitoring should be done within 3 h of delivery if the package is delivered in normal working hours or no later than 3 h from the beginning of the next working day if it is received after working hours.

Two types of monitoring are performed: survey for external exposure and wipe test for removable contamination on the surface of the package due to possible leakage of the radioactive material. The external survey is conducted by using a Geiger–Müller (GM) survey meter at the surface and at 1 m from the package. The wipe test for removable contamination is carried out by swabbing three 100-cm^2

areas on the package surface using absorbent paper and counting the swabs in a NaI (Tl) well counter. The NRC limits of these measurements are:

Measurements	Limits
Survey at the surface	$\leq$200 mR/h
Survey at 1 m	$\leq$10 mR/h
Wipe test	$\leq$6600 dpm/300 cm^2

If any of the readings exceeds the limit, the carrier and the RSO should be notified for further corrective action. All the data of monitoring are recorded in a computer.

ALARA Program

Although regulations allow an annual maximum permissible dose to radiation workers, one should make considerable efforts to adopt strict protective measures in working with radiations so as to reduce the radiation dose *as low as reasonably achievable* (ALARA). Under this concept, techniques, equipment, and procedures are critically evaluated and adopted to minimize the radiation dose to the worker. The NRC has set two goals for a radiation worker to achieve: 10% of the occupational dose per quarter (Action level I) and 30% of the occupational dose per quarter (Action level II). If these limits are exceeded, corrective action must be taken or higher limits must be justified for a particular situation. The principles of radiation protection described later should be followed strictly to achieve ALARA compliance.

Radioactive Waste Disposal

Radioactive waste generated in PET facilities contains mostly short-lived radionuclides and is disposed of by the most common method of decay in storage. The solid waste is packaged in a yellow bag properly labeled with the date, radionuclide, and level of activity (in mR) and stored for decay. When the activity level in the bag is equal to or less than the background, the yellow bag is repackaged into a black plastic bag, which is then discarded in the regular trash. Obviously, waste from ^{11}C, ^{13}N, and ^{15}O does not need to be stored for long-term decay in storage because of the short half-lives and needs only to be discarded at the beginning of the next day at the latest. ^{18}F-FDG waste may need to be stored for decay depending on the level of activity and the time of the day when it is stored. For ^{82}Rb, whose half-life is only 75 s, its disposal is not a concern. However, ^{82}Sr ($t_{1/2} = 25.6$ days) and ^{85}Sr ($t_{1/2} = 65$ days) breakthrough in the ^{82}Rb eluate obtained for daily calibration of the ^{82}Sr–^{82}Rb generator for radiochemical yield must be monitored carefully and discarded according to the method recommended by the RSO at the PET facility.

Surveys for Radiation Exposure and Contamination

Working areas, benches, equipment, etc., may be contaminated unknowingly and should be surveyed frequently to avoid unnecessary radiation exposure. Surveys for ambient radiation exposure must be performed in all work areas at the end of the day using a Geiger–Müller (GM) counter. For each area, a trigger level is established from the average of several survey readings taken over a period of time. Daily survey reading should not exceed the trigger level, but if it exceeds, the source of excess radiation is identified and corrective action should be taken.

Wipe tests should be carried out to identify any removable contamination. These tests are done by swabbing the area of 10×10 cm with absorbent paper and counting the swab in a NaI(Tl) well counter. For PET radiopharmaceuticals, the NRC limit is less than 20,000 dpm/100 cm^2 in the radiation areas at the PET facilities and 2000 dpm/100 cm^2 in the unrestricted areas. If the readings exceed the limits, the area or the spot must be decontaminated. These tests should be done once a week.

Syringe and Vial Shields

Since PET radionuclides produce high-energy 511-keV annihilation radiations, vials and syringes containing them should be handled using appropriate lead shields. A variety of syringe shields and vial shields for PET radiopharmaceuticals are available from commercial vendors. A typical PET syringe shield and a syringe holder are shown in Figs. 10.2 and 10.3. Both the syringe or syringe shield and the vial shield should be labeled conspicuously, indicating the name of the radiopharmaceutical, the quantity of the activity, and the date and time of calibration.

Fig. 10.2 Lead syringe shield (Photo courtesy of Biodex Medical Systems, Inc., NY)

Fig. 10.3 A PET syringe holder (Photo courtesy of Biodex Medical Systems, Inc., NY)

Use of Dose Calibrator

An accurate dose calibrator is needed to assay the dosage of a PET radiopharmaceutical for administration to humans. The dose calibrator must be calibrated for constancy, accuracy, linearity, and geometry. The readers are referred to Saha (2010) for the details of calibration of the dose calibrator. The activity of a dosage contained in a syringe is measured by placing the syringe in a plastic insert which is placed inside the dose calibrator. The activity is displayed in Ci, mCi, or μCi units or GBq, MBq, or kBq units. Unit dosages (e.g., ^{18}F-FDG) supplied by the commercial suppliers are not required to be assayed again at the receiving facility. However, it is a good practice to assay it anyway.

Radioactive Spill

It is likely in a PET facility that a radioactive spill may occur and appropriate action must be taken. A radioactive spill may be major or minor depending on the nature and extent of contamination involved in the spill. In the case of a major spill where the spread of contamination is large or personnel are contaminated, the incident must be reported immediately to the RSO. In all spills, the principle is to contain the radioactivity, and access to the area should be restricted. Cleaning the contaminated

area by wiping with absorbent paper and using decontaminating liquid (Radiacwash) is all that is needed in most cases. Surveys and wipe tests must be conducted to assess the level of decontamination. In case of nonremovable contamination, a thin foil-type lead shield may be used to cover the area until the activity decays below the trigger level.

Record Keeping

Records must be maintained for the receipt, storage, dispensing, and disposal of all radioactive materials in a PET facility. All patient dosages administered to patients must be recorded with the patient's name, ID number (e.g., clinic number), date and time, and dosage of activity administered. Also, all the survey data must be recorded.

Nowadays commercial software is available for record keeping of all data including those of radiation safety and patient studies. The programs can also be customized to meet specific needs of a customer. These programs obviate the need for paper record keeping.

Principles of Radiation Protection

The cardinal principles of radiation protection from external radiation sources are governed by four factors: time, distance, shielding, and activity.

Time

The radiation dose to an individual from an external source is proportional to the time the person is exposed to the source. The longer the exposure, the higher the radiation dose. It is advisable to spend no more time than necessary near radiation sources.

Distance

The radiation exposure varies inversely with the square of the distance from the source. Each radionuclide has an exposure rate constant, Γ, which is given in units of R-cm^2/mCi-h at 1 cm or in SI units, μGy-m^2/GBq-h at 1 m, and these values for ^{11}C, ^{13}N, ^{15}O, ^{18}F, and ^{82}Rb are given in Table 10.3. The exposure X per hour at distance d(cm) from an n mCi source is given by

Table 10.3 Exposure rate constants of common positron-emitting radionuclides

Radionuclide	Γ (R-cm^2/mCi-h at 1 cm)	Γ (μGy-m^2/GBq-h at 1 m)
^{11}C	7.18	193.7
^{13}N	7.18	193.7
^{15}O	7.18	193.7
^{18}F	6.96	187.9
^{82}Rb	6.10	164.9

$$X = \frac{n\Gamma}{d^2}, \tag{10.1}$$

where Γ is the exposure rate constant of the radionuclide. Working at maximum possible distance from radiation is prudent in reducing radiation exposure.

Problem 10.1 Calculate the cumulative exposure a radiation worker receives from a 15 mCi (555 MBq) ^{18}F-FDG source while standing for 2 h at a distance of 2 m (Γ for ^{18}F-FDG is 6.96 R-cm^2/mCi-h at 1 cm).

Answer:
Since $t_{1/2}$ of ^{18}F is 1.83 h and the worker stands for 2 h, the activity of ^{18}F-FDG decays considerably and hence the cumulative activity for 2 h is calculated as follows: λ for ^{18}F is $0.693/1.83 = 0.3787\ \text{h}^{-1}$

$$\text{The cumulative activity } A_t = A_0 \frac{1 - e^{-\lambda t}}{\lambda} = \frac{15 \times (1 - e^{-0.3787 \times 2})}{0.3787}$$
$$= 21.04\,\text{mCi-h}.$$

Using Eq. (10.1), the cumulative exposure X at 2 m

$$X = \frac{21.04 \times 6.96}{(200)^2} = 0.00366\,\text{R} = 3.66\,\text{mR}.$$

Shielding

Radiations passing through absorbers lose energy by interaction with absorber material. This loss of energy is very effective in high Z materials such as lead, tungsten, etc. Therefore, these high Z materials are conveniently used as shielding

Fig. 10.4 Lead barrier shield (L-block), behind which all formulation and handling of radioactive materials are carried out (Photo courtesy of Biodex Medical Systems Inc., NY)

materials for radiations, and lead is the shielding material of choice in most cases because it is the least expensive. Bricks, syringe shields, L-blocks (Fig. 10.4), and syringe containers made of lead are common examples of shielding. Handling radioactivity behind the lead shield, using syringe shields, carrying dosages in lead containers, etc., are typical examples of minimizing radiation exposure by shielding. The concept of half-value layer (HVL) of absorbing materials for different radiations has been discussed in Chap. 1 and should be kept in mind in handling radioactivity. In PET facilities, 511-keV photons from positron emitters are highly penetrating and, therefore, larger amounts of shielding material are needed in all aspects of radiation protection.

Problem 10.2 If the HVL of lead for 511-keV photons of ^{18}F is 0.55 cm, calculate the thickness of the lead shield required to reduce the exposure by 90% from a 20 mCi (370 MBq) ^{18}F-FDG dosage in a vial.

Answer:
According to Eq. (1.19), linear attenuation coefficient,

$$\begin{aligned}\mu &= \frac{0.693}{\text{HVL}} \\ &= \frac{0.693}{0.55} \\ &= 1.26\,\text{cm}^{-1}.\end{aligned}$$

Because the initial beam is reduced by 90%, the transmitted beam is 10%.

$$0.1 = 1 \times e^{-1.26 \times x}$$
$$\ln(0.1) = -1.26 \times x$$
$$2.303 = 1.26 \times x$$
$$x = 1.82\,\text{cm}.$$

Thus, 1.82 cm of lead will be needed to reduce the exposure from a 20 mCi (370 MBq) dosage by 90%.

Note that the 20-mCi (370-MBq) dosage does not come into calculation because 90% reduction remains the same regardless of the quantity of dosage. However, the absolute exposure value in roentgen will depend on the dosage. The exposure X beyond the 1.82-cm lead shield is calculated using Eq. (10.1):

$$X = \frac{0.1 \times 20 \times 6.96}{(1.82)^2} = 4.2\,\text{R/h}.$$

Activity

Understandably, the lesser amount of radioactivity will result in less radiation exposure and dose. One should use only a necessary amount of radioactivity.

Do's and Don'ts in Radiation Protection Practice

Do wear laboratory coats and gloves when working with radioactive materials.
Do work in a ventilated fume hood while working with volatile material.
Do handle radioactivity behind a lead barrier shield, such as L-block.
Do cover the trays and workbench with absorbent paper.
Do store and transport radioactive material in lead containers.
Do wear a film badge while working in the radiation laboratory.
Do identify all radionuclides and dates of assay on the containers.
Do survey work areas for contamination as frequently as possible.
Do clean up spills promptly and survey the area after cleaning.
Do not eat, drink, or smoke in the radiation laboratory.
Do not pipette any radioactive material by mouth.
Do monitor hands and feet after the day's work.
Do notify the RSO in the case of a major spill or other emergencies related to radiation.

Department of Transportation

The Department of Transportation (DOT) regulates the transportation of radioactive materials and sets the regulations and guidelines for packaging, types of packaging material, limits of radioactivity in a package, and exposure limits for packages. All these regulations are contained in Title 49 of the Code of Federal Regulations (49CFR).

The packages for radioactive shipping must pass certain tests, such as the drop test, corner drop test, compression test, and 30-min water spray test. A special shipping container made of lead that can ship 3 unit dosages of PET radiopharmaceuticals (e.g., ^{18}F-FDG) is shown in Fig. 10.5.

Radioactive packages must be properly labeled before transportation. There are three types of labels (Fig. 10.6) based on the *transportation index*, TI, which is defined as the exposure reading in mR/h at 1 m from the surface of the package. The maximum permissible TI is 10. The criteria for the three shipping labels are

Fig. 10.5 Special shipping containers made of lead that can ship 3 unit dosages of PET radiopharmaceuticals (Photo courtesy of Biodex Medical Systems, Inc., NY)

Fig. 10.6 Three types of US DOT labels required for transportation of radioactive materials. (Fig. 16.3 on p 329, *Radiation Regulations and Protection*, in: Gopal B Saha (2013), Physics and Radiobiology of Nuclear Medicine, Springer; With kind permission from Springer Science and Business Media)

Table 10.4 Labeling categories for packages containing radioactive materials

	Exposure (mR/h)	
Type of label	At surface	At 1 m
White-I	<0.5	–
Yellow-II	$>0.5 \leq 50$	<1
Yellow-III	>50	>1

Note: No package shall exceed 200 mR/h at the surface of the package or 10 mR/h at 1 m. Transport index is the reading in mR/h at 1 m from the package surface and must not exceed 10

given in Table 10.4. The label "RADIOACTIVE" containing the value of TI must be placed on the outside of the package. For liquids, the label "THIS SIDE UP" must be pasted on the package. The label also must identify the contents and amounts of the radionuclides in becquerels. A shipping document containing all the above information must be placed inside the package.

According to 49CFR173.421, certain transportation requirements are exempted for radionuclides, if only a limited quantity is shipped. These limits for ^{11}C, ^{13}N, and ^{18}F are 1.4 mCi (or 50 MBq) and those for ^{82}Sr and ^{85}Sr (for ^{82}Sr–^{82}Rb generator) are 0.54 mCi (or 20 MBq) and 5.4 mCi (or 200 MBq), respectively. The surface exposure readings should not exceed 0.5 mR/h at all points of the package surface and the wipe test measurements should be below 6600 dpm/300 cm^2. A notice or label, "Radioactive—Limited Quantity," must be enclosed inside or pasted outside or forwarded to the shipper along with the package. This notice must include the name of the shipper and the consignee and the statement, "This package conforms to the conditions and limitations specified in 49CFR173.421 for radioactive material, excepted package-limited quantity of material, UN2910," in or on the package.

Employees who ship hazardous material, including radioactive material, must have hazmat training to be able to recognize and identify hazardous material, to conduct their specific functions, and to enforce safety procedures to protect the public. The training is given to a new employee within 90 days of employment and then repeated every 3 years. The training is provided by the employer or by other public or private sources, and a record of training must be maintained.

Distribution of ^{18}F-FDG

The need for ^{18}F-FDG is increasing over time as the demand for PET procedures for various clinical indications, particularly oncologic indications, increases worldwide. Although the number of cyclotron facilities is increasing in the USA, many hospitals have PET scanners but no cyclotron facility. These hospitals need ^{18}F-FDG to be supplied on a routine basis by a cyclotron facility.

The distribution of ^{18}F-FDG is quite challenging, because of the short half-life (110 min) and the distance to cover for delivery. For controlled, reliable, and economical delivery, ground shipping or air transport may be employed depending on the distance between the cyclotron facility and the PET imaging site. A maximum distance of about 200 miles may be appropriate for ground transportation, but air transport must be employed for longer distances. Air transport is risky, because of flight delay or inclement weather, and is 3–4 times costlier than ground transport. A dedicated charter aircraft is needed for reliable and timely delivery of ^{18}F-FDG. On the other hand, ground transportation is slower than air transport, but is more reliable. It is not as affected by inclement weather. Air transport requires delivery of ^{18}F-FDG by ground transportation from the cyclotron facility to the airport and from the airport to the client. This might negate the advantage of faster delivery by air transport.

Scheduling of delivery by ground or air transportation is the key to a successful and economically viable distribution of ^{18}F-FDG. All orders of FDG dosages are received a day before, and deliveries to different client sites by a courier are scheduled with minimal routing. Deliveries to widely separated sites that cannot be served by one courier are made by separate couriers. Production schedule of ^{18}F-FDG batches must be synchronized with the different deliveries by separate couriers.

The shipping of ^{18}F-FDG must meet all regulations of DOT mentioned above, including approved shipping containers (DOT 7A containers, Fig. 10.5) and DOT training for all FDG shippers. The interstate commercial distribution of ^{18}F-FDG requires that the vendor must obtain a license from the state to operate as a distributor.

Because of increased demand for PET procedures using ^{18}F-FDG, several commercial vendors have set up cyclotron facilities at many locations around the country and distribute ^{18}F-FDG to distant customers. PETNET Solution, a division of Siemens Medical Solutions, Inc., has more than four dozen distribution centers

around the world and provides more than 50% of FDG dosages in the USA. Cardinal Health and IBA have the major share of the remaining FDG sales. Many smaller suppliers as well as many academic sites have come into the market.

Questions

1. The NRC controls the radiation aspect of PET radiopharmaceuticals. True _____; False _____.
2. The registration with the state is required for the following equipment:
   (a) Cyclotron: yes, no, depends on state
   (b) PET/CT: yes, no, depends on state
   (c) PET scanner: yes, no, depends on state
3. Review thoroughly the regulations pertaining to the practice of nuclear medicine technologists in performing PET/CT imaging.
4. Define roentgen, rad, rem, and effective dose.
5. Define restricted area, radiation area, high radiation area, and very high radiation area.
6. In a room in a nuclear medicine department, one could receive 0.15 rem (1.5 mSv) in an hour at 30 cm from the radioactive sources. What type of sign is needed on the door of the room?
7. What are the responsibilities of a radiation safety officer?
8. The occupational dose limits for radiation workers are: effective dose _____; dose to the lens of the eye _____; and dose to extremities _____.
9. The annual radiation dose limit to: (a) the declared pregnant woman during the gestation period is _____; (b) to the minor _____; and (c) to the individual member of the public _____.
10. What is the common method of personnel monitoring?
11. What are the regulatory requirements for receiving and monitoring the radioactive packages?
12. Describe the principles of ALARA program.
13. What is the most common method of radioactive waste disposal of ^{18}F-FDG in a PET facility?
14. What are the limits for the GM survey and wipe test in the laboratory where PET radiopharmaceuticals are prepared and dispensed?
15. When is the personnel monitoring required of a person in a radiation laboratory?
16. Discuss the cardinal principles in radiation protection.
17. Calculate the cumulative exposure a technologist receives from a 10 mCi (370 MBq) 6-^{18}F-L-fluorodopa while standing for 2 h at a distance of 1 m from the source (Γ for ^{18}F is 6.96 R-cm^2/mCi-h at 1 cm).

18. Calculate the amount of lead necessary to reduce the exposure rate from a 200 mCi ^{18}F-FDG source to less than 15 mR/h at 30 cm from the source (Γ for $^{18}F = 6.96$ R-cm^2/mCi-h at 1 cm; HVL of lead for ^{18}F is 0.39 cm).
19. If 1% of the primary beam exits through a patient, calculate the exposure (%) at the midline of the patient.
20. Define transport index TI. What is the maximum TI allowed by DOT for transportation of radiopharmaceuticals?
21. Elucidate the criteria for shipping "limited quantity" of radioactive material.
22. A technologist who packages and ships radioactive material must have hazmat training. True _____; False _____.

References and Suggested Reading

International Commission on Radiological Protection. General principles for the radiation protection of workers. ICRP 75. New York: Elsevier; 1997.

National Council on Radiation Protection and Measurements. Radiation protection and allied health personnel (NCRP 105). Bethesda: NCRP Publications; 1989.

National Council on Radiation Protection and Measurement. Limitation of exposure to ionizing, radiation (NCRP 116). Bethesda: NCRP Publications; 1993.

Nuclear Regulatory Commission. Standards for protection against radiation. 10CFR part 20. Washington, DC: Nuclear Regulatory Commission; 1995.

Nuclear Regulatory Commission. Medical uses of byproduct material. 10CFR part 35. Washington, DC: Nuclear Regulatory Commission; 2007.

Saha GB. Fundamentals of nuclear pharmacy. 6th ed. New York: Springer; 2010.

Chapter 11
Reimbursement for PET Procedures

Background

Healthcare providers (physicians, hospitals, clinics, etc.) operate and are sustained by the reimbursement or payment for care they provide to patients. In the USA, revenue for healthcare services comes from a variety of sources including the patient, insurance companies (i.e., Blue Cross and Blue Shield, Cigna, Aetna), and the Centers for Medicare and Medicaid Services (CMS). The CMS provides healthcare insurance for Medicare and Medicaid beneficiaries, which most insurance companies follow. When interfacing with an insurance company or the CMS, there are three fundamental reimbursement concepts that must be considered to assure appropriate revenue for services provided. These include the concepts of coverage, coding, and payment.

Coverage

Coverage can be defined as the range or extent of healthcare that an insurer will pay for based on the terms of the insurance plan. The CMS under Medicare Act has developed two pathways to secure coverage policies or guidelines for reimbursement for clinical procedures or drugs: national coverage determination (NCD) and local coverage determination (LCD). An NCD is a determination by the CMS if a procedure or service is reasonable and necessary for reimbursement and is initiated either by the request of an outside party or by the CMS. Several factors are considered when developing an NCD for reimbursement for a service: (1) it meets a defined benefit category; (2) it is reasonable and necessary for the care of a patient; and (3) the radiopharmaceutical is approved by the FDA for safety and effectiveness. (Some exceptions are made for products that are in clinical trials.) In addition, the CMS may request an evaluation of the health outcome of a particular

G.B. Saha, *Basics of PET Imaging*, DOI 10.1007/978-3-319-16423-6_11

procedure prior to making a national coverage decision. The CMS employs contractors, the Office of Health Technology Assessment (OHTA) in the Department of Human and Health Services, or literature reviews for the assessment of health outcome of different procedures. It is important to note that an NCD does not specify the code nor the amount of payment. The LCDs are similar to NCDs but are established by the Medicare Administrative Contractors at local levels and applies to reasonable and necessary procedures or services and must specify diagnosis code (see later) for reimbursement. They can be superseded by NCDs. In the past the majority of LCDs were made by two categories of CMS contractors: for Medicare Part A, "fiscal intermediaries" processed claims from facilities/hospitals, and for Medicare Part B, the "carriers" processed claims from physicians or freestanding imaging facilities. Beginning in 2003, for the purpose of improved services to beneficiaries and healthcare providers, Medicare started replacing the fiscal intermediates and carriers with Medicare Administrative Contractors who now provide services for both Part A and Part B.

NCDs have been developed and are currently in place for most clinical PET procedures. Private payers generally follow similar policies and procedures when establishing their coverage guidelines.

Coding

CPT, HCPCS, and APC Codes

Simply defined, coding systems are used by providers and health plans to document the delivery of healthcare services for reimbursement purposes as well as to track services provided. Two major types of codes are important to consider for all clinical procedures: *Current Procedural Terminology* (CPT) codes introduced by the American Medical Association (AMA) and *Healthcare Common Procedure Coding System* (HCPCS) codes developed by a committee composed of private insurers and CMS representatives. The CMS requires the use of CPT codes for reimbursement for a clinical condition except in a few cases where HCPCS codes are required. The HCPCS codes are divided into two categories: Level I and Level II. Level I of HCPCS consists of AMA CPT-4 and is a uniform coding system to identify medical services and procedures furnished by physicians and other healthcare professionals. Level II of HCPCS is a standardized coding system that is used primarily to identify products, supplies, and services not included in the CPT-4 codes, such as ambulance services, durable medical equipment, prosthetics, orthotics, and supplies when used outside a physician's office. Codes are updated at least annually to adjust to the change in conditions and cost over time.

It is important to note that the applicable code for a service or a drug may vary based on the site of service (hospital inpatient, hospital outpatient, freestanding imaging facility) and payer type (Medicare versus non-Medicare). CPT codes

primarily describe the procedures for different clinical indications and can be used for indications that are not covered by Medicare. Ambulatory Payment Classifications or APCs are the CMS method of paying for outpatient services in the Medicare B program, which is discussed later in this section.

The current CPT codes (2015 CPT codes, AMA) used for all approved PET studies of different clinical indications are summarized in Table 11. 1. Initially, reimbursement by the CMS for these indications was limited to their diagnosis, staging, restaging, recurrence, and monitoring of therapy. Currently, this grouping of assessment has been replaced by two categories of assessment—*initial treatment strategy* (replacing former diagnosis and initial staging) and *subsequent treatment strategy* (replacing former treatment monitoring, restaging, and detection of suspected recurrence). All cancer PET studies listed in Table 11.1 are reimbursed for both initial and subsequent treatment strategies. Some examples of this group of cancer indications are the stomach, small intestine, pancreas, kidney, bladder, primary brain, and so on.

Diagnosis Codes

In addition to CPT or HCPCS codes, the CMS also requires specific codes for diagnosis of diseases for inpatient, outpatient, and physician office utilization for efficient claims processing and appropriate reimbursement. These codes, called the diagnosis (Dx) codes, are listed in the International Classification of Diseases, Tenth Revision, Clinical Modification (ICD-10-CM) for diagnosis for inpatient hospital procedure coding. ICDs have been developed by the World Health Organization (WHO) to promote international comparability in the collection, processing, classification, and presentation of mortality statistics. However, WHO has authorized the development of an adaptation of ICD-10 for use in the USA for government purposes. So the CMS uses these adapted codes for classification of diseases for reimbursement purposes. Along with CPT/HCPCS codes, Dx (ICD-10-CM) codes must be provided on the claim form for appropriate reimbursement. These codes are annually reviewed and updated. A few current examples of Dx (ICD-10-CM) codes for the diagnosis of diseases by PET studies are given in Table 11.2.

Payment

As with coding, payment for healthcare services also varies based on the site of service (hospital inpatient versus outpatient, physician office setting, or freestanding imaging facility) and payer type. Note that the CMS pays only for medically necessary procedures, requires precertification for many specific procedures, and does not pay for PET studies for screening purposes.

Table 11.1 CPT and HCPCS codes related to PET and PET/CT procedures

CPT[a]/HCPCS codes[b]	Description
CPT 78811	Tumor imaging, positron emission tomography (PET); limited area (e.g., chest, head/neck)
CPT 78812	Tumor imaging, positron emission tomography (PET); skull base to mid thigh
CPT 78813	Tumor imaging, positron emission tomography (PET); whole body
CPT 78814	Tumor imaging, positron emission tomography (PET) with concurrently acquired computed tomography (CT)[c] for attenuation correction and anatomical localization; limited area (e.g., chest, head/neck)
CPT 78815	Tumor imaging, positron emission tomography (PET) with concurrently acquired computed tomography (CT) for attenuation correction and anatomical localization; skull base to mid thigh
CPT 78816	Tumor imaging, positron emission tomography (PET) with concurrently acquired computed tomography (CT) for attenuation correction and anatomical localization; whole body
CPT 78459	Myocardial imaging, positron emission tomography (PET); metabolic evaluation
CPT 78491	Myocardial imaging, positron emission tomography (PET), perfusion; single study at rest or stress
CPT 78492	Myocardial imaging, positron emission tomography (PET), perfusion; multiple studies at rest and/or stress
CPT 78608	Brain imaging, positron emission tomography (PET); metabolic evaluation
CPT 78609	Brain imaging, positron emission tomography (PET); perfusion evaluation
HCPCS G0219	PET imaging whole body; melanoma for noncovered indications
HCPCS G0235	PET imaging, any site not otherwise specified (not covered by Medicare)
HCPCS A9526	Nitrogen N-13 ammonia, diagnostic, per study dose, up to 40 mCi (1.48 GBq)
HCPCS A9580	Sodium fluoride F-18, diagnostic, per study dose, up to 30 mCi (1.1 GBq)
HCPCS A9552	Fluorodeoxyglucose F-18 FDG, diagnostic, per study dose, up to 45 mCi (1.67 GBq)
HCPCS A9555	Rubidium Rb-82, diagnostic, per study dose, up to 60 mCi (2.22 GBq)
HCPCS A9586	Florbetapir F-18, diagnostic, per study dose, up to 10 mCi (370 MBq)
HCPCS A9559	Radiopharmaceutical, diagnostic, for beta-amyloid positron emission tomography

[a]Adopted from American Medical Association CPT 2015 Professional Edition under the provision of fair use of copyrighted material
[b]HCPCS codes are obtained from www.icd10data.com
[c]For diagnostic CT when performed in conjunction with PET/CT, it should be billed separately with Modifier 59

Table 11.2 Examples of current diagnosis codes (ICD-10-CM) for PET studies

Major clinical condition	ICD-10-CM code	Specific diagnosis or staging of disease
Cardiac perfusion	I25	Chronic ischemic heart disease
	I24	Myocardial infarction
	I20	Angina pectoris
	I50	Heart failure
Cardiac metabolism	I70.1	Acute, chronic ischemia atherosclerosis
Esophageal cancer	C15	Malignant neoplasm of esophagus
Breast cancer (female)	C50	Malignant breast cancer
Seizure	G40	Epilepsy
Lung	C34	Malignant neoplasm of the bronchus and lung
Colorectal cancer	C18	Colon cancer
	C20	Cancer of rectum, rectosigmoid junction and anus
Melanomas	C43	Malignant melanoma
Lymphomas	C90	Multiple myeloma
	C81	Hodgkin's
	C91	Lymphoid leukemia
Head and neck	C00–C14	Lip, oral cavity, and pharynx cancer
	C30	Nasal cavities, middle ear cancer
	C32	Larynx cancer
All above organs except the heart/brain	D49	Neoplasm of unspecified behavior

The diagnosis codes are listed in broad categories, i.e., each of these codes has subcategories for specific diagnosis. These values are obtained from http://www.icd10data.com/ICD10CM/Codes/C00-D49

Hospital Inpatient Services: Medicare Part A

Faced with the need to try to contain rising hospital inpatient costs, the CMS introduced a prospective payment system known as diagnosis-related groups (DRG) in the early 1980s. Under the DRG program, a lump-sum payment is made for all services for hospital inpatient stay based on the patient's course of hospitalization and discharge diagnosis. This payment is the same for all patients with a specific disease regardless of the length of the hospital stay.

Hospital Outpatient Services: Medicare Part B

For hospital outpatient cost issues, the CMS implemented the Hospital Outpatient Prospective Payment System (HOPPS) on August 1, 2000, based on APC Groups. APCs are groupings of procedures that are clinically comparable and similar in terms of resource utilization and cost. APCs are similar to the hospital inpatient

DRGs in that a fixed rate is paid for a grouping of procedures based on the reported hospital outpatient costs. APCs apply to hospital-based outpatient services only; professional fees are paid separately. Under HOPPS, all outpatient services are grouped into APCs based on the CPT or HCPCS codes. The CMS annually evaluates reported cost figures and revises and updates the APCs to establish a payment schedule for the year. Payment is also adjusted for regional variations. The rate published annually by the CMS is the national rate, which must be multiplied by a locality-specific factor to take into account the geographical variations in the cost of services provided.

Payment for PET Radiopharmaceuticals

For PET procedures performed in the hospital outpatient department, there is no separate payment for the radiopharmaceuticals. They are packaged into APC rates for one consolidated payment for the procedure and the radiopharmaceutical. The CMS has letter coded the radiopharmaceuticals to differentiate the status of payment of a radiopharmaceutical. For example, letter N is designated to ^{18}F-FDG to signify that it is paid at the packaged rate. Letter G is used for ^{18}F-florbetapir indicating that it is a pass-through radiopharmaceutical and is paid separately from APC rates for a certain period (3–5 years) to assess the usefulness of the product. All pass-through products are packaged into APC rates after the trial period. In the case of freestanding facilities and private medical practices, radiopharmaceuticals are reimbursed at 95% of the average wholesale price or are carrier-priced and may be paid separately or globally.

Physician's Payment by Medicare

Imaging studies such as PET, CT, and MRI have two components—technical and professional—and each component is paid separately by the CMS. The technical component is paid under DRG or APC depending on if the patient is inpatient or outpatient. Professional fees for the physicians providing services for the patients are paid separately. However, in the case of freestanding facilities such as imaging center or private medical practice, the technical and professional fees are lumped together and a global reimbursement is made for the entire service.

Since 1992, physicians are reimbursed for their services according to a standardized fee schedule established by the CMS based on a system called the resource-based relative value system (RBRVS). The cost of a service consists of three components: physician's work (time, skill, and intensity), practice expense (rent, employee wages, etc.), and professional liability or malpractice insurance (insurance premiums). According to RBRVS, each of these components is assigned a relative value unit (RVU) based on the nature of service and a geographic practice cost index (GPCI) to adjust for the variation in cost in different geographical regions. The total RVU for a service is calculated as the sum of the products of

each component RVU and component GPCI, and the payment is calculated by multiplying the total RVU by a conversion factor CF (a dollar value determined by the CMS). So the RVU for a service is:

$$\text{Total RVU} = (\text{work RVU} \times \text{work GPCI}) + (\text{expense RVU} \times \text{expense GPCI}) + (\text{malpractice RVU} \times \text{malpractice GPCI}).$$

Payment for the service then is calculated as

$$\text{Payment} = \text{total RVU} \times \text{CF}.$$

Every 5 years, the RBRVS fee schedule is reviewed by the CMS, whereas the physician's work RVU and CF are updated every year.

Freestanding Facilities: Medicare

In the freestanding facilities such as imaging centers and physician's private practices, the physician's professional service is considered a part of the entire procedure and is included in the global payment for the service.

Non-Medicare Payers: All Settings

Private insurance companies have a variety of payment arrangements with providers and primarily follow the guidelines of the CMS.

Billing

There are two ways of billing: component billing and global billing. In component billing, there are two components for a given PET procedure: professional and technical components, which are billed separately. The professional component is billed for the physician interpretation services and the technical component for facility services such as equipment, personnel time, and supplies. The global billing is made for both the technical and professional services together, usually applicable to freestanding facilities and private medical practices.

Claims for reimbursements must be submitted to the CMS using CPT codes for PET procedures along with Dx (ICD-10-CM) codes for all approved clinical indications. For billing purposes, several CPT codes have been assigned for all PET procedures with a few exceptions, which require HCPCS codes for billing.

CPT codes can be used for "denial" of reimbursement for noncovered procedures. Private payers may be billed using CPT codes, while some private payers may require the use of the CMS HCPCS codes.

Billing Process

This section describes how a billing for a given study is processed from the beginning to the end. Prior to any study performed on a patient, the demographic data of the patient including the insurance information are entered into the computer by the admitting personnel or receptionist. This becomes a part of the overall medical record of the patient and should be available in the RIS and HIS via PACS. A diagnostic or therapeutic service is performed on the patient and the corresponding CPT or HCPCS codes are entered into the computer. These codes for most studies are usually formatted into bar codes on a template. The technologist performing the examination enters its code into the computer by swiping its bar code on the template using a penlight or a bar code reader. The physician then interprets the study and the report is stored. For each study, the Dx (ICD-10-CM) code is either entered by the technologist or by the physician during dictation, depending on the way it is set up at each facility.

Next, the data for each patient are forwarded electronically to the billing department, which then assembles the data into the proper format of a claim form, normally using a computer billing software. In some complicated studies, manual billing may be done and their paper records are saved. The computer-generated bill is then sent to the insurance company or Medicare who, after proper verification of whether it meets its criteria, accepts or rejects the claim for payment. In most cases, the amount for each examination is paid by the rate set by the insurance company or Medicare, not what is billed. There are several scenarios for Medicare payment. For hospital inpatients, Medicare pays the entire amount at the DRG rate. For hospital outpatient services, Medicare sets up a payment rate for a service, which is divided into two payments—one by Medicare and the other by the patient. The ratio between Medicare and patient payments varies with different services but tends to be around 80:20, i.e., Medicare pays 80% of an eligible charge and the patient pays 20%. If the healthcare provider is in an "assignment" contract with Medicare, it cannot charge the patient more than 20% per contract agreement.

The payment by the private insurers varies depending on the contract between the insurer and the patient. These payments may be based on the usual and customary rates (UCR) set for a region or by company-set RVU-type values or according to the cost of the services provided. It is essential to work with the private insurers in the region to establish a reasonable payment rate for PET studies.

Rejection of a claim often arises from improper coding, incomplete billing information, and errors in demographic data of the patient entered initially. At times, insurance companies may not even notify denials, and so a follow-up by the billing personnel is required. Even if a payment is made, it may be an incorrect amount. The

resolution of nonpayment or incorrect payment may take months, if it is accomplished at all, which is quite aggravating. Electronic billing through portals such as WebMD has eliminated many of these errors and substantially improved billing and collection.

It is essential that properly trained and knowledgeable personnel staff the billing department to avoid rejection and incorrect payment by the CMS. The reimbursement rate for PET studies is at the high end, and many PET centers are paying special attention to the billing process and employ a skilled billing individual as a special point man to concentrate on PET reimbursement. The point man interacts with the payers to clarify the criteria of these studies and explain to them the appropriateness of each PET study.

Healthcare financing is changing and evolving with time, with a continuous decline in reimbursement, while the cost of healthcare itself is growing. It is absolutely critical to attempt to maximize collection of reimbursement for each study, and this can be achieved only through understanding of codes for each study, providing proper codes and other information in the claim form and appropriate follow-up in the case of rejection or incorrect payment.

Chronology of Reimbursement for PET Procedures

For many years, PET procedures were considered by the CMS as experimental and research based and so were not reimbursed, although some private insurers did pay for the PET studies for very specific cases. Based on the approval of ^{82}Rb-RbCl by the FDA in 1989 for myocardial perfusion studies, and after a thorough review of scientific literature on the outcome of the PET study, the CMS first approved reimbursement for PET myocardial perfusion scans using ^{82}Rb-RbCl for both rest and pharmacological stress studies for patients suspected of having coronary artery disease. Similarly, based on the FDA approval and after considerable review of the literature, the CMS approved reimbursement starting in 1998 for two oncologic indications: staging of non-small-cell lung carcinoma (NSCLC) for metastasis and characterization of solitary pulmonary nodules (SPN) for evidence of primary tumor supported by the computed tomography (CT). In 1999, with further evidence of efficacy of ^{18}F-FDG in oncologic indications, the CMS included coverage for the PET study of three more cancers: (1) localization of recurrent colorectal tumors indicated by rising levels of carcinoembryonic antigen (CEA) (not covered for staging), (2) staging of lymphoma confirmed by pathology and as an alternative to a gallium scan, (3) evaluation of recurrent melanoma, prior to surgery, as an alternative to a gallium scan.

In 2001, the CMS made a dramatic change in its approach to coverage for PET procedures and announced an NCD on PET procedures, based on a request by UCLA and Duke University for broad reimbursement coverage. This coverage request contained the summary and analysis of the literature of ^{18}F-FDG PET studies on cancer, cardiovascular disease, epilepsy, and Alzheimer's disease. In this broad coverage, reimbursement for diagnosis, staging, and therapy assessment

and for recurrence of lung, colorectal, melanoma, lymphoma, head and neck, and esophageal cancers was approved. Also included in this coverage was reimbursement for diagnosis for refractory seizure and myocardial viability using ^{18}F-FDG PET following inconclusive SPECT. Later, limited coverage for breast cancer, restaging of recurrent or residual thyroid cancer of follicular cell origin by ^{18}F-FDG PET, and perfusion study of the heart using ^{13}N-NH_3 PET were added for CMS reimbursement.

The CMS limited the above coverage only to PET procedures that were performed using dedicated PET scanners and excluded those performed with dual-head coincidence cameras. For Medicare coverage, the dedicated PET scanners must use BGO, NaI(Tl), or other detectors of equal or superior performance characteristics and may be full-ring or partial-ring types. Note that the CMS and private insurers do not distinguish between PET and PET/CT procedures and reimbursement is identical, i.e., there is no additional reimbursement for the CT part of PET/CT procedures. However, if the CT study is specifically performed for the diagnosis of a particular indication without the PET examination, then the procedure is reimbursed separately. However, physician payment for Medicare Part B is made at a higher rate for PET/CT than PET alone.

National Oncologic PET Registry

Medicare coverage for reimbursement is currently limited to certain types of cancers. To extend the coverage for noncovered indications, the CMS proposed a mechanism, referred to as *coverage with evidence development* (CED), that requires collection of PET data demonstrating the patient's health outcome. Under the CED initiative, the National Oncologic PET Registry (NOPR) was sponsored by the Society of Nuclear Medicine and Molecular Imaging and managed by the American College of Radiology (ACR) through the American College of Radiology Imaging Network (ACRIN). In this registry process, the CMS assesses the efficacy of the FDG procedures for specific indications to qualify for reimbursement. Facility registration began in November 2005 and the patient registration in May 2006. Any PET facility that is approved for billing the CMS is eligible to participate in the NOPR, and Medicare patients who are referred for PET studies for cancer indications that are not currently reimbursed under Medicare can participate in the registry.

The NOPR calls for registration of facilities, patients, and referring physicians for PET studies with the NOPR. It requires an initial facility registration fee of $50 and an escrow fee for each patient having the PET study. Each eligible patient must be registered with the NOPR providing the pre-PET clinical and demographic data via a Web form filled out by the referring physician. The NOPR then assigns a registration number for the patient and enters pre-PET information into the NOPR database prior to the day of scan. The patient must consent to the inclusion of the study data in the future NOPR research.

After the completion of the PET study, the data are sent to the NOPR, which then sends out the post-PET form for the study to be filled out by the referring physician. The referring physician must return the form within 30 days. When the database for the patient is complete and the PET facility is notified by the NOPR about the completion, the PET facility then bills the CMS for reimbursement for technical and professional components separately or globally depending on the setup of the facility. Billing is made using appropriate CPT codes with a special modifier assigned for NOPR studies. Detailed information about the NOPR is available at http://www.cancerPETregistry.org.

Note that as of June 2013, the CMS has ended the requirement of a CED for ^{18}F-FDG for oncologic indications that were covered earlier under CED. However, all other PET radiopharmaceuticals and CMS-designated cancer types can still be pursued under CED.

Questions

1. Which federal agency is responsible for Medicare payment for healthcare services?
2. Describe briefly how a Medicare payment for a particular clinical study is decided by the Centers for Medicare and Medicaid Services.
3. What are the different types of codes that need to be provided in a claim for reimbursement?
4. What is a relative value unit (RVU)?
5. Elucidate different steps taken in generating a bill for reimbursement for a study performed on a patient.
6. Name the PET radiopharmaceuticals for which reimbursements have been approved for specific clinical indications.
7. Describe the NOPR process for a PET procedure. What is the purpose of NOPR?
8. Can ^{18}F-FDG be used under NOPR?
9. Reimbursement for a PET procedure is the same in New York, NY, and Duluth, MN. True_____; False_____.
10. DRG is a reimbursement system for _____ and APC is a reimbursement code for _____.

Disclaimer The codes provided in Tables 11. 1 and 11.2 are valid at the time of this writing, but may change over time following rule changes by the CMS and other regulatory agencies.

References and Suggested Reading

AMA. CPT codes. Professional ed. Chicaco: The American Medical Association; 2015.

Centers for Medicare and Medicaid Services proposed rules. Medicare: hospital outpatient services: prospective payment system. Fed Regist. 2001;66:44671.

Food and Drug Administration notices. Human drugs: positron emission tomography drug products: safety and effectiveness. Fed Regist. 2000;65:12999.
Health care financial rules. Medicare hospital outpatient services: prospective payment system. Fed Regist. 2002;65:18433.
Keppler JS. Federal regulations and reimbursement for PET. J Nucl Med Technol. 2001;29:173.
Medicare national coverage determinations manual. pub 100-03. 2009. http://www.cms.hhs.gov/manuals/iom
Positron Emission Tomography (PET) Scans, Medicare Coverage Issues manual, Section 50-36, Transmittal R147. 2002. http://www.cms.gov//transmitals/downloads/R147cim.pdf
Society of Nuclear Medicine Physician Coding & Reimbursement Committee. Educational material on coding PET/CT with integrated PET systems. 2005 (updated, 2006).

Chapter 12
Design and Cost of PET Center

Introduction

PET/CT has become one of the most common and useful modalities for detection and monitoring of treatment of human diseases because of its high diagnostic efficacy and accuracy. PET centers are growing in large number throughout the world as hospitals and outpatient imaging centers are utilizing PET/CT increasingly for patient care. Smaller facilities normally possess only a single unit of PET/CT and procure their PET radiopharmaceuticals from commercial vendors that have a cyclotron facility. Larger and academic institutes have PET centers that are large enough in area to accommodate several PET/CT scanners, one or more cyclotrons, and a radiochemistry laboratory. These centers produce PET radiopharmaceuticals in their own cyclotron and use them for both patient care and research. The following is a brief description of the design of a relatively large PET center based on the clinical operation of one PET/CT scanner, a radiochemistry laboratory, and a cyclotron.

The design of a PET center hinges on a number of factors: site, floor loading, size of the rooms needed, traffic pattern inside the building, heating and cooling, electrical and water supply, and importantly, shielding requirement in the facility to comply with the NRC or state regulations. These factors vary from facility to facility and from equipment to equipment from various vendors. The discussion here pertains to a generic PET center with minimal requirements for these entities, and a schematic layout of a PET center is illustrated in Fig. 12.1.

G.B. Saha, *Basics of PET Imaging*, DOI 10.1007/978-3-319-16423-6_12

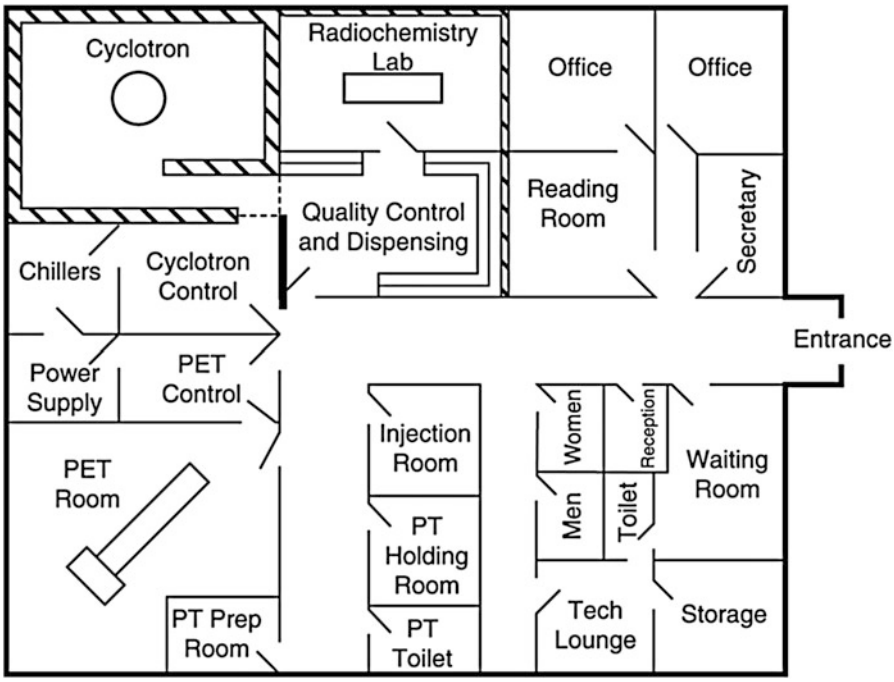

Fig. 12.1 A schematic layout of a PET center with a cyclotron. Note that the cyclotron and PET scanner rooms are on one side and the office area is on the opposite side of the center

Site Planning

To build a modern PET center, it is essential to have a good site planning for a smooth and efficient installation of different units such as the scanner and the cyclotron. An architectural blueprint must be drawn before construction begins. It is difficult and costly to make revisions after the completion of the project. Since a PET center involves the use of radiation, it must comply with all regulations of the NRC or the state regarding the radiation exposure to the worker and the public. Logically, it is preferred to have the PET center far away from heavy traffic areas in the building to minimize exposure to nonradiation workers.

It is more challenging to set up a PET center in an existing facility (such as in a nuclear medicine department) than in a totally new secluded area. Redesigning the rooms, tearing down the walls, rerouting the electrical supply and water pipes, etc., are common difficulties that are faced in modifying the existing facility to set up a PET center. Often, certain requirements may be compromised to go along with the available features at the facility. On the other hand, it is preferred and much easier to build a PET center from scratch in a new area without much compromise in requirements.

Due to the heavy weight of the shielding and magnet, the cyclotron needs to be installed on the ground floor or in the basement, and soil and underground condition must be assessed. If the water level is too shallow, or the sewer is running under, these areas are avoided or must be supported by additional support materials. Because of relatively lighter weight, the PET scanner, however, can be installed on a strong reinforced cement floor. In seismic areas, various units need to be properly anchored in compliance with local applicable seismic codes.

Passage

Passage is an important factor to receive and bring the PET and cyclotron units inside the PET center. The hallway must be wide enough and unhindered for easy delivery of these units to the installation site. Similarly, the door to the PET or cyclotron room also should be wide enough for easy access of the delivery crates. Normally a passage of 8×8 ft in width and height should be optimal for the purpose. At times, in existing facilities where the current passage cannot be used, a new passage may have to be opened to allow for the delivery, thus adding to the cost.

PET Center

The PET center should be divided into three adjacent sections: one for the PET scanner facility, one for the cyclotron facility, and the third for the office area. The size of the first two sections depends on the dimensions of each vendor's equipment, and the third section depends on the size and scope of the operation in a given facility.

Scanner Section

The scanner section should have six rooms: a scan room, a control room, an electronics room, a patient preparation room, an injection room, and a patient uptake room. The scanner room size depends on the dimension of the PET/CT scanner, but the variations in dimensions of scanners from different vendors are not significant. A room of at least 25×20 ft can be optimally used to install a PET/CT scanner from any vendor, along with storage for all supplies.

Adjacent to the scan room are the electronics room for all electrical units, connecting wires, etc., and the control room where the console for the operation of the scanner is installed. There should be a glass viewing window possibly of lead, between the scanning room and the control room for the operator to observe the

patient during the study. Alternatively, a video camera in the scanner room and the monitor in the control room can be installed. The dimension of the electronics room should be approximately 10×8 ft and that of the control room should be about 10×10 ft. However, these dimensions can vary, if needed. All these rooms are interconnected for easy access to each room. Because the electronics modules and scanners generate heat during operation, cooling is essential for the equipment and an efficient cooling and ventilation system must be installed. There should be a sink in the scanner room.

The patient preparation room should be preferably next to the above three rooms, but may be in an area not too distant from the scanner. Such a room should have a dimension of 6×6 ft. This room is primarily used for the patient to change for preparation for the study. This room may also be used as the injection room for administration of PET radiopharmaceuticals such as ^{18}F-FDG, if a separate injection room is not affordable.

An injection room of 6×6 ft should be equipped with a comfortable chair with armrest for the patient to sit on and a sink. All appropriate supplies should be stored in the room. A lead-shielded sharps container for syringe disposal and lead-shielded storage bin for other waste disposals are kept in the room.

Patients injected with ^{18}F-FDG are required to wait for 45–60 min before PET scanning and need to stay in a separate uptake room not to cause radiation exposure to the worker or the public. The PET room, the preparation room (if it is used as an injection room), and the uptake room should be well shielded to comply with the limits on radiation exposure to workers and the public. This will be discussed later in the chapter.

Cyclotron Section

The cyclotron facility should be situated at the farthest location from the inside traffic in the PET center, since its operation is not directly related to the patient and the level of radiation exposure is relatively high in this area. It should consist of a minimum of four rooms: cyclotron room, control room, cooling room, and radiochemistry laboratory. The size of these rooms depends on the size of equipment and space available at the facility, and they should be adjacent to each other.

The size and structural features of a medical cyclotron vary from vendor to vendor and so require rooms of various dimensions. A room of 25×25 ft should be adequate for most compact medical cyclotrons and should be equipped with a floor drain. The power supply unit may be installed in the cyclotron room or in a separate room.

Contaminated air from the cyclotron is exhausted to the outside atmosphere after passing through a HEPA filter and carbon filters. A stack monitor consisting of a gamma detector is installed to constantly monitor the level of radioactivity exhausted to meet the regulatory limits.

The weight of the magnet of a medial cyclotron runs around 22,000 lbs. Some cyclotrons are self-shielded with lead blocks weighing more than 35,000 lbs. Such heavy weight needs special consideration of the condition of the soil and the floor on which the cyclotron is to be installed. Entrance to the cyclotron room should be monitored by an electronic alarm to prevent accidental entrance to the room during the operation of the cyclotron.

The control room houses a workstation, a printer, and other auxiliary terminals to operate the cyclotron. A room with the size of 10×10 ft should be adequate and should have easy access to the cyclotron room, but entrance must be monitored by an alarm.

The cooling system is required because of the heat generated by the electromagnet of the cyclotron and power supply unit associated with it. It consists of chillers with heat exchanger/deionizer water system that recirculates cooled water between the cyclotron and the power supply. The temperature of the system is maintained at around 7–15 °C, depending on the type of cyclotron. Chillers are installed in a room adjacent to the cyclotron and power supply rooms, although they are sometimes installed on the roof of the cyclotron building. The room size for chillers should be of the size 10×10 ft and a floor drain is required in the room.

The radiochemistry room should be adjacent to the cyclotron for convenience of transfer of irradiated targets for processing and subsequent synthesis of PET radiopharmaceuticals. This room should be equipped with conventional labware along with a hot cell, a minicell, a synthesis box, a fume hood (preferably sterile), a sink, and a steel workbench all around. The optimal size of the room should be 20×20 ft, and a floor drain must be installed in the room. Appropriate shielding of this room is essential because a high level of radioactivity is handled inside. To this end, the walls of this room should be thick concrete (on the order of 40 cm). The room should be well ventilated at a negative pressure and maintained at a comfortable temperature using appropriate heating and air conditioning. A section or a separate room within the radiochemistry room is designated for quality control and dispensing of PET radiopharmaceuticals and should have a laminar fume hood.

Office Area

The office area in a PET center should have various administrative offices, a waiting room, a reading room, a storage room for supplies, a toilet, a file storage room, etc. The administrative offices include physicians' offices, receptionist's office, and secretary's office. Depending on the scope of the operation, the office area varies in size. In a smaller operation, all activities mentioned above are carried out in one or two rooms, while in a larger operation, several rooms are utilized for various activities for efficient operation of the PET center, as shown in Fig. 12.1. The receptionist area should be in the front section of the center to receive the patients on arrival at the center. The entire area should be designed with the idea in mind that the area is an unrestricted area and so there is minimal radiation exposure not to

exceed the regulatory limits from the adjacent PET scanner and the cyclotron rooms. An area between 400 and 600 square feet is an optimal estimate for the office suite in a relatively large PET center.

Caveat

A great deal of detail is involved in the planning and construction of a PET center with a cyclotron. To insure a successful project, it is essential to have one person charged with the responsibility of managing the entire project. This person should have a strong background and experience in medical facility construction and should be involved from the beginning to the end of the project. If such a person is not available locally, an outside planner or construction manager is recommended. This person should be the contact and liaison between the vendor and the PET center management.

As with any construction project, a construction permit must be obtained from the local authority. All local construction codes must be adhered to regarding the electricity and water supply and fire safety. A health physicist or a medical physicist should be consulted to address the issues of shielding and personnel traffic in restricted areas. A radioactive material license from the appropriate authority must be in possession for the use of PET radiopharmaceuticals, before the PET center goes into operation. Authorized physicians must be included on the license.

Shielding

A major concern in the setting up of a PET center is the shielding requirement for the walls, floors, and ceilings of the PET room, the uptake room for injected patients, the cyclotron room, and the radiochemistry room, because of the high-energy 511-keV photons from positron emitters handled in these areas. As mentioned, the cyclotron should be in an area away from the inside traffic and typically is installed on the lowest floor because of the heavy weight. Also, most compact cyclotrons are self-shielded with lead blocks. Even then, the cyclotron is housed in a room with thick concrete walls to reduce the radiation exposure outside the room. An unshielded cyclotron requires a very thick concrete vault with a lengthy maze for neutron exposure reduction. The radiochemistry room is also made of thick concrete walls and normally situated away from the inside traffic. Moreover, several enclosures made of lead bricks thick enough to considerably reduce radiation exposure are utilized in the laboratory for handling the radioactivity in the synthesis of PET radiopharmaceuticals.

The shielding requirement for the PET room is somewhat different because most facilities having a PET scanner is located in an area surrounded by areas often frequented by nonoccupational individuals. To meet the regulatory exposure limit

for these individuals, sufficient shielding in the walls and the ceiling should be provided in the PET scanner room, the injection room, and the patient uptake room. It is often required to calculate how much shielding is needed for a new PET room or how much shielding should be added to the wall in an existing room that is to be converted to a PET scanner room. The occupational workers work mostly inside the PET suite and satisfy their radiation exposure limit of 5 rem (0.05 Sv) per year by adopting ALARA principles and all radiation protection principles within the working area. A major consideration for shielding arises for the walls, ceiling, and floor that separate the scanner room and patient uptake room from unrestricted areas. The radiation exposure limit for nonoccupational individuals is 100 mrem (1 mSv) per year. Appropriate shielding should be estimated and provided for these areas to meet the regulatory limit. Several factors must be taken into consideration in estimating these shielding requirements, and these are discussed below.

(a) *Source of radiation*. The source of radiation exposure is primarily the patient injected with a PET radiopharmaceutical. The patient may be on the PET scanning table or in the uptake room after injection. The PET radiopharmaceutical dosages are contained in lead-shielded containers and are not likely to contribute to the exposure. Since a patient is considered an extended source of radiation, annihilation radiation is attenuated by the body and so the dose rate is significantly reduced. Based on literature data, the AAPM Task Group (2006) has recommended a patient dose rate of 0.092 μSv-m^2/MBq-h (0.34 mrad-m^2/mCi-h) immediately after administration of ^{18}F-FDG. This corresponds to an effective attenuation factor of 0.36 and a transmission factor f of 0.64, which should be included in the calculation of shielding for 511-keV photons.

(b) *Amount of activity*. The amount of activity administered to the patient determines the radiation exposure. Since the administered activity varies from patient to patient, an average value may be assumed in the estimation of shielding.

(c) *Decay of activity*. The activity in a patient decays over time and so radiation exposure also decreases with time from a given patient. So, how long a patient stays in the PET center determines the exposure. The exposure can be calculated from the cumulative activity integrated over time the patient stays in the uptake room and the PET scanner room. Thus, the cumulative activity A_c is given by

$$A_c = A_0 \frac{1 - e^{-\lambda t}}{\lambda}, \tag{12.1}$$

where A_0 is the initial administered activity, λ is the decay constant of the radionuclide in question, and t is the time the patient with activity stays at the facility. This time includes the time from injection to the end of scanning, i.e., the waiting time after injection (e.g., ^{18}F-FDG injection) plus the scanning time.

(d) *Number of patients per day*. Radiation exposure occurs when a patient is injected with radioactivity and scanned, i.e., for the duration the patient

stays at the facility after injection of radiopharmaceutical. There is no exposure in the absence of a patient injected with radiopharmaceutical. Therefore, the number of patients studied per day is an important factor in calculating the shielding.

(e) *Distance*. The radiation exposure decreases inversely with the square of the distance between the source and the walls, floor, or ceiling. The exposure X at a distance d from a point source of A mCi (MBq) activity is given by

$$X = \frac{A\Gamma}{d^2}, \tag{12.2}$$

where Γ is the exposure rate constant of the radionuclide, which is discussed at length in Chap. 10. The larger room cuts down the radiation exposure due to longer separation between the source and the outside of the wall.

(f) *Shielding material*. Radiations are attenuated by absorbing material, and the attenuation depends on the atomic number and density of the material. Heavier metals such as lead, tungsten, etc., are effective shielding material to reduce radiation exposure. Construction materials such as plaster, gypsum boards, steel, and concrete have lower attenuation coefficients and thus have lesser shielding effect. The linear attenuation coefficients (μ) of some of the shielding materials are given in Table 12.1. Using these μ values, one can calculate the thickness of shielding required for an initial exposure I_0, to reduce to I_x by the following formula:

$$I_x = I_0 e^{-\mu x}, \tag{12.3}$$

where I_x is the exposure beyond a thickness x of the shielding material with linear attenuation coefficient μ.

Equation (12.3) is valid for a narrow-beam geometry from a point source, and scattered radiations in the absorbing material are excluded. That is, each photon is either completely absorbed or transmitted. In reality, Compton scattering of 511-keV photons occurs within the shielding material, and some of the photons which were heading away from the location point of

Table 12.1 Properties of different shielding materials

Material	Atomic no. (Z)	Density ρ (g/cc)	Attenuation coefficient μ (cm^{-1})[a,b]
Concrete	–	2.2	0.080
Iron	26	7.9	0.433
Tungsten	74	19.3	2.165
Lead	82	11.4	1.260

[a]Adapted from Towson JEC (2003). Radiation dosimetry and protection in PET. In: Valk PE, Bailey DL, Townsend DW, Maisey MN (eds) Positron emission tomography, Springer, New York

[b]Based on broad-beam geometry

Table 12.2 Suggested occupancy factors T[a]

Occupancy level	Type of area	T
Full	Work areas, laboratories, nursing stations, living quarters, offices, children's play area	1
Partial	Corridors, restrooms, unattended parking lots	1/4
Occasional	Waiting rooms, toilets, stairways, elevators, closets	1/16

[a]Values suggested in NCRP 49

exposure may be scattered back toward it, thus adding to the exposure. This broad-beam geometry gives rise to what is called a *buildup factor*, B, which is given by:

$$B = \frac{\text{Intensity of primary plus scattered radiations}}{\text{Intensity of primary radiations only}}.$$

The value of B is always greater than 1 and depends on the thickness of the shielding material. It initially increases with the thickness of the shielding material and then reaches a plateau after a certain thickness. Also, the value of B is higher in low atomic number material than in high atomic number material, due to relatively more Compton scattering in the former. Thus, the buildup factor in gypsum board is higher than in lead. In lead, it can be assumed to be 1. In this case, the human body can be modeled to be segmented into different sections and iterative methods can be applied to estimate the shielding requirement. A phantom called *bottle manikin absorption* (BOMAB) is available, simulating various regions of human anatomy (arms, thigh, abdomen, chest, head) and can be used to estimate shielding need (ANSI 1999).

(g) *Occupancy factor*. The occupancy of an area refers to the amount (fraction) of time the area is occupied by an individual per week. The suggested occupancy factors T are given in Table 12.2.

Combining all the above factors, one can formulate an equation for radiation exposure as follows:

$$X = \frac{A_0 \Gamma f B N \left(1 - e^{-\lambda t}\right) e^{-\mu x} T}{d^2 \lambda}, \tag{12.4}$$

where

X = exposure (rem or Sv per week) at distance d from the patient and beyond the thickness x of shielding material
A_0 = activity in mCi (MBq) administered per patient
Γ = exposure rate constant (R-cm^2/mCi-h at 1 cm or μGy-m^2/GBq-h at 1 m)
f = transmission factor that accounts for exposure coming from the patient
B = buildup factor due to broad-beam geometry

N = number of patients per week
λ = decay constant (h^{-1}) of the radionuclide
t = time (h) the patient spends in the PET facility after receiving tracer injection
μ = linear attenuation coefficient (cm^{-1}) of photons in shielding material
T = occupancy factor for the area in question
d = distance from the patient in meter or centimeter
x = thickness (cm) of shielding material

CT causes radiation exposure to a varying degree due to scattered X-ray radiations from the patient during the study depending on the KV and mAs applied. The shielding required for 511-keV photons should be sufficient for the low-energy (70–140 keV) X-rays, even though the X-ray beam intensity is extremely high compared to the intensity of 511-keV photons. Normally, one-eighth inch of lead is sufficient for both 511 keV and X-rays.

We will now illustrate an example of estimation of shielding requirements for a simple specific case in a PET center.

Case Study

A drywall separates the PET room and a common waiting room and stands at 2 m away from the center of the PET scanner. The facility performs six ^{18}F-FDG PET studies per day using 15 mCi (555 MBq) dosage per patient. How much shielding of lead will be needed on the wall to meet the regulatory radiation exposure limit ($t_{1/2}$ of ^{18}F = 1.833 h; Γ for ^{18}F = 6.96 R-cm^2/mCi-h at 1 cm; μ for ^{18}F in lead = 1.26 cm^{-1})?

The common waiting area is considered a public area, and the exposure limit is 100 mrem/year or 100 mrem/50 weeks = 2 mrem/week.

Number of patients/week	=6 × 5 days/week = 30
Activity/patient, A_0	=15 mCi
Distance, d	=2 m or 200 cm
Time patient stayed after injection, t (assumed)	=40 min (wait) + 20 min (scan)
	=60 min
	=1 h
Occupancy factor T for waiting room	=1/16
B for lead	=1
f for patient attenuation	=0.64 (suggested above by AAPM)
Radiation exposure limit/week	=2 mrem/week
	=0.002 rem/week
Exposure rate constant Γ of ^{18}F	=6.96 R-cm^2/mCi-h at 1 cm
	=6.96 rem-cm^2/mCi-h at 1 cm
μ for ^{18}F in lead	=1.26 cm^{-1}
Decay constant λ for ^{18}F	$= \frac{0.693}{1.833} = 0.378\,h^{-1}$
x (thickness of shielding)	=?

Thus,

$$0.002(\text{rem/week}) = \frac{15 \times 6.96 \times 0.64 \times 30 \times 1 \times (1 - e^{-0.378 \times 1}) \times e^{-1.26x}}{200^2 \times 0.378 \times 16}$$

$$= \frac{4009 \times 0.3147 \times e^{-1.26x}}{241920}$$

$$e^{-1.26x} = 0.3835$$

Taking logarithm,

$$-1.26x = -0.9584$$

$$x = 0.76\,\text{cm}$$

$$\sim 0.30\,\text{in.}$$

Thus, assuming the drywall provides no shielding, approximately 0.3 in. of lead shielding would be needed to add to the wall in order to reduce radiation exposure in the waiting area below the regulatory limit of 100 mrem/year to the public.

Cost of PET/CT and Cyclotron Operation

During the past decades, the growth of PET/CT has been phenomenal all over the world, especially in the USA. Many community hospitals and academic institutions now have one or more PET/CT scanners, because PET/CT studies for many oncologic indications are reimbursed by the CMS. In the past, the supply of ^{18}F-FDG was limited to only a few academic centers that owned a cyclotron, and PET studies were available only at these facilities. Nowadays, commercial nuclear pharmacies produce ^{18}F-FDG for daily distribution to many facilities, small or large, for clinical PET/CT studies thus obviating the need for a cyclotron in a facility. These facilities benefit from this arrangement without having to possess a cyclotron that is expensive to purchase as well as to operate. However, academic and research institutions that are interested in research using different PET radiopharmaceuticals in addition to clinical ^{18}F-FDG are more likely to have a full-pledged PET center with a cyclotron and a radiochemistry laboratory. While the cost of operation and maintenance of a PET/CT scanner is moderate, that of a cyclotron is very high including personnel. The following is a brief estimate of expenses for different items pertinent to a PET/CT scanner and a cyclotron.

The price of a PET/CT scanner ranges between $1.7 and $2.5 million, depending on the choice of various features. At present, a 10–18-MeV medical cyclotron costs around $1–1.5 million dollars. The operational and maintenance cost of a cyclotron

is high because of power consumption and shielding requirement. Cost of equipment for the radiochemistry laboratory may run into $1 million. While PET/CT can be run by regular nuclear medicine technologists sharing their daily responsibilities with other nuclear medicine studies, dedicated individuals trained in cyclotron operation are needed for a cyclotron. One or more radiochemists, radiopharmacists, and technicians are required depending on the extent and scope of the operation, to synthesize the PET tracer of interest, to do its quality control, and to dispense it for patients. While a radiochemist is responsible for synthesis aspect and routine operation of the cyclotron, a radiopharmacist is required to validate and dispense the patient dosages. All these individuals earn a high-end salary of more than $100,000, with the exception of technicians who earn slightly less. The cost of licensing, service contract, and insurance of a cyclotron is quite high ranging in several hundred thousand dollars. An additional item of cost in the cyclotron operation is the target material that can be quite expensive depending on the enrichment and availability.

If an institution having a cyclotron operates a business venture to distribute ^{18}F-FDG to other facilities for PET/CT studies, it must have a distribution license from the state, which will add to the overall cost. In addition, delivery of dosages calls for drivers or courier services prompting additional expense. Considering the expenses, facilities that have no research plan or business of distribution are better off without a cyclotron avoiding the cost of cyclotron operation while fulfilling the clinical demand by purchasing unit dosages of ^{18}F-FDG from commercial vendors at a substantial financial benefit.

Questions

1. What are the different factors one should consider in designing a PET center without any cyclotron?
2. In designing a cyclotron facility, the major concern is shielding. Elaborate on different factors that must be taken into consideration in the estimation of shielding around the facility.
3. In a PET center, a clinical laboratory is situated on the other side of a plaster wall of the PET room. Calculate the amount of lead shielding required to be added to meet the regulatory limit, given the following information: number of FDG studies per week = 25; ^{18}F-FDG dosage per patient = 10 mCi; linear attenuation coefficient of 511-keV photons in lead = 1.26 cm^{-1}; Γ for ^{18}F = 6.96R-cm^2/mCi-h at 1 cm; distance between the scanner and the wall is 250 cm; and patient stays in the department for a total of 1 h after injection.
4. What is a stack monitor? Where is it used?

References and Suggested Reading

American National Standards Institute/Health Physics Society. Specifications for the bottle manikin absorption phantom. ANSI/HPS N13. McLean: Health Physics Society; 1999. p. 35.

Courtney JC, Mendez P, Hidalgo-Salvatierra O, Bujenovic S. Photon shielding for a positron emission tomography suite. Health Phys. 2001;81:S24.

Kearfott KJ, Carey JE, Clemenshaw MN, Faulkner DB. Radiation protection design for a clinical positron emission tomography imaging suite. Health Phys. 1992;63:581.

Madsen MT, Anderson JA, Halama JR, et al. AAPM Task Group 108: PET and PET/CT shielding requirements. Med Phys. 2006;33:4.

Mathe B. Shielding design for a PET imaging suite: a case study. Health Phys. 2003;84:S83.

Chapter 13
Sample Procedures for PET Studies

Introduction

In this chapter, different protocols for common PET procedures are described to provide a general understanding of how a PET study is performed. Only five procedures are included, namely, whole-body PET imaging with ^{18}F-FDG, PET/CT whole-body imaging with ^{18}F-FDG, ^{18}F-florbetapir PET/CT imaging of amyloid plaque in Alzheimer's patients, myocardial perfusion imaging with ^{82}Rb-RbCl, and myocardial metabolic imaging with ^{18}F-FDG. The procedures described here are generic in that there are variations in the detail of each procedure from institution to institution. Different institutions employ different techniques in immobilizing the patient on the table. Use of CT contrast agents in PET/CT is still a debatable issue, and some investigators use them, while others do not. While glucose loading is essential for myocardial ^{18}F-FDG studies in patients with low fasting glucose levels, there are varied opinions as to the lowest limit of glucose level at which glucose loading should be provided and what amount of glucose should be given orally. In lymphoma and colorectal studies, it is desirable to have a Foley catheter secured to the patient to eliminate extraneous activity in the bladder, but perhaps it is not universally employed by all.

In view of the above discussion, it is understandable that the procedures described below are a few among many with variations in detail, but the basics of PET or PET/CT imaging remain the same.

G.B. Saha, *Basics of PET Imaging*, DOI 10.1007/978-3-319-16423-6_13

Whole-Body PET Imaging with ^{18}F-FDG

Physician's Directive

1. A nuclear medicine physician fills out a scheduled patient's history form indicating where the scan begins and ends on the body.
2. If the patient weighs over 250 lbs, the physician authorizes a dosage of ^{18}F-FDG higher than the normal dosage.

Patient Preparation

3. The patient is instructed to fast 6 h prior to scan.
4. Insert an IV catheter into the patient's arm for administration of ^{18}F-FDG.
5. For melanoma patients, injection must not be made in the affected extremity. Injection should be made away from the affected area.
6. A Foley catheter is required for patients with colorectal carcinoma and lymphoma, for voiding urine.
7. Remove all metallic items such as belts, dentures, jewelry, bracelets, hearing aids, bra, etc., from the patient.
8. The patient wears a snapless gown.

Dosage Administration

9. Inject ^{18}F-FDG (10–15 mCi or 370–555 MBq in a shielded syringe) into the patient through the IV catheter. Flush with 20-mL saline.
10. The patient waits for 40–60 min with instructions to remain calm and quietly seated during this waiting period.

Scan

11. Enter patient's name, birth date, weight, and ID number into the computer.
12. Obtain a blank transmission scan without the patient in the scanner for attenuation correction using the rotating ^{68}Ge source before the first patient is done. This blank scan is used for all subsequent patients for the day.
13. After the waiting period, the patient lies supine on the scan table with the head toward the PET scanner and with arms up or down depending on the area to be scanned.

14. Position the patient inside the scanner to the upper limit of the scan as designated by the physician. This position is marked by the computer control on the console.
15. The patient is then moved to the lower limit of the scan and the position is marked by the computer control on the console.
16. The computer determines the length of the scan field from the positions marked in Steps 14 and 15. From the manufacturer's whole-body scanner chart, determine the number of bed positions needed for the length of the scan field.
17. Set the PHA at 430–650 keV.
18. Enter into the computer all pertinent information, e.g., dosage of ^{18}F-FDG, injection time, and number of bed positions.
19. Position the patient to the upper limit of scan in the scanner.
20. Collect a patient's transmission scan with the ^{68}Ge source.
21. Start the patient's emission scan collecting data for a preset count or time.
22. Move the table to the next bed position and repeat Steps 19 and 20. Note: Steps 19–21 are automatically done by the computer control.
23. The scanner stops when the lower limit of the scan is completed (i.e., scanning at all bed positions is completed).
24. The patient is released after the complete acquisition of the data.

Reconstruction and Storage

25. Attenuation correction factors are calculated from the blank transmission scan (Step 12) and patient transmission scan (Step 19). Reconstruct images using the corrected data with appropriate reconstruction algorithms (FBP or iterative method), provided by the manufacturer.
26. Images are sent to the workstation for display and interpretation.
27. Images are stored and archived in PACS for future use.

Whole-Body PET/CT Imaging with ^{18}F-FDG

Physician Directive

1. The nuclear physician evaluates the history of the patient and sets the scan limits of the body.
2. The physician authorizes a higher dosage of ^{18}F-FDG, if needed based on the patient's weight.

Patient Preparation

3. The patient is asked to fast for 6 h prior to scan.
4. Remove metallic items from the patient, including dentures, pants with zipper, bra, belts, bracelets, etc.
5. The patient wears a snapless gown.
6. Insert an IV catheter in the patient's arm for administration of ^{18}F-FDG.

Dosage Administration

7. If the patient is diabetic, check the blood glucose level. If the level is <200 mg/dL, inject ^{18}F-FDG into the patient a dosage of 0.22 mCi/kg (8.1 MBq/kg). If the level is >200 mg, consult the physician. The cutoff value for glucose level varies with the institution. Measure the residual in the syringe to determine the administered activity.
8. The patient waits for 45–60 min after ^{18}F-FDG administration and is instructed to remain quiet with minimal movement until the completion of the PET/CT scan.
9. The patient is asked to void prior to scanning.

Scan

10. Enter the patient's information into the computer, such as name, clinic or hospital number, birth date, and weight as well as the dosage of ^{18}F-FDG.
11. Collect a blank CT transmission scan at the beginning of the day. It is used for subsequent patients for the day.
12. The patient lies supine on the scan table with the head toward the gantry and is positioned by laser light. The patient's arms are positioned up (suspected thorax) or down (suspected head and neck) depending on the area to be scanned. Comfortable supports are provided for the head and neck, the arms, and the knees.
13. The table advances by computer control toward the gantry (first CT). Acquire a topogram to define axial range of the body for scanning. The patient is asked not to move and close eyes and breathe normally during this phase. When the area to be scanned is covered by the topogram, scanning is stopped.
14. Position the patient in the CT scan field and procure a spiral CT transmission scan that takes less than 1 min.
15. After the completion of the CT scan, the table is automatically advanced into the PET scanner with the patient in the scan field. The PHA is set at 430–650 keV. The number of bed positions is automatically calculated from the axial range defined by the topogram in Step 13. Data are acquired for a set time for each bed position.
16. After the completion of the PET data acquisition for the last bed position, the patient is released.

Reconstruction and Storage

17. Because CT images are collected in a short time, they are ready for calculation of attenuation correction factors before the first PET emission scan is completed. The attenuation correction factors are calculated from the blank scan (Step 11) and patient's transmission scan (Step 14) by the appropriate algorithm.
18. Attenuation correction factors are applied to acquired PET data (Step 15). PET images are then reconstructed from corrected data using either the FBP or iterative method depending on the vendor's software.
19. The appropriate software fuses the CT and PET images of each slice.
20. The CT, PET, and fused PET/CT images are then sent to the workstation for display and interpretation.
21. Images are stored and archived in PACS for future use.

Amyloid-Plaque Imaging in Alzheimer's Patients Using ^{18}F-Florbetapir PET/CT

Patient Preparation

1. Insert and secure an intravenous catheter for ^{18}F-florbetapir administration in one arm of the patient and keep it patent with 0.9% NaCl solution.
2. Remove all metallic items from the patient including dentures, pants with zipper, bra, belts, bracelets, etc.

Dosage Administration

3. Administer 10 mCi (370 MBq) of ^{18}F-florbetapir through the catheter followed by flushing with ~20 cc of 0.9% NaCl solution. Wait for 40–45 min.

Scan

4. Enter into the computer patient's information such as name, clinic ID number, birth date, weight, and administered dosage.
5. Take blank CT scan at the beginning of the day that is used for all subsequent patients for the day.
6. Let the patient lie supine on the scanning table. Secure the patient's head in the head holder with tape and Velcro to prevent any head movement.

7. Push the table inside the scanner to position the patient's head in the field of view identified by scanner's laser.
8. Take a topogram to define the axial length of field for the head.
9. Move the table in the CT field and take a spiral CT transmission scan for attenuation correction. It takes less than a minute.
10. After the completion of the CT scan, the table with the patient is automatically advanced into the PET axial field of view and set PHA at 430–650 keV. Collect data for a preset time or counts at each of bed positions that are calculated from axial range defined by the topogram in Step 8. The total acquisition time is about 15 min.
11. Note that data acquisition must be finished within 90 min after ^{18}F-florbetapir administration.
12. After data acquisition is complete, the patient is released.

Reconstruction and Storage

13. Since CT scan is obtained in a short time, the attenuation correction factors are calculated during PET emission data acquisition using the blank scan in Step 5 and the patient's transmission scan in Step 9.
14. Attenuation correction is applied to PET data (Step 10) and PET images are reconstructed using the FBP or iterative method provided by the vendor.
15. Fuse the PET image with CT image of each slice.
16. Store and archive the images in PACS for future use.

Myocardial Metabolic PET or PET/CT Imaging with ^{18}F-FDG

Patient Preparation

1. The patient is instructed to fast for 6–12 h prior to scan.
2. Place an IV catheter in the arm of the patient for FDG administration.
3. Blood glucose level of the patient is checked. A variety of situations can arise as to glucose loading to titrate blood glucose level and several protocols have been developed. For details, refer to the American Society of Nuclear Cardiology Practice Guidelines: Imaging guidelines for Nuclear Cardiology Procedures: PET myocardial Perfusion and Metabolism Clinical Imaging (Bacharach et al. 2003). One of the protocols is adopted as follows:

   (a) If fasting glucose level is $<$110 mg/dL and no diabetes, give the patient 25–100 g of glucose orally and monitor the blood glucose and follow the insulin administration guidelines below. If the fasting glucose level is

>110–130 mg/dL or if the patient is diabetic, glucose loading remains suboptimal and so follow the insulin administration guidelines below as well. No glucose needs to be administered if the blood glucose level is >250 mg/dL. If at 45–60 min after administration, the glucose level is

130–140 mg/dL, give 1 U regular insulin IV
140–160 mg/dL, give 2 U regular insulin IV
160–180 mg/dL, give 3 U regular insulin IV
180–200 mg/dL, give 5 U regular insulin IV
>200 mg/dL, notify physician

Dosage Administration

4. After blood glucose monitoring, administer 5–15 mCi (185–555 MBq) ^{18}F-FDG to the patient. The patient is asked to wait for 45–60 min.
5. For a PET-only study, obtain a blank transmission scan with a ^{68}Ge source before the first patient is done. This scan is used for all subsequent patients for the day. For a PET/CT scan, obtain a blank CT scan and store it for attenuation correction for subsequent patients on the day.

Scan

6. The patient lies supine on the scan table with arms up away from the field of the heart. Position the patient in the scanner with the heart in the axial field of view.
7. In PET/CT studies, obtain a topogram (scout scan) with CT to define the positioning of the patient.
8. Procure a transmission (for attenuation correction) scan of the patient using the rotating ^{68}Ge source for the PET-only study or with the patient in the CT field of view and collecting CT transmission scan for the PET/CT study.
9. Next, using pulse height window of 430–650 keV, collect PET emission scan data for a preset time or count in a sinogram matrix of a chosen size. It should take about 10–30 min.

Reconstruction and Storage

10. Calculate attenuation correction factors from the blank transmission scan (Step 5) and patient's transmission scan (Step 8), and apply them to the acquired emission data. Reconstruct images using the attenuation-corrected emission data by the FBP or iterative method (e.g., OSEM) provided by the manufacturer. The pixel size in reconstructed images should be 2–4 mm.
11. The gating technique may be applied, if desired.

12. Images are then sent to the workstation for viewing and interpretation.
13. Next, images are stored in PACS for future use.

Myocardial Perfusion PET or PET/CT Imaging with ^{82}Rb-RbCl

Patient Preparation

1. The patient removes all clothing above the waist and wears a slip-on gown.
2. Twelve-lead EKG connections are then applied to the patient for monitoring vital signs during stressing.
3. The patient lies supine on the scan table with arms stretched out beyond the scanner gantry. The head and neck and the arms are kept comfortable and immobile with supports.
4. Insert an IV catheter into the arm for ^{82}Rb and pharmacologic agent (dipyridamole, lexiscan, or adenosine) infusion. The IV line is kept patent with saline. Patient's information is entered into the computer.

Dosage Administration and Scan

5. For a PET-only study, collect a blank transmission scan at the beginning of the day by the ^{68}Ge source before the first patient is positioned in the PET scanner. This blank scan is used for all subsequent patients for the day. For a PET/CT study, collect a blank CT scan and store for subsequent patients for the day.
6. Position the patient so that the heart is within the scan field.
7. Connect the ^{82}Rb generator tubing from the infusion pump (see Chap. 14) to the patient's catheter. A low dosage of 10–20 mCi (370–740 MBq) ^{82}Rb is administered by the infusion pump and a topogram (scout scan) is obtained to ensure the position of the heart is in the correct scan field. In the case of PET/CT study, a topogram is obtained with CT to set the axial scan range.
8. Take a patient's transmission scan with the rotating ^{68}Ge source or with a spiral CT.
9. Administer ^{82}Rb by the infusion pump (see Chap. 14) for a cumulative activity of 40–60 mCi (1.48–2.22 GBq) for 2D acquisition or 20–40 mCi (0.74–1.48 GBq) for 3D acquisition. Infusion should be completed in a period of maximum 30 s.
10. Set the energy window at 430–650 keV. Start rest emission scan 70–90 s after the ^{82}Rb infusion for normal left ventricular function and about 110–130 s for poor ventricular function. Gated acquisition also can be performed, if desired.

11. Infuse the pharmacologic agent (dipyridamole at 0.57 mg/kg over 4 min, adenosine at 140 μg/kg/min for 6 min, or lexiscan at 0.4 mg/5 mL by rapid injection) using a pump, after the rest scan.
12. Administer ^{82}Rb by the infusion pump at the peak stress the same cumulative activity as for the rest scan in Step 9.
13. Start stress emission scan at the peak stress collecting data for a preset count or time.
14. The patient is released after the completion of the PET scan.

Reconstruction and Storage

15. Attenuation correction factors are calculated for each pixel from the transmission scan (Step 8) and the blank scan (Step 5) and applied to the PET emission data. Reconstruct images using the corrected data by the FBP or iterative method based on the algorithm provided by the vendor. The reconstruction should use a Butterworth or low-pass filter and a pixel size of 2–3 mm.
16. Images are sent to the workstation for display and interpretation.
17. Images are stored and archived in PACS for future use.

References and Suggested Reading

Bacharach SL, Bax JJ, Case J et al. American society of Nuclear Cardiology Practice guidelines. PET Myocardial glucose metabolism and perfusion imaging. Part 1. Guidelines for patient preparation and data acquistion. J Nucl Cardiol. 2003;10:543.

Chapter 14
Topics of Interest

Estimated Absorbed Dose from Intravenous Administration of ^{18}F-FDG and ^{82}Rb-RbCl in Humans

The dose estimate D in a human organ is made by using the following internal dosimetry equation (Saha 2013):

$$D = \tilde{A} \times S, \tag{14.1}$$

where $\tilde{A}$ is the cumulated activity and S is the mean absorbed dose per cumulated activity. $\tilde{A}$ is calculated from the initial administered activity and the biodistribution and residence time of the tracer in each organ and has the unit of $\mu Ci \cdot h$ or $MBq \cdot h$. S is calculated from the knowledge of physical characteristics of the radiation in question, the mass of the organ, and the absorption fraction of the radiation in the target organ and has the unit of $rad/\mu Ci \cdot h$ or $mGy/MBq \cdot h$. The values of S are available in literature for most common radiopharmaceuticals including ^{18}F-FDG and ^{18}Rb-RbCl. The experimental data for biodistribution and residence time are available in literature and used to calculate $\tilde{A}$. The following two tables give the absorbed doses per administered activity based on these calculations for ^{18}F-FDG and ^{82}Rb-RbCl, respectively (Tables 14.1 and 14.2).

Evaluation of Tumor Uptake of ^{18}F-FDG by PET

PET imaging is widely used for the detection of a variety of tumors such as breast, colorectal, esophageal, head and neck, lung, thyroid, melanoma, lymphoma, and other cancers, because of its high sensitivity, specificity, and accuracy. In the interpretation of tumor FDG-PET images, it is desirable to compare the relative tumor FDG uptake

G.B. Saha, *Basics of PET Imaging*, DOI 10.1007/978-3-319-16423-6_14

Table 14.1 Absorbed dose per unit administered activity of ^{18}F-FDG[a]

Target organ	mGy/MBq	rad/mCi
Brain	0.046 ± 0.012	0.17 ± 0.044
Heart wall	0.068 ± 0.036	0.25 ± 0.13
Kidneys	0.021 ± 0.0059	0.078 ± 0.022
Liver	0.024 ± 0.0085	0.088 ± 0.031
Lungs	0.015 ± 0.0084	0.056 ± 0.031
Pancreas	0.014 ± 0.0016	0.052 ± 0.0060
Red marrow	0.011 ± 0.0017	0.040 ± 0.0062
Spleen	0.015 ± 0.0021	0.056 ± 0.0078
Urinary bladder wall[b]	0.073 ± 0.042	0.27 ± 0.16
Ovaries[c]	0.011 ± 0.0015	0.041 ± 0.0055
Testes[c]	0.011 ± 0.0016	0.041 ± 0.0057
Whole body[d]	0.012 ± 0.00077	0.043 ± 0.0023
Effective dose[d,e]	0.0190	0.070

[a]Reproduced with permission from Hays MT, Watson EE, Thomas ER, et al (2002). MIRD dose estimate report no.19: radiation absorbed dose estimates from ^{18}F-FDG. J Nucl Med 43:210

[b]Dose to urinary bladder wall is based on 120-min void intervals, starting 120 min after dosing, using traditional static MIRD model

[c]Doses to ovaries and testes include doses from residence times in urinary bladder and remainder of body as calculated from data in: Hays MT, Segall GM (1999) A mathematical model for the distribution of fluorodeoxyglucose in humans. J Nucl Med 40:1358

[d]The calculation of whole-body dose is based on total energy deposited in the body divided by its total mass, whereas the total effective dose reported by the ICRP is calculated by applying risk-based weighting factors to individual organ doses to estimate a uniform whole-body dose that in theory gives the same risk as the nonuniform pattern that actually occurred. The two values are based on different concepts and not comparable

[e]From ICRP (1999) Publication No. 80. Pergamon Press, New York

with the adjacent normal tissue uptake. Such a comparison offers information on the degree of tumor progression and provides clues to appropriate management of the tumor. In radiation therapy or chemotherapy of tumors, comparative evaluation of tumor FDG-PET images before and after therapy is even more useful to assess the effect of therapy on tumor. In all cases, the reconstructed images are used to determine the tumor uptake of FDG relative to the normal tissue uptake.

There are several methods, visual, quantitative, and semiquantitative, to determine the tumor uptake of FDG. Visual assessment is commonly used in tumor diagnosis and staging and is based on differences in contrast between tumor and adjacent tissue. This is a simplified method requiring only a single static image at a set time after injection and can be equally applied to assess the therapeutic response of the tumor. In the visual technique, it is important to adjust the image intensities of the tumor and adjacent tissues to the same gray or color scale.

While visual assessment of tumor is widely accepted in many nuclear medicine facilities, the quantitative or even semiquantitative method improves the detection

Table 14.2 Absorbed dose per unit administered activity of ^{82}Rb-RbCl

Adult absorbed radiation doses[a]		
Organ	mGy/2220 MBq	rads/60 mCi
Adrenals	2.15	0.22
Stomach	1.91	0.19
Small intestine	3.11	0.32
Upper large intestine	1.91	0.19
Lower large intestine	1.91	0.19
Heart wall	4.22	0.42
Kidneys	19.1	1.92
Liver	1.91	0.19
Lungs	3.77	0.38
Ovaries	0.84	0.084
Pancreas	1.38	0.14
Red marrow	0.84	0.084
Testes	0.67	0.066
Total body	0.95	0.096
Effective dose[b]	7.5	0.755

[a]Obtained from package insert
[b]Obtained from ICRP Publication No. 80. Pergamon Press, New York, 1999

and comparative assessment significantly and therefore is highly desirable. Quantitative methods, also called the kinetic methods, include two methods: compartmental analysis and Potlak analysis. Compartmental analysis is based on the fitting of the time–activity curve to a two-compartmental model, using measured arterial activity (input function) and nonlinear regression. The time course of activity in tissue is followed by serial imaging and arterial blood sampling. The metabolic rate of glucose given by this method is expressed in mol/min/mL. Potlak analysis provides similar information requiring a fewer data and only the integral of the blood activity for input function. Both methods are too complex demanding much resources and therefore are less favorable for routine clinical application. The details of these methods are beyond the scope of this book and the readers are referred to standard texts on kinetic modeling.

In semiquantitative methods, static images are utilized as in visual assessment to determine the tissue activity and compare the relative tumor uptake. One method uses an index, the tumor-to-normal tissue activity ratio (T/N), using data from the normal and tumor regions on the reconstructed images. The ratios are independent of the administered dosage and patient's weight or blood glucose level. The T/N ratio assessment is somewhat similar to visual assessment. The choice of an appropriate normal reference site, particularly in the abdomen and pelvic area, is critical in this analysis.

The most versatile semiquantitative technique is the *standard uptake value* (SUV) method that is widely used in nuclear medicine and molecular imaging. This value is also less commonly referred to as the differential uptake ratio (DUR). It is defined by the tissue concentration of activity as determined from the region of interest (ROI) on the PET image, divided by the injected dosage of the tracer, and multiplied by a calibration factor, which is basically the body weight, body surface, or body lean mass. Thus,

$$\text{SUV} = (C_{\text{ROI}}/A) \times WT, \tag{14.2}$$

where C_{ROI} is the decay-corrected radiotracer concentration in μCi/g or (MBq/g) of tissue in ROI, A is the injected radiotracer dosage in μCi (MBq), and WT is the body weight of the patient. In SUV calculation, an ROI is chosen by the reader on the reconstructed image that is displayed on the computer monitor. The computer then calculates the average count density or maximum count density in the ROI, corrects it for the decay for the uptake period and counting efficiency, estimates the area of ROI from the knowledge of pixel size and the number of pixels in ROI, and finally converts the corrected count density to activity per gram of tissue (assuming tissue density is equal to 1 g/cm^3). From the knowledge of the body weight of the patient, and the injected dosage in μCi (MBq), the SUV is calculated for the ROI using Eq. (14.2). The ^{18}F-FDG SUV values are unitless numbers and for some normal tissues are <1 for soft tissues, 1.5–2.0 for blood pool 1 h after injection, $\sim$2.5 for liver, and $\sim$3.5 for renal cortex. The SUV values for various neoplastic tissues range from 2 to as high as 25, depending on the avidity of different cancer cells for ^{18}F-FDG. Note that if all of the tracer were uniformly distributed throughout the body, the SUV in each region would be 1. It implies that the SUV serves as a normalized *T*/*N* ratio index.

It is important to note that the SUV values are affected by several factors. The time period between tracer injection and scanning (i.e., the uptake period) is perhaps the largest single source of error in determining the SUV. Time to reach maximum uptake in a given tissue varies with the type and condition of tissue, i.e., different forms of neoplasm and also with tissues before and after therapy. Tissue uptake of FDG decreases with increasing blood glucose level, which affects the SUV. Excess body fat falsely elevates the SUV, which many investigators correct by using body lean mass instead of body weight. Also, many investigators found better values of SUVs using body surface area in place of body weight. The use of maximum pixel count density versus average value for all pixels in an ROI also affects the SUV values, although the average value now is less commonly used. Thus, SUVs reported in literature are not exactly comparable unless all these parameters are specified.

Infusion Pump for ^{82}Sr–^{82}Rb Generator

Rubidium-82 ($t_{1/2} = 75$ s) is available from the ^{82}Sr–^{82}Rb generator (CardioGen-82 supplied by Bracco Diagnostics, Inc.). Because of its short half-life, an automated infusion pump is employed for its delivery from the generator to the patient. The infusion pump is a device distributed by Bracco Diagnostics, Inc., that delivers ^{82}Rb-RbCl by pumping 0.9% NaCl (normal saline) through the generator. A schematic diagram of the infusion pump is shown in Fig. 14.1. The lead-shielded generator is mounted on a mobile cart. A large-volume plastic syringe is connected through a three-way stopcock to a saline bottle or bag to supply saline to the generator for ^{82}Rb elution. The syringe is filled with saline and then pushes it through the generator to elute ^{82}Rb under the action of an electronically controlled pump. An outlet tubing from the generator carries the ^{82}Rb activity in saline under the action of the pump to either a waste bottle or the patient. A divergence valve placed along the outlet tubing switches the line between the patient and the waste bottle. The initial low-level activity is discarded into the waste bottle, and later the uniform activity is directed to the patient. In the midway of the tubing before the divergence valve, a positron detector made of plastic scintillator coupled with a photomultiplier tube is installed to measure the activity passing through the tubing.

The infusion pump is operated electronically and equipped with several controls on a console that select the total volume (mL), total dosage (mCi or MBq), dosage rate (mCi/s or MBq/s), and flow rate (mL/min). A printer is included in the device to print out all parameters related to the infusion of the ^{82}Rb activity. Before the infusion pump is used for a given day, the pump device needs to be calibrated.

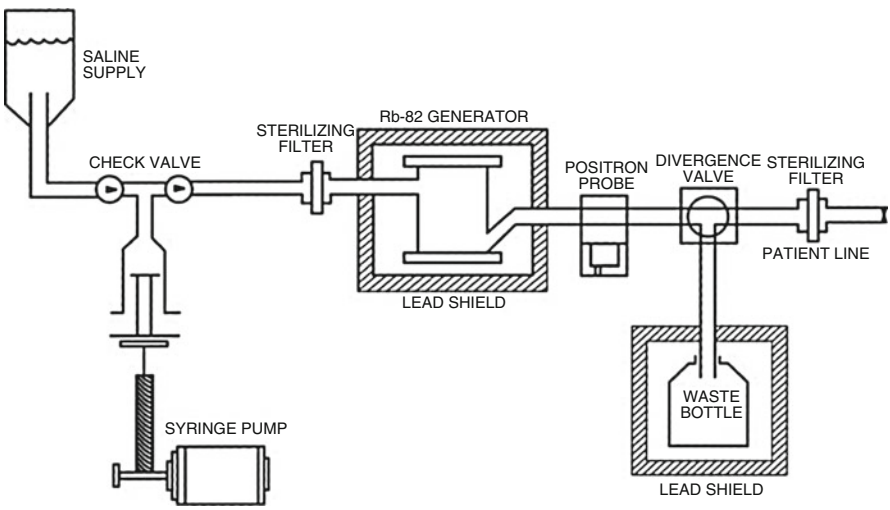

Fig. 14.1 A schematic illustration of the infusion pump for the ^{82}Sr–^{82}Rb generator. The details of the operation of the pump are given in the text

There is a control knob on the console that sets a specified calibration factor for the generator. Calibration is performed at the beginning of the day prior to patient study using the manufacturer's calibration factor given for the generator. Initial 50 mL of eluate is discarded, and after 10-min wait for the growth of ^{82}Rb, 50 mL of the activity is collected in a stoppered vial and measured in a dose calibrator immediately after the elution is over. One can use the dose calibrator setting given by Bracco or use ^{60}Co setting and dividing the reading by 0.548. The measured activity is corrected for decay to the end of infusion and compared with the activity printed out by the printer. The discrepancy, beyond the specifications of the manufacturer, is corrected by adjusting the calibration factor and repeating the calibration. In this calibration experiment, the amounts of ^{82}Sr ($t_{1/2} = 25.6$ days) and ^{85}Sr ($t_{1/2} = 65$ days) breakthrough are also determined by allowing the ^{82}Rb activity in the vial to decay completely and then measuring the activity of these two radionuclides, as described below.

For a patient study, the patient gets an IV catheter that is connected to the patient line of the infusion pump. The desired total volume, the total activity to be administered, and the flow rate are all set on the console by the operator prior to the start of infusion. First, the low activity volume of saline as detected by the detector is flushed out to the waste bottle by applying the purge button. After purging, when the preset dose rate threshold is achieved as detected by the detector, the activity is directed to the patient line, and the set amount of the cumulated activity is administered. The pump stops after the infusion of the desired amount of activity, and all relevant parameters are printed out by the printer. The procedure for myocardial perfusion study in humans using the ^{82}Rb generator and infusion pump is presented in Chap. 13.

The waste bottle should be emptied every morning prior to or at the end of system usage. The ^{82}Rb generator is supplied every month and a half, which is installed in the infusion cart replacing the old generator. Each new generator is supplied with a new tubing set (called the administration set), which replaces the old set. The old generator is returned to the supplier, Bracco Diagnostics, Inc.

Calculation of ^{82}Sr and ^{85}Sr Breakthrough in ^{82}Rb Eluate

The breakthrough of ^{82}Sr and ^{85}Sr in the ^{82}Rb eluate must be within the limits set by the NRC, which are 0.02 μCi of ^{82}Sr per mCi of ^{82}Rb (0.02 kBq of ^{82}Sr per MBq of ^{82}Rb) and 0.2 μCi of ^{85}Sr per mCi of ^{82}Rb (0.2 kBq of ^{85}Sr per MBq of ^{82}Rb). According to Bracco Diagnostics, Inc., product brochure, the method of determining the breakthrough is as follows: The generator is initially flushed with 50 mL of 0.9% NaCl solution to clear any residual activity in the tubing. It is then eluted with another 50 mL of 0.9% NaCl solution and immediately the ^{82}Rb activity is measured in a dose calibrator and decay corrected to the end of elution. The ^{82}Rb activity is allowed to decay almost completely for an hour and the residual activity (A) containing ^{82}Sr and ^{85}Sr is measured. The ratio P, ^{85}Sr/^{82}Sr, for the day of calibration

is provided on the generator label, and the correction factors (F) for the ratio P for subsequent days of use are provided by the manufacturer in the generator brochure.

Next the ratio R, $^{85}Sr/^{82}Sr$, on a given day of measurement is calculated as

$$R = P \times F. \tag{14.3}$$

The ^{85}Sr contribution to the total breakthrough activity A is further corrected by a factor, Q (0.478). So the ^{82}Sr activity is calculated as

$$^{82}Sr(\mu Ci) = A/(1 + R \times Q) \tag{14.4}$$

The ^{82}Sr breakthrough is calculated by dividing the ^{82}Sr (μCi or MBq) activity from Eq. (14.4) by the ^{82}Rb (mCi or MBq) activity at the end of elution. The ^{85}Sr breakthrough is obtained by multiplying the ^{82}Sr breakthrough calculated above by R from Eq. (14.3). If on a day these values exceed 1/10th of the specified limits, i.e., 0.002 μCi of ^{82}Sr per mCi of ^{82}Rb (0.002 kBq of ^{82}Sr per MBq of ^{82}Rb) and 0.02 μCi ^{85}Sr per mCi of ^{82}Rb (0.02 kBq of ^{85}Sr per MBq of ^{82}Rb), these breakthrough measurements must be performed twice daily (e.g., morning and noon).

The use of the ^{82}Sr–^{82}Rb generator is discontinued if ^{82}Sr and ^{85}Sr breakthroughs exceed the specified limits, 0.02 μCi (740 Bq) and 0.2 μCi (7.4 kBq), respectively, and if the cumulative volume of ^{82}Rb eluate exceeds 17 L. The useful shelf-life of the generator is 42 days after which its use is discontinued.

Questions

1. Define SUV.
2. SUV depends on the administered activity. True_____; False_____.
3. What is the shelf-life of the ^{82}Sr–^{82}Rb generator?
4. Describe how to determine the ^{82}Sr and ^{85}Sr breakthrough in ^{82}Rb eluate.
5. SUV decreases with increasing blood sugar. True_____; False_____.
6. What are the limits of ^{82}Sr and ^{85}Sr in the ^{82}Rb eluate?

References and Suggested Reading

CardioGen-82 (Bracco Diagnostics Inc): FDA package insert. medlibrary.org/lib/rx/meds/cardiogen-82-1

Saha GB. Physics and radiobiology of Nuclear Medicine. 4th ed. New York: Springer; 2013. page 248

Appendix A: Abbreviations Used in the Text

ALARA	As low as reasonably achievable
ANDA	Abbreviated new drug application
APC	Ambulatory payment classification
APD	Avalanche photodiode
BET	Bacterial endotoxin test
BGO	Bismuth germanate
CMS	Centers for Medicare and Medicaid Services
CPT	Current Procedural Terminology
CTDI	CT dose index
CZT	Cadmium–zinc–tellurium
DICOM	Digital Imaging and Communications in Medicine
DOI	Depth of interaction
DOT	Department of Transportation
DRG	Diagnosis-related group
EC	Electron capture
eIND	Exploratory Investigational New Drug
eaIND	Expanded Access Investigational New Drug
FBP	Filtered backprojection
FDA	Food and Drug Administration
FDG	Fluorodeoxyglucose
FID	Free induction decay
FOV	Field of view
FWHM	Full width at half maximum
GSO	Gadolinium oxyorthosilicate
HCPCS	Healthcare Common Procedure Coding System
HIPAA	Hospital Insurance Portability and Accountability Act
HIS	Hospital Information System
HOPPS	Hospital Outpatient Prospective Payment System

G.B. Saha, *Basics of PET Imaging*, DOI 10.1007/978-3-319-16423-6

HPLC	High-performance liquid chromatography
HVL	Half-value layer
ICD-10-CM	International Classification of Disease, Tenth Revision, Clinical Modification
ICRP	International Committee on Radiological Protection
IND	Notice of Claimed Investigational Exemption for a New Drug
IRB	Institutional Review Board
IT	Isomeric transition
kV	Kilovolt
LAL	Limulus amebocyte lysate
LAN	Local area network
LCD	Liquid crystal display
LOR	Line of response
LSO	Lutetium oxyorthosilicate
LYSO	Lutetium yttrium oxyorthosilicate
MIRD	Medical internal radiation dose
MLEM	Maximum-likelihood expectation maximization
NCA	No carrier added
NCD	National coverage determination
NCRP	National Council on Radiation Protection and Measurement
NDA	New drug application
NECR	Noise equivalent count rate
NEMA	National Electrical Manufacturers Association
NRC	Nuclear Regulatory Commission
OSEM	Ordered subset expectation maximization
PACS	Picture Archival and Communication System
PET	Positron emission tomography
PM	Photomultiplier (tube)
PHA	Pulse height analyzer
PS-APD	Position-sensitive avalanche photodiode
QF	Quality factor
RBE	Relative biologic effectiveness
RDRC	Radioactive Drug Research Committee
RIS	Radiology Information System
RSC	Radiation Safety Committee
RSO	Radiation Safety Officer
RVU	Relative value unit
SiPM	Silicon photomultiplier tube
SF	Scatter fraction
SNR	Signal-to-noise ratio
SPECT	Single photon emission computed tomography
SUV	Standard uptake value
TEDE	Total effective dose equivalent

TLC	Thin layer chromatography
TLD	Thermoluminescent dosimeter
TOF	Time of flight
USP	US Pharmacopeia

Appendix B: Terms Used in the Text

Absorption	A process by which the total energy of a radiation is removed by a medium through which it passes.
Annihilation radiation	Gamma radiations of 511 keV energy emitted at 180° after a β^+ particle is annihilated by combining with an electron in matter.
Antineutrino	A particle of no charge and mass emitted during β^- decay.
Atomic mass unit (amu)	By definition, one-twelfth of the mass of ^{12}C, equal to 1.66×10^{-24} g or 931 MeV.
Atomic number (Z)	The number of protons in the nucleus of an atom.
Attenuation	A process by which the intensity of radiation is reduced by absorption and/or scattering during its passage through matter.
Auger electron	An electron ejected from the outer electron shell by an X-ray by transferring all its energy.
Average life (τ)	See mean life.
Avogadro's number	The number of molecules in 1 g-mol of a substance or the number of atoms in 1 g atom of an element. It is equal to 6.02×10^{23}.
Becquerel (Bq)	A unit of radioactivity. One becquerel is equal to 1 disintegration per second.
Binding energy	The energy to bind two entities together. In a nucleus, it is the energy needed to separate a nucleon from other nucleons in the nucleus. In a chemical bond, it is the energy necessary to separate two binding partners by an infinite distance.
Biological half-life (T_b)	The time by which one-half of an administered dosage of a substance is eliminated by biological processes such as urinary and fecal excretion.

G.B. Saha, *Basics of PET Imaging*, DOI 10.1007/978-3-319-16423-6

Bremsstrahlung	Gamma ray photons produced by deceleration of charged particles while passing near the nucleus of an atom.
Carrier	A stable element that is added in detectable quantities to a radionuclide of the same element, usually to facilitate chemical processing of the radionuclide.
Carrier-free	A term used to indicate the absence of any stable isotopic atom in a radionuclide sample.
Chelating agent	A compound that binds to a metal ion by more than one coordinate covalent bond.
Committed dose equivalent ($H_{T,50}$)	The dose equivalent to organs or tissues of reference (T) that will be received from an intake of radioactive material by an individual during the 50-year period following intake.
Committed effective dose equivalent ($H_{E,50}$)	It is the sum of the products of the tissue weighting factors (W_T) applicable to each of the body organs or tissues that are irradiated and the committed dose equivalent to the corresponding organ or tissue ($H_{E,50} = \Sigma W_T \times H_{T,50}$). W_T accounts for the tissue sensitivity to radiation, and their values are given in Table 10.2. Note that this is due to committed dose equivalent from only internal uptake of radiation. This quantity is referred to as the effective dose.
Conversion electron (e^-)	See internal conversion.
Cross section (σ)	The probability of occurrence of a nuclear reaction or the formation of a radionuclide in a nuclear reaction. It is expressed in a unit termed barn; $1\ b = 10^{-24}\ cm^2$.
Curie (Ci)	A unit of activity. A curie is defined as 3.7×10^{10} disintegrations per second.
Cyclotron	A machine to accelerate charged particles in circular paths by means of an electromagnetic field. The accelerated particles such as α-particles, protons, deuterons, and heavy ions possess high energies and can cause nuclear reactions in target atoms by irradiation.
Decay constant (λ)	The fraction of atoms of a radioactive element decaying per unit time. It is expressed as $\lambda = 0.693/t_{1/2}$ where $t_{1/2}$ is the half-life of the radionuclide.
Deep-dose equivalent (H_d)	Dose equivalent at a tissue depth of 1 cm (1000 mg/cm^2) due to external whole-body exposure.
Dosage	A general term for the amount of a radiopharmaceutical administered in microcuries or millicuries or becquerels.

Dose	The energy of radiation absorbed by any matter.
Dosimeter	An instrument to measure the cumulative dose of radiation received during a period of radiation exposure.
Dosimetry	The calculation or measurement of radiation absorbed doses.
Effective dose equivalent (H_E)	It is the sum of the products of the dose equivalent to the organ or tissue (H_T) and the tissue weighting factors (W_T) applicable to each of the body organs or tissues that are irradiated ($H_E = \Sigma W_T H_T$).
Effective half-life (T_e)	Time required for an initial administered dose to be reduced to one-half due to both physical decay and biological elimination of a radionuclide. It is given by $T_e = (T_p \times T_b)/(T_p + T_b)$, where T_e is the effective half-life and T_p and T_b are the physical and biological half-lives, respectively.
Electron (e^-)	A negatively charged particle circulating around the atomic nucleus. It has a charge of 4.8×10^{-10} esu and a mass of 9.1×10^{-28} g, equivalent to 0.511 MeV or equal to 1/1836 of the mass of a proton.
Electron capture (EC)	A mode of decay of a proton-rich radionuclide in which an orbital electron is captured by the nucleus, accompanied by emission of a neutrino and characteristic X-rays.
Electron volt (eV)	The kinetic energy gained by an electron when accelerated through a potential difference of 1 V.
Erg	The unit of energy or work done by a force of 1 dyne through a distance of 1 cm.
Fission (f)	A nuclear process by which a heavy nucleus divides into two nearly equal smaller nuclei, along with the emission of 2–3 neutrons.
Generator, radionuclide	A device in which a short-lived daughter nuclide is separated chemically from a long-lived parent nuclide adsorbed on an adsorbent material. For example, ^{99m}Tc is separated from ^{99}Mo from the ^{99}Mo–^{99m}Tc generator with saline.
Gray (Gy)	The unit of radiation dose in SI units. One gray is equal to 100 rad.
Half-life ($t_{1/2}$)	A unique characteristic of a radionuclide, defined by the time during which an initial activity of a radionuclide is reduced to one-half. It is related to the decay constant λ by $t_{1/2} = 0.693/\lambda$.

Half-value layer (HVL)	The thickness of an absorbing material required to reduce the intensity or exposure of a radiation beam to one-half of the initial value when placed in the path of the beam.
Internal conversion	An alternative mode to γ-ray decay in which nuclear excitation energy is transferred to an orbital electron which is then ejected from the orbit.
Ion	An atom or group of atoms with a positive charge (cation) or a negative charge (anion).
Ionization chamber	A gas-filled instrument used to measure radioactivity or exposure in terms of ion pairs produced in gas by radiations.
Isobars	Nuclides having the same mass number, that is, the same total number of neutrons and protons. Examples are $^{57}_{26}$Fe and $^{57}_{27}$Co.
Isomeric transition (IT)	Decay of the excited state of a nuclide to a lower excited state or the ground state.
Isomers	Nuclides having the same atomic and mass numbers but differing in energy and spin of the nuclei. For example, ^{99}Tc and ^{99m}Tc are isomers.
Isotones	Nuclides have the same number of neutrons in the nucleus. For example, $^{131}_{53}$I and $^{132}_{54}$X are isotones.
Isotopes	Nuclides having the same atomic number, that is, the same number of protons in the nucleus. Examples are $^{14}_{6}$C and $^{12}_{6}$C.
K capture	A mode of radioactive decay in which an electron from the *K* shell is captured by the nucleus.
$LD_{50/60}$	A dosage of a substance that, when administered or applied to a group of any living species, kills 50% of the group in 60 days.
Linear attenuation coefficient (μ)	The fraction of radiation energy absorbed and scattered per unit thickness of absorber.
Linear energy transfer (LET)	Energy deposited by radiation per unit length of the matter through which the radiation passes. Its usual unit is keV/mm.
Mass number (A)	The total number of protons and neutrons in a nucleus of a nuclide.
Mean life (τ)	The period of time a radionuclide exists on the average before disintegration. It is related to the half-life and decay constant by $\tau = 1/\lambda = 1.44\, t_{1/2}$.
Metastable state (m)	An excited state of a nuclide that decays to a lower excited state or the ground state with a measurable half-life.

Neutrino (v)	A particle of no charge and mass emitted with variable energy during β^+ and electron capture decays of radionuclides.
No carrier added (NCA)	A term used to characterize the state of a radioactive material to which no stable isotope of the compound has been added purposely.
Nucleon	A common term for neutrons or protons in the nucleus of a nuclide.
pH	The unit of hydrogen ion concentration. It is given by the negative common logarithm of the hydrogen ion concentration in a solution: $pH = -\log_{10}[H^+]$.
Phantom	A volume of material artificially made to simulate the property of an organ or part of the body when exposed to radiation.
Physical half-life (T_p)	See half-life.
Quality factor (QF)	A factor dependent on linear energy transfer that is multiplied by absorbed doses to calculate the dose equivalents in rem. It is used in radiation protection in order to take into account the relative radiation damage caused by different radiations. It is 1 for X-ray, γ-ray, and β-ray, 10 for protons, and 20 for α-particles.
Rad	The unit of radiation absorbed dose. One rad is equal to 100 ergs of radiation energy deposited per gram of any matter or 10^{-2} J/kg of any medium.
Radiation weighting factor (W_r)	See quality factor.
Radiochemical purity	The fraction of the total radioactivity in the desired chemical form. If ^{99m}Tc-MAA is 90% pure, then 90% of the radioactivity is in the ^{99m}Tc-MAA form.
Radionuclidic purity	The fraction of the total radioactivity in the form of the stated radionuclide. Any extraneous radioactivity such as ^{99}Mo in ^{99m}Tc-radiopharmaceuticals is an impurity.
Radiopharmaceutical	A radioactive drug that can be administered safely to humans for diagnostic and therapeutic purposes.
Rem. (H_r)	A dose equivalent defined by the absorbed dose (rad) times the relative biological effectiveness or quality factor or radiation weighting factor of the radiation in question. $H_r = \text{rad} \times W_r$
Roentgen	The quantity of X-rays or γ radiations that produces one electrostatic unit of positive or negative charge in 1 cm^3 of air at 0 °C and 760 mmHg pressure (STP). It is equal to 2.58×10^{-4} C/kg air.

Sensitivity	The number of counts per unit time detected by a scanner for each unit of activity present in a source. It is given by counts per second per microcurie (cps/μCi) or (cps/kBq).
Shallow-dose equivalent (H_s)	Dose equivalent at a tissue depth of 0.007 cm (7 mg/cm^2) averaged over an area of 1 cm^2 due to external exposure to the skin.
Sievert (Sv)	The international unit of dose equivalent and equal to 100 rem.
Spatial resolution	A measure of the ability of a scanner to faithfully reproduce the image of an object. It is empirically defined as the minimum distance between two points on an image that can be delineated by a scanner.
Tissue weighting factor (W_T)	A factor related to the radiosensitivity of different tissues in living systems.
Tracer	A radionuclide or a compound labeled with a radionuclide that may be used to follow its distribution or course through a chemical, physical, or metabolic process.

Appendix C: Units and Constants

Energy	
1 electron volt (eV)	$= 1.602 \times 10^{-12}$ erg
1 kiloelectron volt (keV)	$= 1.602 \times 10^{-9}$ erg
1 million electron volts (MeV)	$= 1.602 \times 10^{-6}$ erg
1 joule (J)	$= 10^{7}$ ergs
1 watt (W)	$= 10^{7}$ ergs/s
	= 1 J/s
1 rad	$= 1 \times 10^{-2}$ J/kg
	= 100 ergs/g
1 gray (Gy)	= 100 rad
	= 1 J/kg
1 sievert (Sv)	= 100 rem
	= 1 J/kg
1 horsepower (HP)	= 746 W
1 calorie (cal)	= 4.184 J

Charge	
1 coulomb (C)	$= 6.25 \times 10^{18}$ charges
1 electronic charge	$= 4.8 \times 10^{-10}$ esu
	$= 1.6 \times 10^{-19}$ C
1 ampere (A)	= 1 C/s

Mass and energy	
1 atomic mass unit (amu)	$= 1.66 \times 10^{-24}$ g
	= 1/12 the atomic weight of ^{12}C
	= 931 MeV
1 electron rest mass	= 0.511 MeV

(continued)

G.B. Saha, *Basics of PET Imaging*, DOI 10.1007/978-3-319-16423-6

Mass and energy	
1 proton rest mass	= 938.78 MeV
1 neutron rest mass	= 939.07 MeV
1 pound	= 453.6 g
1 ounce	= 28.3 g

Length	
1 angstrom (Å)	$= 10^{-8}$ cm
1 micrometer or micron (μm)	$= 10^{-6}$ m
	$= 10^{4}$ Å
1 nanometer (nm)	$= 10^{-9}$ cm
1 fermi (F)	$= 10^{-13}$ cm
1 inch	= 2.54 cm
1 mile	= 1.6 km

Activity	
1 curie (Ci)	$= 3.7 \times 10^{10}$ disintegrations per second (dps)
	$= 2.22 \times 10^{12}$ disintegrations per minute (dpm)
1 millicurie (mCi)	$= 3.7 \times 10^{7}$ dps
	$= 2.22 \times 10^{9}$ dpm
1 microcurie (μCi)	$= 3.7 \times 10^{4}$ dps
	$= 2.22 \times 10^{6}$ dpm
1 becquerel (Bq)	= 1 dps
	$= 2.703 \times 10^{-11}$ Ci
1 kilobecquerel (kBq)	$= 10^{3}$ dps
	$= 2.703 \times 10^{-8}$ Ci
1 megabecquerel (MBq)	$= 10^{6}$ dps
	$= 2.703 \times 10^{-5}$ Ci
1 gigabecquerel (GBq)	$= 10^{9}$ dps
	$= 2.703 \times 10^{-2}$ Ci
1 terabecquerel (TBq)	$= 10^{12}$ dps
	= 27.03 Ci

Constants	
Avogadro's number	$= 6.02 \times 10^{23}$ atoms/g-atom
	$= 6.02 \times 10^{23}$ molecules/g-mol
π	= 3.1416
e	= 2.7183

Appendix D: Answers to Questions

Chapter 1

5. False
6. True
11. 85 keV
14. 110 keV
16. 220 min
18. 4.6 mCi
19. 31.1 mCi
20. 1.56 h
21. 1.55 h
23. (a) False, (b) False, (c) True
25. (a) False, (b) True
26. 325 keV
29. (a) 8.3 HVLs, (b) 9 HVLs
30. 1 HVL
31. 2.56 cm
32. False

Chapter 2

4. (a)
5. (b)
6. *N*/2
7. (b)
8. (c)
14. (a) True, (b) False, (c) True
15. 120 cm
16. (c)
18. True
19. (c)

G.B. Saha, *Basics of PET Imaging*, DOI 10.1007/978-3-319-16423-6

Chapter 3

2. (a)
3. (b)
4. (b)
5. 0.313 cm
7. True
8. (c)
12. (a), (c)
13. True
15. 0.135
17. True
18. (b)
19. 5.6
20. True
22. A (a), B (b), C (b), D (a)
23. (a) False, (b) False
26. True (a), Random (b), Scatter (a)
28. (a) True, (b) True

Chapter 4

6. False
7. True
8. (b)
10. True

Chapter 6

1. (c)
3. False
4. True
5. 4 mm
7. 1.98 mm
10. (c)
12. 2D: (c), 3D: (a)
13. (c)
17. True
18. (a) True, (b) False
19. (b)
21. False
22. True

Chapter 7

5. True
6. 3.86 Ci

7. ~18 h (6 half-lives of the radionuclide)
9. True
12. True

Chapter 8

10. False
11. False
12. (b)

Chapter 10

1. True
8. 5 rem (0.05 Sv); 15 rem (0.15 Sv); 50 rem (0.5 Sv)
9. 0.5 rem (5 mSv); 0.5 rem (5 mSv); 0.1 rem (1 mSv)
17. 9.76 mR
18. 2.61 cm
19. 10%
22. True

Chapter 11

9. False
10. Hospital inpatient, hospital outpatient

Chapter 12

3. 1.6 cm of lead (assuming occupancy factor 1)

Chapter 14

2. False
3. 42 days
5. True

Index

G.B. Saha, *Basics of PET Imaging*, DOI 10.1007/978-3-319-16423-6